

Stochastic and continuum descriptions of population dynamics with spatial structure

Anudeep Surendran

B.S. (Physical Sciences, IISER-Kolkata)

M.S. (Physical Sciences, IISER-Kolkata)

under the supervision of

Professor Matthew J. Simpson

and

Professor Scott W. McCue

School of Mathematical Sciences

Science and Engineering Faculty

Queensland University of Technology

and external supervision of

Professor Michael J. Plank

School of Mathematics and Statistics

University of Canterbury



2020

SUBMITTED IN FULFILMENT OF THE REQUIREMENTS FOR THE
DEGREE OF DOCTOR OF PHILOSOPHY

To my loving family.

Copyright in relation to this thesis

© Copyright 2020 by Anudeep Surendran. All rights reserved.

Statement of original authorship

The work contained in this thesis has not been previously submitted to meet requirements for an award at this or any other higher education institution. To the best of my knowledge and belief, the thesis contains no material previously published or written by another person except where due reference is made.

Signature:

Date: December 16, 2020

Abstract

Localised interactions among individuals in a population are fundamental to many processes in cell biology and ecology. These interactions can be cell-to-cell interactions or cell-to-extracellular substrate interactions in cell biology and interactions between animals or between plants or between animals and plants in ecology. The short-range interactions, such as competition and cooperation between individuals, and limited dispersal, lead to the formation of macro-scale spatial structures in the population. The most common spatial structures are clustered spatial structure where individuals tend to be seen in close aggregates, and segregated spatial structure where individuals tend to stay away from others. As a result of these specific spatial arrangements, the number of individuals present in the close proximity of an individual will be significantly different from a population without any spatial structure. This subtle effect can influence individuals' event rates and, hence, play a significant role in determining the overall population dynamics. Despite the numerous evidence for the role of spatial structure in determining the dynamics of the population, mathematical models in these contexts are often based on a mean-field assumption. Under the mean-field assumption, the interactions between individuals are assumed to be proportional to the average density of individuals and neglect the spatial correlation between individuals' locations. In this thesis, we develop individual-based models (IBM) that consider various short-range interactions between individuals and accurately predict the resulting spatial structure formation in the population. A mathematically tractable continuum approximation of the IBM is derived in terms of the dynamics of spatial moments. Using these modelling frameworks, we explore the role of spatial structure in biologically and ecologically relevant scenarios, such as the dynamics of cells in the presence of obstacles, chase-escape dynamics, predator-prey dynamics and Allee kinetics.

Acknowledgments

First and foremost, I would like to express my sincere thanks to **Professor Mat Simpson**, my principal supervisor, for providing me with an excellent opportunity to pursue this Ph.D. research project under his supervision and for all of his support, guidance and encouragement throughout my candidature. Thank you Mat, for the generous amount of time you have dedicated to meeting me every week for discussing the research ideas, reading draft manuscripts, and for all opportunities and help provided for enhancing my training for a career in research. Without your continued support and guidance, this thesis would not have been possible. I am deeply grateful for your supervision and I look forward to future opportunities to collaborate.

Second, I would like to thank my external supervisor, **Professor Mike Plank**, for finding time to meet on-line regularly, discuss research ideas and provide guidance throughout my candidature. I would also like to take this opportunity to thank Mike for inviting me to the University of Canterbury, Christchurch. This visit helped me in shaping the research ideas for two chapters in this thesis. I am immensely grateful to Mike for his suggestions on the research projects and for the time he has spent on reading and giving feedback on draft manuscripts.

I would also like to thank my associate supervisor, **Professor Scott McCue**, for his support and encouragement.

I want to acknowledge the financial support from **QUT** and the **Australian Research Council (DP170100474)** that enabled me to pursue my candidature. I would also like to thank the **School of Mathematical Sciences** and the **Institute of Health and Biomedical Research** at QUT for providing financial support for attending conferences.

I would also like to thank my colleagues and friends at QUT for making a positive working environment. In particular, I want to thank **Dr. Alex Matisaka**, **Dr. Claudio Arancibia-Ibarra** and **Mr. Olivier Huet** for all the interesting discussions and coffee breaks.

Last but not least, I want to thank my family and friends. Thanks to my parents, **Surendran** and **Sheela**, my love **Leya**, my brother **Anuvind**, and all other family and friends back in Kerala for always being there for me. Even though you all were so far away from Brisbane, that never stopped you from supporting and encouraging me in all possible ways. Without that love and care you have shown to me, this journey would not have been possible.

List of publications

1. **Surendran Anudeep**, Plank Michael J., Simpson Matthew J. 2018 Spatial moment description of birth-death-movement processes incorporating the effects of crowding and obstacles. *Bulletin of Mathematical Biology* 80: 2828–2855. DOI:[10.1007/s11538-018-0488-1](https://doi.org/10.1007/s11538-018-0488-1). bioRxiv Preprint.
2. **Surendran Anudeep**, Plank Michael J., Simpson Matthew J. 2019 Spatial structure arising from chase-escape interactions with crowding. *Scientific Reports* 9: 14988. DOI:[10.1038/s41598-019-51565-3](https://doi.org/10.1038/s41598-019-51565-3). bioRxiv Preprint.
3. **Surendran Anudeep**, Plank Michael J., Simpson Matthew J. 2020 Small-scale spatial structure affects predator-prey dynamics and coexistence. *Theoretical Ecology* 13: 537–550. DOI:[10.1007/s12080-020-00467-6](https://doi.org/10.1007/s12080-020-00467-6). bioRxiv Preprint.
4. **Surendran Anudeep**, Plank Michael J., Simpson Matthew J. 2020 Population dynamics with spatial structure and an Allee effect. *Proceedings of the Royal Society A: Mathematical, Physical and Engineering Sciences* 476: 20200501. DOI:[10.1098/rspa.2020.0501](https://doi.org/10.1098/rspa.2020.0501). bioRxiv Preprint.

Contents

Abstract	v
Acknowledgments	vii
List of publications	ix
1 Introduction	1
1.1 Background	1
1.2 Research questions	7
1.3 Objectives and outcomes	10
1.4 Structure of the thesis	14
1.5 Statement of joint authorship	15
1.5.1 Chapter 2: Spatial moment description of birth-death-movement processes incorporating the effects of crowding and obstacles	15
1.5.2 Chapter 3: Spatial structure arising from chase-escape interactions with crowding	16
1.5.3 Chapter 4: Small-scale spatial structure affects predator-prey dynamics and coexistence	16
1.5.4 Chapter 5: Population dynamics with spatial structure and an Allee effect	17
2 Spatial moment description of birth-death-movement processes incorporating the effects of crowding and obstacles	19
2.1 Preamble	19
2.2 Abstract	20
2.3 Introduction	20
2.4 Individual-based model	22
2.4.1 IBM for motile, proliferative agents and stationary obstacles	24
2.4.2 Numerical implementation	25
2.5 Continuous description	27
2.5.1 Dynamics of spatial moments	27

2.5.2	Spatial moment description for motile, proliferative agents and stationary obstacles	29
2.6	Bias landscape	33
2.7	Results and discussion	38
2.7.1	Effect of varying the obstacle density	38
2.7.2	Effect of varying the obstacle size	41
2.7.3	Effect of varying the obstacle interaction strength	44
2.8	Conclusions	47
2A	Additional results for Chapter 2	51
2A.1	Definition of spatial moments for general multi-species model	51
2A.2	Conditional probabilities for the presence of individuals	52
2A.3	Calculating the expected event rates and net bias vector	53
2A.4	Dynamics of the second spatial moment	55
2A.5	Numerical methods	56
3	Spatial structure arising from chase-escape interactions with crowding	59
3.1	Preamble	59
3.2	Abstract	59
3.3	Introduction	60
3.4	Stochastic, individual-based model	62
3.4.1	Numerical simulation of the individual-based model	66
3.5	Spatial moment dynamics	67
3.5.1	General spatial moment formulation	67
3.5.2	Summary statistics	69
3.5.3	Numerical methods for spatial moment dynamics	70
3.6	Results	70
3.6.1	Effect of varying the interaction strength	72
3.6.2	Effect of varying the spatial extent of interaction	75
3.6.3	Effect of varying the relative density of species	77
3.7	Conclusions	78
3A	Additional results for Chapter 3	81
3A.1	Derivation of movement displacement PDF	81
3A.2	Spatial moment dynamics for a community consisting of two distinct species	81
3A.3	Moment closure schemes	83
3A.4	Evolution of spatial structure	85
3A.5	Dependence of steady-state spatial patterns on the initial configuration of individuals	87
3A.6	Effect of varying the relative density of species	88

4 Small-scale spatial structure affects predator-prey dynamics and coexistence	91
4.1 Preamble	91
4.2 Abstract	91
4.3 Introduction	92
4.4 Individual-based model	94
4.4.1 Mean-field dynamics	97
4.5 Results	98
4.5.1 Short range dispersal creates intraspecies clustering	101
4.5.2 Short range competition creates intraspecies segregation	103
4.5.3 Short range predation drives interspecies segregation	105
4.5.4 Short-range dispersal and short-range predation enhances resources' survival	106
4.5.5 Effect of short range predation and short range competition	109
4.5.6 Spatial structure drives qualitative departure from the mean-field model	111
4.6 Conclusion	113
5 Population dynamics with spatial structure and an Allee effect	117
5.1 Preamble	117
5.2 Abstract	117
5.3 Introduction	118
5.4 Individual-based model	120
5.5 Spatial moment dynamics	124
5.6 Mean-field dynamics	128
5.7 Results and Discussion	130
5.7.1 Short-range competition reduces the Allee threshold	132
5.7.2 Short-range competition and dispersal encourage population extinction	133
5.7.3 Short-range cooperation and intermediate-range dispersal promotes population growth	136
5.7.4 Survival probability	137
5.8 Conclusions	138
5A Additional results for Chapter 5	141
5A.1 Comparison of long-range and short-range competition	141
5A.2 Numerical implementation of the individual-based model	142
5A.3 Definition of spatial moments	143
5A.4 Conditional probabilities for the presence of individuals	144
5A.5 Computation of variance	145
5A.6 Comparison of moment closure methods	146
5A.7 Numerical methods for solving the moment dynamics equation	148

5A.8 Effect of short-range dispersal	148
6 Conclusions	151
6.1 Summary of the research	151
6.2 Future work	154
6.2.1 Non-homogeneous models	154
6.2.2 Three-dimensional models	155
6.2.3 Incorporation of experimental data and parameter estimation	155
6.2.4 Higher order moment closure methods	156
6.2.5 Multi-species model of Allee effects	156
6.2.6 Impact of directional bias on predator-prey dynamics and Allee kinetics	156
6.2.7 Eco-evolutionary dynamics	157
6.3 Final remarks	157
Bibliography	159

Chapter 1

Introduction

1.1 Background

Interactions between individuals play a crucial role in many biological and ecological processes, such as tissue development and repair, immune response, diseases and predator-prey dynamics, to mention a few (Weijer 2009; Shaw and Martin, 2009; Ilina and Friedl, 2009; Williams and Solnica-Krezel, 2017; Barbosa and Castellanos, 2005). The interaction an individual experiences locally can significantly influence its motility and proliferation. For instance, the interaction through release and detection of chemical signals or mechanical forces such as cell-cell adhesion leads to cells moving in a direction towards or away from other cells, creating a directional bias to the movement (Raz and Mahabaleshwar, 2009; Tambe et al., 2011). Another interaction mechanism is crowding effects such as contact inhibition or stimulation of movement and proliferation, where the event rates of an individual depend on the local cell density (Abercrombie, 1979; Roycroft and Mayor, 2015; Pavel et al., 2018). Similar to the biological systems, localised interactions are ubiquitous in ecosystems and play a significant role in determining the population dynamics. For example, in a predator-prey ecosystem, a prey located close to a group of predators experiences increased mortality due to the high risk of predation. Similarly, the competitive interactions within a population for shared resources can amplify the death rate of conspecifics. Another interesting interaction mechanism commonly observed in various animal communities is the chase escape interaction (Vicsek, 2010; Romanczuk et al., 2009). These interactions are characterised by the presence of two types of individuals, namely chasers and escapees, where the chasers are biased to move towards the escapees, and the escapees are biased to move away from the chasers.

Experimental observations in ecology and cell biology suggest that the short-range interactions at the individual level often lead to the development of a macroscale spatial structure in the population, which in turn can influence the population dynamics (Wood and Ackland, 2007; Strombom et al., 2014; Binny et al., 2015; Dini et al., 2018). The typical forms of spatial structures observed are clustering and segregation (Simpson et al., 2013; Gerum et al. 2018).

In a clustered spatial structure, individuals tend to gather together, such as in Figure 1.1(a). In contrast, in a segregated spatial structure, individuals seem to spread out as much as possible from others, as shown in Figure 1.1(b). When a strong spatial structure is present in the population, the effective density of individuals in the local neighbourhood of a reference individual will be significantly different from that without spatial structure. These effects influence the encounter rates of individuals. For example, under clustering, an individual encounters more neighbours in its close neighbourhood than in a population without spatial structure. Similarly, under spatial segregation, an individual encounters fewer neighbours than in a population without spatial structure. These differences influence the event rates and hence impact the overall population dynamics.

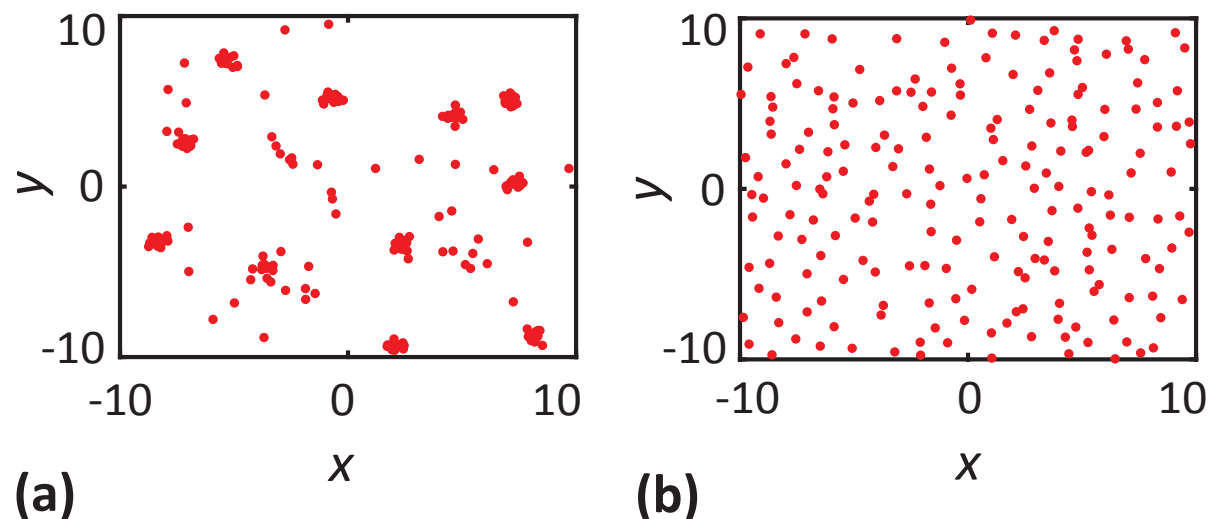


Figure 1.1: An illustration of the most common types of spatial structures. **a** cluster spatial structure. **b** segregated spatial structure.

Mathematical models are convenient tools to enhance our understanding of ecological and biological processes. They enable us to make predictions about the dynamics of the system in question and help us to underpin various mechanisms that lead to the observed dynamics. Traditional mathematical models considering the population dynamics in ecological and biological systems are based on the mean-field assumption (Murray, 1989; Edelstein-Keshet, 2005). Under the mean-field approximation, the population is assumed to be well mixed, and the interaction between the constituent individuals are considered to be proportional to the average density (Law et al., 2003). The use of mean-field approximation means that the spatial correlations between individuals' locations are neglected, and the presence of an individual at one location is independent of the presence or absence of an individual at any other location. Some of the mean-field models, such as the classical logistic growth model and the Lotka-Volterra model of predator-prey dynamics do not incorporate any spatial information. These models are written as ordinary differential equations that govern the time evolution of average density. Spatially explicit mean-field models where the density dynamics is often described using partial differential equations such as the Fisher-Kolmogorov equation are also popular

(Murray, 1989; Hillen and Painter, 2009; Johnston et al., 2015). Even though these spatially explicit models express the density of individuals as a function of spatial location, the interactions between individuals are implicitly assumed to be given by local mean-field conditions described by the average density alone.

While the use of mean-field models is ubiquitous in mathematical biology literature, these frameworks neglect spatial correlations in individual positions because they assume that individuals occupy uniformly the whole extent of the population (Young et al., 2001). Hence, the probability of finding an individual at a particular location is independent of the locations of other individuals. As a result, in a population of $N(t)$ individuals, the interactions between individuals is proportional to $N(t)(N(t) - 1) \approx N^2(t)$ and amounts to the neglect of spatial structure, such as clustering and segregation. A useful alternative is to consider the stochastic individual-based model (IBM) framework, which does not invoke any approximation on the interactions between individuals (Grimm et al., 2006; Surendran et al., 2020b). Typically, IBMs are algorithmic in nature and simulated using stochastic simulation algorithms such as the Gillespie algorithm (Gillespie, 1977). Depending upon the physical domain over which individuals interact and undergo specific events, the IBMs can be classified into two major types (Plank and Simpson, 2012). In the first type known as the lattice-based IBM, the domain is divided into discrete lattice sites. In this framework, each individual is assumed to be of constant size, which occupies one or a few lattice sites. The interactions between individuals and crowding effects are incorporated into the modelling framework by considering an exclusion process, where only a single individual occupies each lattice site (Simpson et al., 2009; Jin et al., 2018). Some of the lattice-based models allow several individuals to occupy the same lattice site (Khalil et al., 2017). The movement of individuals is restricted to a discrete set of directions corresponding to adjacent lattice sites. The restriction of cell movements only to distinct lattice sites enables the simulation of IBM to be computationally efficient, but this comes at an added cost that the model's prediction can be biologically unrealistic. In contrast, for the second type of IBM known as the lattice-free IBM, individuals' location is not restricted to distinct lattice sites (Plank and Simpson, 2013). Instead, the individuals have the freedom to move in any direction on a continuous spatial domain. This framework is more biologically realistic since the movement of cells or animals is not restricted to fixed lattice directions.

As we have shown in Figure 1.1, the number of individuals that an individual encounters in its close vicinity depends on the nature of the spatial structure present in that population. For example, the competition between individuals will be severe in Figure 1.1(a) due to many individuals being crowded together. In contrast, the competition between individuals will be lower in Figure 1.1(b), since the individuals are segregated. To model how spatial structure influences the event rates of individuals (the competition induced death rate in this case), we need to construct a method that accurately accounts for the interactions between individuals. One method to incorporate the interactions between individuals into the lattice-free IBM framework is by using an interaction kernel. To illustrate it, if we consider a population where individuals

compete with each other, the competition interaction kernel measures the competition an individual experiences from another individual in the population depending on the inter-individual distance. The interaction kernels are constructed as a decreasing function of the separation distance between individuals such that the interaction is strongest when individuals are at close proximity, and the extent of interaction decays as the distance between individuals increases. Now we define the competition interaction kernel, denoted by $\omega(|\mathbf{x}_k - \mathbf{x}_n|)$, to measure the competition a reference individual located at \mathbf{x}_n experiences from another individual at \mathbf{x}_k . We can then define the net death rate of the reference individual at \mathbf{x}_n as the overall competition experienced from all of the N individuals present in the population as,

$$D_n = \sum_{\substack{k=1 \\ k \neq n}}^N \omega(|\mathbf{x}_k - \mathbf{x}_n|). \quad (1.1)$$

A realistic choice for the functional form of the interaction kernel is Gaussian, given by,

$$\omega(|\xi|) = \gamma \exp\left(-\frac{|\xi|^2}{2\sigma^2}\right), \quad (1.2)$$

where γ and σ are the interaction strength and range, respectively. A Gaussian kernel implies that the interactions are strongest when individuals are very close and decays with the separation distance $|\xi|$. It is also possible to use other decreasing functions of the pair separation distance as the interaction kernel (Plank et al., 2020). However, we choose a Gaussian kernel in order to be consistent with the previous studies in this field (Law et al., 2003; Binny et al., 2016b). We model various types of interactions such as competition, co-operation and predation by defining an interaction kernel similar to that in Equation 1.2. In the definition of $\omega(|\xi|)$ in Equation 1.2, the parameter σ determines the range over which the interaction is significant. By controlling this parameter, we generate long-range or short-range interactions between individuals. A population with long-range interaction between individuals is analogous to a population under mean-field conditions (Binny et al. 2016b; Law et al., 2003). That means each individual interacts with every other individual as would happen in a well-mixed system. On the other hand, short-range interactions correspond to very localised interactions occurring between closely placed individuals. Note that when the dispersal rate is low, the short-range interactions generate spatial structures in the population. In chapters 2-5, we demonstrate and explore in detail the development of spatial structures from various types of short-range interactions.

We illustrate the difference between long-range (large σ) and short-range (small σ) interactions by considering a sample population where individuals compete with each other, as shown in Figure 1.2. The arrangement of individuals in Figure 1.2(a) and (c) are identical but we consider a long-range competition kernel in Figure 1.2(a)-(b) and a short-range competition kernel in Figure 1.2(c)-(d). In Figure 1.2 we compute the death rate of a test individual located at any

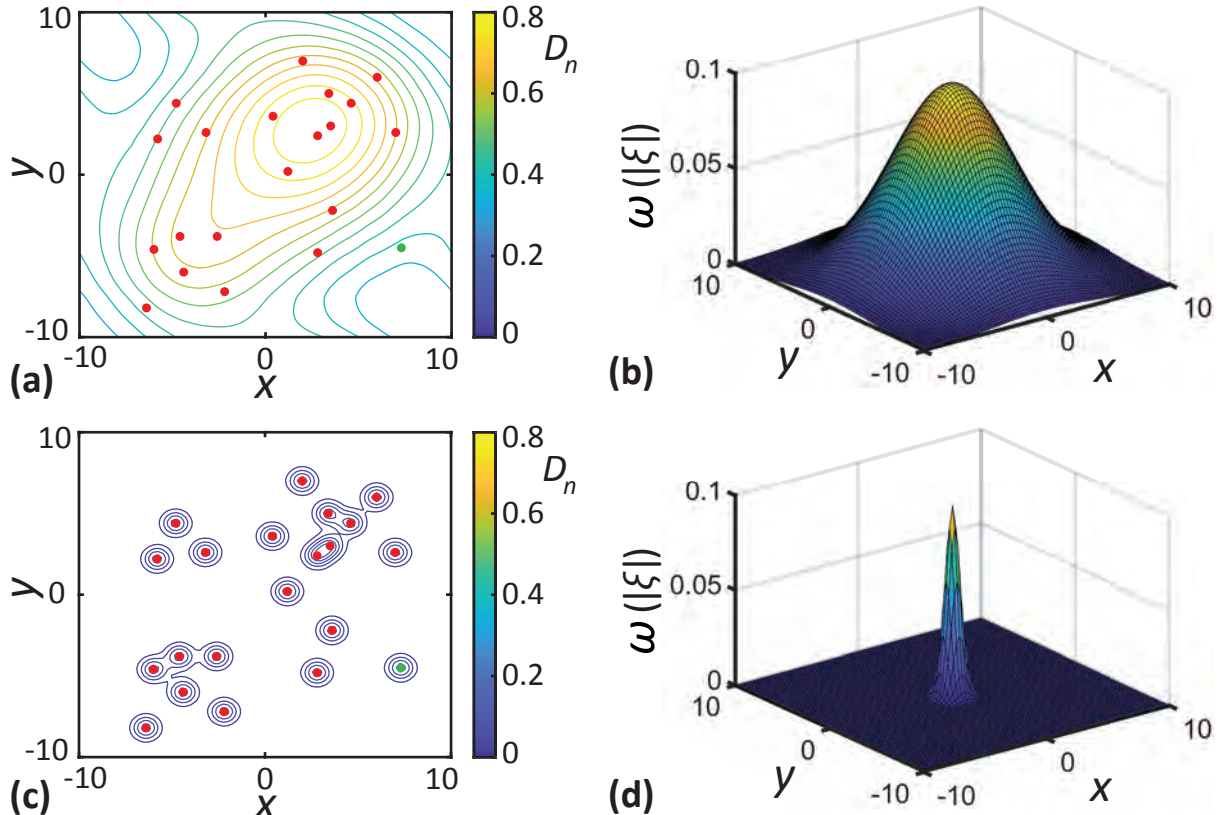


Figure 1.2: Visualising long- and short-range competition interactions. **a, c** shows locations of individuals (dots) superimposed with level curves of D_n for long- and short-range competition, respectively. **b, d** shows the long- ($\sigma = 4.0$) and short-range ($\sigma = 0.5$) competition kernels, respectively, where these kernels are centred at the origin.

location \mathbf{x} . This allow us to treat D_n as a continuous function of position. Level curves of the death rate, D_n , are superimposed in Figure 1.2(a) and (c), and we see that the differences in the length-scale of interaction lead to very different local death rates. For example, when the competition is long-range in Figure 1.2(a)-(b), the death rate for the relatively isolated green individual is non-zero. In contrast, when the competition is short-range in Figure 1.2(c)-(d), the death rate of the same individual is zero, which is very different from the previous case. Note that when the competition is short-range, only those individuals that are very closer to a focal individual contribute to the death rate. The effect of individuals that are further away is very negligible.

Defining various event rates similar to the definition in Equation 1.1 and simulating the IBM using stochastic simulation algorithms such as the Gillespie algorithm (Gillespie, 1977) will reveal the realistic population dynamics. A limitation of stochastic IBMs is that the computational cost becomes prohibitively expensive as we consider large populations. Also, the algorithmic nature of the IBM means that they provide limited mathematical insight into the population dynamics.

The continuum approximation of the IBM in terms of the dynamics of the spatial moments that track the time evolution of the density of individuals, pairs, triplets and so on is a use-

ful tool to explore the impact of spatial structure on population dynamics (Bolker and Pacala, 1997; Murrell and Law, 2000; Plank and Law, 2015). The spatial moment models provide a mathematically tractable description of the IBM, and since there is no stochastic simulation involved, the computation time is independent of the population size. Previous studies reveal that the spatial moment dynamics models provide an accurate continuum description of the IBM when populations have a complete absence of spatial structure or segregated spatial structure (Binny et al., 2015). While the moment closure approximation fails to completely replicate the population dynamics when the population is highly clustered, it provides better results than the traditional mean-field assumption (Binny et al., 2020). Initial studies that used spatial moment modelling framework were predominantly in ecology (Bolker and Pacala, 1997, 1999; Lewis and Pacala 2000; Law et al., 2003; Law et al., 2009). More recently, these ecological models have been extended to consider processes that are motivated by observations from cell biology experiments (Binny et al., 2015, 2016a, 2016b; Middleton et al., 2014; Browning et al., 2018, 2020).

The first spatial moment is defined as the average density of individuals. Note that the mean-field model deals with the time evolution of the average density of individuals, which does not hold any information on the population’s spatial configuration. Considering the second spatial moments defined as the average density of pairs of individuals helps us to explore the spatial structure of the population. The second moment is often expressed in terms of a pair correlation function $C(|\xi|, t)$ (Binder and Simpson, 2013; Ovaskainen et al., 2014). The pair-correlation function denotes the average density of pairs of individuals with separation distance $|\xi|$, at a time, t , normalised by the density of pairs in a population with the complete absence of spatial structure. Hence, for a population without any spatial structure, $C(|\xi|, t) = 1$. When $C(|\xi|, t) < 1$, there are fewer pairs of individuals with a separation distance, $|\xi|$, than in a population without any spatial structure. We refer to this spatial configuration as being segregated. When $C(|\xi|, t) > 1$, we have more pairs of individuals with a separation distance, $|\xi|$, than we would have in a population without any spatial structure and this spatial configuration is referred to as being clustered. To compute the pair-correlation from IBM, we need to calculate the distance between all N individuals. Now, binning the distances that fall into the interval, $[|\xi| - \delta|\xi|/2, |\xi| + \delta|\xi|/2]$ and normalising this bincount using a factor of $2\pi|\xi|\delta|\xi|N(t)(N(t) - 1)/L^2$ gives the $C(|\xi|, t)$. Note that the normalisation of bincount is essential to ensure that $C(|\xi|, t) = 1$ in the absence of spatial structure. An illustration of a population in the absence of spatial structure as well as with clustered and segregated spatial structure are shown in Figure 1.3(a)-(c). The corresponding pair-correlation functions are shown in Figure 1.3(d)-(f).

Constructing a dynamical equation for the time evolution of second spatial moments helps us to explore how the spatial structure of the population changes over time and whether a steady spatial pattern arises in the population at sufficiently large time. Note that the dynamics of the second moment often depend on third-order moments, which can be defined as the average

density of triplets of individuals. Higher-order moments can be defined in a similar fashion and leads to a hierarchy of equations for spatial moments. Typically, moment closure methods are used in approximating higher-order moments in terms of the lower order moments to obtain a solvable system of equations (Murrell et al., 2004; Raghbir et al., 2011).

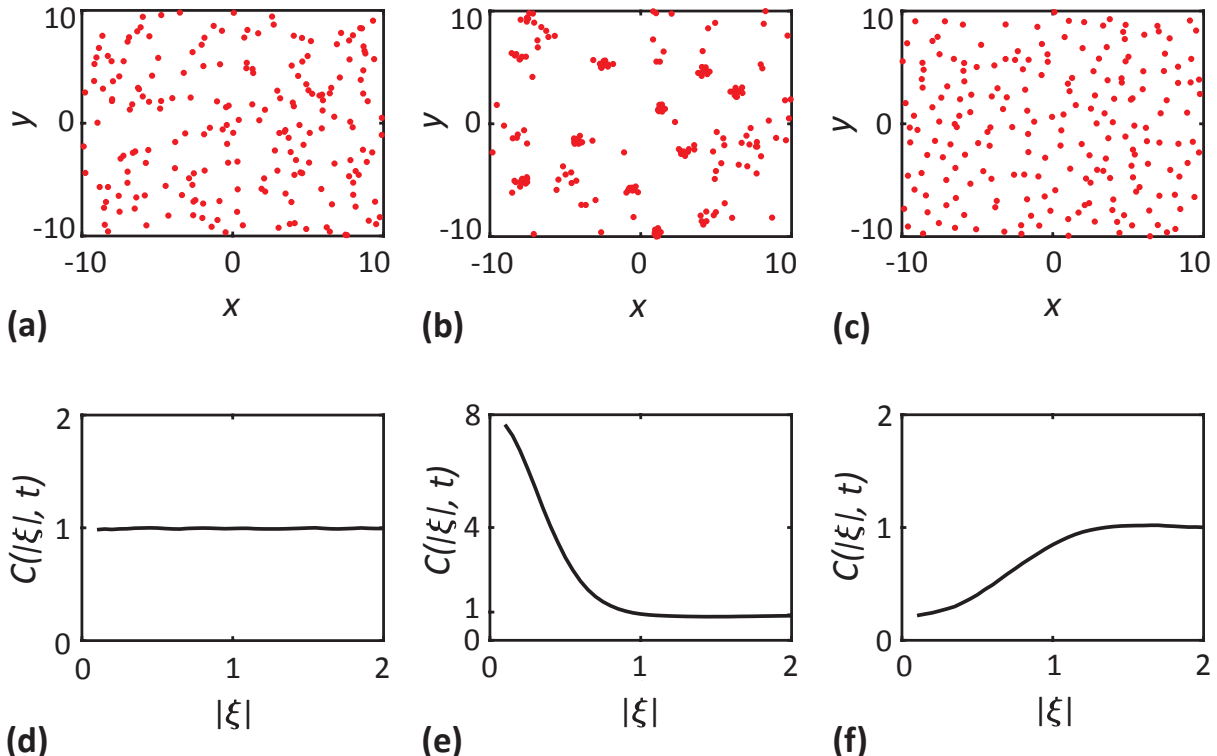


Figure 1.3: An illustration of spatial structures **a-c** and the corresponding pair-correlation functions $C(|\xi|, t)$ **d-f**. **a, d** a population in the absence of spatial structure. **b, e** cluster spatial structure. **c, f** segregated spatial pattern.

1.2 Research questions

This thesis explores and answers the following questions:

- 1. How can we develop models of birth-death-movement processes for cells in an obstacle field by incorporating the realistic effects of short-range interactions, crowding effects and spatial structure?**

A realistic scenario of cell migration and proliferation often involves an environment characterised by various biological structures, such as the extracellular matrix (ECM). The ECM, composed of macromolecules such as polysaccharides and proteins, can be thought of as biological obstacles that influence cell migration in different ways. They mediate cell migration by providing biochemical cues for the movement of cells and by physical forces such as cell-to-substrate adhesion (Harley et al., 2008; Zaman et al., 2006; Yue, 2014). These biological obstacles with varying size and adhesive properties are known to regulate the motility of cancer and immune cells (Condeelis and Segail,

2003; Bajenoff et al., 2006). Another factor relevant in this context is the crowding effects such as contact inhibition of proliferation and contact inhibition of movement, where the presence of many cells at close proximity leads to a reduction in the proliferation and movement rates (Abercrombie, 1979; Roycroft and Mayor, 2015; Warne et al., 2017).

Standard models of population dynamics based on mean-field approximation is insufficient to consider these intricate details. For instance, in a population exhibiting cluster spatial structure, the crowding effects become significant due to the presence of a greater number of cells in a close neighbourhood. Mean-field models in this context disregard the impact of short-range interactions and the spatial configuration of the population and do not account for the local density dependence in the event rates. In Chapter 2, we propose to develop an IBM and its continuum approximation in terms of the dynamics of spatial moments to describe these scenarios accurately. The construction of such a modelling framework also helps us to explore how various properties of obstacles such as density, size, and adhesive properties influence the cell population dynamics.

2. How does the directional movement of individuals arising out of chase-escape interactions generate macroscale spatial structures in a multispecies conservative community?

Chase-escape interactions between two types of individuals, namely chasers and escapees, corresponds to a scenario where chasers are biased to move towards the escapees, and the escapees are biased to move away from the chasers. These types of interactions are known to influence many biological and ecological systems. Chase-escape dynamics between two types of pigment cells, known as melanophores and xanthophores, is critical in the development of skin patterns in zebrafish (Inaba et al., 2012). Other examples include chase-escape dynamics in herding behaviour, such as in the case of dogs herding sheep (King et al., 2012; Strombom et al., 2014). These interactions result in the formation of spatial structure, such as cellular aggregation or animal clusters (Thomas et al., 2006; Wood and Ackland, 2007).

An interesting problem here is to model how the movement of individuals in response to the directional interactions they experience from other individuals leads to the development of spatial structures. To achieve this, we require a multispecies modelling framework that allows various intraspecies and interspecies interactions. To exclusively explore the role of motility and directional bias in generating the spatial structure, we need to consider conservative communities where the population size of each species remains constant. In Chapter 3 we propose to develop an IBM and spatial moment dynamics modelling framework that incorporates all of these details.

3. What impact do short-range interactions and spatial structure have on the predator-prey dynamics?

Classical models of predator-prey dynamics such as the Lotka-Volterra model are based on a mean-field approximation that ignores short-range interactions and spatial structure. In reality, short-range interactions can have a significant role in determining the population dynamics. In a realistic scenario, individual prey can experience increased mortality when close to a cluster of predators. Similarly, in a group of conspecifics, competition for shared resources can increase mortality. Hence the prediction of mean-field models about the long-time behaviour of the population can be erroneous.

To obtain accurate predator-prey population dynamics, we need to consider short-range interactions such as short-range predation, competition and dispersal of offsprings. Hence, in Chapter 4, we focus on developing an IBM that considers various short-range interactions. Comparing the simulation results of IBM with solutions of the classical mean-field model helps us to find out the scenarios where the mean-field model fails.

4. What impact do short-range interactions and spatial structure have on the Allee dynamics?

Mathematical models of population dynamics are routinely built upon the classical logistic growth assumption where a population survives and grows to finite carrying capacity for all initial densities (Murray, 1989; Kot, 2003). Allee effects describe populations that deviate from the logistic growth model, where the long-term survival of a population depends on the initial density (Taylor and Hastings, 2005; Courchamp et al., 2008). A *strong Allee effect* is associated with a net negative growth rate at low densities leading to population extinction below the Allee threshold density. In contrast, a net positive growth rate at higher densities leads to the survival of the population when the initial density is greater than the Allee threshold (Courchamp et al., 1999a). Another type of Allee effect, known as the *weak Allee effect*, describes population growth with a reduced but positive growth rate at low densities (Taylor and Hastings, 2005). Unlike the strong Allee effect, a weak Allee effect does not exhibit any threshold density due to the net positive growth rate.

Mean-field models of population dynamics neglect spatial structure that can arise through short-range interactions, such as competition and cooperation. While spatial effects are well studied for the case of logistic growth (Law et al., 2003), the influence of non mean-field effects has not been studied in the presence of an Allee effect. In Chapter 5, we focus on developing novel IBM and spatial moment dynamics framework to explore the impact of spatial structure and short-range interactions on the Allee type dynamics. Here, we focus only on the strong Allee effect since we are interested in exploring the threshold effects and how spatial structure impacts the Allee threshold.

In Chapters 2-5, which address each of these four research questions, respectively, we employ a common overall approach in modelling and analysis. We first develop stochastic and

continuum mathematical models that incorporate interactions between individuals and the spatial structure of the population. Here the specific types of interactions considered or the number of species considered are different in each chapter and depend on the particular application. The population dynamics of the system is computed by repeated simulation of the stochastic model and through numerically solving the continuum models. From these different methods, we examine the long-time behaviour of the system. We analyse the population's density dynamics by looking at the time evolution of the first spatial moment, and the information about the spatial configuration is revealed by the second moment expressed as a pair correlation function. We use these results to infer how spatial structure and interactions impact the population dynamics in each of the specific applications.

1.3 Objectives and outcomes

The primary objective of this thesis is to develop new mathematical models that incorporate short-range neighbour-dependent interactions and spatial structure of the population into the modelling framework.

The specific objectives of this thesis that addresses each of the four research questions described in Section 1.2, respectively are as follows:

1. Develop an IBM and spatial moment model of birth-death-movement processes for cells in an obstacle field by incorporating the realistic effects of neighbour-dependent interactions, crowding effects and spatial structure.
2. Extend the modelling frameworks developed in objective 1 to consider chase-escape interactions observed in ecology and cell biology processes.
3. Develop an IBM that incorporates predator-prey dynamics and compare the simulation results to the classical mean-field model's solutions to gain insight into scenarios where the mean-field approximation fails.
4. Develop a novel IBM and spatial moment model that incorporate the Allee effect and compare the results to the classical mean-field model's solutions to gain insight into how spatial structure impacts the Allee kinetics.

To achieve the four specific objectives of the thesis, we start by developing a generalized IBM and spatial moment dynamics framework that incorporates short-range interactions and the development of spatial structure from these interactions in Chapter 2. These models consider birth-death-movement processes for a multispecies population. The directional interactions between individuals are incorporated into the modelling framework. We first employ this model to study cell migration and proliferation in the presence of obstacles. In this case, we assume one subpopulation to be motile proliferative cells and other subpopulation to be stationary non-proliferative obstacles.

In Chapter 3, we consider a particular application of the models developed in Chapter 2, where we exclusively look at the importance of the movement and directional bias. In this case, we do not consider proliferation and death. These considerations are particularly interesting since many previous studies focusing on spatial moment dynamics were originally developed to study plant ecology. In those contexts, birth and death are the fundamental mechanisms that generate spatial structure in the population, and the motility is irrelevant (Bolker and Pacala, 1997; Bolker and Pacala, 1999; Murrell and Law, 2003; Law et al., 2003). The recent extensions of these frameworks to model cell biology experiments attributed simultaneous movement and proliferation as the drivers of spatial structure formation (Binny et al., 2016b; Browning et al., 2018). With the model considerations of Chapter 3 we will be able to demonstrate the development of spatial structure in conservative communities solely arising due to the directional movement.

In Chapter 4, we extend the model developed in Chapter 2, to consider the ecologically relevant predator-prey interactions. Here we extend the modelling framework by considering the effect of predation interactions on individuals' event rates.

In Chapter 5, we extend the model developed in Chapter 2, to consider the strong Allee effect. To accommodate the Allee effect into the modelling framework, we have to make substantial changes to the way we defined event rates in Chapters 2-4. We see that incorporating the Allee effect into the modelling framework requires a non-linear dependency of density on the event rates, which is different from all three previous cases. To reflect these differences, we derive a novel IBM and spatial moment dynamics framework in Chapter 5.

This thesis is presented by publication and incorporates four publications in peer reviewed journals. Three of these publications are published in Q1 journals (*Bulletin of Mathematical Biology*, *Scientific Reports* and *Theoretical Ecology*). The final paper is submitted to another Q1 journal (*Proceedings of the Royal Society A: Mathematical, Physical and Engineering Sciences*) and is currently under review. The PhD candidate is the first author and contributed significantly to all four publications. The work presented in this thesis fulfils Queensland University of Technology criteria for the thesis by publication.

This thesis incorporates the following publications:

1. **Surendran Anudeep**, Plank Michael J., Simpson Matthew J. 2018 Spatial moment description of birth-death-movement processes incorporating the effects of crowding and obstacles. *Bulletin of Mathematical Biology* 80: 2828–2855. DOI:[10.1007/s11538-018-0488-1](https://doi.org/10.1007/s11538-018-0488-1). [bioRxiv Preprint](https://www.biorxiv.com/content/early/2018/08/24/263881).

Abstract Birth-death-movement processes, modulated by interactions between individuals, are fundamental to many cell biology processes. A key feature of the movement of cells within *in vivo* environments are the interactions between motile cells and stationary obstacles. Here we propose a multi-species model of individual-level motility, proliferation and death. This model is a spatial birth-death-movement stochastic process,

a class of individual-based model (IBM) that is amenable to mathematical analysis. We present the IBM in a general multi-species framework, and then focus on the case of a population of motile, proliferative agents in an environment populated by stationary, non-proliferative obstacles. To analyse the IBM, we derive a system of spatial moment equations governing the evolution of the density of agents and the density of pairs of agents. This approach avoids making the usual mean-field assumption so that our models can be used to study the formation of spatial structure, such as clustering and aggregation, and to understand how spatial structure influences population-level outcomes. Overall the spatial moment model provides a reasonably accurate prediction of the system dynamics, including important effects such as how varying the properties of the obstacles leads to different spatial patterns in the population of agents.

2. **Surendran Anudeep**, Plank Michael J., Simpson Matthew J. 2019 Spatial structure arising from chase-escape interactions with crowding. *Scientific Reports* 9: 14988. DOI:[10.1038/s41598-019-51565-3](https://doi.org/10.1038/s41598-019-51565-3). bioRxiv Preprint.

Abstract Movement of individuals, mediated by localised interactions, plays a key role in numerous processes including cell biology and ecology. In this work, we investigate an individual-based model accounting for various intraspecies and interspecies interactions in a community consisting of two distinct species. In this framework we consider one species to be *chasers* and the other species to be *escapees*, and we focus on chase-escape dynamics where the chasers are biased to move towards the escapees, and the escapees are biased to move away from the chasers. This framework allows us to explore how individual-level directional interactions scale up to influence spatial structure at the macroscale. To focus exclusively on the role of motility and directional bias in determining spatial structure, we consider conservative communities where the number of individuals in each species remains constant. To provide additional information about the individual-based model, we also present a mathematically tractable deterministic approximation based on describing the evolution of the spatial moments. We explore how different features of interactions including interaction strength, spatial extent of interaction, and relative density of species influence the formation of the macroscale spatial patterns.

3. **Surendran Anudeep**, Plank Michael J., Simpson Matthew J. 2020 Small-scale spatial structure affects predator-prey dynamics and coexistence. *Theoretical Ecology* 13: 537–550. DOI:[10.1007/s12080-020-00467-6](https://doi.org/10.1007/s12080-020-00467-6). bioRxiv Preprint.

Abstract Small-scale spatial variability can affect community dynamics in many ecological and biological processes, such as predator-prey dynamics and immune responses. Spatial variability includes short-range neighbour-dependent interactions and small-scale spatial structure, such as *clustering* where individuals aggregate together, and *segregation*

where individuals are spaced apart from one another. Yet, a large class of mathematical models aimed at representing these processes ignores these factors by making a classical mean-field approximation, where interactions between individuals are assumed to occur in proportion to their average density. Such mean-field approximations amount to ignoring spatial structure. In this work, we consider an individual based model of a two-species community that is composed of *consumers* and *resources*. The model describes migration, predation, competition and dispersal of offspring, and explicitly gives rise to varying degrees of spatial structure. We compare simulation results from the individual based model with the solution of a classical mean-field approximation, and this comparison provides insight into how spatial structure can drive the system away from mean-field dynamics. Our analysis reveals that mechanisms leading to intraspecific clustering and interspecific segregation, such as short-range predation and short-range dispersal, tend to increase the size of the resource species relative to the mean-field prediction. We show that under certain parameter regimes these mechanisms lead to the extinction of consumers whereas the classical mean-field model predicts the coexistence of both species.

4. **Surendran Anudeep**, Plank Michael J., Simpson Matthew J. 2020 Population dynamics with spatial structure and an Allee effect. *Proceedings of the Royal Society A: Mathematical, Physical and Engineering Sciences* 476: 20200501. DOI:[10.1098/rspa.2020.0501](https://doi.org/10.1098/rspa.2020.0501). bioRxiv Preprint.

Abstract Allee effects describe populations in which the long-term survival of individuals depends on the population density. A simple mathematical model of an Allee effect is one where initial densities below the threshold lead to extinction, whereas initial densities above the threshold lead to survival. Mean field models of population dynamics neglect spatial structure that can arise through short-range interactions, such as competition and dispersal. The influence of non mean-field effects has not been studied in the presence of an Allee effect. To address this we develop an individual-based model that incorporates short-range interactions and an Allee effect. To explore the role of spatial structure we derive a mathematically tractable continuum approximation of the IBM in terms of the dynamics of spatial moments. In the limit of long-range interactions where the mean-field approximation holds, our modelling framework recovers the mean-field Allee threshold. We show that the Allee threshold is sensitive to spatial structure neglected by mean-field models. For example, there are cases where the mean-field model predicts extinction but the population actually survives. Through simulations we show that our new spatial moment dynamics model accurately captures the modified Allee threshold in the presence of spatial structure.

1.4 Structure of the thesis

Since the thesis is presented as a thesis by published papers, each of the main chapters (Chapters 2, 3, 4 and 5) are comprised of the publications mentioned in Section 1.3, respectively. Each of the main chapters contains an introduction section that describes our problem of interest, relevant background information and literature review. Since all these chapters are independent publications, there is a slight overlap in the background information of these different chapters. Each of these chapters also includes mathematical methods sections describing the discrete and continuum modelling frameworks developed in the thesis and results and discussion section demonstrating our findings and a discussion on the results. We also provide a conclusion section that summarises our research findings and proposes future avenues for the extension of the study in all of these chapters. The Chapters 2A, 3A and 5A correspond to the supplementary materials associated with the respective publications. These chapters present additional results, definitions and derivations that are not included in the main publications.

Chapter 1 constitute the introduction for the thesis. This chapter introduces the relevant background information from ecology and cell biology, where short-range interactions and spatial structure play a significant role in population dynamics. Also, the chapter provides an overview of mathematical modelling techniques relevant to the study of these systems. The major research questions of the thesis and the objectives and outcomes of the thesis are then stated. The details about the contribution of the candidate and all co-authors to each of the publication are described in Section 1.5.

Chapter 2 addresses objective 1 of the thesis described in Section 1.3. Chapter 2 contains publication 1, where we construct models of birth-death-movement processes for cells in an obstacle field. The key features of cell migration and proliferation in realistic situations, such as the interactions between motile cells and stationary obstacles, crowding effects and spatial structure, are considered while developing the modelling framework. Using the models, we explore important effects such as how varying the properties of the obstacles lead to different spatial patterns in the population and how it influences the population dynamics. Additional information, such as more detailed derivations and definitions associated with publication 1, are described in Chapter 2A.

Chapter 3 addresses objective 2 of the thesis described in Section 1.3. Chapter 3 contains publication 2, where we study how the directional movement of individuals arising out of chase-escape interactions generate macroscale spatial structures. Here, we develop an IBM and a spatial moment dynamics model for the two-species community of *chasers* and *escapees*, by carefully considering various interspecies and intraspecies interactions between them. To focus exclusively on the role of motility and directional bias in determining spatial structure, we consider conservative communities where the number of individuals in each species remains constant. We explore how different features of interactions, including interaction strength, the spatial extent of interaction, and relative density of species influence the formation of the

macroscale spatial patterns. Additional results associated with publication 2, are presented in Chapter 3A.

Chapter 4 addresses objective 3 of the thesis described in Section 1.3. Chapter 4 contains publication 3, where we study the impact of short-range interactions and spatial structure on predator-prey dynamics. We develop an IBM that consider a two-species community of *consumers* and *resources*, where consumers predate on resources. Short-range predation, competition and dispersal of offspring are incorporated into the IBM framework. We compare the simulation results from the IBM with the solution of a classical mean-field approximation, where interactions between individuals are assumed to occur in proportion to the average density and ignore the population's spatial structure. This comparison provides insight into how spatial structure can drive the system away from mean-field dynamics.

Chapter 5 addresses objective 4 of the thesis described in Section 1.3. Chapter 5 contains publication 4, where we study the impact of short-range interactions and spatial structure on the Allee dynamics. We develop models that incorporate short-range interactions and an Allee effect, where survival of the population is only possible if the density is above some threshold level. We investigate how sensitive the Allee threshold is to the spatial structure of the population. A comparison of IBM, spatial moment model, and mean-field model is conducted to gain insight on the effect of spatial structure. Additional results associated with publication 4, are presented in Chapter 5A.

Chapter 6 outline a summary of the research findings from this thesis, and proposes further avenues for future research.

1.5 Statement of joint authorship

In this section we summarize the contributions of the PhD candidate and the co-authors to each publication. All co-authors have agreed to the presentation of these publications in this thesis.

1.5.1 Chapter 2: Spatial moment description of birth-death-movement processes incorporating the effects of crowding and obstacles

The associated publication for this chapter is:

Surendran Anudeep, Plank Michael J., Simpson Matthew J. 2018 Spatial moment description of birth-death-movement processes incorporating the effects of crowding and obstacles. *Bulletin of Mathematical Biology* 80: 2828–2855. DOI:[10.1007/s11538-018-0488-1](https://doi.org/10.1007/s11538-018-0488-1). bioRxiv Preprint.

- **Surendran Anudeep (Candidate)** designed the study, derived the continuum moment dynamics equations, developed the codes for numerical simulation of the IBM and spatial moment model, performed numerical simulations, generated results, interpreted the

results, drafted the manuscript, and revised the manuscript during peer-review process.

- Plank Michael J. designed the study, interpreted the results, edited the manuscript during initial submission and subsequent revision during peer-review process.
- Simpson Matthew J. designed the study, supervised the research, interpreted the results, edited the manuscript during initial submission and subsequent revision during peer-review process and acted as the corresponding author.

1.5.2 Chapter 3: Spatial structure arising from chase-escape interactions with crowding

The associated publication for this chapter is:

Surendran Anudeep, Plank Michael J., Simpson Matthew J. 2019 Spatial structure arising from chase-escape interactions with crowding. *Scientific Reports* 9: 14988. [DOI:10.1038/s41598-019-51565-3](https://doi.org/10.1038/s41598-019-51565-3). [bioRxiv Preprint](https://www.biorxiv.com/content/515653.full.pdf).

- **Surendran Anudeep (Candidate)** designed the study, derived the continuum moment dynamics equations, developed the codes for numerical simulation of the IBM and spatial moment model, performed numerical simulations, generated results, interpreted the results, drafted the manuscript, and revised the manuscript during the peer-review process.
- Plank Michael J. designed the study, interpreted the results, edited the manuscript during the initial submission and subsequent revision during the peer-review process.
- Simpson Matthew J. designed the study, supervised the research, interpreted the results, edited the manuscript during the initial submission and subsequent revision during the peer-review process and acted as the corresponding author.

1.5.3 Chapter 4: Small-scale spatial structure affects predator-prey dynamics and coexistence

The associated publication for this chapter is:

Surendran Anudeep, Plank Michael J., Simpson Matthew J. 2020 Small-scale spatial structure affects predator-prey dynamics and coexistence. *Theoretical Ecology* 13: 537–550. [DOI:10.1007/s12080-020-00467-6](https://doi.org/10.1007/s12080-020-00467-6). [bioRxiv Preprint](https://www.biorxiv.com/content/515653.full.pdf).

- **Surendran Anudeep (Candidate)** designed the study, developed the codes for numerical simulation of the IBM, performed numerical simulations, generated results, interpreted the results, drafted the manuscript, and revised the manuscript during the peer-review process.

- Plank Michael J. designed the study, interpreted the results, edited the manuscript during initial submission and subsequent revision during the peer-review process.
- Simpson Matthew J. designed the study, supervised the research, interpreted the results, edited the manuscript during the initial submission and subsequent revision during the peer-review process and acted as the corresponding author.

1.5.4 Chapter 5: Population dynamics with spatial structure and an Allee effect

The associated publication for this chapter is:

Surendran Anudeep, Plank Michael J., Simpson Matthew J. 2020 Population dynamics with spatial structure and an Allee effect. *Proceedings of the Royal Society A: Mathematical, Physical and Engineering Sciences* 476: 20200501. DOI:[10.1098/rspa.2020.0501](https://doi.org/10.1098/rspa.2020.0501). bioRxiv Preprint.

- **Surendran Anudeep (Candidate)** designed the study, derived the continuum moment dynamics equations, developed the codes for numerical simulation of the IBM and spatial moment model, performed numerical simulations, generated results, interpreted the results, drafted the manuscript, and revised the manuscript during the peer-review process.
- Plank Michael J. designed the study, interpreted the results, edited the manuscript during the initial submission and subsequent revision during the peer-review process.
- Simpson Matthew J. designed the study, supervised the research, interpreted the results, edited the manuscript during the initial submission and subsequent revision during the peer-review process and acted as the corresponding author.

Statement of Contribution of Co-Authors for Thesis by Published Paper

The authors listed below have certified that:

1. they meet the criteria for authorship and that they have participated in the conception, execution, or interpretation, of at least that part of the publication in their field of expertise;
2. they take public responsibility for their part of the publication, except for the responsible author who accepts overall responsibility for the publication;
3. there are no other authors of the publication according to these criteria;
4. potential conflicts of interest have been disclosed to (a) granting bodies, (b) the editor or publisher of journals or other publications, and (c) the head of the responsible academic unit, and
5. they agree to the use of the publication in the student's thesis and its publication on the [QUT's ePrints site](#) consistent with any limitations set by publisher requirements.

In the case of chapter 2:

Surendran Anudeep, Plank Michael J., Simpson Matthew J. 2018 Spatial moment description of birth-death-movement processes incorporating the effects of crowding and obstacles. Bulletin of Mathematical Biology 80: 2828–2855.

Contributor	Statement of contribution*
Anudeep Surendran	Designed the study, derived the continuum moment dynamics equations, developed the codes for numerical simulation of the IBM and spatial moment model, performed numerical simulations, generated results, interpreted the results, drafted the manuscript, and revised the manuscript during peer-review process.
19/08/2020	
Michael J. Plank	Designed the study, interpreted the results, edited the manuscript during initial submission and subsequent revision during peer-review process.
Matthew J. Simpson	Designed the study, supervised the research, interpreted the results, edited the manuscript during initial submission and subsequent revision during peer review process and acted as the corresponding author.

Principal Supervisor Confirmation

I have sighted email or other correspondence from all Co-authors confirming their certifying authorship.
(If the Co-authors are not able to sign the form please forward their email or other correspondence confirming the certifying authorship to the GRC).

MATTHEW SIMPSON
Name


Signature

26/8/2020
Date

Chapter 2

Spatial moment description of birth-death-movement processes incorporating the effects of crowding and obstacles

2.1 Preamble

This chapter is a paper published in the *Bulletin of Mathematical Biology*.

Surendran Anudeep, Plank Michael J., Simpson Matthew J. 2018 Spatial moment description of birth-death-movement processes incorporating the effects of crowding and obstacles. *Bulletin of Mathematical Biology* 80: 2828–2855. DOI:[10.1007/s11538-018-0488-1](https://doi.org/10.1007/s11538-018-0488-1). bioRxiv Preprint.

In this chapter, we address the research question 1 of the thesis: How can we develop models of birth-death-movement processes for cells in an obstacle field by incorporating the realistic effects of short-range interactions, crowding effects and spatial structure? We start by describing the construction of our IBM and spatial moment dynamics modelling frameworks. These fairly general models consider birth-death-movement processes in a multispecies population. Short-range interactions between individuals and spatial structure development from these interactions are incorporated. We then use our models to study cell biology motivated research question about cell migration and proliferation in the presence of obstacles. In this case, we assume one subpopulation to be motile proliferative cells and other subpopulation to be stationary non-proliferative obstacles. Note that the models constructed here act as reference models for further applications in the subsequent chapters, where extensions are made by incorporating additional interaction mechanisms and features.

2.2 Abstract

Birth-death-movement processes, modulated by interactions between individuals, are fundamental to many cell biology processes. A key feature of the movement of cells within *in vivo* environments are the interactions between motile cells and stationary obstacles. Here we propose a multi-species model of individual-level motility, proliferation and death. This model is a spatial birth-death-movement stochastic process, a class of individual-based model (IBM) that is amenable to mathematical analysis. We present the IBM in a general multi-species framework, and then focus on the case of a population of motile, proliferative agents in an environment populated by stationary, non-proliferative obstacles. To analyse the IBM, we derive a system of spatial moment equations governing the evolution of the density of agents and the density of pairs of agents. This approach extends the usual mean-field assumption so that our models can be used to study the formation of spatial structure, such as clustering and aggregation, and to understand how spatial structure influences population-level outcomes. Overall the spatial moment model provides a reasonably accurate prediction of the system dynamics, including important effects such as how varying the properties of the obstacles leads to different spatial patterns in the population of agents.

2.3 Introduction

Movement, birth and death processes are important individual-level mechanisms that can influence population-level outcomes in both biological and ecological systems. Cell migration and cell proliferation, modulated by interactions among neighbouring cells and obstacles, are essential for development (Kurosaka and Kashina, 2008), repair (Martin, 1997) and disease (Friedl and Wolf, 2003). Similarly, in many ecological systems, the movement of individuals, and interactions between individuals, can have important population-level consequences. The emergence of spatial structure in predator-prey systems and plant communities are direct results of interactions between individuals (Tobin and Bjornstad, 2003; Law and Dieckmann, 2000). These common observations from different areas of the life sciences suggest a role for individual-level, mathematical models to represent molecules, cells, plants and animals. Popular modelling frameworks include lattice-based models and continuous space lattice free models (Plank and Simpson, 2012; Dyson and Baker, 2015). Some of these models consider single species populations (Lewis, 2000; Middleton et al., 2014), while others incorporate the influence of interactions among different subpopulations (Jin et al., 2018; Murrell, 2005; Smith et al., 2017).

Cell migration in living tissues involves complicated heterogeneous environments that are occupied by various biological structures and scaffolds of varying size, shape and adhesive properties (Ellery et al., 2014; Ellery et al., 2016). Such obstacles can have a significant impact on the migration of cells due to the interplay between crowding and cell-to-substrate adhesion

(Welch, 2015; Sun and Zaman, 2017; Simpson and Plank, 2017). The extracellular matrix (ECM), composed of polysaccharides and proteins, is an example of a biological obstacle which influences the cell migration in many different ways, such as providing biochemical stimuli, mechanical cues and steric hindrances (Zaman et al., 2006; Harley et al., 2008). ECM geometry can regulate the motility of cancer (Condeelis and Segall, 2003) and immune cells (Bajenoff et al., 2006). The highly compartmentalised structure of the cytoplasm and the presence of macromolecular obstacles such as nucleic acids and proteins within intracellular environments can have a significant impact on biochemical reactions (Tan et al., 2013; Hansen et al., 2016) and physical transport processes inside the cell (Ghosh et al., 2016; Smith et al., 2017). These examples from various biological organisational levels suggest that the incorporation of both obstacles and their crowding effects in a mathematical model of cell migration is important.

Standard models of biological and ecological systems are based on the mean field assumption which, roughly speaking, assumes that individuals in the population encounter each other in proportion to their average density (Law and Dieckmann, 2000). Classical examples of mean field models include Lotka-Volterra models of ecological competition (Murray 1989), the Keller-Segel model of chemotaxis (Keller and Segel, 1971), the logistic growth model to describe population dynamics (Edelstein-Keshet, 2005) and the Fisher-Kolmogorov model to describe wound healing (Johnston et al., 2015). Standard mathematical models based on ordinary and partial differential equations routinely invoke the mean field assumption. In this work we take a more general approach by accounting for spatial correlations by developing continuous descriptions of the dynamics of individuals, dynamics of pairs of individuals, and so on (Plank and Law, 2015). In general this approach leads to an infinite hierarchy of equations governing the spatial moments of the system which we approximate using a moment closure assumption (Murrell et al., 2004; Raghbir et al., 2011).

The first studies that used spatial moments focused on modelling birth-death processes in ecology with a single species (Bolker and Pacala, 1997; Lewis, 2000), and later studies examined competition and prey-predator interactions in a multi-species birth-death framework (Murrell, 2005; Barraquand and Murrell, 2013). More recently these ecological models have been extended to include movement processes that are motivated by observations from cell biology experiments (Baker and Simpson, 2010; Simpson et al., 2013b). However, these first models that include movement are lattice-based, which means that the movement of individuals is restricted to an artificial lattice. Lattice-free moment dynamics models of cell migration and cell proliferation are much more recent (Middleton et al., 2014; Binny et al., 2015, 2016a, 2016b). Unlike the lattice-based models in which volume exclusion is strictly enforced, lattice-free models use interaction kernels to give a more realistic description of interactions because cells are able to deform as they move close to neighbouring cells (Le Clainche and Carlier, 2008). In this work we present a lattice-free model of cell migration, cell proliferation and cell death. In an attempt to make the model relevant to *in vivo* conditions, we take a multi-species approach so that we can consider one species to be a population of motile and proliferative

cells, whereas the other population represents an immobile subpopulation of obstacles.

2.4 Individual-based model

A key feature of the individual-based model (IBM) is that we consider the total population to be composed of several different subpopulations. This gives great flexibility since the model can be used to study the movement, proliferation and death of different types of individuals, and it also allows for different types of interactions between the different subpopulations. The state of the IBM depends on the position of each individual, and the properties of agents within each subpopulation. In the model, we have a total of $N(t)$ agents that are associated with I subpopulations. The location of the n^{th} agent is $\mathbf{x}_n \in \mathbb{R}^2$, and each agent belongs to a particular subpopulation, $i_n \in \{1, 2, \dots, I\}$, where $n = 1, 2, \dots, N(t)$. We always initiate the IBM with individuals distributed according to a spatial Poisson process, meaning that the IBM is relevant to spatially homogeneous problems without macroscopic gradients in density of individuals (Jin et al., 2018).

Individuals undergo movement, proliferation and death events with a rate per unit time given by \widehat{M}_n , \widehat{P}_n and \widehat{D}_n respectively. The IBM is a continuous-time Markov process, where the probability of agent n undergoing a movement during a short time interval, of duration δt , is $\widehat{M}_n \delta t + O(\delta t^2)$. Similar expressions govern the probability of proliferation and death events occurring within a short time interval. The total event rates are comprised of a neighbour independent, intrinsic component, and a neighbour-dependent component accounting for interactions with neighbouring individuals. The neighbourhood contribution is specified by an interaction kernel that depends upon the distance, $|\xi|$, between pairs of individuals. We assume the interaction kernel is isotropic and decays to zero at larger distances, $|\xi|$, ensuring that only relatively close individuals interact. For movement events, the intrinsic component of the movement rate of an individual from subpopulation i is denoted by m_i , and the interactions from a neighbouring agent from subpopulation j is governed by an interaction kernel $\omega_{ij}^{(m)}(|\xi|)$. Hence we write the net movement rate of individual n as,

$$\widehat{M}_n = \max \left(0, m_{i_n} + \sum_{r \neq n} \omega_{i_n j_r}^{(m)}(|\mathbf{x}_r - \mathbf{x}_n|) \right). \quad (2.1)$$

Here, $i_n = 1$ if individual n is from the first subpopulation, and $i_n = 2$ if individual n is from the second subpopulation, and so on. Similarly, we write the net proliferation and net death rates as,

$$\widehat{P}_n = \max \left(0, p_{i_n} + \sum_{r \neq n} \omega_{i_n j_r}^{(p)}(|\mathbf{x}_r - \mathbf{x}_n|) \right), \quad (2.2)$$

$$\widehat{D}_n = \max \left(0, d_{i_n} + \sum_{r \neq n} \omega_{i_n j_r}^{(d)}(|\mathbf{x}_r - \mathbf{x}_n|) \right), \quad (2.3)$$

where p_i and d_i are the intrinsic proliferation and death rates, respectively, for an individual from subpopulation i . For simplicity, we assume a constant death rate and a fixed distribution for the direction of placement of daughter agents which is unaffected by the interactions with other individuals.

When an individual from subpopulation i undergoes a movement event, it travels a displacement ξ that is drawn from a probability density function (PDF) $\mu_i^{(m)}(\xi)$. If an individual from subpopulation i proliferates, a daughter of the same subpopulation is placed at a displacement ξ , that is drawn from a PDF $\mu_i^{(p)}(\xi)$. We refer to the placement of daughter agents as a result of a successful proliferation event as agent *dispersal*. Now we generalise the movement displacement PDF by introducing a neighbour-dependent bias vector, to accommodate the influence of neighbouring individuals upon the direction of movement. We introduce an interaction kernel, $\omega_{ij}^{(b)}(|\xi|)$, to account for neighbour-dependent directional bias acting on the reference individual, from subpopulation i , due to the presence of a second individual, from subpopulation j , at a displacement ξ . The neighbour-dependent bias is defined as the gradient of the interaction kernel, $\nabla \omega_{ij}^{(b)}(|\xi|)$. This definition is same as that of Binny et al. (2016b), however here we generalise that previous model to account for the contributions to the directional bias arising from multiple subpopulations. The net bias vector is the sum of contributions from each of the neighbouring individuals, and a constant neighbour-independent global bias $\mathbf{b}_{i_n} \in \mathbb{R}^2$, giving

$$\widehat{\mathbf{B}}_n = \mathbf{b}_{i_n} + \sum_{r \neq n} \nabla \omega_{i_n j_r}^{(b)}(|\mathbf{x}_r - \mathbf{x}_n|). \quad (2.4)$$

The angular direction of the net bias vector, denoted by $\arg(\widehat{\mathbf{B}}_n) \in [0, 2\pi]$, is the preferred direction of movement for a particular individual. In this framework, the preferred direction of movement is driven, in part, by the sum of the gradient of the interaction kernels. The strength of bias is given by the magnitude of bias vector, $|\widehat{\mathbf{B}}_n|$. Now we assume that the neighbouring individuals affect the direction of movement $\arg(\xi) \in [0, 2\pi]$, but not the actual distance moved, $|\xi|$.

During a movement event, the direction of movement is drawn from a von Mises distribution, $g(\theta; \widehat{\mathbf{B}}_n)$ whose concentration parameter is $|\widehat{\mathbf{B}}_n|$, and the mean direction is given by $\arg(\widehat{\mathbf{B}}_n)$,

$$g(\theta; \widehat{\mathbf{B}}_n) = \frac{\exp(|\widehat{\mathbf{B}}_n| \cos(\theta - \arg(\widehat{\mathbf{B}}_n)))}{2\pi I_0(|\widehat{\mathbf{B}}_n|)}, \quad (2.5)$$

where I_0 is the zero order modified Bessel function. This PDF ensures that individuals are most likely move in the direction of $\arg(\widehat{\mathbf{B}}_n)$, and the bias to move in this preferred direction increases with $|\widehat{\mathbf{B}}_n|$. When the net bias is zero, $\widehat{\mathbf{B}}_n = \mathbf{0}$, the von Mises distribution reduces to the uniform distribution (Binny et al., 2016b). Individuals located where the gradient is steep will have a large $|\widehat{\mathbf{B}}_n|$, and are more likely to move in the direction of $\widehat{\mathbf{B}}_n$. Individuals located where the gradient is relatively flat will have a weaker bias and the direction of movement becomes

almost uniformly distributed (Browning et al., 2017). We assume that the distance moved by an agent is independent of local crowding, and is given by a fixed PDF, $u_i(|\xi|)$. Hence the net movement displacement PDF is the product of the distance PDF and the direction PDF, giving

$$\mu_i^{(m)}(\xi; \widehat{\mathbf{B}}_n) = \frac{u_i(|\xi|) g(\arg(\xi); \widehat{\mathbf{B}}_n)}{|\xi|}. \quad (2.6)$$

2.4.1 IBM for motile, proliferative agents and stationary obstacles

The IBM can be applied to numerous problems involving populations composed of various combinations of motile and stationary subpopulations by appropriate choice of parameters. Here we focus on an important scenario with two distinct subpopulations, $I = 2$. We consider the first subpopulation, $i = 1$, to be a group of agents undergoing movement, proliferation and death events. This first subpopulation can be thought of as a population of motile, proliferative cells. The first subpopulation interacts with a second subpopulation, $i = 2$, that is composed of stationary, non-proliferating obstacles. The event rates for individual agents in the first subpopulation will be influenced by the presence of both obstacles and other agents in their neighbourhood, given by Equations (2.1)-(2.3). Since the obstacles never undergo birth, death or movement events, they contribute to the overall dynamics by interactions between the obstacles and the agents.

We introduce interaction kernels: $\omega_{ij}^{(m)}(|\xi|)$; $\omega_{ij}^{(p)}(|\xi|)$; and $\omega_{ij}^{(b)}(|\xi|)$, to account for the contribution from surrounding agents and obstacles to the movement rate, proliferation rate, and the directional bias of an agent, respectively. We choose these interaction kernels to be two-dimensional Gaussian functions. The movement interaction kernel is given by,

$$\omega_{ij}^{(m)}(|\xi|) = \gamma_{ij}^{(m)} \exp\left(-\frac{|\xi|^2}{2(\sigma_{ij}^{(m)})^2}\right), \quad (2.7)$$

where $\gamma_{ij}^{(m)}$ and $\sigma_{ij}^{(m)} > 0$ represent the interaction strength and the spatial extent of interaction, respectively. We assume a similar form for the proliferation and bias kernels, given by,

$$\omega_{ij}^{(p)}(|\xi|) = \gamma_{ij}^{(p)} \exp\left(-\frac{|\xi|^2}{2(\sigma_{ij}^{(p)})^2}\right), \quad (2.8)$$

$$\omega_{ij}^{(b)}(|\xi|) = \gamma_{ij}^{(b)} \exp\left(-\frac{|\xi|^2}{2(\sigma_{ij}^{(b)})^2}\right). \quad (2.9)$$

In our simulations we have two subpopulations. The first subpopulation, denoted $i = 1$, corresponds to the motile and proliferative agents. The second subpopulation, denoted $i = 2$, corresponds to the stationary, non-proliferative obstacles. The intrinsic rates of movement and proliferation of agents are m_1 and p_1 , respectively. These rates for obstacles are zero. The pres-

ence of subpopulations of agents and obstacles results in different types of interactions. The interactions involving the pairs of individuals of same type such as, agent-agent and obstacle-obstacle pairs, are specified by $\omega_{11}^{(m)}(|\xi|)$ and $\omega_{22}^{(m)}(|\xi|)$, respectively. Similar kernels apply for proliferation and bias. Interactions involving individuals from different subpopulations are specified by the interaction kernels $\omega_{12}^{(m)}(|\xi|)$ and $\omega_{21}^{(m)}(|\xi|)$. Since obstacles are both stationary and non-proliferative, the presence of neighbouring agents and obstacle do not affect the dynamics and spatial arrangement of obstacles in any way. Hence the interaction strengths $\gamma_{21}^{(m)}$ and $\gamma_{22}^{(m)}$ are both set to zero. Positive $\gamma_{11}^{(m)}$ and $\gamma_{12}^{(m)}$ values enhance the movement rate of agents, and can be thought of as representing contact stimulation of migration (Barbaric et al., 2014; Binny et al., 2015). In contrast, a negative interaction strength results in a reduction of the movement rate, which can be thought of as representing contact inhibition of migration (Abercrombie, 1979; Cai et al., 2007). Similarly, the net proliferation rate of agents, and the nature of directional bias depend on the sign of interaction strength (Green et al., 2010; Kim et al., 2011; Kay et al., 2012; Binny et al., 2016a, 2016b).

We use a univariate Gaussian distribution, with mean $\mu_1^{(s)}$ and standard deviation $\sigma_1^{(s)}$, to specify the distribution of movement distance for agents $u_1(|\xi|)$. The PDFs of movement displacement, $\mu_1^{(m)}(\xi, t)$ and $\mu_2^{(m)}(\xi, t)$, also require the specification of the movement distance distribution, $u_1(|\xi|)$, and the neighbour-dependent direction probability density function given by Equation (2.5). For simplicity, the PDF for the dispersal of daughter agents arising from proliferation events, $\mu_1^{(p)}(\xi)$, is chosen to be neighbour independent, and specified as a bivariate Gaussian distribution with zero mean and standard deviation $\sigma_1^{(d)}$.

2.4.2 Numerical implementation

We simulate the IBM using the Gillespie algorithm (Gillespie, 1977) implemented in FORTRAN. In each simulation the population is initially composed of $N_1(0)$ agents and $N_2(0)$ obstacles, distributed according to a spatial Poisson process across a square domain of size $L \times L$. The movement, proliferation and death rates of the agents are computed using Equations (2.1)-(2.3). For this study, we use a constant death rate for all the agents, hence the neighbour-dependent term in Equation (2.3) is set to zero. The sum of event rates of all agents is given by,

$$\lambda(t) = \sum_{n=1}^{N_1(t)} (\widehat{M}_n + \widehat{P}_n + \widehat{D}_n). \quad (2.10)$$

Since the event rates for obstacles are always zero, those terms do not contribute to $\lambda(t)$. The time interval between consecutive events is exponentially distributed with mean $1/\lambda(t)$. At each event time, one of the three possible events occurs to an agent. The probability of occurrence of an event is proportional to the rate of that event. For a movement event, the agent moves a displacement specified by the bias vector and movement displacement PDF in Equation (2.4) and Equation (2.6), respectively. For a proliferation event, the proliferative agent disperses a

daughter agent at a displacement specified by the PDF $\mu_1^{(p)}(\xi)$, and the total number of agents increases by one. For a death event the total number of agents is reduced by one.

To provide a mathematical description of the IBM we analyse the dynamics of the first and second spatial moments of the agents and obstacles. The first moment of agents and obstacles is given by dividing the total number of agents and obstacles by the area of the domain, giving $N_1(t)/L^2$ and $N_2(t)/L^2$, respectively. We use a pair correlation function (PCF) to quantify the second spatial moment. Here the PCF depends on both the separation distance, r , and time, t (Angew et al., 2014; Dini et al., 2018). However, to be consistent with previous studies, our notation focuses on the separation distance, r , only. Since there are two different subpopulations, we will have two different PCFs. First, we denote the auto-correlation PCF between agents as $C_{11}(r)$. Second, we denote the cross-correlation between agents and obstacles as $C_{12}(r)$. To compute the auto-correlation function, we consider a reference agent at \mathbf{x}_i , and calculate all distances, $r = |\mathbf{x}_j - \mathbf{x}_i|$, to the other $N_1 - 1$ agents. We follow the same procedure with each of the remaining agents until all agents have acted as the reference agent. Note that we always take care to measure distances across periodic boundaries. With this information, the auto-correlation PCF is constructed by enumerating the distances between pairs of agents that fall into the interval, $[r - \delta r/2, r + \delta r/2]$. That means we use a bin width of δr . To ensure that $C_{11}(r) = 1$ in the absence of spatial structure, we normalise the bin count by a factor of $N_1(t)(N_1(t) - 1)(2\pi r \delta r)/L^2$. When $C_{11}(r) > 1$, we have a larger number of pairs of agents separated by a distance r than we would have in the spatially random population. In contrast, for $C_{11}(r) < 1$, we have a smaller number of pairs of agents separated by a distance r than we would have in the spatially random population. Similarly, we compute the cross-correlation PCF, $C_{12}(r)$, by counting, binning and normalising all distances between agents and obstacles. A similar calculation could be made for $C_{22}(r)$, by counting, binning and normalising all distances between pairs of obstacles. However, since obstacles are stationary, non-proliferative and initialised at random, we always have $C_{22}(r) = 1$. Only when $C_{11}(r) = C_{12}(r) = C_{22} = 1$ are agents and obstacles are arranged at random, which is an implicit assumption in all mean-field models. One of the important features of our model and our analysis is that we can have spatial structure, such as clustering or segregated spatial patterns, present in the population. This is signified by having $C_{11}(r) \neq 1$ and $C_{12}(r) \neq 1$.

There are several key variables relevant to specifying different obstacle fields and different obstacle properties. These include obstacle density, obstacle size and obstacle interactions, such as whether obstacles are adhesive or repulsive. We will explore how systematically varying these properties influences the development of spatial structure in a population of motile and proliferative agents that are placed into an environment containing obstacles. We first explore this by performing repeated realizations of the IBM and analysing averaged ensemble data in terms of the first spatial moment and PCF. Second, we then compare these results with the prediction from our analysis of spatial moment dynamics in Section 2.7. A summary of key variables and notation for these calculations is given in Table 2.1.

2.5 Continuous description

Here, we derive a continuum approximation for the IBM in terms of spatial moments. To keep our work as general as possible, we present the derivation for an arbitrary number of motile and proliferative subpopulations. Then we present a specific case of the continuous description where there are two subpopulations: the first subpopulation is a population of motile and proliferative agents and the second subpopulation is a population of stationary and non-proliferative obstacles. As previously described, we consider a spatially homogeneous environment. This means that the probability of finding an individual in a given small region is independent of the position of that small region. Hence the key quantity of interest is the displacement between individuals. The first spatial moment, $Z_{1,i}(t)$, is the average density of individuals from subpopulation i . The second spatial moment, $Z_{2,ij}(\xi, t)$, is the average density of pairs of individuals, consisting of an individual from subpopulation j at a displacement ξ from an individual belonging to subpopulation i . The third spatial moment, $Z_{3,ijk}(\xi, \xi', t)$, is the average density of triplets of individuals. Here, this triplet consists of an individual from subpopulation j at displacement ξ from an individual belonging to subpopulation i , and an individual from subpopulation k at displacement ξ' from the individual belonging to subpopulation i . Mathematical definitions of these spatial moments are presented in Section 2A.1.

2.5.1 Dynamics of spatial moments

The expected rates of movement and proliferation of an individual, denoted $M_{1,i}(t)$ and $P_{1,i}(t)$, depend on the contribution from another individual at a displacement ξ . The conditional probability of having an individual from subpopulation j located at $\mathbf{x} + \xi$ given that an individual from subpopulation i is located at \mathbf{x} , is $Z_{2,ij}(\xi, t)/Z_{1,i}(t)$. The derivation of the conditional probability in terms of the spatial moments is provided in Section 2A.2. The expected movement and proliferation rates of an individual from subpopulation i is given by multiplying this conditional probability by the corresponding interaction kernels, $\omega_{ij}^{(m)}(|\xi|)$ or $\omega_{ij}^{(p)}(|\xi|)$, respectively, and integrating over all possible displacements, and adding over all individuals j . These details are outlined in Section 2A.3, and lead to

$$M_{1,i}(t) = m_i + \sum_j \int \omega_{ij}^{(m)}(|\xi|) \frac{Z_{2,ij}(\xi, t)}{Z_{1,i}(t)} d\xi, \quad (2.11)$$

$$P_{1,i}(t) = p_i + \sum_j \int \omega_{ij}^{(p)}(|\xi|) \frac{Z_{2,ij}(\xi, t)}{Z_{1,i}(t)} d\xi. \quad (2.12)$$

We now consider the dynamics of the first moment. The first moment dynamics depends solely on the balance between the expected rate of proliferation, $P_{1,i}(t)$, and death rate, d_i . The movement and neighbour-dependent directional bias does not directly influence the dynamics of the

first moment. The time evolution of the first moment is given by,

$$\frac{d}{dt}Z_{1,i}(t) = (P_{1,i}(t) - d_i)Z_{1,i}(t). \quad (2.13)$$

The dynamics of the average density of pairs of agents depends on the conditional occupancy of a third agent in the neighbourhood. The conditional probability of having an individual from subpopulation k located at $\mathbf{x} + \boldsymbol{\xi}'$ given that an individual from subpopulation i is located at \mathbf{x} and an individual from subpopulation j located at $\mathbf{x} + \boldsymbol{\xi}$, is $Z_{3,ijk}(\boldsymbol{\xi}, \boldsymbol{\xi}', t)/Z_{2,ij}(\boldsymbol{\xi}, t)$. The expected movement and proliferation rates for an individual from subpopulation i , which forms a pair with an individual from subpopulation j , separated by a displacement $\boldsymbol{\xi}$, denoted by $M_{2,ij}(\boldsymbol{\xi}, t)$ and $P_{2,ij}(\boldsymbol{\xi}, t)$, respectively. These rates depend on the conditional presence of another individual from subpopulation k at a displacement $\boldsymbol{\xi}'$. Hence, the expected rates are found by multiplying $Z_{3,ijk}(\boldsymbol{\xi}, \boldsymbol{\xi}', t)/Z_{2,ij}(\boldsymbol{\xi}, t)$ by the interaction kernels and integrating over all possible displacements as follows,

$$M_{2,ij}(\boldsymbol{\xi}, t) = m_i + \sum_k \int \omega_{ik}^{(m)}(|\boldsymbol{\xi}'|) \frac{Z_{3,ijk}(\boldsymbol{\xi}, \boldsymbol{\xi}', t)}{Z_{2,ij}(\boldsymbol{\xi}, t)} d\boldsymbol{\xi}' + \omega_{ij}^{(m)}(|\boldsymbol{\xi}|), \quad (2.14)$$

$$P_{2,ij}(\boldsymbol{\xi}, t) = p_i + \sum_k \int \omega_{ik}^{(p)}(|\boldsymbol{\xi}'|) \frac{Z_{3,ijk}(\boldsymbol{\xi}, \boldsymbol{\xi}', t)}{Z_{2,ij}(\boldsymbol{\xi}, t)} d\boldsymbol{\xi}' + \omega_{ij}^{(p)}(|\boldsymbol{\xi}|). \quad (2.15)$$

The third term on the right of Equations (2.14)-(2.15) accounts for the direct influence of the individual from subpopulation j at a displacement $\boldsymbol{\xi}$ from the individual from subpopulation i .

The gradient of the interaction kernel specifies the contribution of other individuals to the bias vector. The expected net bias vector for an individual from subpopulation i , conditional on presence of an individual from subpopulation j , is given by,

$$\mathbf{B}_{2,ij}(\boldsymbol{\xi}, t) = \mathbf{b}_i + \sum_k \int \nabla \omega_{ik}^{(b)}(|\boldsymbol{\xi}'|) \frac{Z_{3,ijk}(\boldsymbol{\xi}, \boldsymbol{\xi}', t)}{Z_{2,ij}(\boldsymbol{\xi}, t)} d\boldsymbol{\xi}' + \nabla \omega_{ij}^{(b)}(|\boldsymbol{\xi}|). \quad (2.16)$$

Again, the third term on the right of Equation (2.16) accounts for the direct influence of an individual from subpopulation j , at a displacement $\boldsymbol{\xi}$, from the individual belonging to subpopulation i . We note that Equation (2.16) combines directional bias (Binny et al., 2016a, 2016b) with multi-species spatial moment equations (Law and Dieckmann, 2000; Murrell, 2005; Plank and Law, 2015) in a way that has not been considered previously. Now we consider the PDF for the movement displacement $\boldsymbol{\xi}'$ for an individual from subpopulation i conditional on the presence of an individual from subpopulation j at displacement $\boldsymbol{\xi}$ as,

$$\mu_{2,ij}^{(m)}(\boldsymbol{\xi}', \boldsymbol{\xi}, t) = \mu_i^{(m)}(\boldsymbol{\xi}'; \mathbf{B}_{2,ij}(\boldsymbol{\xi}, t)). \quad (2.17)$$

For the dynamics of the second moment, we must consider two factors: (i) the loss of pairs of agents at displacement $\boldsymbol{\xi}$; and (ii) the creation of pairs at displacement $\boldsymbol{\xi}$. The loss of pairs

occurs either by movement or death events, whereas the creation of pairs occurs through movement or proliferation events. The time evolution of the second moment is given by,

$$\begin{aligned} \frac{\partial}{\partial t} Z_{2,ij}(\xi, t) = & - \left(M_{2,ij}(\xi, t) + M_{2,ji}(-\xi, t) + d_i + d_j \right) Z_{2,ij}(\xi, t) \\ & + \int \left(\mu_{2,ij}^{(m)}(\xi', \xi' + \xi, t) M_{2,ij}(\xi' + \xi, t) \right. \\ & \left. + \mu_i^{(p)}(\xi') P_{2,ij}(\xi' + \xi, t) \right) Z_{2,ij}(\xi' + \xi, t) d\xi' \\ & + \int \left(\mu_{2,ji}^{(m)}(\xi', \xi' - \xi, t) M_{2,ji}(\xi' - \xi, t) \right. \\ & \left. + \mu_j^{(p)}(\xi') P_{2,ji}(\xi' - \xi, t) \right) Z_{2,ji}(\xi' - \xi, t) d\xi' \\ & + 2\delta_{ij}\mu_j^{(p)}(-\xi) P_{1,j}(t) Z_{1,j}(t). \end{aligned} \quad (2.18)$$

In Equation (2.18), the two integral terms and the factor of two in the last term on the right arises due to the fact that a pair can be created or destroyed by either of the individuals in that pair. A detailed description of the derivation of the dynamics of the second spatial moment is provided in Section 2A.4.

Just as the dynamics of the first moment depends on the second moment, we see that the dynamics of the second moment depends on the third moment. If we continue in this way we could develop an infinite hierarchy of equations which is difficult to analyse (Ovaskainen and Cornell, 2006; Finkelshtein et al., 2009; Ovaskainen et al., 2014). However, previous studies focusing on applications in cell biology (Binny et al., 2016a, 2016b) and ecology (Law and Dieckmann, 2000) provide useful results by closing the infinite system of moment equations to produce an approximate truncated system. Here we follow a similar approach and approximate the third order terms in Equations (2.14)-(2.16) using a moment closure approximation. While various approximations, such as the power-1 closure, power-2 closure and Kirkwood superposition approximation, are available (Murrell et al., 2004), in this study we focus on the power-2 closure scheme (Law et al., 2003) that is given by,

$$\begin{aligned} Z_{3,ijk}(\xi, \xi', t) = & \frac{1}{5} \left(4 \frac{Z_{2,ij}(\xi, t) Z_{2,ik}(\xi', t)}{Z_{1,i}(t)} + \frac{Z_{2,ij}(\xi, t) Z_{2,jk}(\xi' - \xi, t)}{Z_{1,j}(t)} \right. \\ & \left. + \frac{Z_{2,ik}(\xi', t) Z_{2,jk}(\xi' - \xi, t)}{Z_{1,k}(t)} - Z_{1,i}(t) Z_{1,j}(t) Z_{1,k}(t) \right). \end{aligned} \quad (2.19)$$

2.5.2 Spatial moment description for motile, proliferative agents and stationary obstacles

For clarity, we now present the governing equations for the specific case of a population of motile, proliferative agents in an environment containing stationary, non-proliferative obstacles. The first spatial moment of agents and obstacles are denoted $Z_{1,1}(t)$ and $Z_{1,2}(t)$, respectively. The second spatial moments, corresponding to the density of pairs are denoted: $Z_{2,11}(\xi, t); Z_{2,12}(\xi, t)$;

$Z_{2,21}(\xi, t)$; and $Z_{2,22}(\xi, t)$. The terms $Z_{2,11}(\xi, t)$ and $Z_{2,22}(\xi, t)$ correspond to the average densities agent-agent pairs and obstacle-obstacle pairs. The other two terms, $Z_{2,12}(\xi, t)$ and $Z_{2,21}(\xi, t)$, corresponds to the average densities of agent-obstacle pairs, and obstacle-agent pairs.

The expected rate of movement of an agent, $M_{1,1}(t)$, is given by multiplying the interaction kernels of movement, $\omega_{11}^{(m)}(|\xi|)$ or $\omega_{12}^{(m)}(|\xi|)$, by the conditional probability of having an agent or obstacle present at a displacement ξ from the reference agent, and integrating over all possible displacements. These conditional probabilities of either an agent or obstacle located at a displacement ξ are given by $Z_{2,11}(\xi, t)/Z_{1,1}(t)$ and $Z_{2,12}(\xi, t)/Z_{1,1}(t)$, respectively. The expected proliferation rate is also calculated in the same way by replacing the movement kernels with proliferation kernels, $\omega_{11}^{(p)}(|\xi|)$ and $\omega_{12}^{(p)}(|\xi|)$. Using this information, the expected rate of movement and proliferation of an agent is given by,

$$M_{1,1}(t) = m_1 + \frac{1}{Z_{1,1}(t)} \int (\omega_{11}^{(m)}(|\xi|)Z_{2,11}(\xi, t) + \omega_{12}^{(m)}(|\xi|)Z_{2,12}(\xi, t)) d\xi, \quad (2.20)$$

$$P_{1,1}(t) = p_1 + \frac{1}{Z_{1,1}(t)} \int (\omega_{11}^{(p)}(|\xi|)Z_{2,11}(\xi, t) + \omega_{12}^{(p)}(|\xi|)Z_{2,12}(\xi, t)) d\xi. \quad (2.21)$$

The expected movement and proliferation rates of obstacles $M_{1,2}(t)$ and $P_{1,2}(t)$ are zero.

The time evolution of density of agents depends only on the expected rate of proliferation and death of agents. The density of obstacles remains constant. Hence we have,

$$\frac{d}{dt} Z_{1,1}(t) = (P_{1,1}(t) - d_1) Z_{1,1}(t), \quad (2.22)$$

$$\frac{d}{dt} Z_{1,2}(t) = 0. \quad (2.23)$$

The conditional probability of having an agent located at ξ' , given that an another agent is present at ξ , is $Z_{3,111}(\xi, \xi', t)/Z_{2,11}(\xi, t)$. Similarly three more conditional probabilities can be specified by considering different arrangements of agents and obstacles around the reference agent at displacement $\mathbf{0}$. The expected event rates, $M_{2,11}(\xi, t)$ and $P_{2,11}(\xi, t)$, of an agent conditional on the presence of another agent at displacement ξ can be computed by multiplying these conditional probabilities by the corresponding interaction kernels and integrating over all possible displacements. The expected rates are given by,

$$M_{2,11}(\xi, t) = \frac{1}{Z_{2,11}(\xi, t)} \int (\omega_{11}^{(m)}(|\xi'|)Z_{3,111}(\xi, \xi', t) + \omega_{12}^{(m)}(|\xi'|)Z_{3,112}(\xi, \xi', t)) d\xi' + m_1 + \omega_{11}^{(m)}(|\xi|), \quad (2.24)$$

$$P_{2,11}(\xi, t) = \frac{1}{Z_{2,11}(\xi, t)} \int (\omega_{11}^{(p)}(|\xi'|)Z_{3,111}(\xi, \xi', t) + \omega_{12}^{(p)}(|\xi'|)Z_{3,112}(\xi, \xi', t)) d\xi' + p_1 + \omega_{11}^{(p)}(|\xi|). \quad (2.25)$$

Using similar arguments, we compute the remaining movement and proliferation rates of an

agent arising from the presence of an obstacle at a displacement ξ as follows,

$$\begin{aligned} M_{2,12}(\xi, t) &= \frac{1}{Z_{2,12}(\xi, t)} \int (\omega_{11}^{(m)}(|\xi'|) Z_{3,121}(\xi, \xi', t) + \omega_{12}^{(m)}(|\xi'|) Z_{3,122}(\xi, \xi', t)) d\xi' \\ &\quad + m_1 + \omega_{12}^{(m)}(|\xi|), \end{aligned} \quad (2.26)$$

$$\begin{aligned} P_{2,12}(\xi, t) &= \frac{1}{Z_{2,12}(\xi, t)} \int (\omega_{11}^{(p)}(|\xi'|) Z_{3,121}(\xi, \xi', t) + \omega_{12}^{(p)}(|\xi'|) Z_{3,122}(\xi, \xi', t)) d\xi' \\ &\quad + p_1 + \omega_{12}^{(p)}(|\xi|). \end{aligned} \quad (2.27)$$

The gradient of the bias kernel gives the contribution of agents and obstacles to the bias vector of the neighbouring agent. The expected net bias vector of an agent conditional on presence of another agent is given by,

$$\begin{aligned} \mathbf{B}_{2,11}(\xi, t) &= \mathbf{b}_1 + \frac{1}{Z_{2,11}(\xi, t)} \int (\nabla \omega_{11}^{(b)}(|\xi'|) Z_{3,111}(\xi, \xi', t) \\ &\quad + \nabla \omega_{12}^{(b)}(|\xi'|) Z_{3,112}(\xi, \xi', t)) d\xi' + \nabla \omega_{11}^{(b)}(|\xi|). \end{aligned} \quad (2.28)$$

Similarly, the expected net bias vector of an agent conditional on presence of an obstacle is given by,

$$\begin{aligned} \mathbf{B}_{2,12}(\xi, t) &= \mathbf{b}_1 + \frac{1}{Z_{2,12}(\xi, t)} \int (\nabla \omega_{11}^{(b)}(|\xi'|) Z_{3,121}(\xi, \xi', t) \\ &\quad + \nabla \omega_{12}^{(b)}(|\xi'|) Z_{3,122}(\xi, \xi', t)) d\xi' + \nabla \omega_{12}^{(b)}(|\xi|). \end{aligned} \quad (2.29)$$

Now we develop the equations governing the dynamics of the second moments. The equations for the density of pairs involving agents depends on the loss of pairs of agents at displacement ξ , which can occur either by movement or death, and creation of pair at displacement ξ which can occur through movement or proliferation. The density of pairs of obstacles, $Z_{2,22}(\xi, t)$, remains constant over time. The equations governing the dynamics of second moments for the

agent-obstacle population are given by,

$$\begin{aligned} \frac{\partial}{\partial t} Z_{2,11}(\xi, t) = & - \left(M_{2,11}(\xi, t) + M_{2,11}(-\xi, t) + 2d_1 \right) Z_{2,11}(\xi, t) \\ & + \int \left(\mu_{2,11}^{(m)}(\xi', \xi' + \xi, t) M_{2,11}(\xi' + \xi, t) \right. \\ & \left. + \mu_1^{(p)}(\xi') P_{2,11}(\xi' + \xi, t) \right) Z_{2,11}(\xi' + \xi, t) d\xi' \\ & + \int \left(\mu_{2,11}^{(m)}(\xi', \xi' - \xi, t) M_{2,11}(\xi' - \xi, t) \right. \\ & \left. + \mu_1^{(p)}(\xi') P_{2,11}(\xi' - \xi, t) \right) Z_{2,11}(\xi' - \xi, t) d\xi' \\ & + 2\mu_1^{(p)}(-\xi) P_{1,1}(t) Z_{1,1}(t), \end{aligned} \quad (2.30)$$

$$\begin{aligned} \frac{\partial}{\partial t} Z_{2,12}(\xi, t) = & - \left(M_{2,12}(\xi, t) + d_1 \right) Z_{2,12}(\xi, t) \\ & + \int \left(\mu_{2,12}^{(m)}(\xi', \xi' + \xi, t) M_{2,12}(\xi' + \xi, t) \right. \\ & \left. + \mu_1^{(p)}(\xi') P_{2,12}(\xi' + \xi, t) \right) Z_{2,12}(\xi' + \xi, t) d\xi', \end{aligned} \quad (2.31)$$

$$\begin{aligned} \frac{\partial}{\partial t} Z_{2,21}(\xi, t) = & - \left(M_{2,12}(-\xi, t) + d_1 \right) Z_{2,21}(\xi, t) \\ & + \int \left(\mu_{2,12}^{(m)}(\xi', \xi' - \xi, t) M_{2,12}(\xi' - \xi, t) \right. \\ & \left. + \mu_1^{(p)}(\xi') P_{2,12}(\xi' - \xi, t) \right) Z_{2,12}(\xi' - \xi, t) d\xi', \end{aligned} \quad (2.32)$$

$$\frac{\partial}{\partial t} Z_{2,22}(\xi, t) = 0. \quad (2.33)$$

A description of the numerical methods we use to solve Equations (2.30)-(2.33) are given in Section 2A.5.

Table 2.1: Model parameters and typical values.

Parameter	Symbol	Value
Densities		
Agents	$Z_{1,1}(t)$	0.25 to 0.9
Obstacles	$Z_{1,2}(t)$	0.0 to 0.375
Initial density of agents	$Z_{1,1}(0)$	0.25
Initial density of obstacles	$Z_{1,2}(0)$	0.0 to 0.375
Intrinsic rates		
Birth	p_1, p_2	1, 0
Death	d_1, d_2	0.5, 0
Movement	m_1, m_2	5, 0
Neighbour-dependent interaction strengths		
Birth	$\gamma_{11}^{(p)}, \gamma_{12}^{(p)}, \gamma_{21}^{(p)}, \gamma_{22}^{(p)}$	-0.38 to 0
Movement	$\gamma_{11}^{(m)}, \gamma_{12}^{(m)}, \gamma_{21}^{(m)}, \gamma_{22}^{(m)}$	0
Bias	$\gamma_{11}^{(b)}, \gamma_{12}^{(b)}, \gamma_{21}^{(b)}, \gamma_{22}^{(b)}$	-0.2 to 0.4
Spatial extent of interactions		
Birth	$\sigma_{11}^{(p)}, \sigma_{12}^{(p)}, \sigma_{21}^{(p)}, \sigma_{22}^{(p)}$	0.25 to 0.6
Movement	$\sigma_{11}^{(m)}, \sigma_{12}^{(m)}, \sigma_{21}^{(m)}, \sigma_{22}^{(m)}$	0.25 to 0.6
Bias	$\sigma_{11}^{(b)}, \sigma_{12}^{(b)}, \sigma_{21}^{(b)}, \sigma_{22}^{(b)}$	0.25 to 0.6
Movement and dispersal distance		
Mean movement distance	$\mu_1^{(s)}, \mu_2^{(s)}$	0.4
Standard deviation movement distance	$\sigma_1^{(s)}, \sigma_2^{(s)}$	0.1
Standard deviation dispersal distance	$\sigma_1^{(d)}, \sigma_2^{(d)}$	0.5

2.6 Bias landscape

A key feature of the IBM is the neighbour-dependent bias. This formalism helps us understand how the spatial arrangement of obstacles and other agents affects the movement of a particular reference agent. To interpret and visualise the neighbour-dependent bias, we define the *bias landscape* as,

$$Q(\mathbf{x}) = Q_1(\mathbf{x}) + Q_2(\mathbf{x}), \quad (2.34)$$

where,

$$Q_1(\mathbf{x}) = \sum_{n \in N_1} \omega_{11}^{(b)}(|\mathbf{x}_n - \mathbf{x}|), \quad (2.35)$$

$$Q_2(\mathbf{x}) = \sum_{n \in N_2} \omega_{12}^{(b)}(|\mathbf{x}_n - \mathbf{x}|), \quad (2.36)$$

are contributions to overall bias landscape from the agents and the obstacles, respectively. For an agent located at \mathbf{x} , $Q(\mathbf{x})$ acts as a measure of the degree of crowding. The neighbour-dependent bias vector, \mathbf{B}_n , is the negative gradient of the bias landscape, $-\nabla Q(\mathbf{x})$. With these definitions it is straightforward to see that agents move in response to the gradient of the bias landscape. Writing the negative gradient of the bias landscape in terms of the contributions from the two subpopulations, $-\nabla Q(\mathbf{x}) = -\nabla Q_1(\mathbf{x}) - \nabla Q_2(\mathbf{x})$, it is clear that the spatial arrangements of both the agents and the obstacles play a role in influencing the movement of agents in the IBM. The incorporation of bias owing to interactions within a particular subpopulation, and interactions from other subpopulations is a very simple, yet powerful feature of our IBM and this can be used to explore a range of behaviours such as enabling the simulation of attraction of individuals within the same subpopulation, and repulsion between pairs of individuals from different subpopulations. This kind of detail, which has never been considered before in the context of a spatial moment model, can be incorporated very simply in our modelling framework.

The influence of bias depends on the spatial arrangement of the agents and obstacles, and properties of the interaction kernels, $\omega_{11}^{(b)}(|\xi|)$ and $\omega_{12}^{(b)}(|\xi|)$, respectively. When the kernels are decreasing functions of $|\xi|$, agents experience a repulsive bias that encourages them to move away from the regions of high crowding. Figure 2.1 shows how the repulsive bias affects the movement of agents in a particular arrangement. The bias landscape and corresponding level curves due to agent-agent interactions alone are shown in Figure 2.1(a)-(b). The locations of agents are represented by red dots, and the arrows indicate the preferred direction of movement. The length of these arrows indicates the strength of bias. We note that crowded agents experience a repulsive bias, and prefer to move towards a lower density region. Figure 2.1(c)-(d) shows the crowding effects generated by obstacles only, and Figure 2.1(e)-(f) shows how both the agent-agent and agent-obstacle interactions sum to give the total bias landscape. Note that, if the bias interaction strength is negative, then the interaction kernels $\omega_{11}^{(b)}(|\xi|)$ and $\omega_{12}^{(b)}(|\xi|)$ are increasing functions of $|\xi|$. In that case, the orientation of the bias landscape structure would be reversed, and we would have an attractive bias.

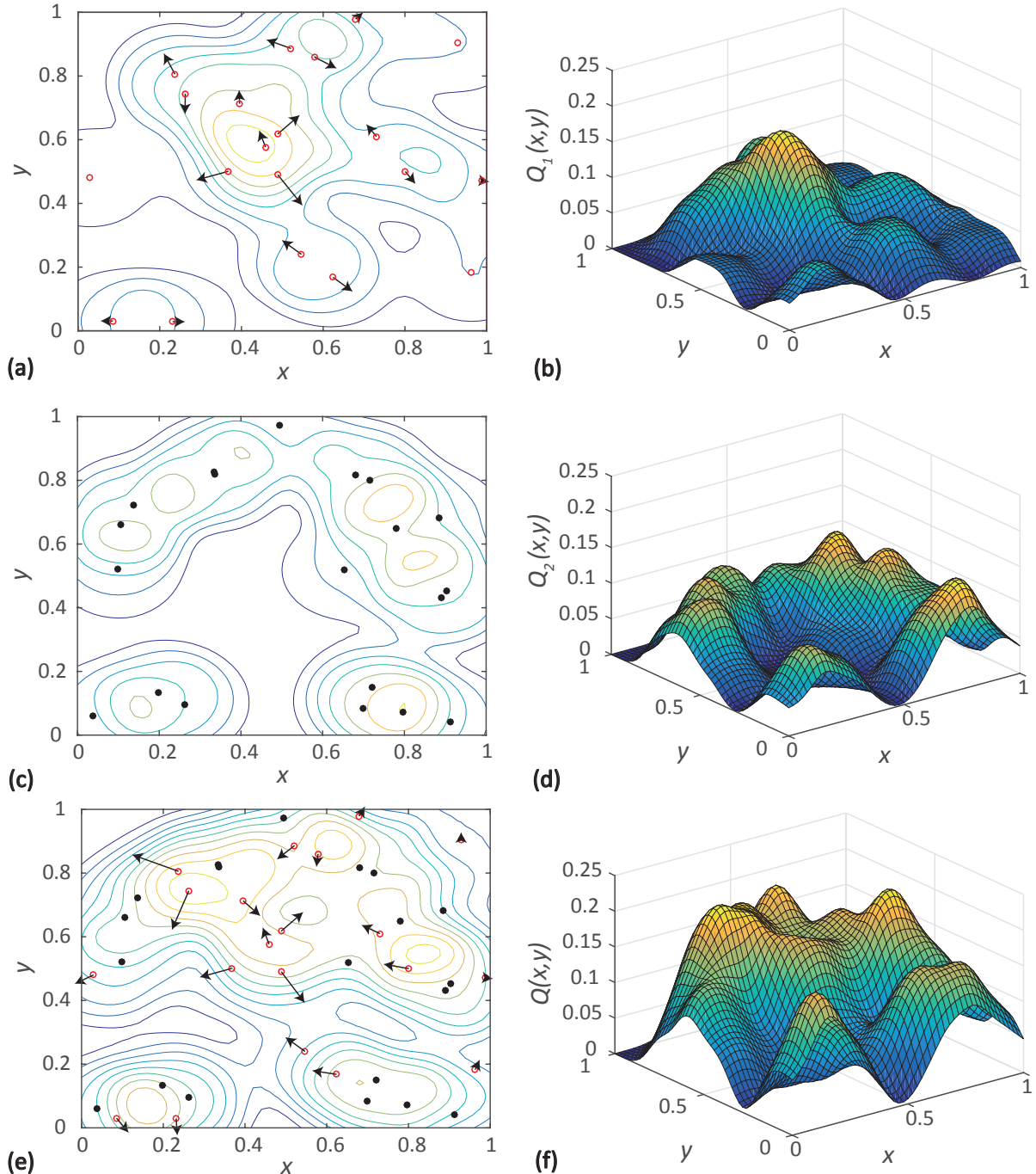


Figure 2.1: Neighbour-dependent bias visualised for a particular arrangement of 20 agents (red open circles) and 20 obstacles (black dots). In this case we have a positive Gaussian interaction kernel to specify the interactions among agents as well as the interactions between agents and obstacles. **a** Locations of agents (red open circles). **c** Locations of obstacles (black dots). **e** Location of both agents (red open circles) and obstacles (black dots). In each subplot, **a,c,e**, the locations of individuals are superimposed with the level curves of various components of the bias landscape. **b,d,f** shows the different components of the bias landscape: $Q_1(\mathbf{x})$; $Q_2(\mathbf{x})$; and $Q(\mathbf{x})$, respectively. The bias vectors are denoted by black arrows. The bias vectors in **a** show $-\nabla Q_1(\mathbf{x}_n)$, which is the negative gradient of the component of the bias landscape corresponding to agent-agent interactions. For some agents where the bias vector is sufficiently small we do not show the bias vector. In addition, the bias vectors for stationary obstacles are omitted since the obstacles are stationary. The bias vectors in **e** show $-\nabla Q(\mathbf{x}_n)$, which is the negative gradient of the net bias landscape corresponding to the sum of agent-agent and agent-obstacle interactions. The length of arrows indicate the strength of bias. Results in **a-b** correspond to interactions between agents only. Results in **c-d** show interactions between obstacles. Results in **e-f** show the net interactions between agents and obstacles. Parameters are $\gamma_{11}^{(b)} = \gamma_{12}^{(b)} = 0.2$ and $\sigma_{11}^{(b)} = \sigma_{12}^{(b)} = 0.5$.

Another key variable in the IBM is the size of the obstacles, which determines the spatial extent of the obstacle-agent bias. We use the parameter describing the spatial extent of interactions, $\sigma_{12}^{(b)}$, as a proxy for obstacle size. Here we make the natural assumption that larger obstacles correspond to increased $\sigma_{12}^{(b)}$, so that larger obstacles tend to exert an influence over a larger neighbourhood. Note that we maintain the bias strength, $\gamma_{12}^{(b)}$, as a constant and we only vary $\sigma_{12}^{(b)}$ to mimic the influence of obstacle size. Results in Figure 2.2 show the same spatial arrangement of 20 agents and 20 obstacles as in Figure 2.1, except that we reduce $\sigma_{12}^{(b)}$ so that the obstacles in Figure 2.2 influence a smaller neighbourhood than the obstacles in Figure 2.1. This change in obstacle size does not affect the agent-agent component of the bias landscape, $Q_1(\mathbf{x})$, but it does affect the agent-obstacle component, $Q_2(\mathbf{x})$.

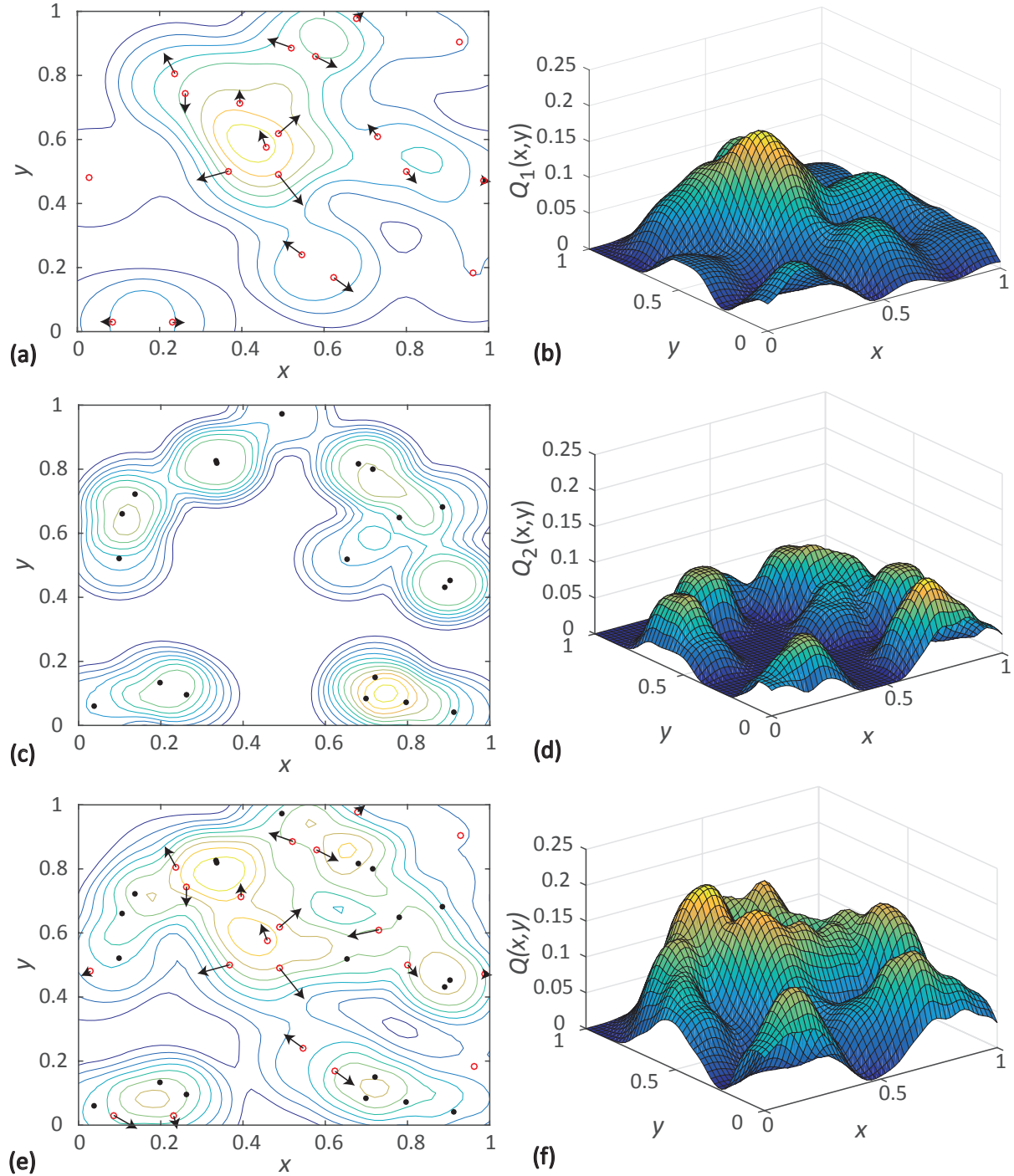


Figure 2.2: Neighbour-dependent bias visualised for a particular arrangement of 20 agents (red open circles) and 20 smaller obstacles (black dots). In this case we have a positive Gaussian interaction kernel to specify the interactions among agents as well as the interactions between agents and obstacles. **a** Locations of agents (red open circles). **c** Location of obstacles (black dots). **e** Locations of both agents (red open circles) and obstacles (black dots). In each subplot, **a,c,e**, the locations of individuals are superimposed with the level curves of various components of the bias landscape. **b,d,f** shows the different components of the bias landscape: $Q_1(\mathbf{x})$; $Q_2(\mathbf{x})$; and $Q(\mathbf{x})$, respectively. The bias vectors are denoted by black arrows. The bias vectors in **a** show $-\nabla Q_1(\mathbf{x}_n)$, which is the negative gradient of the component of the bias landscape corresponding to agent-agent interactions. For some agents where the bias vector is sufficiently small we do not show the bias vector. In addition, the bias vectors for stationary obstacles are omitted since the obstacles are stationary. The bias vectors in **e** show $-\nabla Q(\mathbf{x}_n)$, which is the negative gradient of the net bias landscape corresponding to the sum of agent-agent and agent-obstacle interactions. The length of arrows indicate the strength of bias. Results in **a-b** correspond to interactions between agents only. Results in **c-d** show interactions between obstacles. Results in **e-f** show the net interactions between agents and obstacles. Parameters are $\gamma_{11}^{(b)} = \gamma_{12}^{(b)} = 0.2$, $\sigma_{11}^{(b)} = 0.5$ and $\sigma_{12}^{(b)} = 0.25$.

2.7 Results and discussion

In this section we present snapshots from the IBM to explore the dynamics of the two species agent-obstacle system. In these simulations we systematically vary the density of obstacles, the size of obstacles, and the interactions between agents and obstacles. In addition to presenting IBM simulations, we also present solutions of the spatial moment dynamics model to explore how well the model predicts the dynamics of the different conditions we consider. Another outcome is to examine how various properties of obstacle field influence spatial structure.

2.7.1 Effect of varying the obstacle density

Here we explore how variations in the density of obstacles influence the spatial structure and the dynamics of the agent subpopulation. Results in Figure 2.3 show a series of snapshots from the IBM. Each row shows snapshots at $t = 0, 10, 20$ and 60 , whereas each column shows results for different densities of obstacles. The initial number of obstacles is varied from $N_2(0) = 0, 50, 100$ to 150 , in the columns from left-to-right, respectively. In all cases we consider a constant initial number of agents, $N_1(0) = 100$, and a random initial placement of obstacles and agents. Results in Figure 2.3(a)-(d) show the most fundamental case where there are no obstacles present, and we note that the multi-species model simplifies to the previous single species model presented by Binny et al. (2016b) in this case. We use this first scenario to emphasise the differences in the population dynamics for the agent subpopulation in presence and absence of obstacles, which are shown in the second, third and fourth column of Figure 2.3. By repeating the stochastic simulations in Figure 2.3 many times, we can calculate the density of obstacles, the density of agents, the auto-correlation PCF and the cross-correlation PCF, as shown in Figure 2.4.

Results in Figure 2.3(a)-(d) show the evolution of the population of agents and the associated spatial structure in the absence of obstacles. Overall we see that the initially small population of agents increases with time until there is a balance of net proliferation and death, leading to the formation of a steady density of agents at later time. For this choice of parameters we observe the formation of a segregated spatial pattern. The main reason for the emergence of segregation is the choice of a positive bias strength, $\gamma_{11}^{(b)} > 0$ which means that agents tend to move away from regions of high density. The segregated nature of the distribution of agents is evident in the auto-correlation PCF as we see that $C_{11}(r) < 1$ over relatively short distances, r .

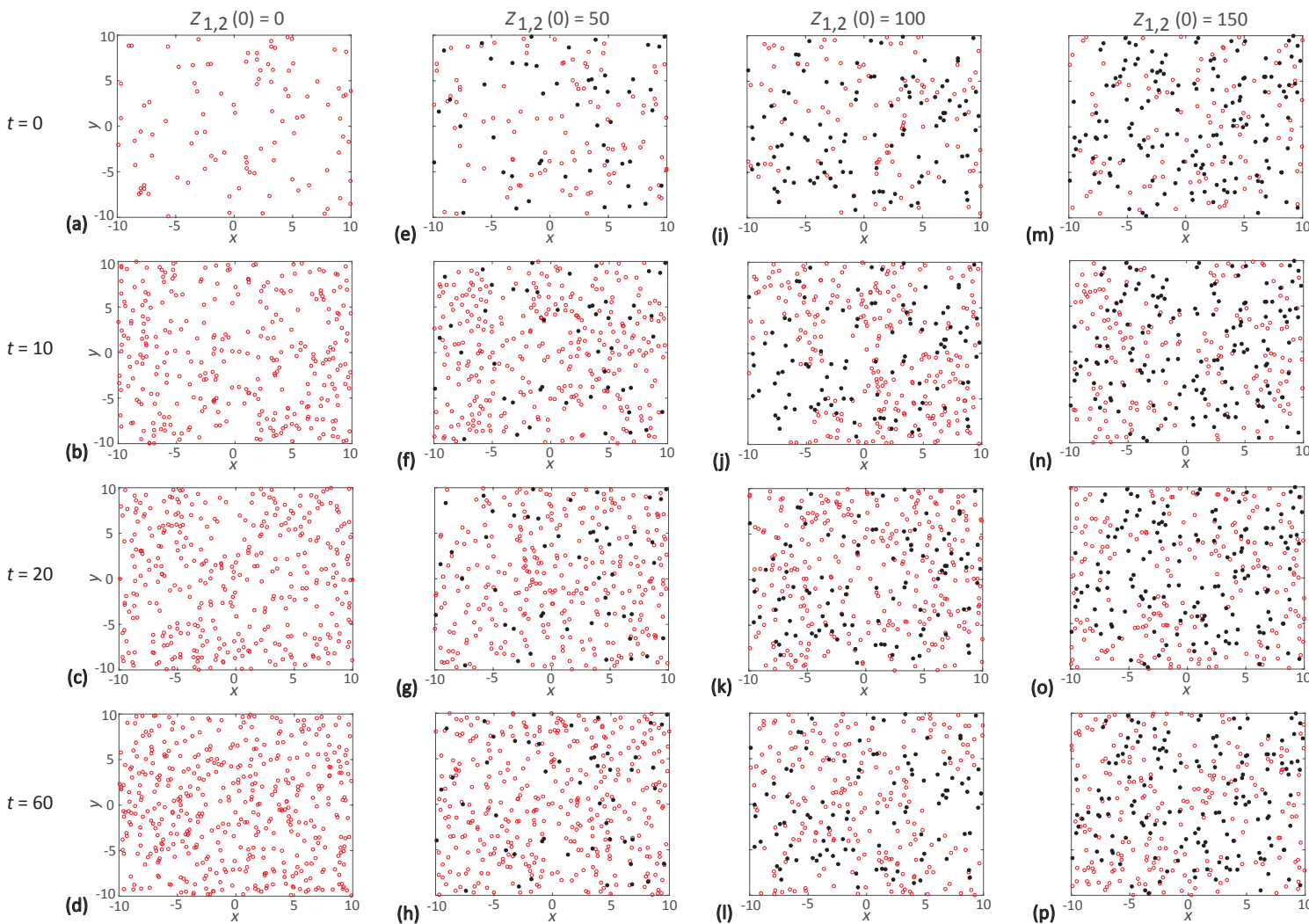


Figure 2.3: IBM snapshots showing the impact of increasing obstacle density. Each row shows a snapshot of the IBM at $t = 0, 10, 20$ and 60 , respectively. Results in **a-d** show the evolution of a population of agents in the absence of obstacles. Results in **e-h**, **i-l** and **m-p** show the evolution of a population of agents among a population of 50 , 100 and 150 obstacles, respectively. In all cases agents are red and obstacles are black. Parameter values are $p_1 = 1$, $d_1 = 0.5$, $m_1 = 5$, $p_2 = d_2 = m_2 = 0$, $\gamma_{11}^{(p)} = -0.38$, $\gamma_{12}^{(p)} = -0.38$, $\gamma_{21}^{(p)} = \gamma_{22}^{(p)} = 0$, $\gamma_{11}^{(b)} = 0.1$, $\gamma_{12}^{(b)} = 0.1$, $\gamma_{21}^{(b)} = 0$, $\gamma_{22}^{(b)} = 0$, $\gamma_{11}^{(m)} = \gamma_{12}^{(m)} = \gamma_{21}^{(m)} = \gamma_{22}^{(m)} = 0$, $\sigma_{11}^{(p)} = 0.5$, $\sigma_{12}^{(p)} = 0.5$, $\sigma_{21}^{(p)} = 0.5$, $\sigma_{22}^{(p)} = 0.5$, $\sigma_{11}^{(b)} = 0.5$, $\sigma_{12}^{(b)} = 0.5$, $\sigma_{21}^{(b)} = 0.5$, $\sigma_{22}^{(b)} = 0.5$, $\sigma_{11}^{(m)} = 0.5$, $\sigma_{12}^{(m)} = 0.5$, $\sigma_{21}^{(m)} = 0.5$, $\sigma_{22}^{(m)} = 0.5$, $\mu_1^{(s)} = 0.4$, $\mu_2^{(s)} = 0.4$, $\sigma_1^{(s)} = 0.1$, $\sigma_2^{(s)} = 0.1$, $\sigma_1^{(d)} = 0.5$, and $\sigma_2^{(d)} = 0.5$.

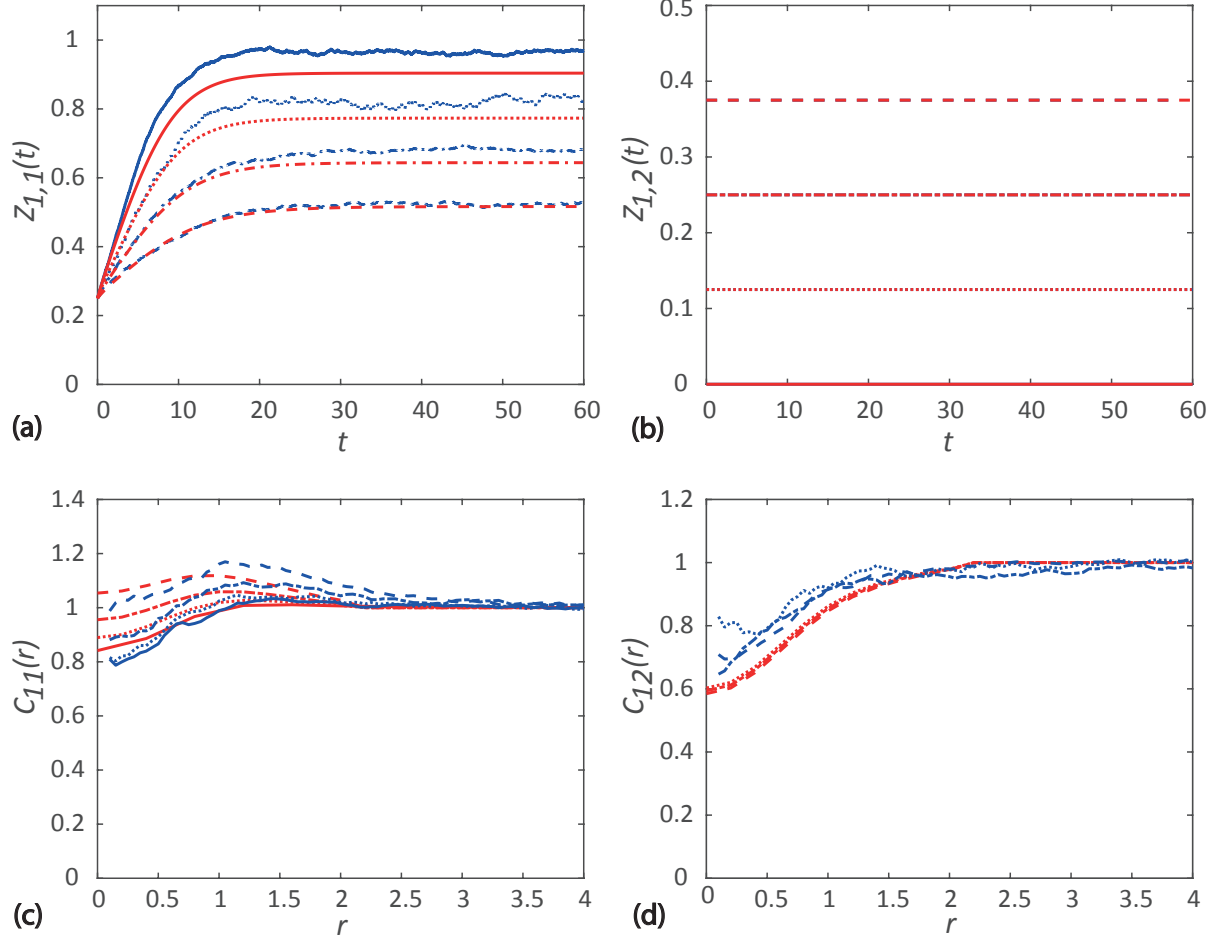


Figure 2.4: Comparison of spatial moment results and averaged data from 40 identically-prepared realizations of the IBM. Results in **a** show the evolution of the first spatial moment for the agents, $Z_{1,1}(t)$. Various results are superimposed for different obstacle densities of obstacles: $Z_{1,2}(0) = 0/400$ (solid), $Z_{1,2}(0) = 50/400$ (dotted), $Z_{1,2}(0) = 100/400$ (dash-dotted) and $Z_{1,2}(0) = 150/400$ (dashed). Results in **b** show the constant first spatial moment for the obstacles. Results in **c-d** show the second spatial moment of agents expressed in terms of $C_{11}(r)$ and $C_{12}(r)$, respectively. Both PCFs are given at $t = 60$. The curves in red correspond to results from the spatial moment dynamics model, whereas curves in blue correspond to averaged data from the IBM. Parameter values are $p_1 = 1$, $d_1 = 0.5$, $m_1 = 5$, $p_2 = d_2 = m_2 = 0$, $\gamma_{11}^{(p)} = -0.38$, $\gamma_{12}^{(p)} = -0.38$, $\gamma_{21}^{(p)} = \gamma_{22}^{(p)} = 0$, $\gamma_{11}^{(b)} = 0.1$, $\gamma_{12}^{(b)} = 0.1$, $\gamma_{21}^{(b)} = \gamma_{22}^{(b)} = 0$, $\gamma_{11}^{(m)} = \gamma_{12}^{(m)} = \gamma_{21}^{(m)} = \gamma_{22}^{(m)} = 0$, $\sigma_{11}^{(p)} = 0.5$, $\sigma_{12}^{(p)} = 0.5$, $\sigma_{21}^{(p)} = 0.5$, $\sigma_{22}^{(p)} = 0.5$, $\sigma_{11}^{(b)} = 0.5$, $\sigma_{12}^{(b)} = 0.5$, $\sigma_{21}^{(b)} = 0.5$, $\sigma_{22}^{(b)} = 0.5$, $\mu_1^{(s)} = 0.4$, $\mu_2^{(s)} = 0.4$, $\sigma_1^{(s)} = 0.1$, $\sigma_2^{(s)} = 0.1$, $\sigma_1^{(d)} = 0.5$, and $\sigma_2^{(d)} = 0.5$.

The incorporation of obstacles in the system leads to a reduction in the long time steady density of agents, as shown in Figure 2.4(a). In general we see that the more obstacles present, the smaller the steady state density of agents. This results makes intuitive sense as the presence of obstacles in the system increases the role of agent-obstacle interactions, which acts to reduce the net proliferation rate. These results also show that the accuracy of the spatial moment prediction increases with the density of obstacles. Results in Figure 2.4(b) show the time evolution of density of obstacles and we see the expected result that the density remains constant. However, the presence of obstacles influences the spatial structure of the population of agents by contributing to the directional bias. Since the obstacles are stationary, the obstacles prevent agents residing in certain regions of the domain. As we increase the obstacle density,

we observe a progressive shift from the long time segregated spatial pattern of agents over short distances when there are no obstacles present, to a more clustered long time pattern of agents as the obstacle density increases. The auto-correlation PCF for each of the cases shown in Figure 2.4(c) illustrates this transition. The cross-correlation PCF between agents and obstacles appears to be less sensitive to the density of obstacles than the auto-correlation PCF. For all cases we see that $C_{12}(r) < 1$ over relatively short distances, r , for all the cases considered, indicating segregated spatial pattern of agents and obstacles.

2.7.2 Effect of varying the obstacle size

Next, we explore how variations in obstacle size influence the spatial structure and dynamics of the agent subpopulation. The notion of obstacle size is incorporated into the model by varying the spatial extent of the interaction of obstacles, $\sigma_{12}^{(p)}$ and $\sigma_{12}^{(b)}$. We assume that larger obstacles interact with agents over a greater distance than smaller obstacles. Therefore, we vary the size of the obstacles and examine how this impacts the evolution of the density of agents, and the spatial structure. We consider a total population composed of agents and obstacles with initial population sizes, $N_1(0) = N_2(0) = 100$, respectively, as shown in Figure 2.5. We then consider increasing the obstacle size, shown from left-to-right in Figure 2.5, where we have $\sigma_{12}^{(p)} = \sigma_{12}^{(b)} = 0.25, 0.4, 0.5$, and 0.6 , respectively. By repeating the stochastic simulations in Figure 2.5 many times, we can calculate the density of obstacles, the density of agents, the auto-correlation PCF and the cross-correlation PCF, as shown in Figure 2.6.

Results in Figure 2.6(a)-(b) show the time evolution of the density of agents and the density of obstacles in each of the four cases considered. As the size of obstacles increase, we observe a decrease in the long time steady agent density. The wider range of interactions for the larger obstacles enables them to influence the proliferation rate of more distant agents. Even though the obstacle density is same, the proliferation rate of more agents reduces in the presence of large obstacles, leading to a reduced long time density of agents. Another mechanism that plays a crucial role in reducing long time steady agent density is the indirect effect of reduction in the effective system size (i.e., the fraction of the domain available for agents) as obstacle size increases. This reduction in system size increases agent-agent interaction and effectively enhances the contact inhibition of agents' proliferation, leading to lower long time steady agent density.

Figure 2.5 shows the snapshot of the spatial structure of population for each case considered and corresponding auto-correlation and cross-correlation PCFs are given in Figure 2.6(c)-(d). The population consisting of small obstacles shows a small-scale segregated spatial pattern of agents. Due to the narrow interaction range of the smaller obstacles, a relatively small number of agents are affected by the obstacles. However, the agents are also subject to a repulsive bias from other agents, which results in a small scale segregated spatial pattern of agents for this choice of parameters. The cross-correlation PCF is less than unity over short displacements,

thereby suggesting segregated spatial structure between agents and obstacles, but the effects are less pronounced than the spatial patterns between agents. As the obstacle size increases, the agent population became less segregated, and the case we consider with the largest, $\sigma_{12}^{(p)} = 0.6$, leads to agent clustering over short distances.

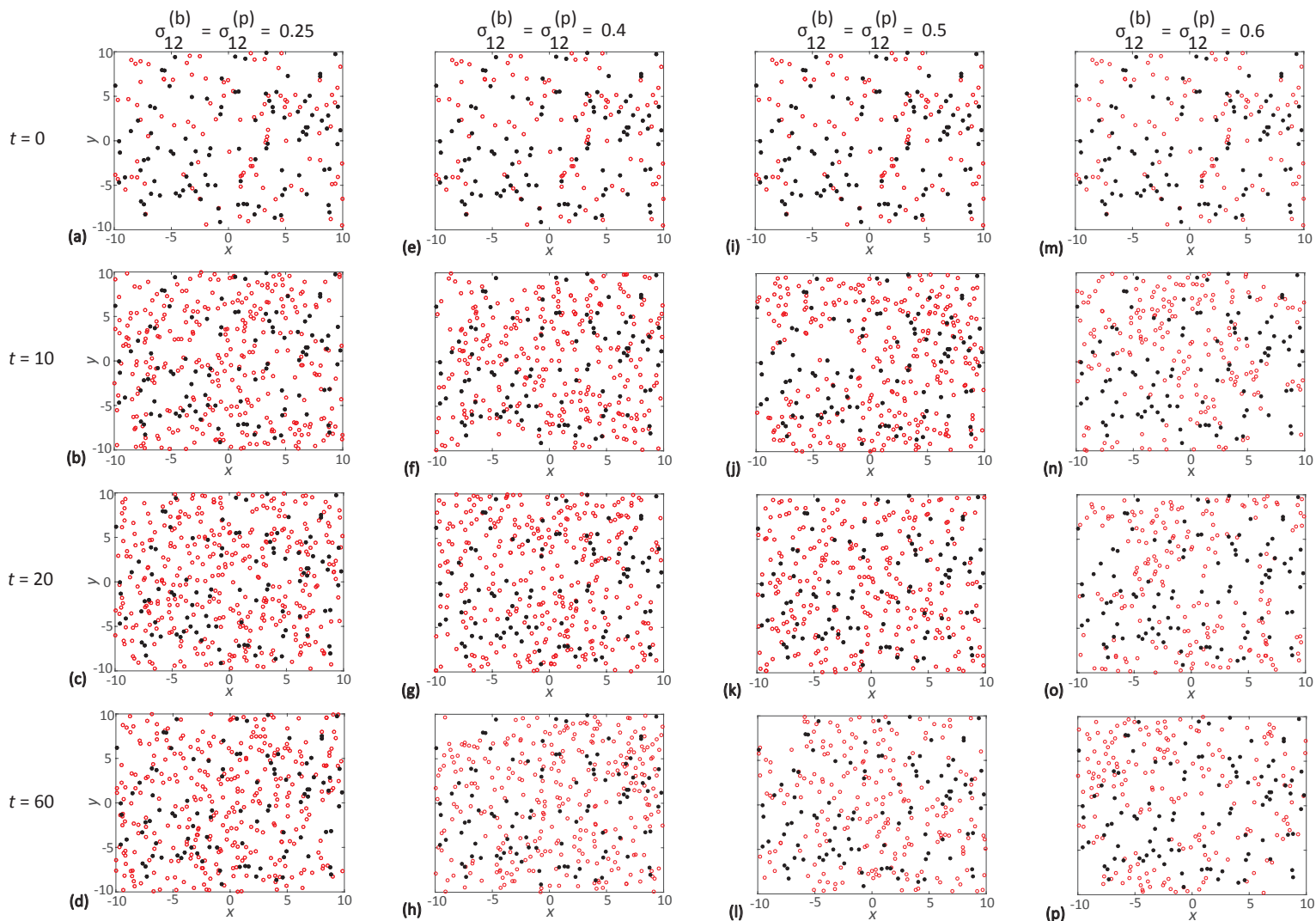


Figure 2.5: IBM snapshots showing the impact of increasing obstacle size. Each row shows a snapshot of the IBM at $t = 0, 10, 20$ and 60 , respectively. Results in **a-d**, **e-h**, **i-l** and **m-p** show the evolution of a population of agents where $\sigma_{12}^{(p)} = \sigma_{12}^{(b)} = 0.25$; $\sigma_{12}^{(p)} = \sigma_{12}^{(b)} = 0.40$; $\sigma_{12}^{(p)} = \sigma_{12}^{(b)} = 0.50$; and $\sigma_{12}^{(p)} = \sigma_{12}^{(b)} = 0.60$, respectively. In each case the initial number of obstacles is 100. In all cases agents are red and obstacles are black. Parameter values are $p_1 = 1, d_1 = 0.5, m_1 = 5, p_2 = d_2 = m_2 = 0, \gamma_{11}^{(p)} = -0.38, \gamma_{12}^{(p)} = -0.38, \gamma_{21}^{(p)} = \gamma_{22}^{(p)} = 0, \gamma_{11}^{(b)} = 0.1, \gamma_{12}^{(b)} = 0.1, \gamma_{21}^{(b)} = \gamma_{22}^{(b)} = 0, \gamma_{11}^{(m)} = \gamma_{21}^{(m)} = \gamma_{22}^{(m)} = 0, \sigma_{11}^{(p)} = 0.5, \sigma_{11}^{(b)} = 0.5, \sigma_{11}^{(m)} = 0.5, \mu_1^{(s)} = 0.4, \mu_2^{(s)} = 0.4, \sigma_1^{(s)} = 0.1, \sigma_2^{(s)} = 0.1, \sigma_1^{(d)} = 0.5$, and $\sigma_2^{(d)} = 0.5$.

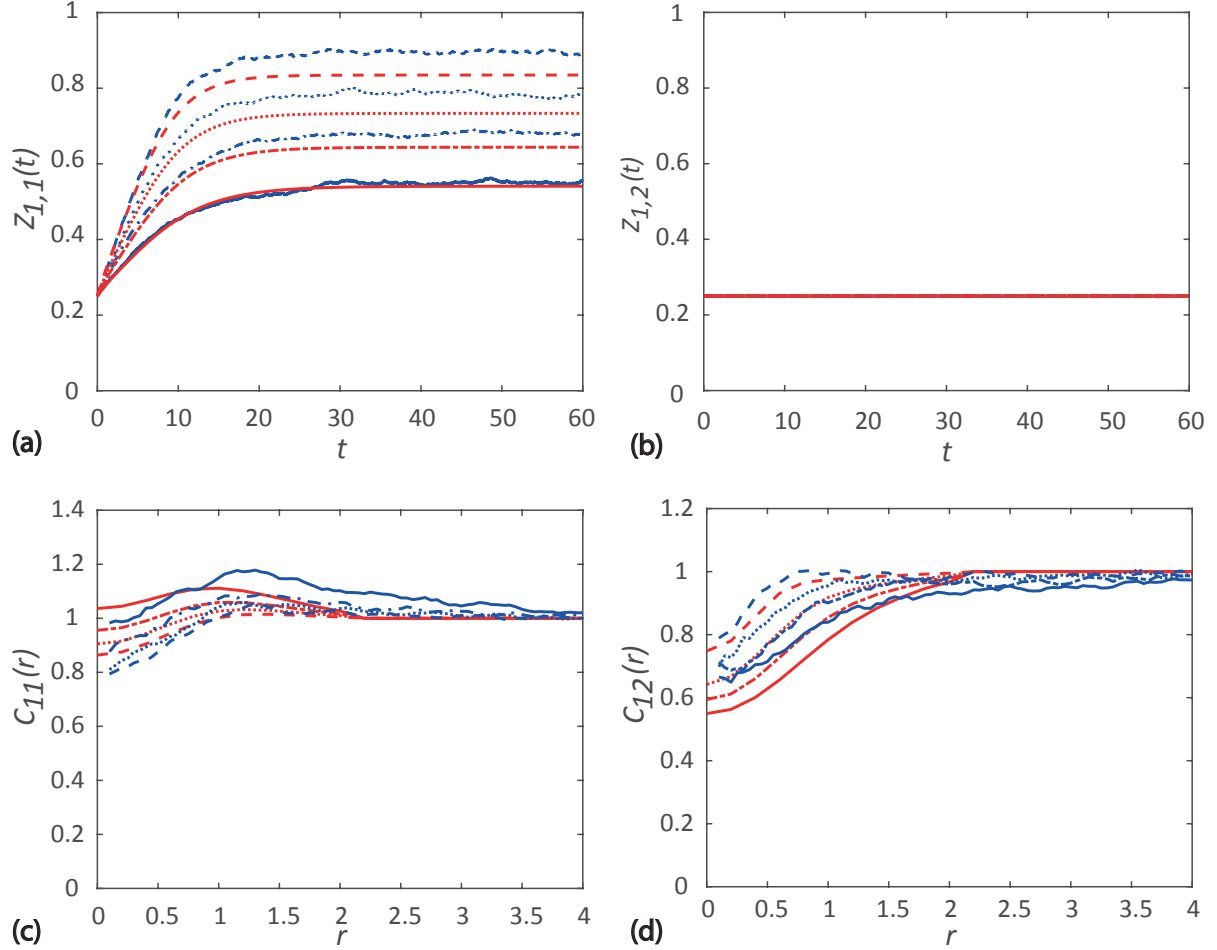


Figure 2.6: Comparison of spatial moment results and averaged data from 40 identically-prepared realizations of the IBM. Results in **a** show the evolution of the first spatial moment for agents, $Z_{1,1}(t)$. Various results are superimposed for different obstacle size: $\sigma_{12}^{(p)} = \sigma_{12}^{(b)} = 0.25$ (dashed); $\sigma_{12}^{(p)} = \sigma_{12}^{(b)} = 0.40$ (dotted); $\sigma_{12}^{(p)} = \sigma_{12}^{(b)} = 0.50$ (dash-dotted); and $\sigma_{12}^{(p)} = \sigma_{12}^{(b)} = 0.60$ (solid). Results in **b** show the constant first spatial moment for the obstacles. Results in **c-d** show the second spatial moment of agents expressed in terms of $C_{11}(r)$ and $C_{12}(r)$, respectively. Both PCFs are given at $t = 60$. **d** The curves in red correspond to results from the spatial moment dynamics model, whereas curves in blue correspond to averaged data from the IBM. Parameter values are $p_1 = 1$, $d_1 = 0.5$, $m_1 = 5$, $p_2 = d_2 = m_2 = 0$, $\gamma_{11}^{(p)} = -0.38$, $\gamma_{12}^{(p)} = -0.38$, $\gamma_{21}^{(p)} = \gamma_{22}^{(p)} = 0$, $\gamma_{11}^{(b)} = 0.1$, $\gamma_{12}^{(b)} = 0.1$, $\gamma_{21}^{(b)} = \gamma_{22}^{(b)} = 0$, $\gamma_{11}^{(m)} = \gamma_{12}^{(m)} = \gamma_{21}^{(m)} = \gamma_{22}^{(m)} = 0$, $\sigma_{11}^{(p)} = 0.5$, $\sigma_{12}^{(b)} = 0.5$, $\sigma_{11}^{(m)} = 0.5$, $\mu_1^{(s)} = 0.4$, $\mu_2^{(s)} = 0.4$, $\sigma_1^{(s)} = 0.1$, $\sigma_2^{(s)} = 0.1$, $\sigma_1^{(d)} = 0.5$, and $\sigma_2^{(d)} = 0.5$.

2.7.3 Effect of varying the obstacle interaction strength

Finally, we explore how variations in interaction strength, and the nature of the interactions between agents and obstacles, influence the spatial structure and the dynamics of the agent population. We examine the influence of both attractive interactions, as well as repulsive interactions. Similar to the previous simulations in Figure 2.5, we consider a random initial spatial distribution of agents and obstacles with initial population size $N_1(0) = N_2(0) = 100$. We then vary the strength of interactions, $\gamma_{12}^{(b)}$, between 0.4 and -0.2. This means that we consider both attractive and repulsive interactions between agents and obstacles in this suite of simulations. Snapshots from the IBM are shown in Figure 2.7, and by repeating these stochastic simulations

many times, we can calculate the density of obstacles, the density of agents, the auto-correlation PCF and the cross-correlation PCF, as shown in Figure 2.8.

Results in Figure 2.7(a)-(d) show the spatial structure arising when there is a relatively strong repulsive bias between the obstacles and agents. This repulsion means that agents tend to move away from the obstacles, leading to the formation of a segregated spatial structure among agent-obstacle pairs. The PCFs, given in Figure 2.8(c)-(d), are consistent with this as we have $C_{12}(r) < 1$ over small distances. Here we note that the repulsive interactions between agents are sufficiently strong to counteract the short-range dispersal of agents. Hence we also observe a segregated spatial pattern among agents over short distances. Results in Figure 2.7(e)-(h) and Figure 2.7(i)-(l) show a similar spatial pattern, but the effects are less pronounced due to the reduced repulsion. Results in Figure 2.7(m)-(p) are quite different since we have attraction between the agents and obstacles, and the agents are biased to move towards the obstacles.

Figure 2.8(a) shows the density dynamics of agents for each of the cases considered. The agent density decreases as the bias strength decreases and the density is lowest when bias strength is negative. When the obstacle bias strength is negative, corresponding to attractive obstacles, agents form clusters around obstacles. Since a large number of agents present at short distances, the proliferation rate of agents in clusters reduces significantly. Hence the population size increases more slowly than the case where obstacles are repulsive. Figure 2.8(b) shows the constant density of obstacles in each of the four cases.

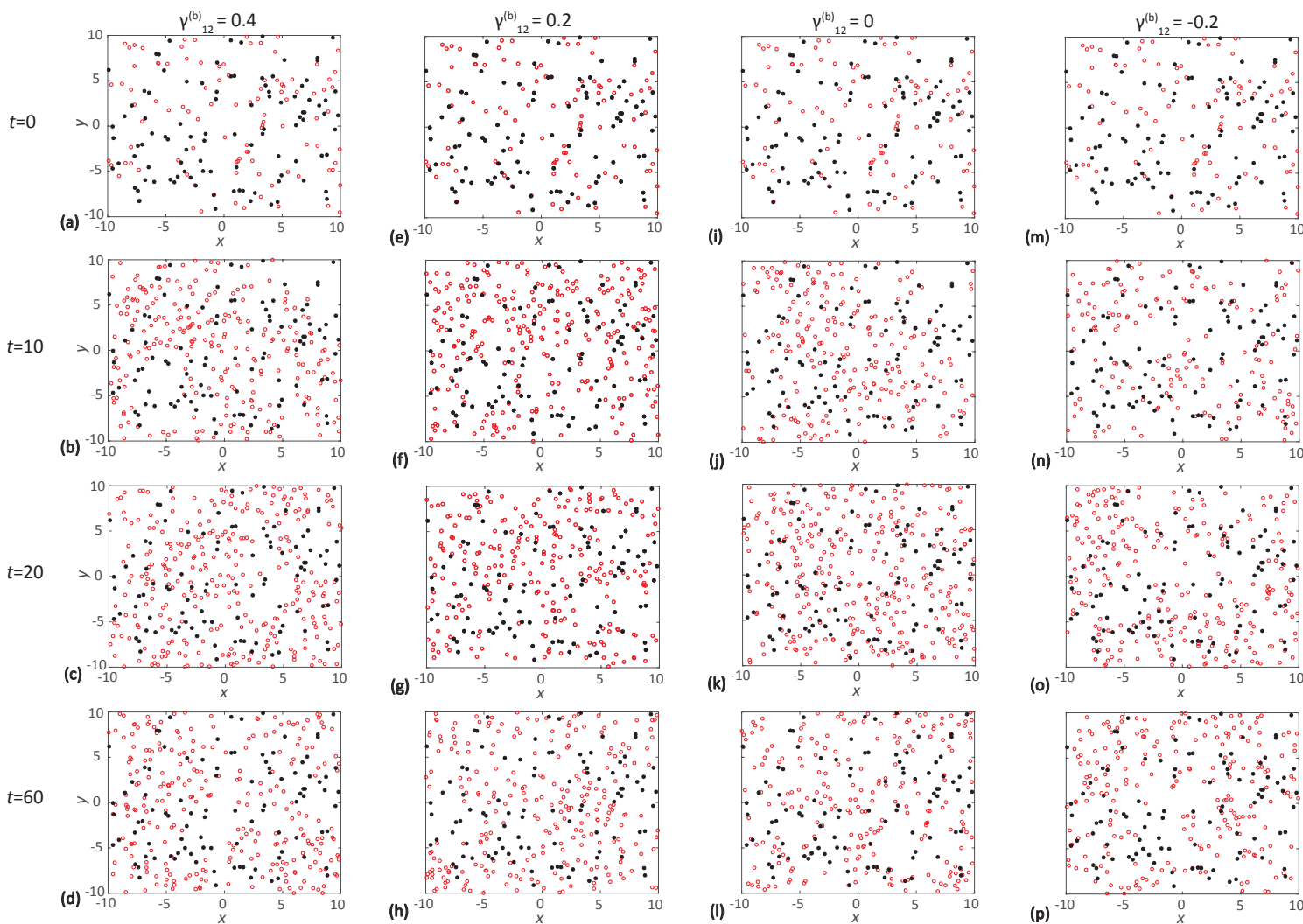


Figure 2.7: IBM snapshots showing the impact of varying the obstacle interaction strength. Each row shows a snapshot of the IBM at $t = 0, 10, 20$ and 60 , respectively. Results in **a-d**, **e-h**, **i-l** and **m-p** show the evolution of a population of agents where $\gamma_{12}^{(b)} = 0.4$; $\gamma_{12}^{(b)} = 0.2$; $\gamma_{12}^{(b)} = 0.0$; and $\gamma_{12}^{(b)} = -0.2$, respectively. In each case the initial number of obstacles is 100. In all cases agents are red and obstacles are black. Parameter values are $p_1 = 1$, $d_1 = 0.5$, $m_1 = 5$, $p_2 = d_2 = m_2 = 0$, $\gamma_{11}^{(p)} = -0.38$, $\gamma_{12}^{(p)} = -0.38$, $\gamma_{21}^{(p)} = \gamma_{22}^{(p)} = 0$, $\gamma_{11}^{(b)} = 0.1$, $\gamma_{21}^{(b)} = \gamma_{22}^{(b)} = 0$, $\gamma_{11}^{(m)} = \gamma_{12}^{(m)} = \gamma_{21}^{(m)} = \gamma_{22}^{(m)} = 0$, $\sigma_{11}^{(p)} = 0.5$, $\sigma_{12}^{(p)} = 0.5$, $\sigma_{21}^{(p)} = 0.5$, $\sigma_{22}^{(p)} = 0.5$, $\sigma_{11}^{(b)} = 0.5$, $\sigma_{12}^{(b)} = 0.5$, $\sigma_{21}^{(b)} = 0.5$, $\sigma_{22}^{(b)} = 0.5$, $\sigma_{11}^{(m)} = 0.5$, $\sigma_{12}^{(m)} = 0.5$, $\sigma_{21}^{(m)} = 0.5$, $\sigma_{22}^{(m)} = 0.5$, $\mu_1^{(s)} = 0.4$, $\mu_2^{(s)} = 0.4$, $\sigma_1^{(s)} = 0.1$, $\sigma_2^{(s)} = 0.1$, $\sigma_1^{(d)} = 0.5$, and $\sigma_2^{(d)} = 0.5$.

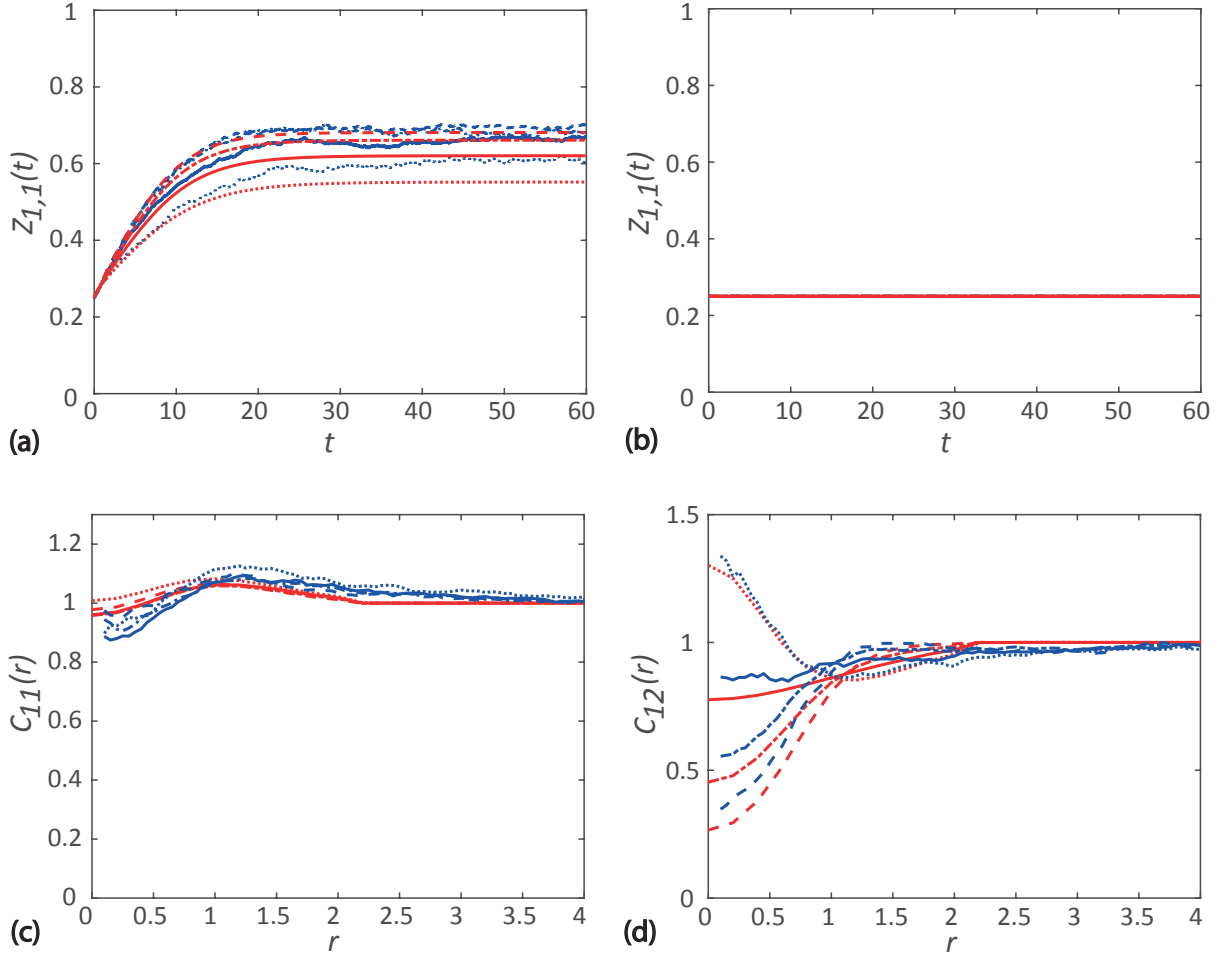


Figure 2.8: Comparison of spatial moment results and averaged data from 40 identically-prepared realizations of the IBM. Results in **a** show the evolution of the first spatial moment for agents, $Z_{1,1}(t)$. Various results are superimposed for different obstacle interaction strength: $\gamma_{12}^{(b)} = 0.4$ (dashed); $\gamma_{12}^{(b)} = 0.2$ (dash-dotted); $\gamma_{12}^{(b)} = 0.0$ (solid); and $\gamma_{12}^{(b)} = -0.2$ (dotted). Results in **b** show the constant first spatial moment for the obstacles. Results in **c-d** show the second spatial moment of agents expressed in terms of $C_{11}(r)$ and $C_{12}(r)$, respectively. Both PCFs are given at $t = 60$. **d** The curves in red correspond to results from the spatial moment dynamics model, whereas curves in blue correspond to averaged data from the IBM. Parameter values are $p_1 = 1$, $d_1 = 0.5$, $m_1 = 5$, $p_2 = d_2 = m_2 = 0$, $\gamma_{11}^{(p)} = -0.38$, $\gamma_{12}^{(p)} = -0.38$, $\gamma_{21}^{(p)} = \gamma_{22}^{(p)} = 0$, $\gamma_{11}^{(b)} = 0.1$, $\gamma_{21}^{(b)} = \gamma_{22}^{(b)} = 0$, $\gamma_{11}^{(m)} = \gamma_{12}^{(m)} = \gamma_{21}^{(m)} = \gamma_{22}^{(m)} = 0$, $\sigma_{11}^{(p)} = 0.5$, $\sigma_{12}^{(p)} = 0.5$, $\sigma_{21}^{(p)} = 0.5$, $\sigma_{22}^{(p)} = 0.5$, $\sigma_{11}^{(b)} = 0.5$, $\sigma_{12}^{(b)} = 0.5$, $\sigma_{21}^{(b)} = 0.5$, $\sigma_{22}^{(b)} = 0.5$, $\sigma_{11}^{(m)} = 0.5$, $\sigma_{12}^{(m)} = 0.5$, $\sigma_{21}^{(m)} = 0.5$, $\sigma_{22}^{(m)} = 0.5$, $\mu_1^{(s)} = 0.4$, $\mu_2^{(s)} = 0.4$, $\sigma_1^{(s)} = 0.1$, $\sigma_2^{(s)} = 0.1$, $\sigma_1^{(d)} = 0.5$, and $\sigma_2^{(d)} = 0.5$.

2.8 Conclusions

In this chapter, we develop an IBM describing multi-species neighbour-dependent birth-death-movement processes, and we derive a continuum approximation of the stochastic dynamics using a spatial moment framework. We incorporate various processes such as neighbour-dependent directional bias from multiple subpopulations, and crowding effects such as contact inhibition of proliferation and contact inhibition of motility. We use this general framework to explore the case where one subpopulation is stationary and non-proliferative, and we treat this subpopulation as acting like biological obstacles in an *in vivo* environment. This framework

allows us to explore how different properties of obstacles such as density, size and interaction strength influence the dynamics and emergence of spatial structure in the population.

Repeated simulations of the IBM are computationally inexpensive when the total number of individuals in the population is relatively small. However, such repeated simulations become computationally prohibitive as the population size increases. A useful feature of the spatial moment dynamics approximation is that the computational overhead is independent of the population size. Furthermore, if we were to explore the parameter space using the IBM to understand how variations in the interaction strength and the spatial extent of interactions lead to the emergence of spatial patterns, we would need to consider a large number of repeated stochastic simulations for each point in the parameter space. As we have shown in Figure 2.4 and Figure 2.6, simulations with certain parameter values lead to larger populations than other parameter combinations and the computational overhead associated with the IBM to describe these situations with larger population size could be significant. Under these situations, it might be more convenient to explore the parameter space using the spatial moment approximation since the computational cost is independent of the final population size.

Some previous models of cell movement treat individuals as hard spheres with a fixed radius to incorporate volume exclusion effects (e.g. Bruna and Chapman, 2012; Dyson and Baker, 2015; Plank and Simpson, 2012). The main assumption behind these models is that the individual cells occupy space in the domain and any events would lead to other individuals overlapping the same space are prohibited. Our modelling framework does not impose absolute restrictions on the locations an individual can occupy. Instead, the probabilistic motility of individuals along with the neighbour-dependent bias kernel mean that events that lead to individuals being very close are assigned a low probability. Specifying neighbourhood interaction through an interaction kernel can be thought of as a proxy model for deformable, non-spherical individuals. This is an advantage of our model over volume exclusion models because cells are known to deform in the vicinity of other cells or obstacles (Hu et al., 2007; Le Clainche and Carlier, 2008; Simpson et al., 2010b).

Overall we see that the details of the dynamics of the population of agents and the spatial structure predicted using many identically prepared realisations of the IBM is reasonably well approximated by the solution of the spatial moment model. Our results reveal some interesting features that are not obvious without careful consideration. For example, results in Figure 2.3-2.4 show that as we increase the obstacle density, we observe that the steady state density of agents decreases, as we might expect. However, when we find that the accuracy of the spatial moments prediction increases with the density of obstacles, which is not obvious. Through our exploration we see the emergence of interesting spatial patterns as we vary the properties of obstacles. For example, results in Figure 2.3-2.4 shows that the long time steady arrangement of agents is segregated at short distances when there is a sufficiently low density of obstacles present. In contrast, we see a clustered arrangement of agents at short distances when there is a sufficiently large density of obstacles present.

While our modelling framework is relatively general, there are many ways that it could be extended. For example, in this work we consider a spatially uniform initial distribution of individuals, and this kind of simulation is relevant to study certain cell biology experiments, such as a *proliferation assay*. However, other kinds of experiments, such as *scratch assays*, are initiated by considering an initial density of cells that varies spatially. To deal with this generalisation, both the IBM and our analysis needs modification. Furthermore, in this study we always consider stationary obstacles. However, in some applications it is thought that mobile obstacles are more relevant (Wedemeier et al., 2009), and this could be dealt with by setting the obstacle motility rate to be positive. Previous studies in ecology focusing on the birth-death processes of sessile organisms such as plants, consider fixed points in space corresponding to the locations of maximum resource availability in the habitats with an associated kernel (North and Ovaskainen, 2007). Evaluating and summing the kernel over all these points leads to an environmental surface which measures the quality of habitats in the context of the evolution of dispersal. We note that the neighbour-dependent birth-death-movement model presented here can be extended to include the dispersal dependent upon densities of conspecifics or heterospecifics, or on habitat quality for both sessile and motile organisms (North et al., 2011). We leave these extensions for future consideration.

Chapter 2A

Additional results for Chapter 2

2A.1 Definition of spatial moments for general multi-species model

We define a random variable, $N_i(A)$, to be the number of individuals from subpopulation i in a region $A \subset \mathbb{R}^2$ at a given time t . Let $D_h(\mathbf{x}) \subset \mathbb{R}^2$ denote a disc of radius h centred on $\mathbf{x} \in \mathbb{R}^2$. Since we are considering population dynamics in a spatially homogeneous environment, we assume without loss of generality that one of the individual is located at the origin, $\mathbf{x} = \mathbf{0}$. In our simulations, we approximate the first spatial moment, $Z_{1,i}(t)$, by dividing the population size of individuals from subpopulation i , given by $N_i(t)$, by the area of the domain, L^2 . Formally we have,

$$Z_{1,i}(t) = \lim_{h \rightarrow 0} \frac{1}{h} \mathbb{E}[N_i(D_h(\mathbf{0}))]. \quad (2A.1)$$

The second spatial moment, $Z_{2,ij}(\boldsymbol{\xi}, t)$, is the average density of pairs of individuals. For a pair of individuals consisting of an individual from subpopulation i present at $\mathbf{x} = \mathbf{0}$, and an individual from subpopulation j present at a displacement $\boldsymbol{\xi}$, we have

$$Z_{2,ij}(\boldsymbol{\xi}, t) = \lim_{h \rightarrow 0} \frac{1}{h^2} \mathbb{E}[N_i(D_h(\mathbf{0}))N_j(D_h(\boldsymbol{\xi})) - \delta_{ij}N_i(D_h(\mathbf{0}) \cap D_h(\boldsymbol{\xi}))]. \quad (2A.2)$$

The second term in the expectation in Equation (2A.2) is necessary to avoid counting self-pairs. If the discs $D_h(\mathbf{0})$ and $D_h(\boldsymbol{\xi})$ are non-overlapping, this term becomes zero (Plank and Law, 2015). The third spatial moment is the density of triplets of individuals, and is similarly

defined as,

$$\begin{aligned} Z_{3,ijk}(\boldsymbol{\xi}, \boldsymbol{\xi}', t) = & \lim_{h \rightarrow 0} \frac{1}{h^3} \mathbb{E} \left[N_i(D_h(\mathbf{0})) N_j(D_h(\boldsymbol{\xi})) N_k(D_h(\boldsymbol{\xi}')) \right. \\ & - \delta_{ij} N_i(D_h(\mathbf{0}) \cap D_h(\boldsymbol{\xi})) N_k(D_h(\boldsymbol{\xi}')) \\ & - \delta_{ik} N_i(D_h(\mathbf{0}) \cap D_h(\boldsymbol{\xi}')) N_j(D_h(\boldsymbol{\xi})) \\ & - \delta_{jk} N_j(D_h(\boldsymbol{\xi}) \cap D_h(\boldsymbol{\xi}')) N_i(D_h(\mathbf{0})) \\ & \left. + 2\delta_{ijk} N_i(D_h(\mathbf{0}) \cap D_h(\boldsymbol{\xi}') \cap D_h(\boldsymbol{\xi})) \right]. \end{aligned} \quad (2A.3)$$

Again, the extra terms in Equation (2A.3) are needed to avoid counting non-distinct triplets.

2A.2 Conditional probabilities for the presence of individuals

In this section, we derive an expression for the probability of finding individuals separated by a given displacement, conditional on the presence of other individuals. The conditional probability of finding an individual from subpopulation j at a displacement $\boldsymbol{\xi}$, given the reference individual from subpopulation i is located at $\mathbf{0}$, is defined as,

$$\lim_{h \rightarrow 0} \frac{1}{h} \mathbb{P} [N_j(D_h(\boldsymbol{\xi})) = 1 \mid N_i(D_h(\mathbf{0})) = 1]. \quad (2A.4)$$

Using the following property of conditional probability,

$$\mathbb{P}[A \mid B] = \frac{\mathbb{P}[A \cap B]}{\mathbb{P}[B]}, \quad (2A.5)$$

we rewrite Equation (2A.4) as,

$$\lim_{h \rightarrow 0} \frac{1}{h} \frac{\mathbb{P}[N_j(D_h(\boldsymbol{\xi})) = 1 \cap N_i(D_h(\mathbf{0})) = 1]}{\mathbb{P}[N_i(D_h(\mathbf{0}))]} \quad (2A.6)$$

Using the definitions of spatial moments, as defined in Section 2A.1, we write the probabilities appearing in the numerator and denominator of Equation (2A.6) as,

$$\mathbb{P}[N_i(D_h(\mathbf{0})) = 1] = Z_{1,i}(t)h, \quad (2A.7)$$

$$\mathbb{P}[N_j(D_h(\boldsymbol{\xi})) = 1 \cap N_i(D_h(\mathbf{0})) = 1] = Z_{2,ij}(\boldsymbol{\xi}, t)h^2. \quad (2A.8)$$

Hence the conditional probability of finding an individual from subpopulation j at a displacement ξ from the reference individual from subpopulation i at $\mathbf{0}$ can be written as,

$$\lim_{h \rightarrow 0} \frac{1}{h} \mathbb{P}[N_j(D_h(\xi)) = 1 \mid N_i(D_h(\mathbf{0})) = 1] = \frac{Z_{2,ij}(\xi, t)}{Z_{1,i}(t)}. \quad (2A.9)$$

Similarly, we write the conditional probability of finding an individual from subpopulation k at a displacement ξ' , given that a pair of individuals from subpopulations j and i , located at ξ and $\mathbf{0}$, respectively, as

$$\begin{aligned} & \lim_{h \rightarrow 0} \frac{1}{h} \mathbb{P}[N_k(D_h(\xi')) = 1 \mid N_j(D_h(\xi)) = 1 \cap N_i(D_h(\mathbf{0})) = 1] \\ &= \lim_{h \rightarrow 0} \frac{1}{h} \frac{\mathbb{P}[N_k(D_h(\xi')) = 1 \cap N_j(D_h(\xi)) = 1 \cap N_i(D_h(\mathbf{0})) = 1]}{\mathbb{P}[N_j(D_h(\xi)) = 1 \cap N_i(D_h(\mathbf{0})) = 1]}, \\ &= \frac{Z_{3,ijk}(\xi, \xi', t)}{Z_{2,ij}(\xi, t)}. \end{aligned} \quad (2A.10)$$

2A.3 Calculating the expected event rates and net bias vector

Here, we derive expressions for expected event rates and net bias vector using Equations (2A.9)-(2A.10). These expected rates are required to develop the equations for the time evolution of the density of individuals and the density of pairs of individuals. The expected movement rate for an individual from subpopulation i depends on the presence of an individual from subpopulation j at a displacement ξ . The contribution from the neighbouring individual to the expected movement rate is given by the interaction kernel, $\omega_{ij}^{(m)}(|\xi|)$. To compute the net contribution, we multiply the interaction kernel by the conditional probability of having an individual present, and integrate over all possible displacements. This gives,

$$M_{1,i}(t) = m_i + \lim_{h \rightarrow 0} \sum_j \int \omega_{ij}^{(m)}(|\xi|) \frac{P[N_j(D_h(\xi)) = 1 \mid N_i(D_h(\mathbf{0})) = 1]}{h} d\xi, \quad (2A.11)$$

where m_i is the intrinsic contribution to the expected movement rate. Now we use the expression for the conditional probability for the presence of individual, Equation (2A.9), to rewrite Equation (2A.11) in terms of the spatial moments, giving

$$M_{1,i}(t) = m_i + \sum_j \int \omega_{ij}^{(m)}(|\xi|) \frac{Z_{2,ij}(\xi, t)}{Z_{1,i}(t)} d\xi. \quad (2A.12)$$

Similarly, we compute the expected proliferation rate of an individual from subpopulation i as,

$$\begin{aligned} P_{1,i}(t) &= p_i + \lim_{h \rightarrow 0} \sum_j \int \omega_{ij}^{(p)}(|\xi|) \frac{P[N_j(D_h(\xi)) = 1 \mid N_i(D_h(\mathbf{0})) = 1]}{h} d\xi, \\ &= p_i + \sum_j \int \omega_{ij}^{(p)}(|\xi|) \frac{Z_{2,ij}(\xi, t)}{Z_{1,i}(t)} d\xi. \end{aligned} \quad (2A.13)$$

To derive the dynamics of the second spatial moments, we need to compute the expected event rates for an individual from subpopulation i , which forms a pair with another individual associated with subpopulation j and separated by a displacement ξ . In this case, the neighbour-dependent component of the event rates depends on the conditional presence of another individual from subpopulation k at a displacement ξ' . We compute the neighbour-dependent component of the expected movement rate of an individual from subpopulation i , that forms a pair with another individual from subpopulation j . To do this we multiply the movement interaction kernel, $\omega_{ij}^{(m)}(|\xi|)$, with the conditional probability of having a pair of individuals, at a displacement ξ , given that an individual from subpopulation k is present at a displacement ξ' , and integrating over all possible displacements, ξ' . The integration over ξ' does not account for the contribution of the individual from subpopulation j located at displacement ξ , which forms a pair with the reference individual, and so an additional term, $\omega_{ij}^{(m)}(|\xi|)$, must be added to incorporate contributions from all neighbouring individuals. Hence the net expected movement rate is given by,

$$\begin{aligned} M_{2,ij}(\xi, t) &= m_i + \omega_{ij}^{(m)}(|\xi|) \\ &+ \lim_{h \rightarrow 0} \sum_k \int \omega_{ik}^{(m)}(|\xi'|) \frac{P[N_k(D_h(\xi')) = 1 \mid N_j(D_h(\xi)) = 1 \cap N_i(D_h(\mathbf{0})) = 1]}{h} d\xi' \end{aligned} \quad (2A.14)$$

Now we use Equation (2A.10) to re-write Equation (2A.11) in terms of the spatial moments as,

$$M_{2,ij}(\xi, t) = m_i + \sum_k \int \omega_{ik}^{(m)}(|\xi'|) \frac{Z_{3,ijk}(\xi, \xi', t)}{Z_{2,ij}(\xi, t)} d\xi' + \omega_{ij}^{(m)}(|\xi|). \quad (2A.15)$$

Similarly, we compute the expected proliferation rate of an individual from subpopulation i , which is in pair with an individual of subpopulation j as,

$$\begin{aligned} P_{2,ij}(\xi, t) &= p_i + \omega_{ij}^{(p)}(|\xi|) \\ &+ \lim_{h \rightarrow 0} \sum_k \int \omega_{ik}^{(p)}(|\xi'|) \frac{P[N_k(D_h(\xi')) = 1 \mid N_j(D_h(\xi)) = 1 \cap N_i(D_h(\mathbf{0})) = 1]}{h} d\xi', \\ &= p_i + \sum_k \int \omega_{ik}^{(p)}(|\xi'|) \frac{Z_{3,ijk}(\xi, \xi', t)}{Z_{2,ij}(\xi, t)} d\xi' + \omega_{ij}^{(p)}(|\xi|). \end{aligned} \quad (2A.16)$$

Next, we compute the net bias vector $\mathbf{B}_{2,ij}(\xi)$ for an individual from subpopulation i conditional on the presence of another individual from subpopulation j at a displacement ξ . The contribution of the neighbouring individual to the directional bias of the reference individual is defined as the gradient of the bias kernel, $\nabla\omega_{ij}^{(b)}(|\xi|)$ (Binny et al. 2016a). We compute the neighbour-dependent contribution to the net bias vector of an individual from subpopulation i that forms a pair with another individual from subpopulation j , by multiplying the gradient of the bias interaction kernel with the conditional probability of having a pair of individuals at a displacement ξ , given that an individual from subpopulation k is present at a displacement ξ' , and integrating over all possible displacements ξ' . As before, an additional term, $\nabla\omega_{ij}^{(b)}(|\xi|)$, is required to account for the contribution of the individual from subpopulation j located at the displacement ξ , which forms a pair with the reference individual. Hence the net bias vector is given by,

$$\begin{aligned}\mathbf{B}_{2,ij}(\xi, t) &= \mathbf{b}_i + \nabla\omega_{ij}^{(b)}(|\xi|) \\ &+ \lim_{h \rightarrow 0} \sum_k \int \nabla\omega_{ik}^{(b)}(|\xi'|) \frac{P[N_k(D_h(\xi')) = 1 \mid N_j(D_h(\xi)) = 1 \cap N_i(D_h(\mathbf{0})) = 1]}{h} d\xi', \\ &= \mathbf{b}_i + \sum_k \int \nabla\omega_{ik}^{(b)}(|\xi'|) \frac{Z_{3,ijk}(\xi, \xi', t)}{Z_{2,ij}(\xi, t)} d\xi' + \nabla\omega_{ij}^{(b)}(|\xi|).\end{aligned}\quad (2A.17)$$

2A.4 Dynamics of the second spatial moment

In this section, we outline the derivation of the equations governing the dynamics of the average density of pairs of individuals. To derive the equation governing the rate of change of pair density, we need to consider events that result in loss of existing pairs and events that lead to the creation of new pairs. Figure 2A.1 shows a schematic representation of possible configurations that lead to change in the total number of pairs separated by a displacement ξ . Figure 2A.1(a) shows a pair of individuals, separated by a displacement ξ , where the pair is composed of individuals from subpopulations i and j , respectively. A movement or death event for either of these individuals results in the destruction of the pair. The movement of an individual occurs with a rate $M_{2,ij}(\xi, t)$ and the death occurs with a rate d_i .

Now we consider the case where the creation of a new pair of individuals separated by a displacement ξ occurs. Figure 2A.1(b) shows a pair composed of individuals from subpopulation i and j , separated by a displacement $\xi' + \xi$. When an individual moves a displacement ξ' , or places a daughter at a displacement ξ' , as shown in Figure 2A.1(b), a pair of individuals is created at a displacement ξ . The movement of the individual from subpopulation i that forms a pair with an individual from subpopulation j separated by a displacement $\xi' + \xi$, to a displacement ξ' occurs at a rate $\mu_{2,ij}^{(m)}(\xi', \xi' + \xi, t)M_{2,ij}(\xi' + \xi, t)$. Similarly, the placement of a daughter from subpopulation i at a displacement ξ' after a proliferation event occurs at rate $\mu_i^{(p)}(\xi')P_{2,ij}(\xi' + \xi, t)$. Figure 2A.1(c) shows the case when an individual from subpopulation i

proliferates, and places a daughter at a displacement $-\xi$, generating a pair of individuals at a displacement of ξ . The rate for this event is $\mu_i^{(p)}(-\xi) P_{1,i}(t)$. By combining these terms describing the rate at which pairs of individuals are lost and gained, we obtain,

$$\begin{aligned} \frac{\partial}{\partial t} Z_{2,ij}(\xi, t) = & - \left(M_{2,ij}(\xi, t) + M_{2,ji}(-\xi, t) + d_i + d_j \right) Z_{2,ij}(\xi, t) \\ & + \int \left(\mu_{2,ij}^{(m)}(\xi', \xi' + \xi, t) M_{2,ij}(\xi' + \xi, t) \right. \\ & \left. + \mu_i^{(p)}(\xi') P_{2,ij}(\xi' + \xi, t) \right) Z_{2,ij}(\xi' + \xi, t) d\xi' \\ & + \int \left(\mu_{2,ji}^{(m)}(\xi', \xi' - \xi, t) M_{2,ji}(\xi' - \xi, t) \right. \\ & \left. + \mu_j^{(p)}(\xi') P_{2,ji}(\xi' - \xi, t) \right) Z_{2,ji}(\xi' - \xi, t) d\xi' \\ & + 2\delta_{ij}\mu_j^{(p)}(-\xi) P_{1,j}(t) Z_{1,j}(t). \end{aligned} \quad (2A.18)$$

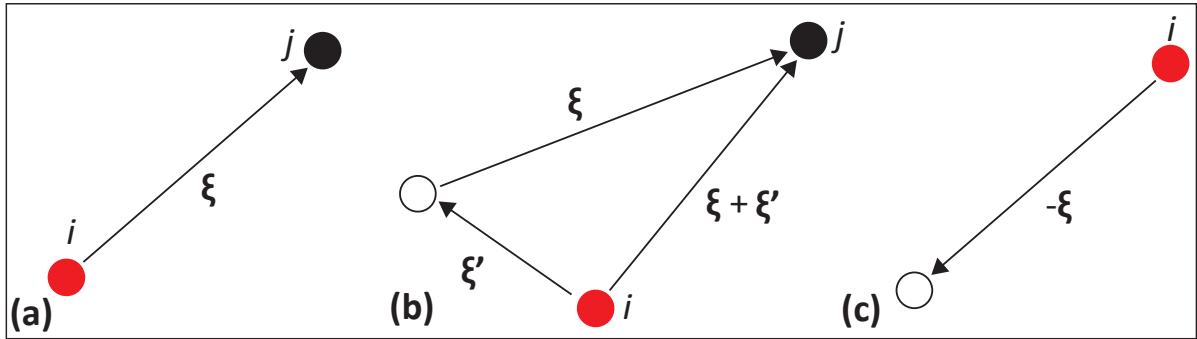


Figure 2A.1: Schematic representation of the possible configurations of individuals which results in a change of the density of pairs of individuals separated by a displacement ξ . **a** A pair of individuals associated with subpopulations i and j separated by a displacement ξ . A movement or death event acting on either individual leads to the loss of the pair. **b** A pair of individuals associated with subpopulations i and j separated by a displacement $\xi + \xi'$. A movement event or the placement of a daughter individual after a proliferation event over a displacement ξ' results in the creation of a pair of individuals separated by a displacement ξ . **c** The placement of a daughter individual at a displacement $-\xi$ results in the creation of a pair of individuals separated by a displacement ξ .

2A.5 Numerical methods

The system of equations governing the dynamics of the second spatial moments, Equations (2.30)-(2.33) are solved numerically using the forward Euler method. The numerical solutions are obtained using the MATLAB programming language. The numerical scheme involves spatially discretising the displacement, $\xi = (\xi_x, \xi_y)$, over the domain $\{-\xi_{\max} \leq \xi_x, \xi_y \leq \xi_{\max}\}$, with a grid spacing $\Delta\xi$. In all cases we have $\Delta\xi = 0.2$, and our calculations show that this choice is sufficient to produce grid-independent results. We choose ξ_{\max} to be sufficiently large so that $Z_{2,ij}(\xi, t) \approx Z_{1,i}(t) \times Z_{1,j}(t)$ at the boundary. The integral terms in Equations (2.20)-(2.21) and Equations (2.24)-(2.33) are approximated using the trapezoid rule. To evaluate the integrals we

need the values of $Z_{2,ij}(\xi + \xi', t)$. For sufficiently large ξ and ξ' , these values will lie outside of the computational domain. In that case, we replace those terms with the value of $Z_{2,ij}(\xi, t)$ at the boundary, $Z_{2,ij}((\xi_{\max}, \xi_{\max}), t)$. The movement and dispersal PDFs are normalised using the trapezoid rule with the same spatial discretisation such that $\int \mu_{2,ij}^{(m)}(\xi, \xi', t) d\xi = 1$ and $\int \mu_i^{(p)}(\xi) d\xi = 1$, for a fixed value of ξ' .

To solve the system of equations corresponding to the second spatial moments, Equations (2.30)-(2.33), we also need the values of $Z_{1,1}(t)$ and $Z_{1,2}(t)$. The large computational domain, together with the fact that we only consider local interactions, means that the usual mean-field condition will hold at large displacements. This means that we can evaluate the first moments without solving the Equations (2.22)-(2.23). At each time step, we use values of $Z_{2,11}(\xi, t)$ and $Z_{2,22}(\xi, t)$ at the boundary to compute the first moments since we have $Z_{1,1}(t) = \sqrt{Z_{2,11}((\xi_{\max}, \xi_{\max}), t)}$ and $Z_{1,2}(t) = \sqrt{Z_{2,22}((\xi_{\max}, \xi_{\max}), t)}$, respectively. To compare predictions from the spatial moment model with results from the IBM, we compute the auto-correlation and cross-correlation PCFs, $Z_{2,11}(\xi, t)/Z_{1,1}(t)$ and $Z_{2,12}(\xi, t)/(Z_{1,1}(t)Z_{1,2}(t))$, respectively. The initial condition used in solving the dynamics of the second spatial moment is $Z_{2,ij}(\xi, 0) = Z_{1,i}(0)Z_{1,j}(0)$ at $t = 0$. For all results we set the time step to be $dt = 0.1$, which is sufficiently small so that our numerical solutions are insensitive to this choice.

Statement of Contribution of Co-Authors for Thesis by Published Paper

The authors listed below have certified that:

1. they meet the criteria for authorship and that they have participated in the conception, execution, or interpretation, of at least that part of the publication in their field of expertise;
2. they take public responsibility for their part of the publication, except for the responsible author who accepts overall responsibility for the publication;
3. there are no other authors of the publication according to these criteria;
4. potential conflicts of interest have been disclosed to (a) granting bodies, (b) the editor or publisher of journals or other publications, and (c) the head of the responsible academic unit, and
5. they agree to the use of the publication in the student's thesis and its publication on the [QUT's ePrints site](#) consistent with any limitations set by publisher requirements.

In the case of chapter 3:

Surendran Anudeep, Plank Michael J., Simpson Matthew J. 2019 Spatial structure arising from chase-escape interactions with crowding. *Scientific Reports* 9: 14988.

Contributor	Statement of contribution*
Anudeep Surendran <i>Anudeep Surendran</i>	Designed the study, derived the continuum moment dynamics equations, developed the codes for numerical simulation of the IBM and spatial moment model, performed numerical simulations, generated results, interpreted the results, drafted the manuscript, and revised the manuscript during peer-review process.
19/08/2020	
Michael J. Plank	Designed the study, interpreted the results, edited the manuscript during initial submission and subsequent revision during peer-review process.
Matthew J. Simpson	Designed the study, supervised the research, interpreted the results, edited the manuscript during initial submission and subsequent revision during peer review process and acted as the corresponding author.

Principal Supervisor Confirmation

I have sighted email or other correspondence from all Co-authors confirming their certifying authorship. (If the Co-authors are not able to sign the form please forward their email or other correspondence confirming the certifying authorship to the GRC).

MATTHEW SIMPSON
Name

M. Simpson
Signature

26 | 8 | 2020
Date

Chapter 3

Spatial structure arising from chase-escape interactions with crowding

3.1 Preamble

This chapter is a paper published in the *Scientific Reports*.

Surendran Anudeep, Plank Michael J., Simpson Matthew J. 2019 Spatial structure arising from chase-escape interactions with crowding. *Scientific Reports* 9: 14988. [DOI:10.1038/s41598-019-51565-3](https://doi.org/10.1038/s41598-019-51565-3). [bioRxiv Preprint](#).

In this chapter, we address the research question 2 of the thesis: How does the directional movement of individuals arising out of chase-escape interactions generate macroscale spatial structures in a multispecies conservative community? This chapter can be viewed as a particular application of the models developed in Chapter 2. Here we exclusively look at the importance of the movement and directional interactions and do not consider proliferation and death. Such considerations are of great interest because many previous studies that use spatial moment dynamics framework have origin in plant ecology, where birth and death are considered as the mechanisms that drive spatial structure formation and movement is irrelevant (Bolker and Pacala, 1997; Bolker and Pacala, 1999; Murrell and Law, 2003). Some of the more recent studies that use spatial moment framework in the context of cell biology experiments attributed simultaneous movement and proliferation as the drivers of spatial structure formation (Binny et al., 2016b; Browning et al., 2018). Here we demonstrate that the biased movement of individuals due to directional interactions such as chase-escape interactions can generate spatial structures.

3.2 Abstract

Movement of individuals, mediated by localised interactions, plays a key role in numerous processes including cell biology and ecology. In this chapter, we investigate an individual-based

model accounting for various intraspecies and interspecies interactions in a community consisting of two distinct species. In this framework we consider one species to be *chasers* and the other species to be *escapees*, and we focus on chase-escape dynamics where the chasers are biased to move towards the escapees, and the escapees are biased to move away from the chasers. This framework allows us to explore how individual-level directional interactions scale up to influence spatial structure at the macroscale. To focus exclusively on the role of motility and directional bias in determining spatial structure, we consider conservative communities where the number of individuals in each species remains constant. To provide additional information about the individual-based model, we also present a mathematically tractable deterministic approximation based on describing the evolution of the spatial moments. We explore how different features of interactions including interaction strength, spatial extent of interaction, and relative density of species influence the formation of the macroscale spatial patterns.

3.3 Introduction

Movement of, and interaction between individuals is fundamental to various processes in cell biology and ecology (Williams and Solnica-Krezel, 2017; Oliveira et al., 2016; Janosov et al., 2017). These interactions are generated by a number of factors such as the release and detection of chemical signals, mechanical forces, as well as chase and escape dynamics between animals (Baker et al., 2019; Raz and Mahabaleshwar, 2009; Tambe et al., 2011; Vicsek, 2010), and such interactions can be associated with attractive or repulsive bias (Keeley et al., 2014; Binny et al., 2016a). Typically, chase-escape interactions in animal communities involve interspecies interactions between two species where the chasers are biased to move towards the escapees, and the escapees are biased to move away from the chasers (Vicsek, 2010; Oshanin et al., 2009). Such chase-escape interactions are relevant to the development of skin patterns in zebrafish involving the movement of two types of pigment cells: melanophores and xanthophores. Here, melanophores tend to move away from xanthophores as xanthophores pursue the melanophores (Inaba et al., 2012). An example of chase-escape interaction among a single species is in the case of locusts. Cannibalism within the population is an important source of nutrients for locusts. Here, individual locusts tend to escape in response to the threat of being attacked by its conspecifics. Concurrently, they pursue others in the migratory band in search of nutrients (Bazazi et al., 2008; Guttal et al., 2015; Romanczuk et al., 2009). Another example of chase-escape dynamics includes herding behaviour, such as in the case of dogs herding sheep (King et al., 2012; Wood and Ackland, 2007; Strombom et al., 2014). Neighbour dependent movement and directional bias can act in unison to generate distinct spatial patterns in the cell population such as cellular aggregation (Thomas et al., 2006). Similarly, interactions in animal herds or bird flocks can also lead to the creation of spatial patterns (Delcourt et al., 2016). These observations suggest that individual level interactions have significant implications in the macroscale outcomes and motivates us to develop mathematical models to study how the

directional movement of individuals as they respond to cues from the neighbourhood, leads to the development of spatial structure.

Mathematical modelling frameworks used to describe the movement of individuals within a population include both discrete individual-based models (IBM) and continuum models that are often described in terms of differential equations (Gavagnin and Yates, 2018; Treloar et al., 2014; Binny et al., 2015). To understand the impact of key factors relating to motility, in this work we focus solely on movement processes and neglect proliferation and mortality. Many previous studies focusing on spatial moment dynamics were originally developed to study plant ecology where birth and death are the key mechanisms and motility is irrelevant (Bolker and Pacala, 1997; Bolker and Pacala, 1999; Murrell and Law, 2003; Law et al., 2003). Recently, this framework has been extended to model cell biology experiments where simultaneous movement and proliferation drives the formation of spatial structure (Binny et al., 2016b; Browning et al., 2018). In our previous work (Surendran et al., 2018), we considered a general spatial moment model of birth, death and movement process which is relevant to experimental cell biology where motility and proliferation mechanisms act in unison to generate the spatial structure. Development of spatial structure in conservative communities, solely due to motility and interactions such as chase-escape interactions is an interesting problem and to the best of our knowledge, has not been explored in a spatial moment dynamics framework. Therefore, the present work can be viewed as a particular application of our previous work (Surendran et al., 2018), where we now focus exclusively on the role of motility, and motility bias in a conservative population and we systematically explore how these interactions give rise to spatial structure in the absence of proliferation and death.

In this work we use a lattice-free IBM since this approach allows movement in any direction (Plank and Simpson, 2012). We also employ interaction kernels to specify the interactions between individuals (Plank and Law, 2015). Under this model, individuals are either attracted towards or repelled from neighbouring individuals, depending on their species and distance. Unlike models with strict volume exclusion, here there is no absolute restriction on the location an individual occupies and the strength of the interaction is weighted by a distributed interaction kernel. One of the novel features of our study is the extension of previous structure-forming mechanisms of neighbour-dependent directional bias in single species having identical intrinsic properties (Binny et al., 2016a; 2016b) to two species with differential attractive/ repulsive effects on one another. This significantly expands the types of mechanism that can be modelled, because with a single species it is either attraction or repulsion (or neutral), but with two species there are four types of interaction each of which can be either attraction, repulsion or neutral. In this work the four interactions are: chaser-chaser (c-c); chaser-escapee (c-e); escapee-chaser (e-c); and escapee-escapee (e-e).

Spatial moment analysis is a continuum approximation that tracks the dynamics of the density of individuals, pairs, triples and so on, to describe the spatial correlation present in a population (Bolker and Pacala, 1999; Law and Dieckmann, 2000; Barraquand and Murrell,

2013). Classical macroscale continuum models such as the logistic growth model, disregard the influence of spatial structure by invoking a mean-field approximation such that the interactions between individuals are in proportion to their average density (Murray, 1989). Spatial moment analysis is advantageous over traditional mean-field analysis because it accounts for short-range, neighbour-dependent interactions and spatial correlations, thereby allowing for the analysis of clustered and segregated populations (Plank and Law, 2015).

3.4 Stochastic, individual-based model

We consider a community of two species: *chasers* and *escapees*. We construct the IBM for a spatially homogeneous environment, where the probability of finding an individual in a small region is independent of the location of that region. Hence, the IBM is relevant for communities that do not involve macroscopic density gradients meaning that we do not consider moving fronts or travelling waves (Jin et al., 2018; Johnston et al., 2017). We consider a community with N_c chasers and N_e escapees, distributed over a continuous two-dimensional finite space, $\Omega \in \mathbb{R}^2$. At any instant of time t , the state of the IBM is characterised by the locations of the two types of individuals $\mathbf{x}_n \in \Omega$, where $n = 1, 2, \dots, N_c + N_e$. The intrinsic movement rates of chasers and escapees are m_c and m_e , respectively. We consider a continuous time Markov process where the probabilities that an isolated chaser or an isolated escapee moves during a short time interval of duration δt is $m_c\delta t$ and $m_e\delta t$, respectively.

An important feature of the IBM is the neighbour dependent directional bias where movement directions of individuals are influenced by the interactions with other individuals in the neighbourhood. The interaction between two chasers at a displacement ξ is specified by the bias interaction kernel, $\omega_{cc}(|\xi|)$. We choose these kernels to be two-dimensional Gaussian functions, given by,

$$\omega_{cc}(|\xi|) = \gamma_{cc} \exp\left(-\frac{|\xi|^2}{2\sigma_{cc}^2}\right), \quad (3.1)$$

where γ_{cc} and $\sigma_{cc} > 0$ represent the interaction strength and the spatial extent of interaction, respectively. The intraspecies interaction of escapees as well as interspecies interactions between chasers and escapees are specified by similar interaction kernels, $\omega_{ee}(|\xi|)$, $\omega_{ce}(|\xi|)$, and $\omega_{ec}(|\xi|)$, respectively. The Gaussian shape of the bias kernel means that individuals interact strongly with their immediate neighbours while interactions between more distant pairs are negligible. We ensure that the size of the computational domain is sufficiently large relative to σ_{ij} so that pairs of agents only interact in some local neighbourhood of the domain. The interaction kernel in Equation 3.1 is symmetric, implying that we obtain steady spatial patterns. However, our modelling framework is sufficiently general to incorporate asymmetric kernels if that were of interest. In this case, asymmetric kernels could lead to other types of spatial structures such as stable moving configurations of chasers following escapees (Romanczuk et al., 2009).

The sign of the interaction strength determines the nature of the interaction. A negative

bias strength corresponds to attractive interactions while positive bias strength corresponds to repulsive interactions, and we refer to these interactions as *chase* and *escape* interactions, respectively. The relationship between the directional bias and the nature of the local interactions is best illustrated by considering a few of the possible scenarios in a community of chasers and escapees as shown in Figure 3.1. In Figure 3.1(a), we see that a reference chaser does not have a preferred direction since they feel no bias from neighbouring chasers, because $\gamma_{cc} = 0$. For the intraspecies interactions of escapees, shown in Figure 3.1(b), a positive γ_{ee} results in the reference escapee moves away from other escapees. Similarly, for the interspecies interaction of chasers and escapees, shown in Figure 3.1(c)-(d), a negative γ_{ce} results in chaser attracted to escapees, whereas a positive γ_{ec} results in escapees repelled from chasers. In this way, we have the flexibility of choosing the interspecies interaction to be asymmetric and later we will show that this flexibility can give rise to some very interesting results.

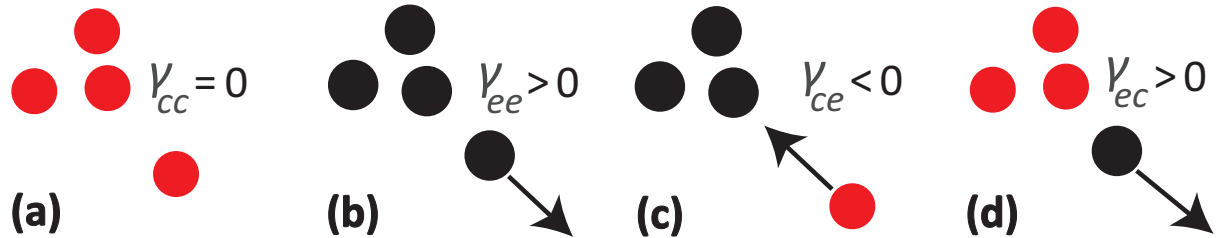


Figure 3.1: Schematic representation of some of the possible interactions arising in a community of chasers (red) and escapees (black). The bias strength of intraspecies interactions of chasers and escapees are γ_{cc} and γ_{ee} , respectively. The bias strengths of interspecies interactions are γ_{ce} and γ_{ec} , respectively. **a** No intraspecies interaction between chasers. **b** Intraspecies repulsion between escapees. **c** Chasers attracted to escapees. **d** Escapees repelled from chasers.

We define a function, $Q(\mathbf{x}, t)$, called the *bias landscape*, which allows us to quantify crowdedness and interactions at location \mathbf{x} and time t . The bias landscape for a chaser is defined as a sum of bias kernels around each individual in the community:

$$Q_c(\mathbf{x}, t) = Q_{cc}(\mathbf{x}, t) + Q_{ce}(\mathbf{x}, t), \quad (3.2)$$

where $Q_{cc}(\mathbf{x}, t) = \sum_{n \in N_c} \omega_{cc}(|\mathbf{x}_n - \mathbf{x}|)$ and $Q_{ce}(\mathbf{x}, t) = \sum_{n \in N_e} \omega_{ce}(|\mathbf{x}_n - \mathbf{x}|)$. The bias landscape for escapees is defined very similarly $Q_e(\mathbf{x}, t) = Q_{ec}(\mathbf{x}, t) + Q_{ee}(\mathbf{x}, t)$. For any individual n , we define the net bias vector to be

$$\widehat{\mathbf{B}}_n = \sum_{r \neq n} \nabla \omega_{i_n j_r} (|\mathbf{x}_r - \mathbf{x}_n|), \quad (3.3)$$

where $i, j \in \{c, e\}$. Two key features of the bias vector are the magnitude, $|\widehat{\mathbf{B}}_n|$, and angular direction, $\arg(\widehat{\mathbf{B}}_n) \in [0, 2\pi]$. The preferred direction of movement is taken to be the angular direction of the net bias vector and this allows us to bias the direction of movement of individuals in response to the local crowdedness. The definition of the bias vector, Equation 3.3, shows that the bias vector is the negative gradient of the bias landscape meaning that each individual

is biased to move in the direction of the steepest descent on the surface. The strength of the bias is determined by the steepness of the bias landscape at any particular individual's location.

The construction of the bias landscape and bias vectors in a community of chasers and escapees is shown in Figure 3.2. The level curves of the intraspecific components of the bias landscapes, $Q_{cc}(\mathbf{x}, t)$ and $Q_{ee}(\mathbf{x}, t)$, are shown in Figure 3.2(a)-(b), respectively. The individual bias vectors point in the direction of steepest descent. In this example we assume no interspecies interaction of chasers ($\gamma_{cc} = 0$), meaning that their bias vector is $\widehat{\mathbf{B}}_n = \mathbf{0}$. This explains why there are no vectors in Figure 3.2(a), and so the direction of movement of chasers is unaffected by other chasers. In contrast, the bias vectors for escapees in Figure 3.2(b) are directed away from each other due to their intraspecies repulsion. The net bias landscape for chasers, $Q_c(\mathbf{x}, t)$, shown in Figure 3.2(c), includes the additional interspecies contribution from escapees so that the chasers are attracted to escapees. Note that, the chaser at approximately $(x, y) = (-0.5, -5)$ is not influenced by the interspecies interaction because it is too far away from the clusters of escapees. Similarly, including the interspecific component of the bias landscape for escapees, shown in Figure 3.2(d), reorients the escapees' bias vectors away from any nearby chasers.

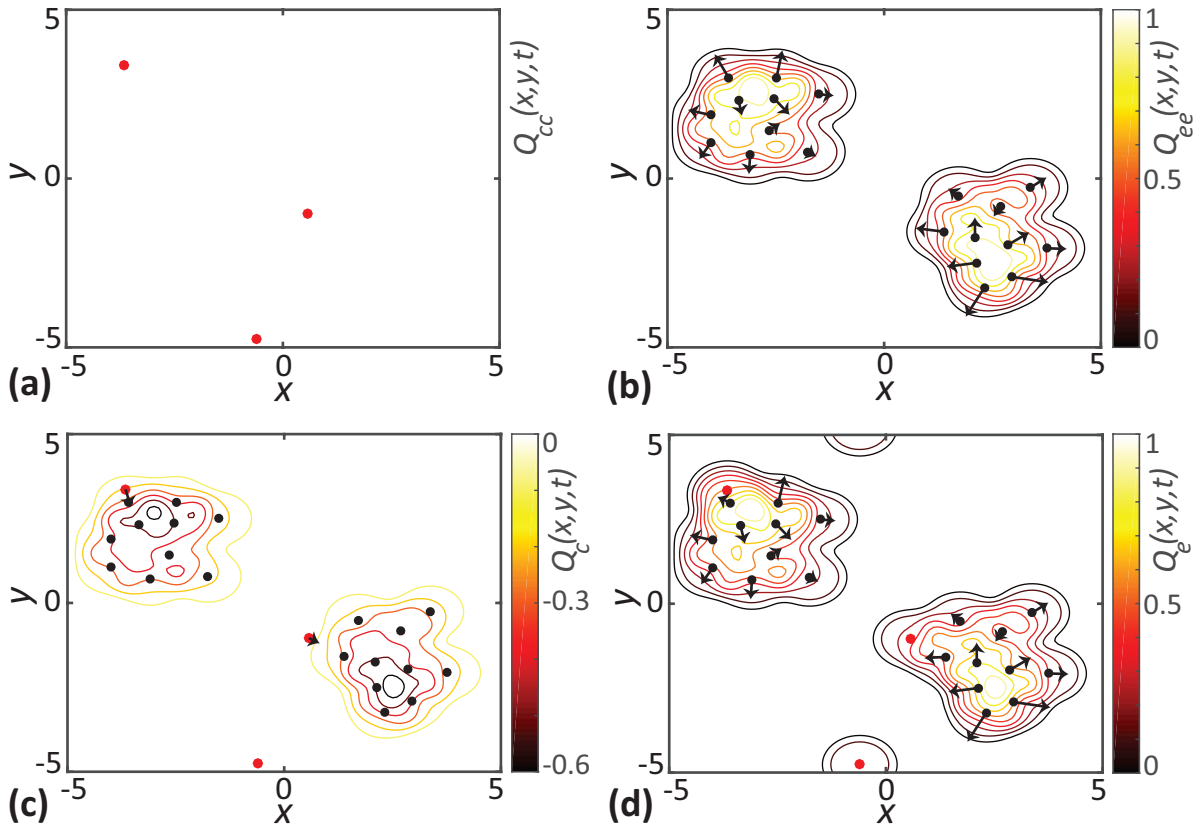


Figure 3.2: Visualisation of directional bias for a community of chasers (red dots) and escapees (black dots). In each subfigure, **a-d**, the locations of individuals are superimposed with the level curves of the bias landscapes. The bias vectors shown with black arrows represent the preferred direction of individuals. The length of arrows indicate the strength of bias. Results in **a** correspond to intraspecies interactions of chasers only. Results in **b** show intraspecies interactions of escapees only. Results in **c** and **d** show the net interaction for both species. Parameter values are $\gamma_{cc} = 0.0$, $\gamma_{ce} = -0.2$, $\gamma_{ec} = \gamma_{ee} = 0.3$ and $\sigma_{cc} = \sigma_{ce} = \sigma_{ec} = \sigma_{ee} = 0.5$. Note that $\gamma_{cc} = 0$, meaning that there are no interactions between chasers in (a), which explains why there is no colour bar on this subfigure.

We now specify the probability density function (PDF) for the displacement that a chaser traverses during a movement event as,

$$\mu_c(\xi; \widehat{\mathbf{B}}_n) = \frac{u_c(|\xi|) g(\arg(\xi); \widehat{\mathbf{B}}_n)}{|\xi|}, \quad (3.4)$$

where $u_c(|\xi|)$ and $g(\arg(\xi); \widehat{\mathbf{B}}_n)$ are two independent PDFs. A derivation of the movement displacement PDF is provided in Section 3A.1. A similar definition holds for the movement displacement PDF of escapees, $\mu_e(\xi; \widehat{\mathbf{B}}_n)$. Here, $u_c(|\xi|)$ is the PDF for the movement distance, $|\xi|$ moved by a chaser. For simplicity, we treat $u_c(|\xi|)$ as a PDF that is independent of the local environment. It is possible to use a constant, deterministic step length in the IBM (Browning et al., 2018). However, since we are interested in deriving a continuous mathematical description of the IBM we use a continuous distribution to describe the step length. Note that the expression for $\mu_c(\xi; \widehat{\mathbf{B}}_n)$ involves a factor of $1/|\xi|$ and so evaluating $\mu_c(\xi; \widehat{\mathbf{B}}_n)$ at $\xi = \mathbf{0}$ results in the PDF becoming infinite. To avoid this, we use a non-zero mean $(\mu_c^{(s)})$ normal distribution with a relatively narrow standard deviation $(\sigma_c^{(s)})$, where $\mu_c^{(s)} > 3\sigma_c^{(s)}$ for the movement distance PDF, $u_c(|\xi|)$. When we evaluate the movement displacement PDF, we set $u_c(|\xi|) = 0$ at distances greater than $\pm 3\sigma_c^{(s)}$ from the mean distance. It is also possible to use other strictly positive distributions for the step length, such as a gamma distribution. However, we choose the truncated Gaussian PDF to be consistent with the previous studies in this field (Binny et al., 2016b; Surendran et al., 2018). Provided the PDF has a relatively narrow distribution around the mean and has zero density at the origin, the exact choice of step length distribution does not qualitatively change the results. Now, $g(\arg(\xi); \widehat{\mathbf{B}}_n)$ is the PDF describing the angular direction of movement, $\arg(\xi) \in [0, 2\pi]$, of a chaser due to the presence of other individuals in the neighbourhood. We choose the PDF for the angular direction of movement to be a von Mises distribution, with mean direction $\arg(\widehat{\mathbf{B}}_n)$ and concentration parameter given by $|\widehat{\mathbf{B}}_n|$,

$$g(\theta; \widehat{\mathbf{B}}_n) = \frac{\exp(|\widehat{\mathbf{B}}_n| \cos(\theta - \arg(\widehat{\mathbf{B}}_n)))}{2\pi I_0(|\widehat{\mathbf{B}}_n|)}, \quad (3.5)$$

where I_0 is the zero order modified Bessel function. In the absence of net bias, $\widehat{\mathbf{B}}_n = \mathbf{0}$, the von Mises distribution reduces to the uniform distribution so that there is no preferred direction of movement (Binny et al., 2016b). This choice of PDF means that the likelihood of individuals moving in the preferred direction, $\arg(\widehat{\mathbf{B}}_n)$, increases with the magnitude of the bias vector. Individuals with large $|\widehat{\mathbf{B}}_n|$, are more likely to move in the direction of $\widehat{\mathbf{B}}_n$. The direction of movement of individuals with a weaker bias becomes almost uniformly distributed. Note that, the magnitude of $\widehat{\mathbf{B}}_n$ does not affect the distance moved.

We implement the IBM using the Gillespie algorithm (Gillespie, 1977) with an initial condition where individuals of each species are distributed uniformly at random in the domain. An alternative simulation method would be to use a constant time-stepping approach, but this

can be less accurate because there is a possibility that multiple events occur in the same time step (Simpson et al., 2010a). Note that, our model considers only the movement direction to be neighbour dependent, and movement rates are chosen to be independent of neighbourhood interactions. In general, our framework could be extended to allow both the movement rates and movement direction to depend upon the crowding surface. However, we choose to work with the simplest implementation where the movement rate does not depend upon the crowding surface since this simpler mechanism gives rise to very interesting spatial patterns.

3.4.1 Numerical simulation of the individual-based model

In our IBM simulations, we consider a community of chasers and escapees with population sizes N_c and N_e , respectively, distributed uniformly at random in a domain of size $L \times L$. The intrinsic movement rates of chasers and escapees are m_c and m_e , respectively. The net movement rate of the community is given by,

$$\lambda = m_c N_c + m_e N_e. \quad (3.6)$$

The time interval between successive movement events is exponentially distributed with mean $1/\lambda$. When a motility event takes place, an individual is chosen to move at random. Depending upon whether the chosen individual is a chaser or escapee, it moves a displacement ξ specified by either of the movement displacement PDFs, $\mu_c(\xi; \widehat{\mathbf{B}}_n)$, and $\mu_e(\xi; \widehat{\mathbf{B}}_n)$. We employ periodic boundary conditions over the $L \times L$ domain in all of our simulations. Typically, the length scales over which interactions take place between individuals are much smaller compared to the overall domain size ($\sigma_{ij} \ll L$). Under these circumstances, the edge effects are negligible, and the periodic boundary condition is a reasonable choice. Also, many previous works that focus on modelling the motility and interactions in ecological and biological systems employ periodic boundary conditions (Wood and Ackland, 2007; Romanczuk et al., 2009; Binny et al., 2016a; Surendran et al., 2018).

We use spatial moments to characterise the spatial structure in the population. The first spatial moment of chasers is $Z_{1,c} = N_c/L^2$ and that of escapees is $Z_{1,e} = N_e/L^2$. We analyse the spatial structure of the community using second spatial moments expressed as the pair correlation function (PCF). Since we have two different types of species in the community, we have three distinct PCFs. These include the auto-PCF of chasers describing the density of pairs of chasers, the auto-PCF of escapees that describes the density of pairs of escapees and the cross-PCF describing the density of pairs involving a chaser and an escapee. To compute the auto-PCF of chasers, $C_{cc}(r)$, we choose a reference chaser located at \mathbf{x}_n and compute all distances, $r = |\mathbf{x}_r - \mathbf{x}_n|$ from all other chasers. We repeat this procedure until each of the remaining $N_c - 1$ chasers act as a reference individual. The PCF is constructed by counting all the distances that fall into the interval $[r - \delta r/2, r + \delta r/2]$. Normalising the bin count by a factor of $N_c(N_c - 1)(2\pi r \delta r)/L^2$ gives C_{cc} such that $C_{cc}(r) = 1$ corresponds to a complete

absence of spatial structure among chasers. To compute C_{ee} and C_{ce} , we repeat this procedure by considering pairs of escapees and pairs involving both chasers and escapees, respectively.

3.5 Spatial moment dynamics

In this section, we derive a macroscale continuum approximation of the IBM by considering the dynamics of spatial moments. For convenience, we present the spatial moment dynamics for a multispecies framework and specific details corresponding to the two species case are presented in Section 3A.2. The spatial point process defined by the IBM is stationary, meaning that statistics of the population in any observation window are independent of the window's location (Plank and Law, 2015). This means that the first spatial moment $Z_{1,i}$, the average density of species i , is independent of location. Since we do not consider the proliferation and death of individuals, the first moment remains constant in time. The second spatial moment, $Z_{2,ij}(\xi, t)$, is the average density of pairs composed of individuals of species i and species j , separated by a displacement ξ . The third spatial moment, $Z_{3,ijk}(\xi, \xi', t)$, is defined as the average density of triplets consisting of individuals of species i , species j and species k where the individuals of species j and k are displaced by ξ and ξ' , respectively from the individual of species i . Note that since the subpopulations are conservative we refer to the average density as $Z_{1,i}$ whereas the second and third moments are time dependent, so we explicitly show the dependence on distance and time by writing $Z_{2,ij}(\xi, t)$ and $Z_{3,ijk}(\xi, \xi', t)$, respectively.

3.5.1 General spatial moment formulation

To derive the equations governing the dynamics of the second spatial moment, we need to derive the expected net bias vector for an individual of species i that is in pair with an individual of species j . This depends on the contribution from another individual of species k at a displacement ξ' . Conditional on a pair consisting of individuals of species i and j existing at a displacement ξ , the probability of an individual of species k being present at a displacement ξ' is $Z_{3,ijk}(\xi, \xi', t)/Z_{2,ij}(\xi, t)$. The expected net bias vector of an individual of species i , conditional on the presence of an individual of species j can be computed by multiplying the gradient of bias kernel with the conditional probability and integrating over all possible displacements, giving,

$$\mathbf{B}_{2,ij}(\xi, t) = \sum_k \int \nabla \omega_{ik}(|\xi'|) \frac{Z_{3,ijk}(\xi, \xi', t)}{Z_{2,ij}(\xi, t)} d\xi' + \nabla \omega_{ij}(|\xi|). \quad (3.7)$$

The second term in Equation 3.7, $\nabla \omega_{ij}(|\xi|)$, accounts for the direct contribution of the individual of species j at displacement ξ . Now we can write the PDF for the movement of an individual of species i over a displacement ξ' , conditional on the presence of an individual of species j at

a displacement ξ as,

$$\mu_{2,ij}(\xi', \xi, t) = \mu_i(\xi'; \mathbf{B}_{2,ij}(\xi, t)). \quad (3.8)$$

We now consider the dynamics of the second spatial moment by considering the change in the density of pairs of individuals at a displacement ξ as a result of the movement of individuals. An existing pair of individuals at displacement ξ can be lost if one of the individuals of the pair moves. Similarly, a new pair with displacement ξ is formed when one of the individuals from an existing pair at a displacement $\xi + \xi'$ moves a displacement ξ' . Accounting for these possibilities means that the time evolution of the second moment is given by,

$$\begin{aligned} \frac{\partial}{\partial t} Z_{2,ij}(\xi, t) = & - (m_i + m_j) Z_{2,ij}(\xi, t) + m_i \int \mu_{2,ij}(\xi', \xi' + \xi, t) Z_{2,ij}(\xi' + \xi, t) d\xi' \\ & + m_j \int \mu_{2,ji}(\xi', \xi' - \xi, t) Z_{2,ji}(\xi' - \xi, t) d\xi'. \end{aligned} \quad (3.9)$$

Given estimates of the first and second moments, we can describe the spatial structure of the community in terms of a pair correlation function (PCF), $C_{ij}(r, t)$, expressed as a function of separation distance, $r = |\xi|$, given by,

$$C_{ij}(r, t) = \frac{Z_{2,ij}(\xi, t)}{Z_{1,i} Z_{1,j}}. \quad (3.10)$$

The normalisation of the second spatial moment by a factor of $Z_{1,i} Z_{1,j}$ in Equation 3.10 ensures that $C_{ij}(r, t) = 1$ in the absence of spatial structure. If $C_{ij}(r, t) > 1$, we have more pairs of an individual of species i separated by a distance r from an individual of species j than if they were in a spatially random configuration. This is referred to as a clustered spatial structure. If $C_{ij}(r, t) < 1$, we have fewer pairs of individuals at a separation distance r than if they were in a spatially random configuration and this is known as a segregated spatial pattern. The PCF is called an auto-PCF when describing the density of pairs involving individuals of the same species and cross-PCF when individuals are from two different species (Binder and Simpson, 2013).

The dynamics of the second spatial moment depend on the third spatial moment via Equation 3.7. To obtain a closed system of equations, we use a moment closure scheme to approximate the third moment as a function of first and second moments (Sharkey et al., 2006; Frasca and Sharkey, 2016). Different closure schemes have been used in the literature including the power-1 closure, power-2 closure and the power-3 Kirkwood superposition approximation (Murrell et al., 2004). A comparison of the performance of various closure methods for the kinds of problems we consider is summarised in Section 3A.3. We find that the asymmetric

power-2 closure (Law et al., 2003) given by,

$$Z_{3,ijk}(\xi, \xi', t) = \frac{1}{5} \left[4 \frac{Z_{2,ij}(\xi, t) Z_{2,ik}(\xi', t)}{Z_{1,i}(t)} + \frac{Z_{2,ij}(\xi, t) Z_{2,jk}(\xi' - \xi, t)}{Z_{1,j}(t)} \right. \\ \left. + \frac{Z_{2,ik}(\xi', t) Z_{2,jk}(\xi' - \xi, t)}{Z_{1,k}(t)} - Z_{1,i}(t) Z_{1,j}(t) Z_{1,k}(t) \right], \quad (3.11)$$

provides the best results for the range of parameters we consider.

3.5.2 Summary statistics

In our analysis of both the IBM and spatial moment model, we focus on examining sufficiently long-time simulations so that we can treat the higher moments and $C_{ij}(r, t)$ as quasi-steady quantities (Simpson et al., 2013b). Under these circumstances, we specify $C_{ij}(r)$ as a function of r only. To summarise the key features of the various possible combinations of spatial structure, we need a simplified measure of spatial structure. Plotting and comparing the various PCFs as a function of distance for each parameter value becomes increasingly challenging as we consider a large parameter space. Under these circumstances, it is more convenient to use a simple measure of spatial structure that expresses the type and extent of the spatial structure as a scalar quantity. A summary statistic based on the difference in the area under the curve of the PCF and the area under a curve made by a constant pair correlation function for a randomly distributed population, $C_{ij}(r) = 1$, is one convenient way to simply express the nature and extent of the spatial structure as a single number. In this work we use,

$$A_{ij} = \int_0^\infty (C_{ij}(r) - 1) dr, \quad (3.12)$$

as such a summary statistic where A_{ij} quantifies the spatial structure between of species i and j as a function of $C_{ij}(r)$. Binny et al. (2016) use a similar measure of spatial structure to describe spatial patterns in a single species framework. Here we use a slightly more general summary statistic since we are interested in populations composed of multiple species. Our definition of A_{ij} is such that, if individuals of species i are more (less) likely to be located in proximity to individuals of species j , then $A_{ij} > 0$ ($A_{ij} < 0$). If there is no correlation between locations of individuals of species i and j then $A_{ij} = 0$. Even though, it is possible to have a positive correlation ($C_{ij}(r) > 1$) at some scales and negative correlation ($C_{ij}(r) < 1$) at other scales, in practice we do not observe this situation. We find that A_{ij} is insensitive to R when we choose R to be sufficiently large since the PCFs approach unity for large separation distances. A summary of the PCF and simple measure of spatial structure values and corresponding spatial structures is provided in Table 3.1.

Table 3.1: A summary of PCF and simple measure of spatial structure values and corresponding spatial structure

Value of PCF	Type of spatial structure
$C_{ij}(r) = 1$	no spatial structure
$C_{ij}(r) > 1$	clustering between species i and j
$C_{ij}(r) < 1$	segregation between species i and j
Value of simple measure of spatial structure	Type of spatial structure
$A_{ij} = 0$	no spatial structure
$A_{ij} > 0$	clustering between species i and j
$A_{ij} < 0$	segregation between species i and j

3.5.3 Numerical methods for spatial moment dynamics

The numerical solution for the dynamical equation of the second spatial moment, Equation 3.9, is computed using the forward Euler method. This scheme involves a spatial discretisation of the displacement, $\xi = (\xi_x, \xi_y)$, using a square grid with constant spacing, $\Delta\xi$, over the domain $\{-\xi_{\max} \leq \xi_x, \xi_y \leq \xi_{\max}\}$. Here, ξ_{\max} is chosen to be sufficiently large such that the second spatial moments are given by a mean field condition at the domain boundaries, giving, $Z_{2,ij}(\xi, t) \approx Z_{1,i} \times Z_{1,j}$. The integral terms in Equation 3.7 and Equation 3.9 are approximated using the trapezoid rule. To compute these integrals, we need to evaluate $Z_{2,ij}(\xi \pm \xi', t)$ for different combinations of ξ and ξ' . Some of these combinations require values of $Z_{2,ij}(\xi \pm \xi', t)$ that lie beyond the computational domain. Whenever this scenario arises, we approximate those terms with the values of $Z_{2,ij}(\xi, t)$ at the boundary, $Z_{2,ij}((\xi_{\max}, \xi_{\max}), t)$.

The initial condition used for solving the spatial moment dynamics is $Z_{2,ij}(\xi, 0) = Z_{1,i} \times Z_{1,j}$. We use a constant grid spacing $\Delta\xi = 0.2$, time step $dt = 0.1$ and $\xi_{\max} = 8$ in all our results. Additional results (not shown) confirms that this choice of spatial and temporal discretisation is sufficient to produce grid-independent results. We compare the numerical solution of the spatial moment dynamics model with the IBM simulation results by computing the auto-PCF and cross-PCF $Z_{2,ii}(\xi, t)/Z_{1,i}^2$ and $Z_{2,ij}(\xi, t)/(Z_{1,i} Z_{1,j})$, respectively.

3.6 Results

Here, we explore how different features of the intraspecies and interspecies interactions influence the spatial structure of a two species community using the IBM and spatial moment models. We examine the influence of variation in factors such as interaction strength, spatial extent of interaction and relative density of species, in determining the macroscale spatial patterns. Our results show that, at a sufficiently large time, $t = 20$, a steady spatial pattern establishes in the community. The evolution of the spatial structure of the community to steady

state is shown in Section 3A.4. Since our interest lies in understanding the long-time impact of individual-level interactions, we focus on presenting and interpreting steady-state solutions of our models. While the time required to attain a steady-state depends on the specific initial distribution of individuals in the domain, the actual steady-state spatial pattern formed is independent of the initial configuration. To illustrate, we provide additional results in Section 3A.5. In all our simulations, the individuals are initially distributed uniformly at random. This choice helps in reducing the computational time and comparing the influence of different types of interactions. A summary of the key parameters in the simulations is given in Table 3.2. Before presenting the details about how different features of interactions influence the spatial structure, we illustrate the types of spatial structure that could arise in a community of chasers and escapees by showing the snapshots of locations of individuals from IBM in Figure 3.3. A community with a complete absence of spatial structure is shown in Figure 3.3(a), where there is no correlation between the locations of chasers and escapees. Figure 3.3(b) shows the interspecies clustering of chasers and escapees, formed due to the interspecies attraction of chasers towards escapees. Here we see more chasers and escapees in close vicinity of each other than in a spatially random configuration. Figure 3.3(c) shows the interspecies segregation formed due to interspecies chase-escape interactions. In this case, the repulsive bias of escapees from chasers is stronger than the attraction of chasers to escapees. Hence we see that escapees are placed away from chasers. Note that, the identification of the spatial structure of a community purely through visual inspection can be challenging in certain cases. Under these scenarios, PCFs are very useful in revealing the type of spatial structure and quantifying it.

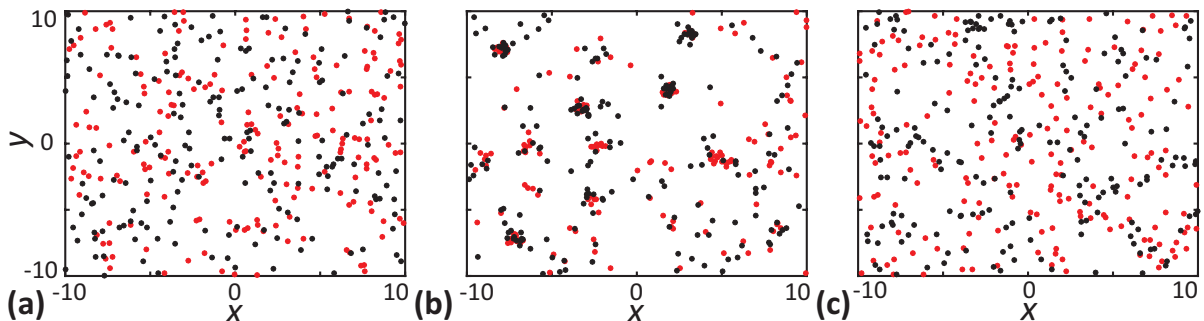


Figure 3.3: Snapshots of the locations of chasers and escapees to illustrate the types of spatial structure arise in our model. **a** Complete absence of spatial structure ($\gamma_{ce} = \gamma_{ec} = 0$). **b** Interspecies cluster spatial structure (chasers and escapees form aggregates, $\gamma_{ce} = -0.25$, $\gamma_{ec} = 0$, $\gamma_{ee} = -0.06$). **c** Interspecies segregation (chasers and escapees are segregated, $\gamma_{ce} = -0.1$, $\gamma_{ec} = 0.3$). Other parameter values are $\gamma_{cc} = \gamma_{ee} = 0$, $\sigma_{cc} = \sigma_{ce} = \sigma_{ec} = \sigma_{ee} = 0.5$, $m_c = m_e = 5.0$, $\mu_c^{(s)} = \mu_e^{(s)} = 0.4$, $\sigma_c^{(s)} = \sigma_e^{(s)} = 0.1$.

Table 3.2: Description of model parameters and variables

Parameter symbol	Description	Default value
γ_{ee}	bias strength with which escapees are repelled by other escapees	0.3
γ_{ce}	bias strength with which chasers are attracted to escapees	-0.2
γ_{ec}	bias strength with which escapees are repelled from chasers	0.3
γ_{cc}	bias strength with which chasers interact with other chasers	0
σ_{ee}	spatial extent of bias over which escapees are repelled from other escapees	0.5
σ_{ce}	spatial extent of bias over which chasers are attracted to escapees	0.5
σ_{ec}	spatial extent of bias over which escapees are repelled from chasers	0.5
σ_{cc}	spatial extent of bias over which chasers interact with other chasers	0.5
$\mu_e^{(s)}$	mean movement distance of escapees	0.4
$\mu_c^{(s)}$	mean movement distance of chasers	0.4
$\sigma_e^{(s)}$	standard deviation movement distance of escapees	0.1
$\sigma_c^{(s)}$	standard deviation movement distance of chasers	0.1
N_e	population size of escapees	200
N_c	population size of chasers	200
m_e	intrinsic movement rate of escapees	5
m_c	intrinsic movement rate of chasers	5
L	domain length for IBM	20
Variable	Description	
t	time	
r	separation distance between a pair of individuals	
$C_{cc}(r)$	PCF corresponding to the pair densities of chasers (auto-PCF of chasers)	
$C_{ee}(r)$	PCF corresponding to the pair densities of escapees (auto-PCF of escapees)	
$C_{ce}(r)$	PCF corresponding to the densities of pairs involving a chaser and escapee (cross-PCF)	
A_{cc}	simple measure of spatial structure computed from $C_{cc}(r)$	
A_{ee}	simple measure of spatial structure computed from $C_{ee}(r)$	
A_{ce}	simple measure of spatial structure computed from $C_{ce}(r)$	

3.6.1 Effect of varying the interaction strength

Here, we investigate how variations in bias interaction strength impact the spatial structure. In our simulations, we consider a two species community of chasers and escapees with population sizes, $N_c = 200$ and $N_e = 200$, distributed according to a spatial Poisson process. We systematically vary the interaction strengths γ_{ce} , γ_{ec} , and γ_{ee} to explore the role of different interactions. For simplicity, we assume $\gamma_{cc} = 0$, which means that the chasers have no intraspecific interactions. We compute the PCFs, $C_{cc}(r)$, $C_{ce}(r)$, and $C_{ee}(r)$ along with simple measures of spatial structure, A_{cc} , A_{ce} and A_{ee} , to quantify the resulting spatial patterns generated in the community, as shown in Figure 3.4.

In Figure 3.4(a)-(d) we vary the bias interaction strength, γ_{ec} , which controls the strength with which escapees are repelled from chasers. When escapees are not repelled from chasers ($\gamma_{ec} = 0$), the chasers move close to escapees due to their attractive bias, leading to the accumulation of chasers around escapees. This results in intraspecies clustering of chasers ($C_{cc}(r) > 1$)

as well as interspecies cluster formation ($C_{ce}(r) > 1$). This is also confirmed by, simple measures of spatial structure, A_{cc} and A_{ce} being positive when $\gamma_{ec} = 0$. We also see a segregated pattern among escapees due to their intraspecies repulsion ($C_{ee}(r) < 1$ and $A_{ee} < 0$). When escapees are repelled from chasers ($\gamma_{ec} > 0$), the clustering we previously observed weakens as the repulsion counteracts the attractive bias of chasers. For a sufficiently large choice of γ_{ec} , here $\gamma_{ec} = 0.3$, spatial structure changes becomes segregated due to the overall segregation of chasers and escapees ($C_{cc}(r) < 1$ and $A_{cc} < 0$ as well as $C_{ce}(r) < 1$ and $A_{ce} < 0$). In spite of the intraspecies repulsion between escapees, the enhanced interspecies repulsion from chasers, force the escapees to come closer to each other. This results in weakening of the segregated spatial structure of escapees as γ_{ec} increases.

In Figure 3.4(e)-(h) we vary γ_{ce} , which controls the strength with which chasers are attracted to escapees. When chasers are not attracted to escapees ($\gamma_{ce} = 0$), the movement of chasers is unbiased so their distribution remains spatially random ($C_{cc}(r) = 1$). In this case, there is no effect opposing the repulsion of escapees from chasers. This results in escapees staying away from chasers, forming an interspecies segregated pattern, as indicated by $C_{ce}(r) < 1$ for small distances and $A_{ce} < 0$. Also, intraspecies repulsion among escapees contributes to the segregated pattern of escapees, indicated by $C_{ee}(r) < 1$ and $A_{ee} < 0$. When chasers are attracted to escapees ($\gamma_{ce} < 0$), an intraspecies segregated spatial structure emerges among chasers ($C_{cc}(r) < 1$ and $A_{cc} < 0$). This is because chasers tend to move towards escapees and the segregated arrangement of escapees forces chasers to occupy spaces around escapees. As the attraction strength is increased (γ_{ce} more negative), the interspecies segregated pattern becomes less pronounced, since the enhanced attractive bias starts to counteract the repulsion from escapees. As γ_{ce} is made more negative, A_{ce} gets closer to zero also confirm this behaviour.

In Figure 3.4(i)-(l) we vary γ_{ee} , which controls the strength with which escapees are repelled by other escapees. As we increase the intraspecies repulsion strength of escapees, we observe a strong segregated spatial pattern emerges among escapees, as indicated by $C_{ee}(r)$ diverges form unity towards zero. The A_{ee} becomes more negative with the increase in γ_{ee} also confirms this behaviour. The development of more pronounced intraspecies segregated spatial structure among escapees can be attributed to the increased repulsion between escapees as γ_{ee} increases. Finally, we observe that the accuracy of the spatial moment prediction increases with the increase in the magnitude of the bias strength.

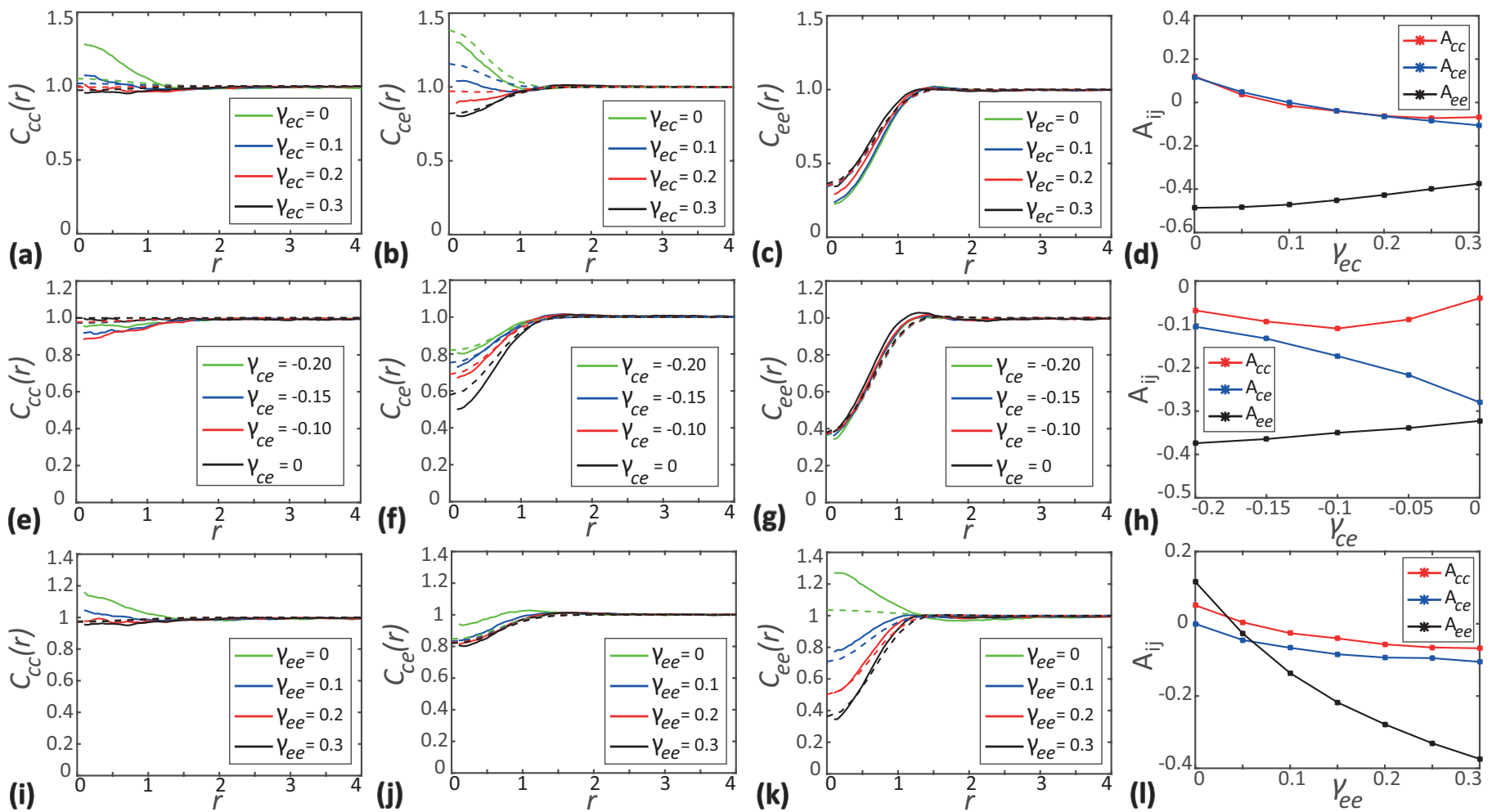


Figure 3.4: Effects of varying the interaction strength. **a-c** show the PCFs $C_{cc}(r)$, $C_{ce}(r)$ and $C_{ee}(r)$ as a function of separation distance for different choices of γ_{ec} . **d** show simple measures of spatial structure A_{cc} , A_{ce} and A_{ee} as a function of γ_{ec} . **e-g** shows PCFs $C_{ij}(r)$ for different choices of γ_{ce} . **h** shows simple measures of spatial structure A_{ij} as a function of γ_{ce} . **i-k** show PCFs $C_{ij}(r)$ for different choices of γ_{ee} . **l** shows simple measures of spatial structure A_{ij} as a function of γ_{ee} . In the subfigures showing the PCFs as a function of r , solid curves show the averaged results from 1000 identically prepared realisations of the IBM, whereas dashed curves correspond to results from spatial moment dynamics model. In all cases $C_{ij}(r)$ and A_{ij} are evaluated at $t = 20$. Parameter values are $\gamma_{cc} = 0$, $\sigma_{cc} = \sigma_{ce} = \sigma_{ec} = \sigma_{ee} = 0.5$, $m_c = m_e = 5.0$, $\mu_c^{(s)} = \mu_e^{(s)} = 0.4$, $\sigma_c^{(s)} = \sigma_e^{(s)} = 0.1$.

3.6.2 Effect of varying the spatial extent of interaction

Here, we investigate how varying the range of interactions impacts the formation of spatial structure. The spatial extent of interaction, σ_{ij} determines the range over which the interactions between individuals are significant. A small choice of σ_{ij} leads to short-range interactions, whereas a large σ_{ij} corresponds to long-range interactions between individuals. Again, we consider a two species community of chasers and escapees with $N_c = 200$ and $N_e = 200$, respectively. As before we set $\gamma_{cc} = 0$, meaning the interactions in between chasers are switched off.

In Figure 3.5(a)-(d) we vary the spatial extent of interaction σ_{ec} , which controls the spatial extent over which escapees are repelled from chasers. For small values of σ_{ec} , we observe a small scale intraspecies clustering among chasers as indicated by the PCF $C_{cc}(r) > 1$ and the simple measure of spatial structure $A_{cc} > 0$. We also observe interspecies clustering between chasers and escapees ($C_{ce}(r) > 1$) as well as a segregated spatial pattern between escapees ($C_{ee}(r) < 1$) at small values of σ_{ec} . Our results showing that $A_{ce} > 0$ and $A_{ee} < 0$ also confirm this behaviour for small σ_{ec} . As σ_{ec} increases, the intraspecies clustering of chasers and interspecies clustering becomes weaker and changes to a segregated spatial structure at a sufficiently large values of σ_{ec} . As the range over which escapees are repelled increases, the escapees experience stronger repulsion due to the influence of more distant chasers resulting in the segregation of chasers and escapees. As we increase σ_{ec} from 0.25 to 0.6, both A_{cc} and A_{ce} change sign from positive to negative. These observations confirm the formation of a segregated spatial structure.

In Figure 3.5(e)-(h) we vary σ_{ce} , which controls the spatial extent over which chasers are attracted to escapees. At small values of σ_{ce} we observe an interspecies segregated spatial structure between chasers and escapees as indicated by $C_{ce}(r) < 1$ and $A_{ce} < 0$. For sufficiently small σ_{ce} , the escapees are repelled from chasers strongly since the small range attraction of chasers to escapees cannot compensate for the relatively long range repulsion. Hence, chasers and escapees segregate from each other forming an interspecies segregated spatial structure. As σ_{ce} increases, we observe the cross-PCF $C_{ce}(r)$ approaches unity and A_{ce} becomes less negative. This suggests a shift from the interspecies segregated spatial structure between chasers and escapees to a less segregated spatial structure. With the increase of the spatial extent of interaction, the distance over which chasers get attracted to escapees increases and results in an enhanced attractive bias. This enhanced attraction counteracts the interspecies repulsion leading to the loss of the segregated spatial pattern between chasers and escapees.

Finally, in Figure 3.5(i)-(l) we vary σ_{ee} , which controls the spatial extend over which escapees repel other escapees. As σ_{ee} increases, we see the $C_{ee}(r)$ diverges from unity and A_{ee} becomes more negative, suggesting the development of stronger segregated spatial structure among escapees. The increase in σ_{ee} enables an escapee to influence more distant escapees, resulting in the enhancement of the segregated structure.

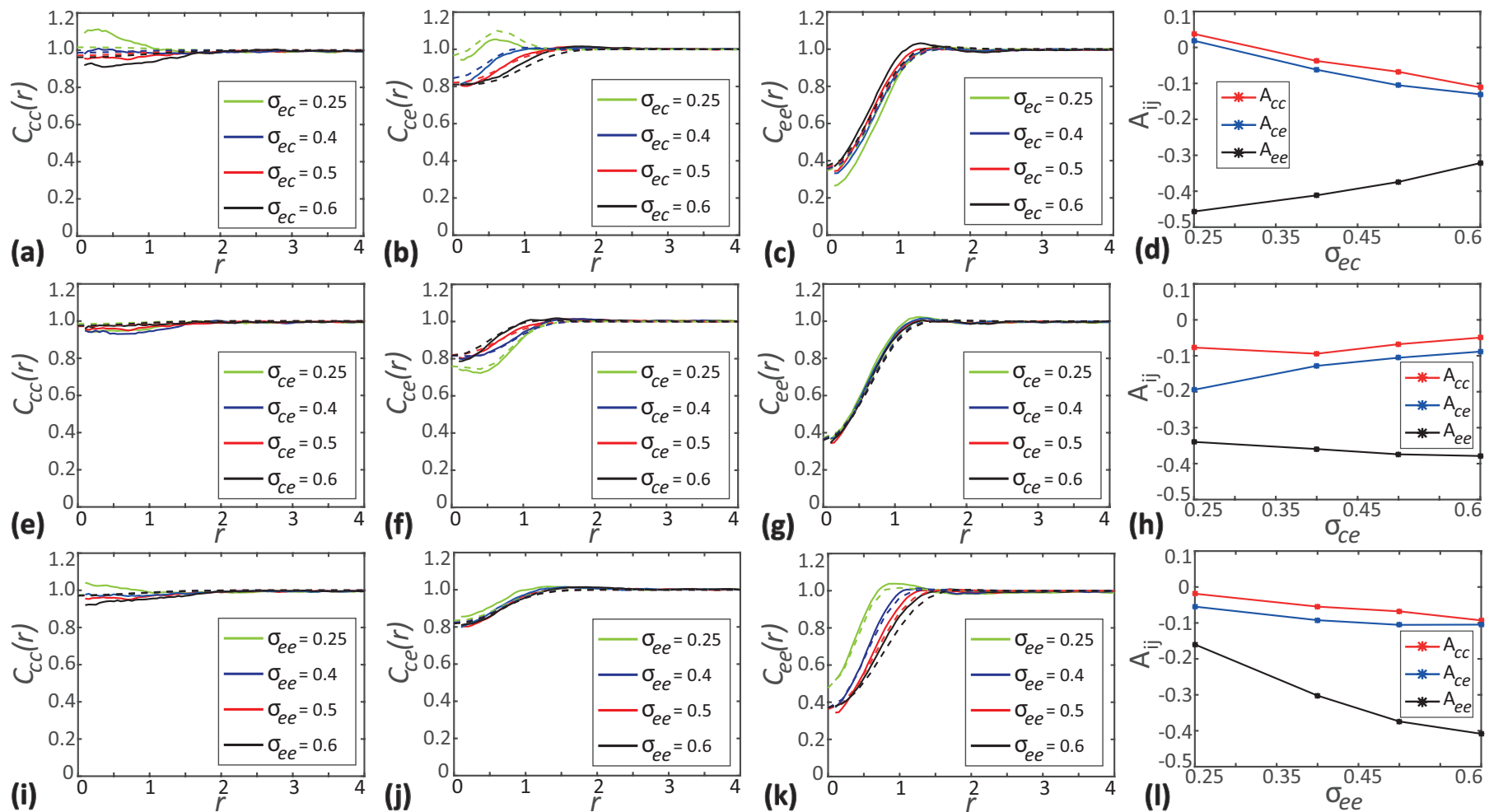


Figure 3.5: Effects of varying the spatial extent of interaction. **a-c** show the PCFs $C_{cc}(r)$, $C_{ce}(r)$ and $C_{ee}(r)$ as a function of separation distance for different choices of σ_{ec} . **d** show simple measures of spatial structure, A_{cc} , A_{ce} and A_{ee} as a function of σ_{ec} . **e-g** shows PCF $C_{ij}(r)$ for different choices of σ_{ce} . **h** shows simple measures of spatial structure A_{ij} as a function of σ_{ce} . **i-k** shows PCFs $C_{ij}(r)$ for different choices of σ_{ee} . **l** shows simple measures of spatial structure A_{ij} as a function of σ_{ee} . In the subfigures showing the PCFs as a function of r , solid curves show the averaged results from 1000 identically prepared realisations of the IBM, whereas dashed curves correspond to results from spatial moment dynamics model. In all cases $C_{ij}(r)$ and A_{ij} are evaluated at $t = 20$. Parameter values are $\gamma_{cc} = 0$, $\gamma_{ce} = -0.2$, $\gamma_{ec} = \gamma_{ee} = 0.3$, $m_c = m_e = 5.0$, $\mu_c^{(s)} = \mu_e^{(s)} = 0.4$, $\sigma_c^{(s)} = \sigma_e^{(s)} = 0.1$.

3.6.3 Effect of varying the relative density of species

We now explore how varying the relative density of chasers and escapees, $Z_{1,c}/Z_{1,e}$, impacts the spatial configuration of the community. We consider a community composed of three different density ratios: $Z_{1,c}/Z_{1,e} = 1/7$, $Z_{1,c}/Z_{1,e} = 1$ and $Z_{1,c}/Z_{1,e} = 7$. To vary the relative density of chasers, the total number of individuals in the community is fixed at $N_c + N_e = 400$ and the population sizes of chasers are varied as $N_1 = 50, 200$ and 350 , respectively. We investigate the behaviour of spatial pattern in the community by plotting $C_{ij}(r)$ and A_{ij} in Figure 3.6.

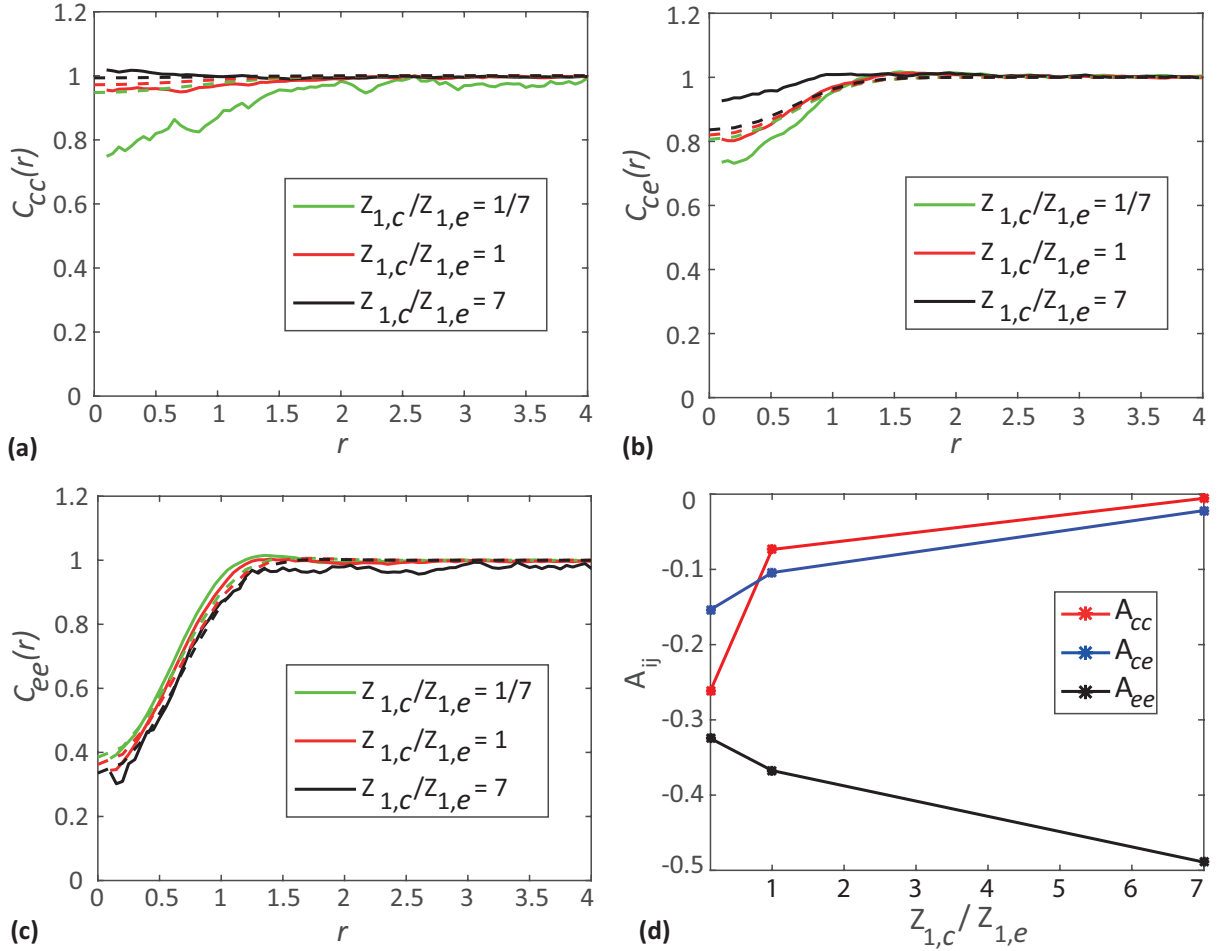


Figure 3.6: Effects of varying the relative density. **a-c** shows $C_{cc}(r)$, $C_{ce}(r)$ and $C_{ee}(r)$ as a function of separation distance, respectively. **d** show simple measures of spatial structure, A_{ij} as a function of relative density. In (a)-(c) solid curves show the averaged results from 1000 identically prepared realisations of the IBM, whereas dashed curves correspond to results from spatial moment dynamics model. In all results, PCFs and simple measures of spatial structure are given at $t = 20$. Parameter values are $\gamma_{cc} = 0$, $\gamma_{ce} = -0.2$, $\gamma_{ec} = \gamma_{ee} = 0.3$, $\sigma_{cc} = \sigma_{ce} = \sigma_{ec} = \sigma_{ee} = 0.5$, $m_c = m_e = 5.0$, $\mu_c^{(s)} = \mu_e^{(s)} = 0.4$, $\sigma_c^{(s)} = \sigma_e^{(s)} = 0.1$.

When the density of chasers is much lower than the density of escapees, the attraction of chasers towards escapees leads to chasers being placed far apart from other chasers. This leads to the formation of segregated spatial structure ($C_{cc} < 1$ and $A_{cc} < 0$) among chasers. In contrast, at a high relative density of chasers, more chasers tend to move towards a particular escapee, resulting in an accumulation of chasers at short distances and a less segregated spatial structure, as indicated by $C_{cc}(r)$ becomes close to unity and A_{cc} becomes closer to zero. An-

other observation is that $C_{ee}(r)$ decreases and A_{ee} becomes more negative with the increase of relative density of chasers. This indicates the emergence of a stronger intraspecies segregation among escapees. This is a potentially counter-intuitive result since we see stronger segregation in escapees as its population size decreases. This is an indirect effect of interactions of escapees with chasers. At a high relative density of chasers, each escapee will be surrounded by many chasers. The repulsive bias of escapees to chasers forbids the possible movement of any escapee, towards other escapees, that are surrounded by chasers. This results in the segregation of escapees. We see $C_{ce}(r)$ becomes close to one and A_{ce} approaches zero as we increase the relative density of chasers, suggesting the weakening of the interspecies segregation. As we increase the relative density of chasers, the attraction of chasers to escapees outweighs the repulsive bias of escapees from chasers, to create a less segregated spatial pattern. We also provide another set of results in Section 3A.6 to emphasise that the impact of variation in relative density is strongly dependent on the choice of interaction strengths.

3.7 Conclusions

The most striking feature of our analysis is that we find the formation of spatial structures that are driven purely by motility. This is interesting because most spatial moment models and analysis have their origin in plant ecology where birth and death, rather than motility, are the key mechanisms (Bolker and Pacala, 1997; Bolker and Pacala, 1999; Law and Dieckmann, 2000; Law et al., 2003). More recent spatial moment models have been developed to mimic cell biology experiments where simultaneous movement and proliferation are important, and these previous studies attribute the formation of spatial structure to the combined effects of motility and proliferation (Binny et al., 2016b; Browning et al., 2018). While other studies have investigated the formation of spatial structures driven by density-dependent movement (Liu et al., 2013, 2016; Delfau et al., 2016), this is the first study to apply spatial moment analysis to a conservative community, composed of multiple distinct populations, without birth or death events. These considerations enable us to focus on how motility alone drives significant spatial patterning, and we find that this is particularly relevant when we consider asymmetric interactions between distinct populations within the community. Our IBM and spatial moment dynamics modelling framework allows us to capture different features of the individual-level motility mechanisms such as neighbour dependent directional bias emerging as a consequence of the interactions among individuals. We explore a range of complex spatial structure arising from the combined impacts of various intraspecies and interspecies interactions, which involve different types of attractive or repulsive bias between individuals in a stereotypical community consisting of two distinct species. We provide an extensive analysis of different features of the intraspecies and interspecies interaction by varying the interaction strength, the spatial extent of interaction and relative densities of individuals of both the species. Our results include several interesting and possibly counter-intuitive results. For example, under self-repulsion of

escapees and chase-escape behaviour, the increase in density of chasers relative to escapees results in weakening of segregated pattern between chasers and enhancement of segregated pattern among escapees.

An interesting extension of the model presented here would be to include interactions which affect the proliferation and mortality of individuals, such as predator-prey interactions or intra and interspecific competition (Dittmann and Schausberger, 2017; Lin et al., 2018). The population dynamics resulting from such interactions will depend on the types of spatial structure examined in this work. Another extension would be to consider spatial processes such as moving fronts that are relevant to many biological processes including malignant invasion and developmental morphogenesis (Smith and Yates, 2018). In this study, we consider the movement of individuals in a two-dimensional spatial domain. However, realistic modelling of *in vivo* cell migration requires consideration of three-dimensional (3D) space. While the extension of the IBM framework and moment dynamics analysis to 3D is relatively straight forward, the numerical evaluation of moment dynamics in 3D can become increasingly complicated. We leave these extensions for future work.

Chapter 3A

Additional results for Chapter 3

3A.1 Derivation of movement displacement PDF

Here, we derive an expression for the probability density function (PDF), for the displacement that a chaser traverses during a movement event. Let us assume that the distance moved is a random variable with PDF $u_c(|\xi|)$ and the direction of movement is specified by an independent random variable with PDF $g(\theta)$. Now, we have the movement vector, $(\xi_x, \xi_y) = (|\xi| \cos(\theta), |\xi| \sin(\theta))$ and the PDF for this bivariate random variable can be computed as,

$$\begin{aligned}\mu_c(\xi) &= \frac{\mathbb{P}(\text{movement vector } (\xi_x, \xi_y) \text{ is in a region of area } dA \in \mathbb{R}^2)}{dA}, \\ &= \frac{u_c(|\xi|) d|\xi| \times g(\theta) d\theta}{|\xi| d|\xi| d\theta}, \\ &= \frac{u_c(|\xi|) g(\theta)}{|\xi|}.\end{aligned}\tag{3A.1}$$

A similar derivation holds for the movement displacement PDF, $\mu_e(\xi)$, of escapees.

3A.2 Spatial moment dynamics for a community consisting of two distinct species

Now, we present the details about the spatial moment dynamics for a specific case of the generalised model, where the community consists of individuals from two distinct species. The average densities of chasers and escapees are denoted by $Z_{1,c}$ and $Z_{1,e}$, respectively. Four different second spatial moments correspond to the average density of pairs of individuals are denoted by $Z_{2,cc}(\xi, t)$, $Z_{2,ce}(\xi, t)$, $Z_{2,ec}(\xi, t)$, and $Z_{2,ee}(\xi, t)$, respectively.

The gradient of the bias kernel gives the contribution of individuals of both species to the bias vector of the neighbouring individual. The expected net bias vector of a chaser conditional

on the presence of another chaser is given by,

$$\begin{aligned}\mathbf{B}_{2,cc}(\xi, t) = & \frac{1}{Z_{2,cc}(\xi, t)} \int (\nabla \omega_{cc}(|\xi'|) Z_{3,ccc}(\xi, \xi', t) \\ & + \nabla \omega_{ce}(|\xi'|) Z_{3,cce}(\xi, \xi', t)) d\xi' + \nabla \omega_{cc}(|\xi|).\end{aligned}\quad (3A.2)$$

Similarly, the expected net bias vector of a chaser conditional on the presence of an escapee is given by,

$$\begin{aligned}\mathbf{B}_{2,ce}(\xi, t) = & \frac{1}{Z_{2,ce}(\xi, t)} \int (\nabla \omega_{cc}(|\xi'|) Z_{3,cec}(\xi, \xi', t) \\ & + \nabla \omega_{ce}(|\xi'|) Z_{3,cee}(\xi, \xi', t)) d\xi' + \nabla \omega_{ce}(|\xi|).\end{aligned}\quad (3A.3)$$

The expected net bias vectors of an escapee conditional on the presence of chaser and escapee, respectively are given by,

$$\begin{aligned}\mathbf{B}_{2,ec}(\xi, t) = & \frac{1}{Z_{2,ec}(\xi, t)} \int (\nabla \omega_{ec}(|\xi'|) Z_{3,ecc}(\xi, \xi', t) \\ & + \nabla \omega_{ee}(|\xi'|) Z_{3,ece}(\xi, \xi', t)) d\xi' + \nabla \omega_{ec}(|\xi|),\end{aligned}\quad (3A.4)$$

$$\begin{aligned}\mathbf{B}_{2,ee}(\xi, t) = & \frac{1}{Z_{2,ee}(\xi, t)} \int (\nabla \omega_{ec}(|\xi'|) Z_{3,eec}(\xi, \xi', t) \\ & + \nabla \omega_{ee}(|\xi'|) Z_{3,eee}(\xi, \xi', t)) d\xi' + \nabla \omega_{ee}(|\xi|).\end{aligned}\quad (3A.5)$$

We now develop the equations governing the dynamics of the second moments. The equations for the density of pairs depends on the loss and gain of pairs at displacement ξ . The equations governing the dynamics of second moments for the community of chasers and escapees are given by,

$$\begin{aligned}\frac{\partial}{\partial t} Z_{2,cc}(\xi, t) = & -2 m_c Z_{2,cc}(\xi, t) \\ & + m_c \int \mu_{2,cc}(\xi', \xi' + \xi, t) Z_{2,cc}(\xi' + \xi, t) d\xi' \\ & + m_c \int \mu_{2,cc}(\xi', \xi' - \xi, t) Z_{2,cc}(\xi' - \xi, t) d\xi',\end{aligned}\quad (3A.6)$$

$$\begin{aligned}\frac{\partial}{\partial t} Z_{2,ce}(\xi, t) = & -(m_c + m_e) Z_{2,ce}(\xi, t) \\ & + m_c \int \mu_{2,ce}(\xi', \xi' + \xi, t) Z_{2,ce}(\xi' + \xi, t) d\xi' \\ & + m_e \int \mu_{2,ec}(\xi', \xi' - \xi, t) Z_{2,ec}(\xi' - \xi, t) d\xi',\end{aligned}\quad (3A.7)$$

$$\begin{aligned} \frac{\partial}{\partial t} Z_{2,ec}(\xi, t) = & - (m_c + m_e) Z_{2,ec}(\xi, t) \\ & + m_e \int \mu_{2,ec}(\xi', \xi' + \xi, t) Z_{2,ec}(\xi' + \xi, t) d\xi' \\ & + m_c \int \mu_{2,ce}(\xi', \xi' - \xi, t) Z_{2,ce}(\xi' - \xi, t) d\xi', \end{aligned} \quad (3A.8)$$

$$\begin{aligned} \frac{\partial}{\partial t} Z_{2,ee}(\xi, t) = & - 2 m_e Z_{2,ee}(\xi, t) \\ & + m_e \int \mu_{2,ee}(\xi', \xi' + \xi, t) Z_{2,ee}(\xi' + \xi, t) d\xi' \\ & + m_e \int \mu_{2,ee}(\xi', \xi' - \xi, t) Z_{2,ee}(\xi' - \xi, t) d\xi'. \end{aligned} \quad (3A.9)$$

3A.3 Moment closure schemes

Here, we compare the accuracy of four popular moment closure schemes. The closure schemes considered include the power-1 closure (P1), symmetric power-2 closure (P2S), asymmetric power-2 closure (P2A) and Kirkwood superposition approximation (KSA) (Murrell et al., 2004; Raghib et al., 2011).

The power-1 closure (P1) is given by,

$$\begin{aligned} Z_{3,ijk}(\xi, \xi', t) = & Z_{1,i} Z_{2,jk}(\xi' - \xi, t) + Z_{1,j} Z_{2,ik}(\xi', t) \\ & + Z_{1,k} Z_{2,ij}(\xi, t) - 2Z_{1,i} Z_{1,j} Z_{1,k}. \end{aligned} \quad (3A.10)$$

The power-2 closure is given by,

$$\begin{aligned} Z_{3,ijk}(\xi, \xi', t) = & \frac{1}{\alpha + \gamma} \left[\alpha \frac{Z_{2,ij}(\xi, t) Z_{2,ik}(\xi', t)}{Z_{1,i}} + \beta \frac{Z_{2,ij}(\xi, t) Z_{2,jk}(\xi' - \xi, t)}{Z_{1,j}} \right. \\ & \left. + \gamma \frac{Z_{2,ik}(\xi', t) Z_{2,jk}(\xi' - \xi, t)}{Z_{1,k}} - \beta Z_{1,i} Z_{1,j} Z_{1,k} \right]. \end{aligned} \quad (3A.11)$$

For the symmetric power-2 closure (P2S), we choose $\alpha = \beta = \gamma = 1$, and for the asymmetric power-2 closure (P2A), we use $\alpha = 4, \beta = 1$, and $\gamma = 1$ (Law et al., 2003).

The Kirkwood superposition approximation (KSA) is given by,

$$Z_{3,ijk}(\xi, \xi', t) = \frac{Z_{2,ij}(\xi, t) Z_{2,ik}(\xi', t) Z_{2,jk}(\xi' - \xi, t)}{Z_{1,i} Z_{1,j} Z_{1,k}}. \quad (3A.12)$$

We compute PCFs using these different closure schemes for a community consisting of two species with $N_c = N_e = 100$ and compare with the averaged results of IBM simulation. Again, in these simulations, we consider a randomly distributed initial arrangement of individuals. Results in Figure 3A.1 compare the auto-PCFs, $C_{cc}(r)$ and $C_{ee}(r)$, and the cross-PCF, $C_{ce}(r)$,

for each of the closure schemes with results from the IBM simulation. Overall, when we consider all three PFCs, we see that the power-2 asymmetric closure provides the best match with the prediction of the IBM simulation for the parameters considered in Figure 3A.1. Our approach in this work is not to promote one particular closure approximation over another closure approximation. Instead, we present a general spatial moment framework that can be implemented with a range of closure assumptions should one particular closure approximation be preferred to another.

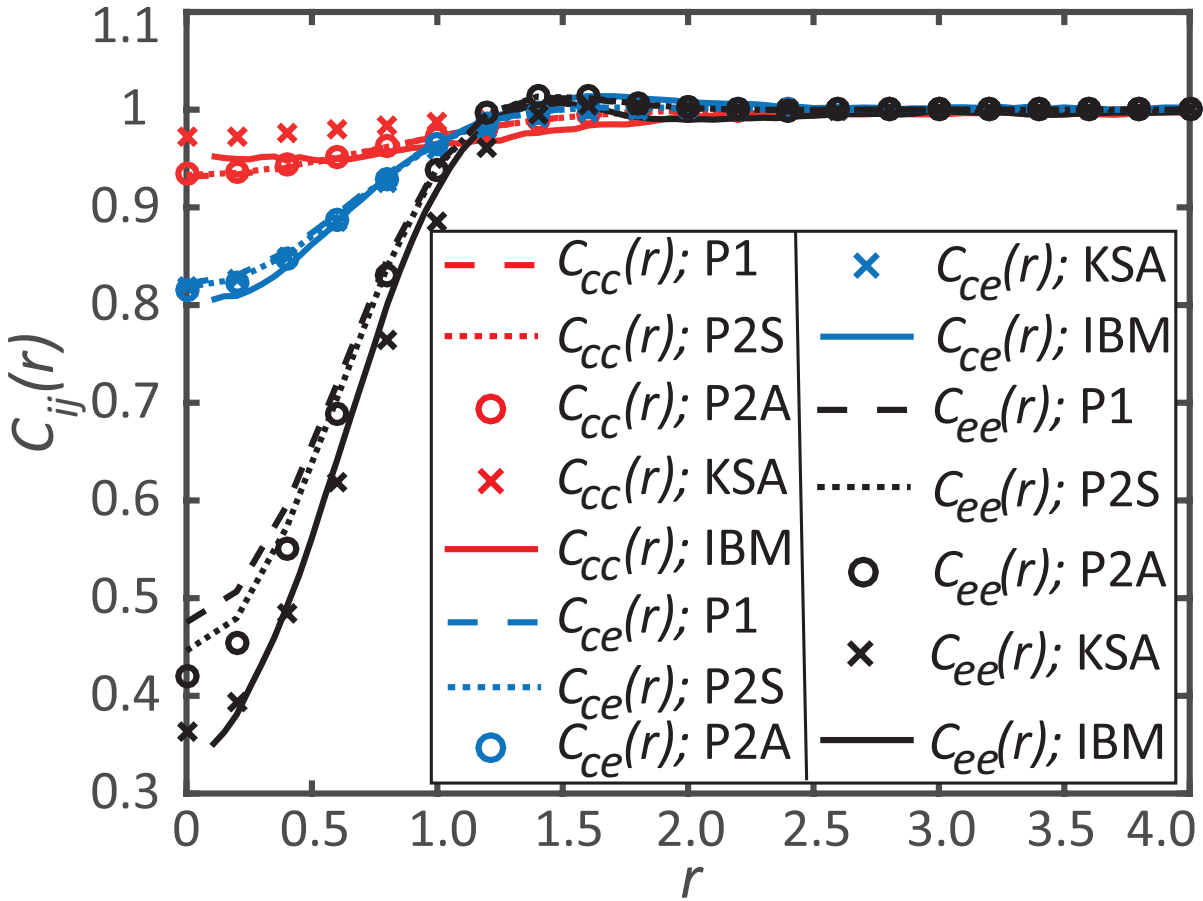


Figure 3A.1: Comparison of spatial moment closure approximation schemes. The curves in red, blue and black correspond to $C_{cc}(r)$, $C_{ce}(r)$ and $C_{ee}(r)$, respectively. In all results, PCFs are given at $t = 20$. All PCFs from IBM correspond to averaged data of 1000 identically prepared realisations. Parameter values are $\gamma_{cc} = 0$, $\gamma_{ce} = -0.2$, $\gamma_{ec} = \gamma_{ee} = 0.3$, $\sigma_{cc} = \sigma_{ce} = \sigma_{ec} = \sigma_{ee} = 0.5$, $m_c = m_e = 5.0$, $\mu_c^{(s)} = \mu_e^{(s)} = 0.4$, $\sigma_c^{(s)} = \sigma_e^{(s)} = 0.1$.

3A.4 Evolution of spatial structure

Here, we explore how the spatial structure evolve as individuals undergo movement events. To illustrate, we consider a sample community consisting of individuals from two distinct species with population sizes $N_c = 30$ and $N_e = 30$. In this suite of simulations, we use a negative γ_{ce} , meaning that the chasers are attracted to escapees. All remaining bias strength parameters are chosen to be positive, which correspond to conspecific repulsions and repulsion of escapees to chasers. Results in Figure 3A.2 show a series of snapshots of the location of individuals and PCFs computed at $t = 0, 1, 20$, and 40 , respectively.

As time progresses, the locations of individuals change due to the movement of individuals as shown in Figure 3A.2(a)-(d). That implies, the local environment around individuals keeps changing and hence the neighbourhood contribution to the bias vector of an individual also varies. The transition of the spatial structure of the community from the initial spatial Poisson process is explored by plotting the PCFs $C_{cc}(r)$, $C_{ee}(r)$ and $C_{ce}(r)$, respectively as shown in Figure 3A.2(e)-(h). Comparing the results at $t = 20$ and $t = 40$, suggests that we have an approximately steady spatial pattern established by $t = 20$. As time progresses, we observe the development of a segregated spatial pattern among subpopulations of chasers and escapees since $C_{cc}(r) < 1$ and $C_{ee}(r) < 1$ for small distances. The reason for the segregated spatial structure is the intraspecies repulsion among both species. Each chaser (escapee) tries to stay apart from other chasers (escapees), hence leading to a segregated spatial structure among chasers (escapees). We also observe a less pronounced interspecies segregation between chasers and escapees. Here, the attractive bias of chasers to escapees counteracts the repulsive bias of escapees to chasers, reducing the extent of the interspecies segregation.

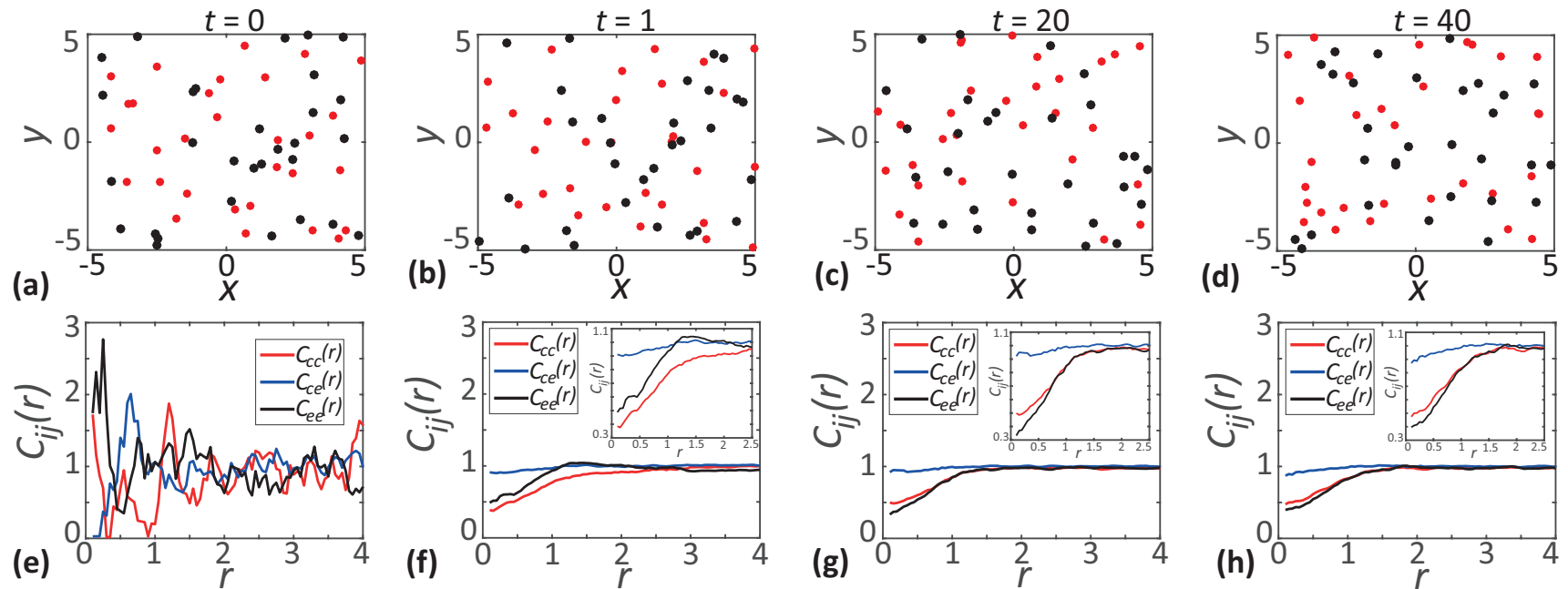


Figure 3A.2: Results in **a-d** show the location of chasers (red dots) and escapees (black dots) at $t = 0, 1, 20$ and 40 , respectively. Results in **e-h** show the PCFs $C_{cc}(r)$, $C_{ce}(r)$, $C_{ee}(r)$ as a function of separation distance r at $t = 0, 1, 20$ and 40 , respectively. The PCFs in **e** corresponds to the randomly distributed initial arrangement of individuals and all PCFs in **f-h** are computed using the average data from 1000 identically prepared realisations of the IBM. Parameter values are $\gamma_{cc} = 0.1$, $\gamma_{ce} = -0.1$, $\gamma_{ec} = \gamma_{ee} = 0.15$ and $\sigma_{cc} = \sigma_{ce} = \sigma_{ec} = \sigma_{ee} = 0.5$.

3A.5 Dependence of steady-state spatial patterns on the initial configuration of individuals

In this section we present additional results which show that the steady-state spatial structure is independent of the initial distribution of individuals. To illustrate, we consider two different initial configurations shown in Figure 3A.3(a)-(b), respectively. Here, the first case corresponds to a uniform distribution of chasers and escapees with population sizes, $N_c = 200$ and $N_e = 200$, respectively. The second case considered corresponds to a spatially non-uniform distribution of chasers and escapees. In this second case, chasers and escapees are placed at the opposite corners of the domain. The population sizes of both the species are kept the same as that in Figure 3A.3(a). To examine whether these different initial conditions affect the long-time spatial structure, we simulate the IBM with these two different types of initial distributions of individuals. In both of these simulations we use identical interaction strengths and spatial extents of interactions.

We observe that a steady spatial pattern emerges in the case of simulation with uniform initial arrangement of chasers and escapees by approximately $t = 20$, whereas the second initial condition requires a longer duration to approach a steady distribution, $t = 100$. To examine the resulting spatial structure we plot the auto and cross-PCFs in Figure 3A.3(c) and these results confirm that the two different initial configurations leads to identical spatial structure.

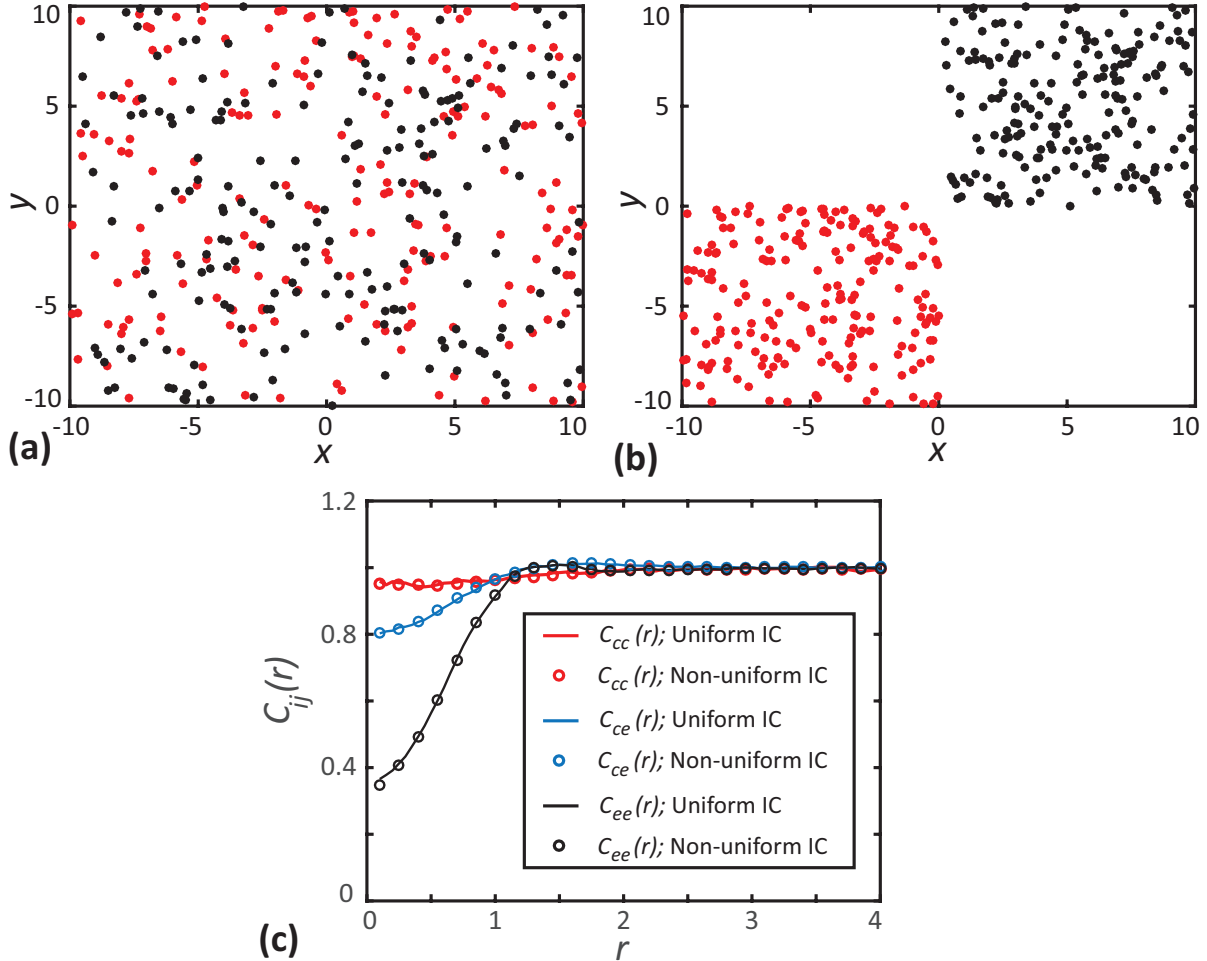


Figure 3A.3: Effect of varying the initial configuration of individuals on the spatial structure. **a** shows a uniformly distributed initial arrangement of chasers (red dots) and escapees (black dots). **b** shows a non-uniform initial arrangement of individuals. In this case, chasers and escapees are placed at the opposite corners of the domain. **c** shows the auto and cross-PCFs computed with uniform and non-uniform initial configurations (IC) at $t = 20$ (solid lines) and $t = 100$ (open circles), respectively. In **c** red, blue and black curves represent $C_{cc}(r)$, $C_{ce}(r)$ and $C_{ee}(r)$, respectively. Parameter values are $\gamma_{cc} = 0$, $\gamma_{ce} = -0.2$, $\gamma_{ec} = \gamma_{ee} = 0.3$ and $\sigma_{cc} = \sigma_{ce} = \sigma_{ec} = \sigma_{ee} = 0.5$.

3A.6 Effect of varying the relative density of species

Here, we present another set of results, as shown in Figure 3A.4, to emphasise that the impact of variation in relative density is strongly dependent on the choice of interaction strengths. To illustrate, we consider a scenario with same parameters and initial placement of individuals as in Figure 3.6, except that we use a positive γ_{ce} that corresponds to repulsion of chasers from escapees. In contrast to the results in Figure 3.6, we observe a strong clustering of chasers at low relative densities of chasers. The presence of more escapees creates a strong repulsion to fewer chasers and the choice of $\gamma_{ce} = 0.3$ forces chasers to move away from the escapees. Since there is no interaction between chasers, both these factors act together to form clusters of chasers. As we increase the relative density, the clustering weakens and leads to a random spatial structure. This is also confirmed by the lowering of simple measure of spatial structure, A_{cc} , from 1.5 at $Z_{1,c}/Z_{1,e} = 1/7$ to close to zero at $Z_{1,c}/Z_{1,e} = 7$.

At low relative densities of chasers we observe an intraspecies segregation of escapees due to the repulsive interaction between escapees. As we increase the relative density of chasers, we observe a peak in PCF, $C_{ee}(r)$, at approximately $r = 1.25$. This peak corresponds to an extreme case of segregation where almost all escapees are separated by approximately the same distance. This case represents the overabundance of a specific distance between pairs of individuals, and hence we call this spatial pattern a regular spatial pattern. The more pronounced regular pattern arises due to the combined effect of the enhanced repulsion of chasers to escapees, due to the increase in the number of chasers compared to escapees, and the repulsive intraspecies interaction of escapees. Overall, we summarise that the interspecies regular spatial structure between chasers and escapees becomes more pronounced as the relative density of chasers increases.

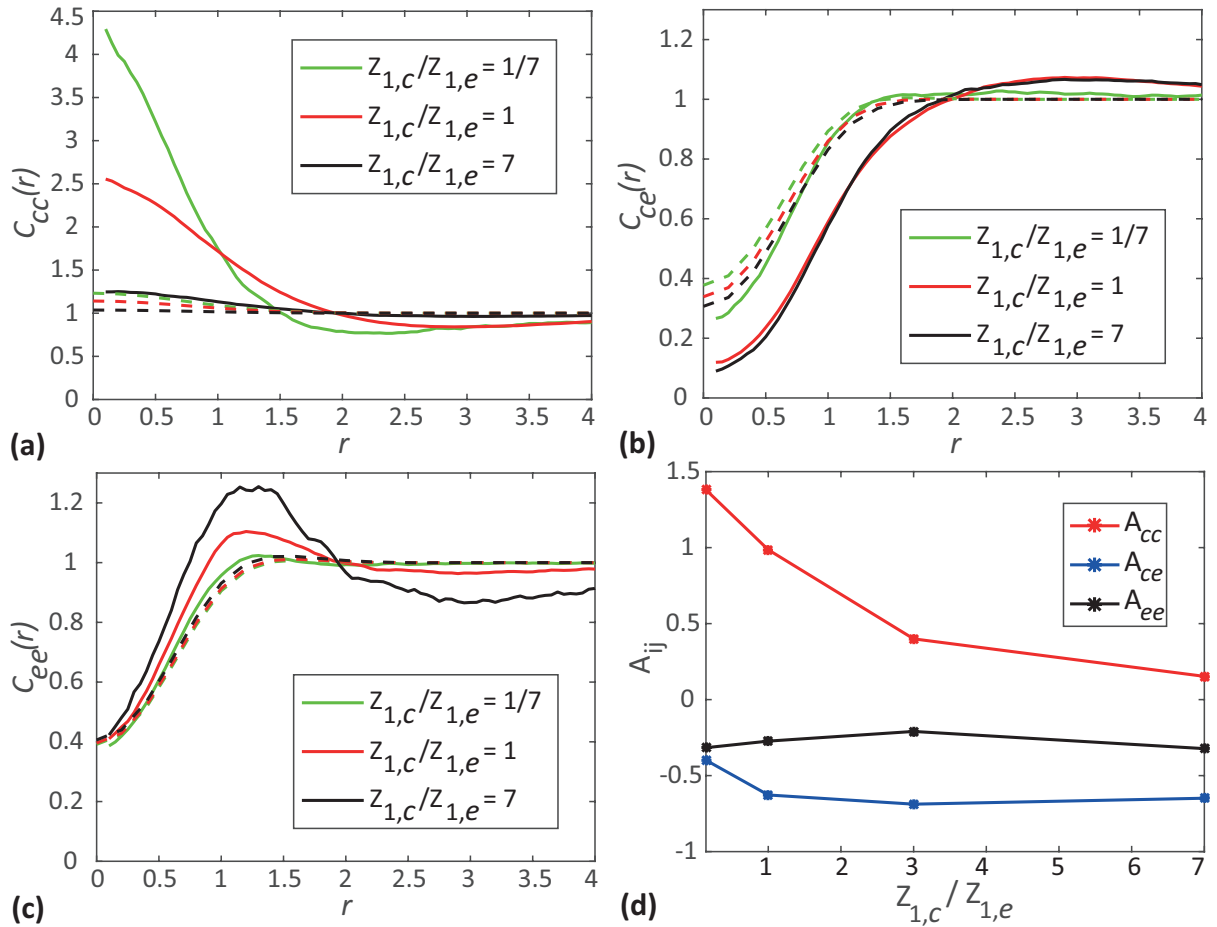


Figure 3A.4: Effects of varying the relative density of species. **a** shows the auto-PCF of chasers as a function of separation distance. **b** shows the cross-PCF as a function of separation distance. **c** shows the auto-PCF of escapees as a function of separation distance. **d** show simple measures of spatial structure, A_{ij} , as a function of relative densities of species. In **(a)-(c)** solid curves show the averaged results from 1000 identically prepared realisations of the IBM, whereas dashed curves correspond to results from spatial moment dynamics model. In all results, PCFs and simple measures of spatial structure are given at $t = 20$. Parameter values are $\gamma_{cc} = 0$, $\gamma_{ce} = \gamma_{ec} = \gamma_{ee} = 0.3$, $\sigma_{cc} = \sigma_{ce} = \sigma_{ec} = \sigma_{ee} = 0.5$, $m_c = m_e = 5.0$, $\mu_c^{(s)} = \mu_e^{(s)} = 0.4$, $\sigma_c^{(s)} = \sigma_e^{(s)} = 0.1$.

Statement of Contribution of Co-Authors for Thesis by Published Paper

The authors listed below have certified that:

1. they meet the criteria for authorship and that they have participated in the conception, execution, or interpretation, of at least that part of the publication in their field of expertise;
2. they take public responsibility for their part of the publication, except for the responsible author who accepts overall responsibility for the publication;
3. there are no other authors of the publication according to these criteria;
4. potential conflicts of interest have been disclosed to (a) granting bodies, (b) the editor or publisher of journals or other publications, and (c) the head of the responsible academic unit, and
5. they agree to the use of the publication in the student's thesis and its publication on the [QUT's ePrints site](#) consistent with any limitations set by publisher requirements.

In the case of chapter 4:

Surendran Anudeep, Plank Michael J., Simpson Matthew J. 2020 Small-scale spatial structure affects predator-prey dynamics and coexistence. *Theoretical Ecology*.

Contributor	Statement of contribution*
Anudeep Surendran	Designed the study, derived the continuum moment dynamics equations, developed the codes for numerical simulation of the IBM and spatial moment model, performed numerical simulations, generated results, interpreted the results, drafted the manuscript, and revised the manuscript during peer-review process. <i>Anudeep Surendran</i>
19/08/2020	
Michael J. Plank	Designed the study, interpreted the results, edited the manuscript during initial submission and subsequent revision during peer-review process.
Matthew J. Simpson	Designed the study, supervised the research, interpreted the results, edited the manuscript during initial submission and subsequent revision during peer review process and acted as the corresponding author.

Principal Supervisor Confirmation

I have sighted email or other correspondence from all Co-authors confirming their certifying authorship. (If the Co-authors are not able to sign the form please forward their email or other correspondence confirming the certifying authorship to the GRC).

MATTHEW SIMPSON
Name

M. Simpson
Signature

26 | 8 | 2020
Date

Chapter 4

Small-scale spatial structure affects predator-prey dynamics and coexistence

4.1 Preamble

This chapter is a paper published in *Theoretical Ecology*.

Surendran Anudeep, Plank Michael J., Simpson Matthew J. 2020 Small-scale spatial structure affects predator-prey dynamics and coexistence. *Theoretical Ecology* 13: 537–550. DOI:[10.1007/s12080-020-00467-6](https://doi.org/10.1007/s12080-020-00467-6). bioRxiv Preprint.

In this chapter, we address the research question 3 of the thesis: What impact do short-range interactions and spatial structure have on the predator-prey dynamics? Here, we extend the modelling framework presented in Chapter 2, to incorporate the ecologically relevant predator-prey interactions. In this extension, we consider a population consisting of two species, namely consumers and resources, where consumers predate on resources. We construct an IBM by considering the effect of predation interactions as well as the conspecific competition interaction of each species on birth and death rates. This chapter’s main objective is to elucidate whether the short-range interactions lead to a qualitatively different population dynamics outcome from that predicted by the classical mean-field predator-prey model. To address this, we derive a continuum model by invoking the mean-field assumption. By comparing the results of IBM simulations with the mean-field model solutions, we examine how short-range interactions and spatial structure drive the population away from the mean-field dynamics.

4.2 Abstract

Small-scale spatial variability can affect community dynamics in many ecological and biological processes, such as predator-prey dynamics and immune responses. Spatial variability includes short-range neighbour-dependent interactions and small-scale spatial structure, such as *clustering* where individuals aggregate together, and *segregation* where individuals are spaced

apart from one another. Yet, a large class of mathematical models aimed at representing these processes ignores these factors by making a classical mean-field approximation, where interactions between individuals are assumed to occur in proportion to their average density. Such mean-field approximations amount to ignoring spatial structure. In this chapter, we consider an individual based model of a two-species community that is composed of *consumers* and *resources*. The model describes migration, predation, competition and dispersal of offspring, and explicitly gives rise to varying degrees of spatial structure. We compare simulation results from the individual based model with the solution of a classical mean-field approximation, and this comparison provides insight into how spatial structure can drive the system away from mean-field dynamics. Our analysis reveals that mechanisms leading to intraspecific clustering and interspecific segregation, such as short-range predation and short-range dispersal, tend to increase the size of the resource species relative to the mean-field prediction. We show that under certain parameter regimes these mechanisms lead to the extinction of consumers whereas the classical mean-field model predicts the coexistence of both species.

4.3 Introduction

Mathematical modelling of ecology and cell biology processes, such as predator-prey dynamics and immune cell-pathogen interactions, can provide insight into the impact of various interaction mechanisms that influence community dynamics. Traditional mathematical models are based on making a mean-field approximation, where the community is assumed to be locally well mixed and the presence of an individual at one location is independent of the presence or absence of an individual at any other location (Law and Dieckmann, 2000; Law et al., 2003; Baker and Simpson, 2010; Grunbaum, 2012). Mean-field models, such as the Lotka-Volterra model of predator-prey dynamics and the logistic growth model do not incorporate any information about the spatial correlation between the locations of individuals. These classical mean-field models are typically written as ordinary differential equations that govern the time evolution of the average density of individuals (Edelstein-Keshet, 2005). Some prey-predator models incorporate different types of functional responses, such as density dependence (Abrams and Ginzburg, 2000; Wang et al., 2009), but do not explicitly consider the role of spatial structure. Spatially explicit mean-field models are also commonly used to help understand various ecology and cell biology processes, where the density dynamics is often described using partial differential equations (Murray, 1989; Hillen and Painter, 2009). Other types of spatially explicit models include coupled map lattices, integro-difference equations, and various kinds of metapopulation models (Britton, 2003). Even though these spatially explicit models express the density of individuals as a function of spatial location, interactions between individuals are implicitly assumed to be given by local mean-field conditions described by the average density alone.

In many situations, short-range interactions are thought to play a significant role in deter-

mining community dynamics (Penczykowski et al., 2016; Galetti et al., 2018). For example, in a prey-predator community, an individual member of the prey population located nearby a cluster of predators could experience increased mortality due to the high risk of predation. Similarly, localised intraspecies competition for shared food resources could lead to an increase in the death rates of conspecific individuals. Neighbour-dependent interactions are known to lead to spatial structures (Tobin and Bjornstad, 2003; Santora et al., 2010). Typical forms of spatial structures relevant to ecological and biological systems include: (i) *clustering* where individuals aggregate together; and (ii) *segregation* where individuals tend to spread out as much as possible (Binny et al., 2015; Treloar et al., 2015; Surendran et al., 2019). These types of spatial structures can occur within communities composed of single or multiple species (Markham et al., 2013; Gerum et al., 2018; Dini et al., 2018).

While spatial structure is known to impact the macroscale density dynamics of a community, commonly-used mean-field models neglect these effects. In contrast, individual based models (IBM) are useful to investigate the effects of short-scale interactions and the formation of spatial structure. Many IBMs are lattice-based, where the interactions between individuals are dictated by an artificial lattice structure (Mobilia et al., 2006; Mobilia et al., 2007; Baker and Simpson, 2010; Dobramysl and Tauber, 2013). A more realistic approach is to consider lattice-free IBMs, where interactions can be incorporated more realistically in a spatially continuous framework. The IBM considered in this study is an extension of our previous work (Surendran et al., 2018) examining the neighbour-dependent interactions between motile agents (e.g. cells) and stationary agents (e.g. obstacles) in the context of experimental cell biology. Here, we extend this framework to accommodate interactions relevant to ecological processes, such as predation and competition. Similar IBMs have been used previously to study the impact of motility and fecundity rates on density dynamics (Murrell, 2005) as well as exploring the impact of spatial patterns on the evolution and natural selection of prey dispersal (Barraquand and Murrell, 2012).

In this work, we explore various spatial structure forming mechanisms such as short-range predation, short-range-dispersal of offspring and short-range intraspecies competition in a community of consumers and resources. We examine the effects of these mechanisms, both in isolation and in combination, and specifically examine how these effects generate spatial structures that lead to deviations from mean-field dynamics. These investigations are conducted by comparing IBM simulations with the solution of appropriate mean-field equations. The spatial configuration of the community is analysed in terms of pair correlation functions (PCF) (Agnew et al., 2014; Binny et al., 2016a, b). The PCFs measure spatial structure within and between species. This analysis assists our interpretation of the impact of spatial structure. We demonstrate scenarios where the mean-field model completely fails to capture the spatial effects and predict qualitatively different behaviours.

4.4 Individual-based model

We consider a community that consists of two distinct species, namely consumers and resources. The consumers are a group of individuals undergoing proliferation, death and movement events. They can be thought of as ecological predators or immune cells (Abrams, 2000; Akira et al., 2006; Soehnlein et al., 2017). These consumers predate on the resources. The resources are also motile and proliferative. The resources can be thought of as a population of ecological prey or biological pathogens (Rincon et al., 2017; Hunt and Brown, 2018; Vijay, 2018). In our model, consumers and resources are distributed on a continuous two dimensional domain of size $L \times L$ with population sizes $N_c(t)$ and $N_r(t)$, respectively. The IBM is constructed for spatially homogeneous problems, where the population density in a small region, averaged over multiple realisations of the IBM, is independent of the location of that region (Plank and Law, 2015). This means our framework is relevant to communities that do not have macroscopic gradients in the density of individuals (Jin et al., 2018).

The death rate of the n^{th} resource individual located at $\mathbf{x}_{r_n} \in \mathbb{R}^2$, where $n = 1, 2, \dots, N_r(t)$, is taken to be a result of both interspecies predation and intraspecies competition that arise from interactions with other individuals in the population,

$$D_{r_n} = \sum_{l=1}^{N_c(t)} \omega_{rc}^p(|\mathbf{x}_l - \mathbf{x}_{r_n}|) + \sum_{k=1}^{N_r(t)} \omega_{rr}^c(|\mathbf{x}_k - \mathbf{x}_{r_n}|). \quad (4.1)$$

The first term on the right of Equation (4.1) is the death rate from predation by consumers, specified by the kernel $\omega_{rc}^p(|\xi|)$. The second term on the right of Equation (4.1) accounts for the contribution of competition to the resources death rate, specified by the kernel $\omega_{rr}^c(|\xi|)$. Both kernels in Equation (4.1) are decreasing functions of distance, $|\xi|$. A schematic representation summarising the impact of predation and competition on the event rates of individuals is given in Figure 4.1.

We consider Gaussian interaction kernels to ensure the strength of interaction between individuals decreases with separation distance. The predation kernel describing the contribution of a neighbouring consumer at a displacement, ξ , to the death rate of a reference resource individual is given by,

$$\omega_{rc}^p(|\xi|) = \gamma_{rc}^p \exp\left(-\frac{|\xi|^2}{2(\sigma_{rc}^p)^2}\right), \quad (4.2)$$

where $\gamma_{rc}^p > 0$ and $\sigma_{rc}^p > 0$ represent the predation strength and the spatial extent of predation, respectively. There is no strict requirement on the functional form of the interaction kernel. Non-Gaussian kernels can be incorporated into the IBM, depending on the specific applications (Plank et al., 2019). Competition kernels also take the same functional form. For simplicity, we assume that resources proliferate at a constant rate, $P_{r_n} = p_r$, and that this rate is unaffected by the presence of other individuals.

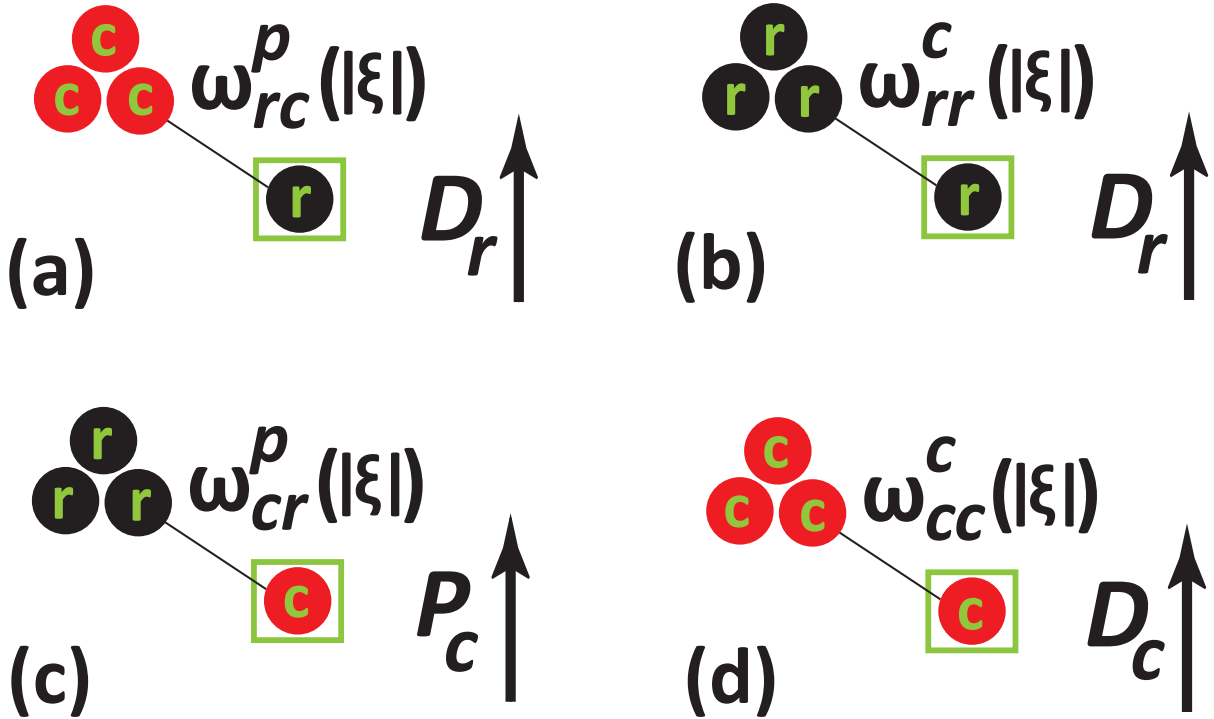


Figure 4.1: Schematic representation of how neighbour-dependent interactions affect proliferation and death rates of resources (black) and consumers (red). The green squares indicate the reference individual whose event rates are altered by the interactions. **a** impact of predation interaction on a resource leading to an increased death rate, D_r . **b** impact of intraspecies competition of resources, leading to an increased death rate, D_r . **c** impact of predation interaction on consumers, leading to an enhanced the proliferation rate, P_c . **d** impact of intraspecies competition of consumers, leading to an increase in the death rate, D_c .

Consumer reproduction is taken to be dependent on the predation and subsequent consumption of resources, which provide the required biomass for offspring. We use a predation kernel, $\omega_{cr}^p(|\xi|)$, to account for the contribution of resources in the enhancement of the proliferation rate of consumers. Setting $\gamma_{cr}^p < \gamma_{rc}^p$ reflects a realistic situation where the consumption of a single resource is insufficient to generate a single consumer. We also make a reasonable assumption that, $\sigma_{cr}^p = \sigma_{rc}^p$, so that the distance over which consumers and resources interact is symmetric. The proliferation rate of consumers is computed by summing the contributions from all the resources,

$$P_{c_n} = \sum_{l=1}^{N_r(t)} \omega_{cr}^p(|\mathbf{x}_l - \mathbf{x}_{c_n}|). \quad (4.3)$$

The mortality of consumers depends on competitive interactions between consumers. The death rate of consumers is given by,

$$D_{c_n} = d_c + \sum_{l=1}^{N_c(t)} \omega_{cc}^c(|\mathbf{x}_l - \mathbf{x}_{c_n}|). \quad (4.4)$$

The first term on the right of Equation (4.4) is a constant intrinsic death rate of consumers which is unaffected by the presence of other individuals in the model. The second term on the right of Equation (4.4) accounts for the contribution of competition between consumers. For

simplicity we assume the movement rate of consumers and resources are constant, and given by m_c , and m_r , respectively.

The IBM is simulated using the Gillespie algorithm (Gillespie, 1977). We use periodic boundary conditions over the computational domain since the domain considered is large enough to avoid any edge effects. Initial population sizes of consumers and resources are $N_c(0)$ and $N_r(0)$, respectively, and the locations of these individuals are initially chosen at random. At each time step, the neighbour-dependent event rates of individuals are computed according to Equation (4.1) and Equations (4.3)–(4.4). The total event rate of all individuals is computed by summing all the intrinsic and neighbour-dependent rates as,

$$\lambda(t) = \sum_{n=1}^{N_r(t)} (P_{r_n} + D_{r_n} + m_r) + \sum_{n=1}^{N_c(t)} (P_{c_n} + D_{c_n} + m_c). \quad (4.5)$$

The time intervals between successive events are distributed according to an exponential distribution with mean $1/\lambda(t)$. At each time increment of the Gillespie algorithm, one of the three possible events occurs. The probability of the occurrence of an event is proportional to the rate of that event (Baker and Simpson, 2010). When a consumer proliferates, a daughter consumer is placed at a displacement, ξ , drawn from a bivariate normal distribution with mean zero and standard deviation, σ_c^d , resulting in an increase of the consumer population by one. Here, σ_c^d is the consumer dispersal range. Similarly, the proliferation of a resource individual involves placing a daughter resource at a displacement sampled from a bivariate normal distribution with mean zero and standard deviation σ_r^d . When a consumer undergoes a movement event, it travels a displacement $(|\xi| \cos(\theta), |\xi| \sin(\theta))$, where the distance moved by a consumer, $|\xi|$, is drawn from a truncated Gaussian distribution with a positive mean μ_c^s and a narrow standard deviation σ_c^s , such that $\sigma_c^s \leq \mu_c^s/4$. To ensure the movement distance is always positive, we truncate the Gaussian at distances greater than $4\sigma_c^s$ from the mean. The direction of movement, $\theta \in [0, 2\pi]$, is uniformly distributed. Movement of a resource is specified by a similar Gaussian distribution with mean μ_r^s and standard deviation σ_r^s .

To analyse the resulting community dynamics, we calculate the average density of consumers and resource by dividing the number of individuals in both the species with the area of the domain as, $Z_c(t) = N_c(t)/L^2$ and $Z_r(t) = N_r(t)/L^2$, respectively. The average density of pairs of individuals reveals the correlation between the locations of individuals (Bolker and Pacala, 1999; Law et al., 2009; Ovaskainen et al., 2014). We calculate several PCFs, defined as the average densities of pairs normalised by the density of pairs in a community without any spatial structure (i.e. a community that evolves in such a way that the mean-field assumption is valid). We define the PCF as a function of the separation distance between pairs of individuals, $|\xi|$, and time, t . Since there are two species in the model, there are three unique PCFs: (i) the auto-PCF of consumers, $C_{cc}(|\xi|, t)$; (ii) the auto-PCF of resources, $C_{rr}(|\xi|, t)$, and, (iii) the cross-PCF, $C_{cr}(|\xi|, t)$, respectively. In the complete absence of spatial structure we have

$C_{cc}(|\xi|, t) = C_{rr}(|\xi|, t) = C_{cr}(|\xi|, t) = 1$. When the auto-PCF of consumers is greater than unity, $C_{cc}(|\xi|, t) > 1$, we have a larger number of pairs of consumers separated by a distance, $|\xi|$, than we would have in a community with spatially random configuration. We refer to this configuration as clustered. When $C_{cc}(|\xi|, t) < 1$, we have a smaller number of pairs of consumers separated by a distance, $|\xi|$, than we would have in a community with spatially random configuration and this situation corresponds to a segregated spatial structure. Similarly, clustered and segregated spatial patterns of resources correspond to $C_{rr}(|\xi|, t) > 1$ and $C_{rr}(|\xi|, t) < 1$, respectively. Interspecies clustering and segregation of consumers and resources correspond to $C_{cr}(|\xi|, t) > 1$ and $C_{cr}(|\xi|, t) < 1$, respectively.

To compute the auto-PCF of consumers, we consider one consumer individual as a reference individual and then calculate the distance between the reference individual and all other $N_c(t) - 1$ consumers. We record the distances between the reference individual and other individuals of the same species. The auto-PCF is constructed by counting the distances that fall into the interval $[\xi - \Delta|\xi|/2, \xi + \Delta|\xi|/2]$ (Binder and Simpson, 2015). The bin count is normalized by a factor of $2\pi|\xi|\Delta|\xi|N_c(N_c - 1)/L^2$ to ensure that $C_{cc}(|\xi|, t) = 1$ in the absence of spatial structure. A similar procedure is followed to compute $C_{rr}(|\xi|, t)$ and $C_{cr}(|\xi|, t)$.

4.4.1 Mean-field dynamics

Here, we present a continuum description of the IBM by invoking the mean-field assumption. We denote the density of species i at time t , averaged over many identically-prepared realisations of the IBM as $Z_i(t)$. Note that, in our model, average density is independent of location owing to the combination of boundary conditions and initial condition used. In the IBM, the presence of other individuals in the neighbourhood of a focal individual is affected by the community's spatial structure. However, the mean-field assumption ignores this dependence by assuming that the probability that there is an individual of species i at any given location ξ at time t is independent of the occupancy of other individuals, and is given by $Z_i(t)$. For example, the expected proliferation rate of a consumer at location ξ and time t is, $\int \omega_{cr}^p(|\xi|) Z_r(t) d\xi = 2\pi\gamma_{cr}^p(\sigma_{cr}^p)^2 Z_r(t)$. Approximating the other birth and death rates in the community in a similar way leads to

$$\frac{d}{dt}Z_c(t) = 2\pi\gamma_{cr}^p(\sigma_{cr}^p)^2 Z_c(t)Z_r(t) - d_c Z_c(t) - 2\pi\gamma_{cc}^c(\sigma_{cc}^c)^2 Z_c(t)^2, \quad (4.6)$$

$$\frac{d}{dt}Z_r(t) = p_r Z_r(t) - 2\pi\gamma_{rc}^p(\sigma_{rc}^p)^2 Z_c(t)Z_r(t) - 2\pi\gamma_{rr}^r(\sigma_{rr}^r)^2 Z_r(t)^2. \quad (4.7)$$

This system of equations can be derived rigorously from the IBM under the mean-field assumption by replacing the second moment of the spatial point process with the product of the first moments (Plank and Law, 2015), but we omit the details of this here. In this work we study the solution of Equations (4.6)–(4.7) numerically using the `ode45` routine in MATLAB (Mathworks, 2019).

4.5 Results

In this section, we compare averaged data from IBM simulations with the solution of the mean-field model to explore the impact of spatial structure on the community dynamics. The auto- and cross-PCFs help to distinguish between different spatial structures formed due to the intra-species and inter-species interactions. Linking the PCFs and averaged densities from the IBM with the solution of the mean-field model provides comprehensive insight into the role of spatial structure in driving community dynamics. We first present simulation results that are in good agreement with the solutions of the mean-field model. We then use these initial results as a benchmark for exploring other parameter combinations. Mean-field dynamics are replicated in the IBM by considering sufficiently large predation, competition and dispersal ranges. Under these conditions the spatial configuration of individuals does not strongly influence community dynamics, and the individuals interact weakly leading to negligible correlations. A summary of parameter values for this first case are given in Table 4.1.

Table 4.1: Description of model parameters and variables

Parameter symbol	Description	Mean-field value
γ_{cc}^c	competition strength of consumers	$\gamma_{cc}^c = 0.001$
γ_{rr}^c	competition strength of resources	$\gamma_{rr}^c = 0.001$
γ_{cr}^p	predation strength with which consumers attack resources	$\gamma_{cr}^p = 0.003$
γ_{rc}^p	predation strength with which resources are attacked by consumers	$\gamma_{rc}^p = 0.004$
σ_{cc}^c	competition range of consumers	$\sigma_{cc}^c = 4.0$
σ_{rr}^c	competition range of resources	$\sigma_{rr}^c = 4.0$
σ_{cr}^p	predation range over which consumers attack resources	$\sigma_{cr}^p = 4.0$
σ_{rc}^p	predation range over which resources are attacked by consumers	$\sigma_{rc}^p = 4.0$
σ_c^d	dispersal range of consumers	$\sigma_c^d = 4.0$
σ_r^d	dispersal range of resources	$\sigma_r^d = 4.0$
$N_c(0)$	initial population size of consumers	$N_c(0) = 100$
$N_r(0)$	initial population size of resources	$N_r(0) = 200$
p_r	intrinsic proliferation rate of resources	$p_r = 0.2$
d_c	intrinsic death rate of consumers	$d_c = 0.1$
m_r	intrinsic movement rate of resources	$m_r = 0.1$
m_c	intrinsic movement rate of consumers	$m_c = 0.1$
μ_c^s	mean movement distance of consumers	$\mu_c^s = 0.4$
μ_r^s	mean movement distance of resources	$\mu_r^s = 0.4$
σ_c^s	standard deviation movement distance of consumers	$\sigma_c^s = 0.1$
σ_r^s	standard deviation movement distance of resources	$\sigma_r^s = 0.1$
L	domain length	$L = 20$
Variable	Description	
t	time	
$ \xi $	separation distance between a pair of individuals	
$Z_c(t)$	average density of consumers	
$Z_r(t)$	average density of resources	
$C_{cc}(\xi , t)$	PCF corresponding to the pair densities of consumers (auto-PCF of consumers)	
$C_{cr}(\xi , t)$	PCF corresponding to the densities of pairs involving a consumer and resource (cross-PCF)	
$C_{rr}(\xi , t)$	PCF corresponding to the pair densities of resources (auto-PCF of resources)	

In Figure 4.2, we show two scenarios where averaged simulation results from the IBM match well with the solution of the mean-field model. The first case, shown in Figure 4.2(a)–(d), corresponds to a scenario that exhibits co-existence of consumers and resources. In this

case, we consider a community of consumers and resources distributed uniformly with $N_c(0) = 100$ and $N_r(0) = 200$, respectively, as shown in Figure 4.2(a). After a sufficiently long time, $t = 200$, we observe that the densities of consumers and resources and the three PCFs appear to become steady. The snapshot of the IBM at $t = 200$ in Figure 4.2(b) does not show any obvious spatial structure, and the auto- and cross-PCFs are approximately unity in Figure 4.2(d), confirming the absence of spatial structure. The temporal dynamics of the community are tracked by plotting the average densities of consumers and resources as a function of time, in Figure 4.2(c). Here, the mean-field model accurately matches the IBM results. These observations are expected since we consider long-range interactions and long-range dispersal.

We present a different example of mean-field dynamics in Figure 4.2(e)–(h), where the consumer species eventually becomes extinct. Here, we choose an identical initial arrangement of individuals and interactions to that of the coexistence case in Figure 4.2(a)–(d). The only difference between the results in Figure 4.2(e)–(h) and Figure 4.2(a)–(d) is that here we specify a higher consumer death rate which leads to the extinction of consumers. The snapshot of the IBM at $t = 200$ in Figure 4.2(f) shows that only resources remain at this time. Consistent with this, the density of consumers in Figure 4.2(g) decays to zero by approximately $t = 20$. The estimate of average densities from IBM and mean-field model match well for this case. Results in Figure 4.2(h) indicate that $C_{rr}(\xi, t) \approx 1$, and this is consistent with the fact that the mean-field approximation is accurate. Note that we only give $C_{rr}(\xi, t)$ in Figure 4.2(h) since consumers are absent from the simulation by $t = 200$.

Given we have established that averaged data from the IBM is consistent with the solution of the mean-field model for the choice of parameters in Figure 4.2, we systematically vary the parameters in the IBM and explore how the resulting spatial structure affects the accuracy of the mean-field description. In all of these subsequent comparisons, we fix the mean-field equilibrium densities of consumers and resources. By fixing the equilibrium densities, we are able to compare different mechanisms and their impacts on the dynamics. Under coexistence, the equilibrium densities of consumers and resources are given by,

$$Z_c^* = \lim_{t \rightarrow \infty} Z_c(t) = \frac{p_r \gamma_{cr}^p (\sigma_{cr}^p)^2 - d_c \gamma_{rr}^c (\sigma_{rr}^c)^2}{2\pi [\gamma_{cr}^p (\sigma_{cr}^p)^2 \gamma_{rc}^p (\sigma_{rc}^p)^2 + \gamma_{cc}^c (\sigma_{cc}^c)^2 \gamma_{rr}^c (\sigma_{rr}^c)^2]}, \quad (4.8)$$

$$Z_r^* = \lim_{t \rightarrow \infty} Z_r(t) = \frac{p_r \gamma_{cc}^c (\sigma_{cc}^c)^2 + d_c \gamma_{rc}^p (\sigma_{rc}^p)^2}{2\pi [\gamma_{cr}^p (\sigma_{cr}^p)^2 \gamma_{rc}^p (\sigma_{rc}^p)^2 + \gamma_{cc}^c (\sigma_{cc}^c)^2 \gamma_{rr}^c (\sigma_{rr}^c)^2]}. \quad (4.9)$$

When we compare different parameter combinations, we take care to choose the interaction ranges and interaction strengths so that Z_c^* and Z_r^* remain constant. This ensures that the long-time solution of the mean-field model is constant between the various conditions that we examine. The specific values of interaction range and strength parameters used in each of our simulations are given in respective figure captions.

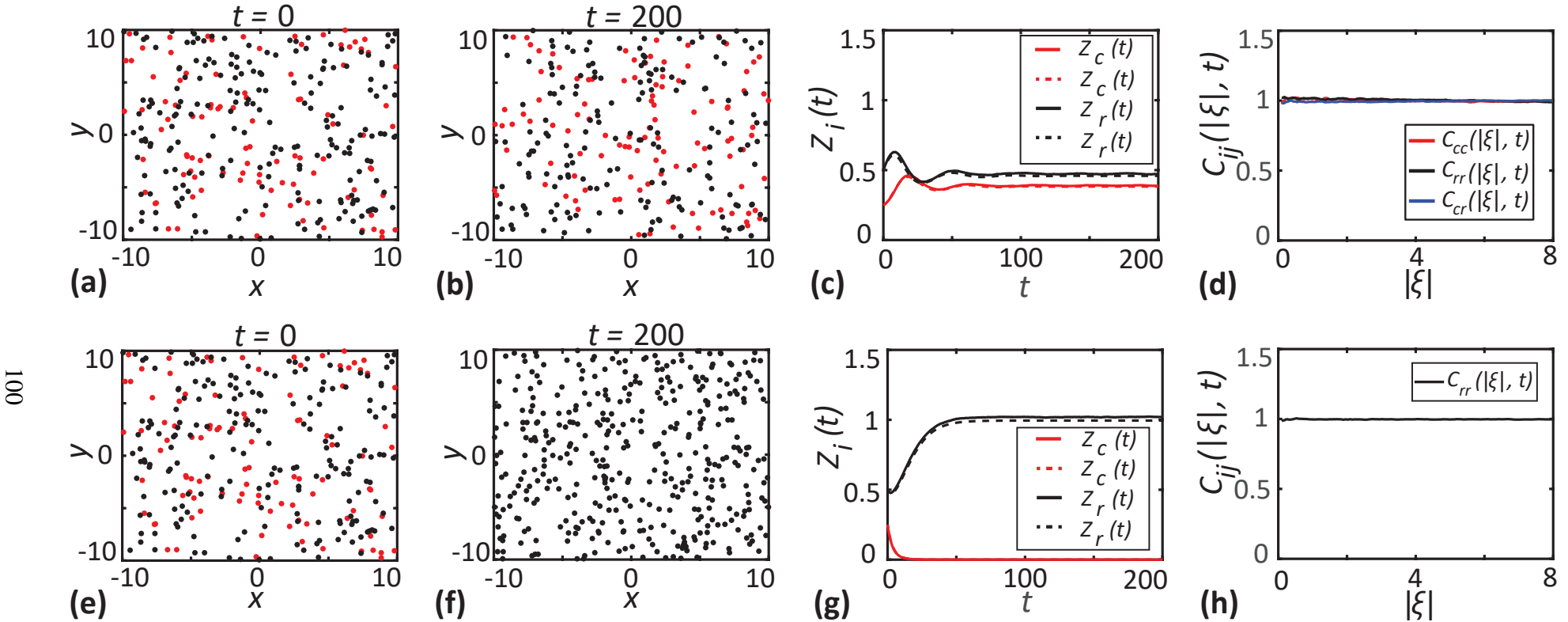


Figure 4.2: Simulation results that match well with the solutions of the mean-field model. Results in **a-d** correspond to a case where consumers and resources coexist ($p_r = 0.2$, $d_c = 0.1$). Results in **e-h** correspond to a case where consumer extinction occurs ($p_r = 0.1$, $d_c = 0.4$). **a, e** show locations of consumers (red dots) and resources (black dots) at $t = 0$. **b, f** show locations of consumers and resources at $t = 200$. **c, g** show the densities of consumers (red lines) and resources (black lines) as a function of time. Solid lines correspond to the averaged results from 1000 realisations of the IBM and dashed lines correspond to the solution of the mean-field model, Equations (4.6)-(4.7). **c, f** show the PCFs computed at $t = 200$ as a function of separation distance. Other parameter values are given in Table 4.1.

4.5.1 Short range dispersal creates intraspecies clustering

Here, we investigate the impact of short-range dispersal of consumers and resources on the spatial structure of the community and how it influences the accuracy of the mean-field model. In these simulations, the predation and competition interactions are long-range, as in Figure 4.2. We first consider short-range dispersal of consumers, as shown in Figure 4.3(a)–(d). This leads to the development of intraspecies clustering among consumers, as shown in Figure 4.3(b), quantified by the auto-PCF with $C_{cc}(|\xi|, t) > 1$ for small $|\xi|$ in Figure 4.3(d). In addition we have, $C_{rr}(|\xi|, t) \approx C_{cr}(|\xi|, t) \approx 1$, suggesting there is no intraspecies spatial structure among resources and no interspecies spatial structure. Since the dispersal of resources is long-range, there is little correlation between the locations of parent and daughter resources, which explains why there is no intraspecies spatial structure among resources. Even though consumers exhibit strong clustering we do not see a large discrepancy between the IBM simulations and the solution of the mean-field model. This observation is due to the long-range predation and competition interactions, under which local spatial structure does not influence the dynamics of the community.

Next, we consider the short-range dispersal of resources in Figure 4.3(e)–(h). After a sufficiently long time, $t = 200$, we see more resource individuals at close distances compared to the initial spatial random distribution. Results in Figure 4.3(h) show $C_{cc} > 1$, confirming clustering of resources. Again, the cluster formation is due to short-range dispersal. Similar to the case of short-range dispersal of consumers, we do not observe strong interspecies spatial structure or any discrepancy between the mean-field model and IBM estimates of the densities of consumers or resources. Finally, we consider the short-range dispersal of both consumers and resources in Figure 4.3(i)–(l). Since resource and consumer parents now place their offspring close to them, we see the development of intraspecies clusters of both consumers and resources.

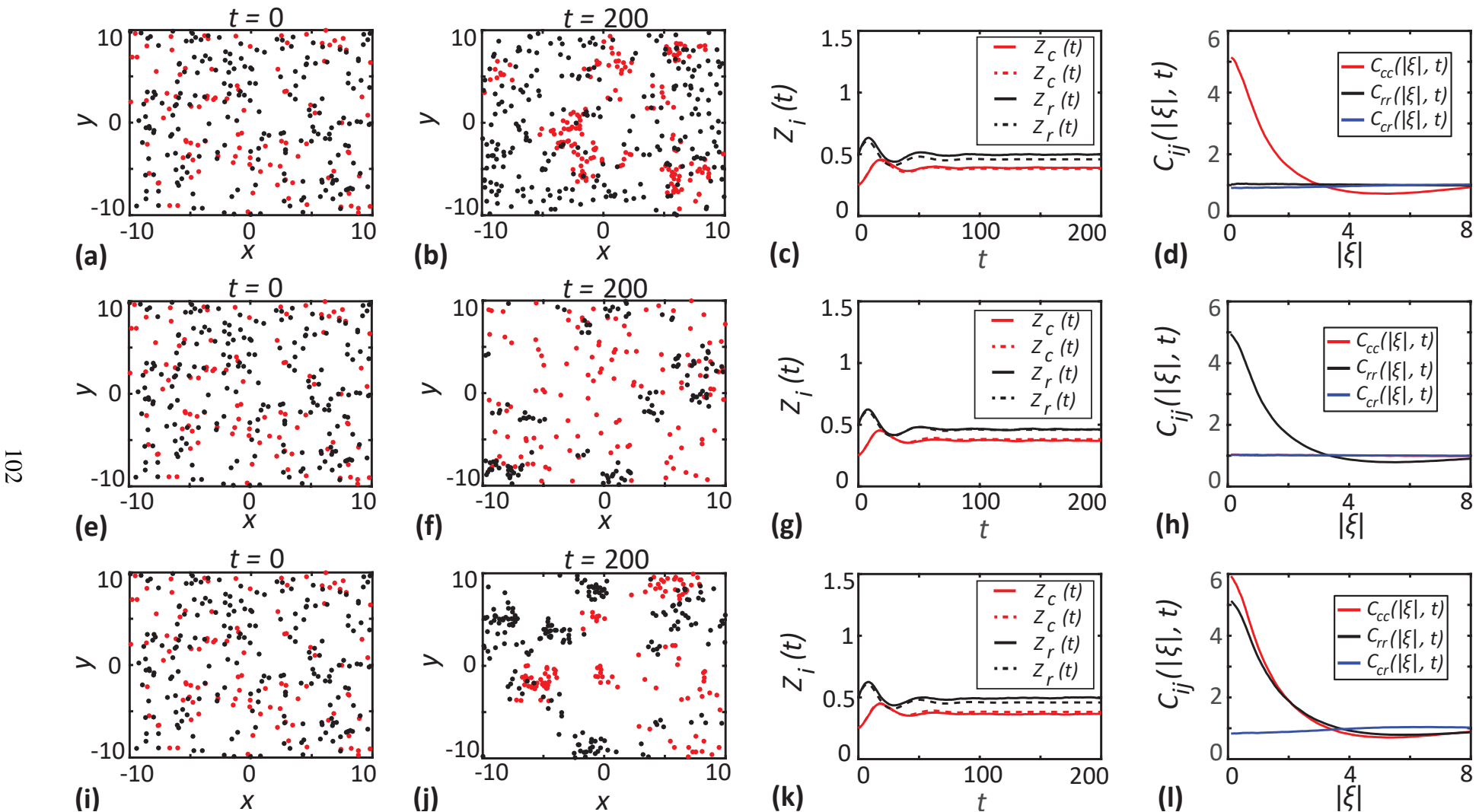


Figure 4.3: Short-range dispersal. Results in **a-d** correspond to short range dispersal of consumers ($\sigma_c^d = 0.5$). Results in **e-h** correspond to short range dispersal of resources ($\sigma_r^d = 0.5$). Results in **i-l** correspond to short range dispersal of both species ($\sigma_c^d = \sigma_r^d = 0.5$). **a, e, i** show the locations of consumers (red dots) and resources (black dots) at $t = 0$. **b, f, j** show the locations of consumers and resources at $t = 200$. **c, g, k** show the densities of consumers (red lines) and resources (black lines) as a function of time. Solid lines correspond to the averaged results from 1000 realisations of the IBM and dashed lines correspond to the solution of the mean-field model, Equations (4.6)-(4.7). **d, h, l** show the PCFs computed at $t = 200$ as a function of separation distance. All other parameters are same as in Table 4.1.

4.5.2 Short range competition creates intraspecies segregation

We first consider short-range competition among consumers in Figure 4.4(a)–(d). After a sufficiently long time, $t = 200$, consumers tend to stay apart from each other, forming an intraspecies segregated spatial pattern, confirmed by $C_{cc}(|\xi|, t) < 1$ in Figure 4.4(d). The intense competition at short distances increases the death rates of nearby consumers, leading to a configuration where consumers are well-separated. In addition we have $C_{rr}(|\xi|, t) \approx C_{cr}(|\xi|, t) \approx 1$, indicating there is no intraspecies spatial structure in resources and no interspecies spatial structure among consumers and resources. Since we consider long-range predation for this case, the consumer-resource interspecies interactions are similar to that of the mean-field case in Figure 4.2. Hence, the spatial structure of consumers does not impact density dynamics, as evident from the good agreement between the IBM results and the solution of the mean-field model in Figure 4.4(b).

Results in Figure 4.4(e)–(h) and Figure 4.4(i)–(l) consider intraspecies competition of resources and intraspecies competition of both species. In both cases, we observe competition-induced segregation. In Figure 4.4(h), $C_{cc}(|\xi|, t) < 1$, confirms the segregation of resources, whereas $C_{cc}(|\xi|, t) < 1$ and $C_{rr}(|\xi|, t) < 1$, respectively in Figure 4.4(l) confirm the interspecies segregation between consumers and resources. Again, we observe that the density dynamics from IBM is in good agreement with the solution of the mean-field model.

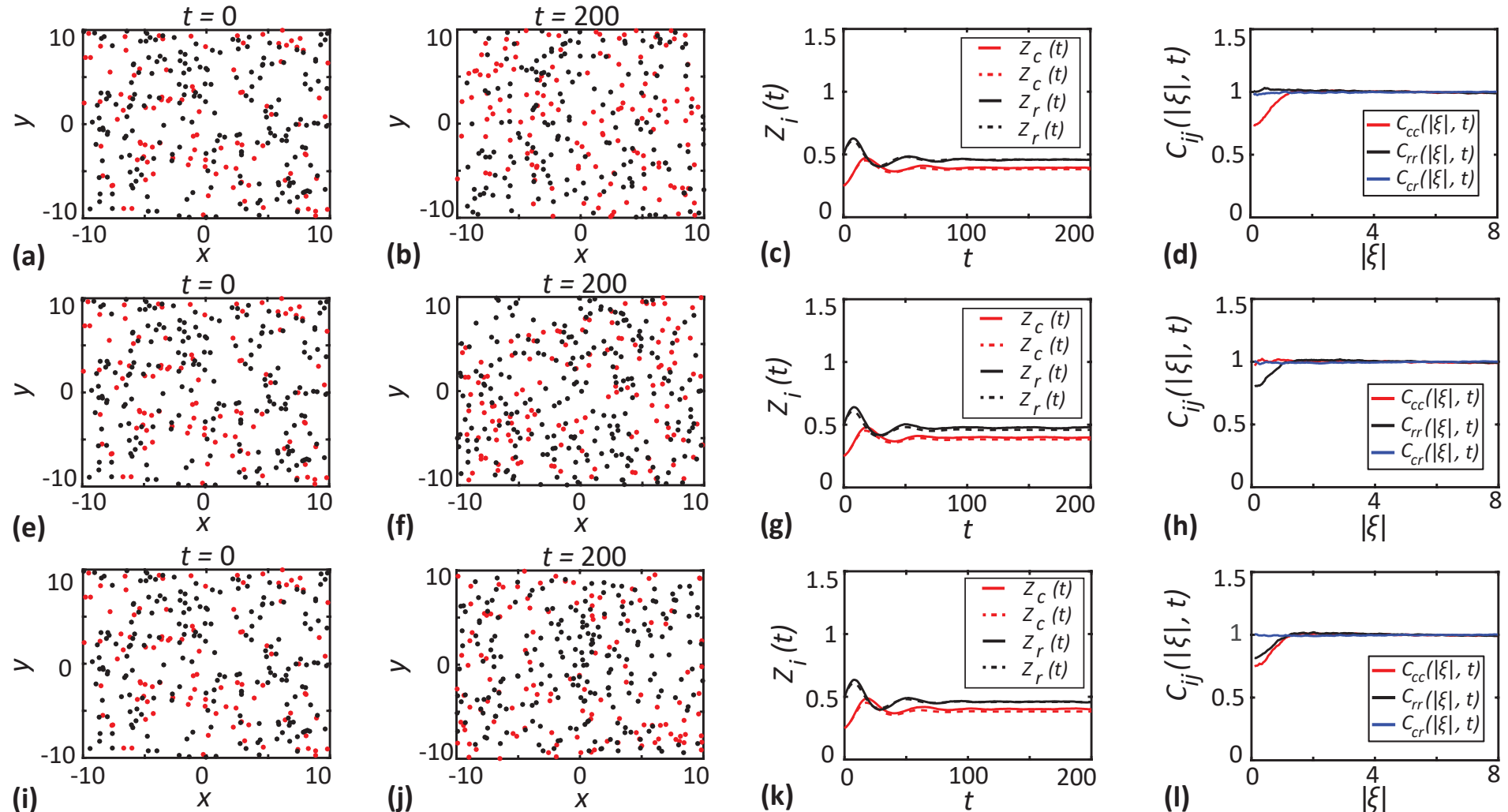


Figure 4.4: Short-range competition. Results in **a-d** correspond to short-range competition of consumers ($\sigma_{cc}^c = 0.5$ and $\gamma_{cc}^c = 0.064$). Results in **e-h** correspond to short-range competition of resources ($\sigma_{rr}^r = 0.5$ and $\gamma_{rr}^r = 0.064$). Results in **i-l** correspond to short-range competition of both species ($\sigma_{cc}^c = \sigma_{rr}^r = 0.5$ and $\gamma_{cc}^c = \gamma_{rr}^r = 0.064$). **a, e, i** show the locations of consumers (red dots) and resources (black dots) at $t = 0$. **b, f, j** show the locations of consumers and resources at $t = 200$. **c, g, k** show the densities of consumers (red lines) and resources (black lines) as a function of time. Solid lines correspond to the averaged results from 1000 realisations of the IBM and dashed lines correspond to the solution of the mean-field model, Equations (4.6)-(4.7). **d, h, l** show the PCFs computed at $t = 200$ as a function of separation distance. All other parameters are same as in Table 4.1.

4.5.3 Short range predation drives interspecies segregation

In this section we explore the impact of short-range predation. In these simulations we fix the range of competition and dispersal to be the same as in Figure 4.2 so that any spatial structure is driven by the influence of short-range predation. Results in Figure 4.5(a)-(b) show the initial spatially random configuration of individuals and the long-time outcome of the IBM, respectively. In this case, visually identifying the nature of the long-time steady spatial structure of the community is difficult. The PCFs shown in Figure 4.5(d), provide insight into the spatial structure. Since the predation is short-range, there is a high probability that each consumer predares upon nearby resources. Hence, the short-range predation by a consumer eventually depletes the resources locally, creating an interspecies segregation. This is confirmed by $C_{cr}(|\xi|, t) < 1$ for short distances in Figure 4.5(d). There is some clustering among resources indicated by $C_{rr}(|\xi|, t) > 1$ at small distances. This is because consumers tend to predate upon nearby resources. Those resources that are not consumed are more likely to be in regions with lower consumer density, which therefore tend to contain small clusters of resources. These spatial structures have an impact on the density dynamics. Results in Figure 4.5(c) show that the mean-field model underestimates the density of resources. The spatial segregation between consumers and resources assists the resources to avoid predation. Results in Figure 4.5(c) also show that the mean-field model underestimates the density of consumers. This may be counter-intuitive but can be attributed to the net increase in the resource population size more than offsetting the decrease in per capita contact rate between consumers and resource due to interspecific segregation.

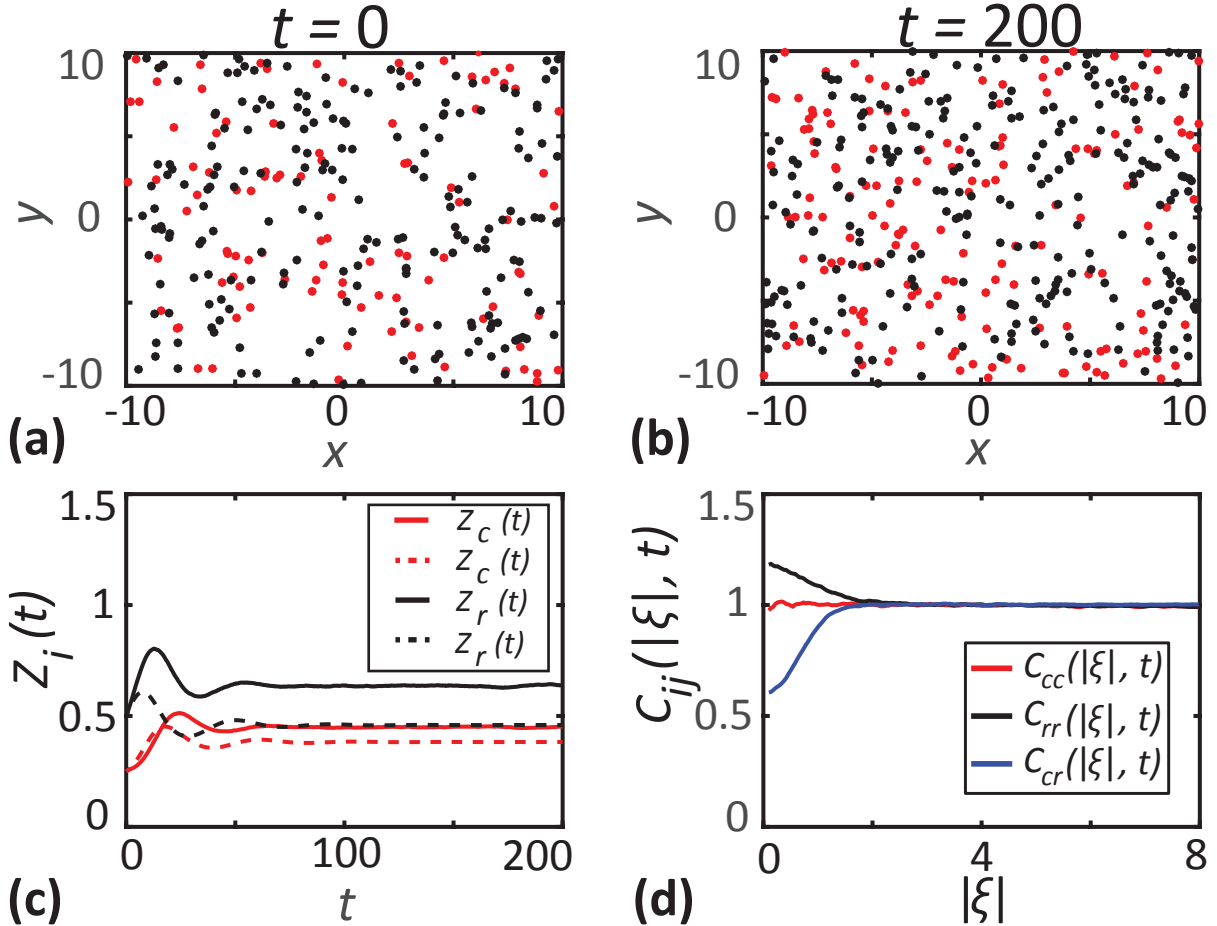


Figure 4.5: Short-range predation. **a–b** show the locations of consumers (red dots) and resources (black dots) at $t = 0$ and $t = 200$, respectively. **c** shows the densities of consumers (red lines) and resources (black lines) as a function of time. Solid lines correspond to the averaged results from 1000 realisations of the IBM and dashed lines correspond to the solution of the mean-field model, Equations (4.6)–(4.7). **d** shows the PCFs computed at $t = 200$ as a function of separation distance. Parameter values are $\sigma_{cr}^p = \sigma_{rc}^p = 0.5$, $\gamma_{cr}^p = 0.192$ and $\gamma_{rc}^p = 0.256$. All other parameters are same as in Table 4.1.

4.5.4 Short-range dispersal and short-range predation enhances resources' survival

Results in Sections 4.5.1–4.5.3 consider the impact of various mechanisms acting in isolation whereas here we investigate multiple mechanisms acting in unison. Note that, when we consider different mechanisms that generate contrasting effects on the density dynamics and spatial structure in unison, the net effect observed in the community depends on the relative strengths of those mechanisms. Hence we are always careful here to choose and report appropriate parameter values relative to previous choices in Figures 4.2–4.5, for which the opposing mechanisms have comparable strengths, such that neither is dominant over the other. If one mechanism is much stronger than others, the results will resemble the case with only that mechanism considered. We start by considering the combined effect of short-range dispersal of consumers and short-range predation in Figure 4.6(a)–(d). In the long-time limit we observe dispersal-induced clustering of consumers and predation-induced interspecies segrega-

tion between consumers and resources, leading to $C_{cc}(|\xi|, t) > 1$ and $C_{cr}(|\xi|, t) < 1$. Segregation between the two species minimises the chances of predation and results in an increase in the density of resources compared to the solution of the mean-field model. Note that the density of resources in Figure 4.6(c) is higher compared to the case in Figure 4.5, where there was only short-range predation. Since the dispersal of resources is long-range, there is a possibility of daughter resources being placed in local neighbourhoods of consumers. The probability of this happening is significantly lower when consumers are clustered rather than uniformly distributed all over the domain as in the case in Figure 4.5.

Next, we consider short-range dispersal of resources with short-range predation in Figure 4.6(e)–(h). These conditions give rise to dispersal induced clustering of resources and predation induced interspecies segregation, where $C_{rr}(|\xi|, t) > 1$ and $C_{cr}(|\xi|, t) < 1$, respectively. The density of consumers and resources from the IBM is greater than the solution from the mean-field model, but the deviation is smaller than in the previous case with short-range dispersal of consumers and short-range predation. Here the consumers are not concentrated on specific regions as compared to the previous case. Hence, the probability of predation is, on average, higher compared to the previous case.

Finally, we consider short-range dispersal of both consumers and resources along with short-range predation in Figure 4.6(i)–(l). In this case we see distinct clusters of consumers and resources due to short-range dispersal of both the species, confirmed by $C_{cc}(|\xi|, t) > 1$ and $C_{rr}(|\xi|, t) > 1$. Here, we observe an increase in the density of resources and a decrease in the density of consumers. Since both the species form clusters and occupy specific regions in the domain, the chances of pairs of consumers and resources separated by short distances is significantly reduced. The short-range predation under these circumstances leaves the consumers with reduced availability of resources for their survival. In contrast, resource grows rapidly due to the reduced risk of predation.

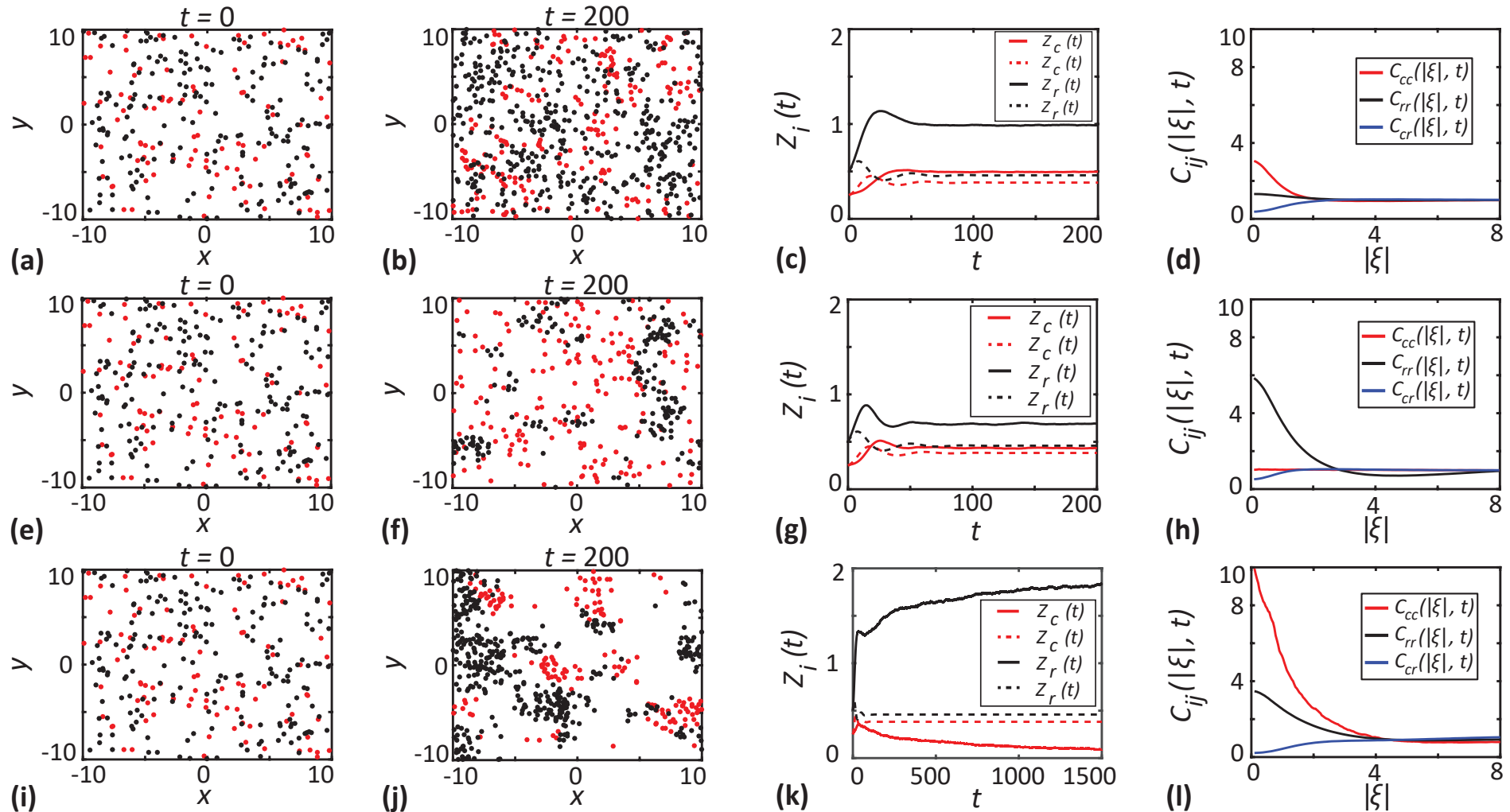


Figure 4.6: Short-range dispersal and short-range predation. Results in **a-d** correspond to short range dispersal of consumers ($\sigma_c^d = 0.5$) and short-range predation ($\sigma_{cr}^p = \sigma_{rc}^p = 0.5$, $\gamma_{cr}^p = 0.192$ and $\gamma_{rc}^p = 0.256$). Results in **e-h** correspond to short-range dispersal of resources ($\sigma_r^d = 0.5$) and short-range predation. Results in **i-l** correspond to short-range dispersal of both species ($\sigma_c^d = \sigma_r^d = 0.5$) and short-range predation. **a, e, i** show the locations of consumers (red dots) and resources (black dots) at $t = 0$. **b, f, j** show the locations of consumers and resources at $t = 200$. **c, g, k** show the densities of consumers (red lines) and resources (black lines) as a function of time. Solid lines correspond to the averaged results from 1000 realisations of the IBM and dashed lines correspond to the solution of the mean-field model, Equations (4.6)-(4.7). **d, h, l** show the PCFs computed at $t = 200$ as a function of separation distance. All other parameters are same as in Table 4.1.

4.5.5 Effect of short range predation and short range competition

We consider the combined effect of short-range competition of consumers and short-range predation in Figure 4.7(a)–(d). Here, we see consumers tend to become isolated from other consumers and resources. While short-range predation creates interspecies segregation, the competition within the consumer subpopulation results in intraspecies segregation, confirmed by $C_{cr}(|\xi|, t) < 1$ and $C_{cc}(|\xi|, t) < 1$, respectively. These results indicate that the density of resources tends to be higher than the solution of the mean-field model since segregation of consumers and resources reduces the effects of predation.

Combined effects of short-range competition of resources and short-range predation are shown in Figure 4.7(d)–(f). These conditions lead to interspecies segregation due to short-range predation. In addition, we see less pronounced intraspecies segregation developing among resources due to the competition between resources. In Figure 4.5, we saw that the effect of short-range predation, when considered in isolation, leads to a small scale clustering of resources. Here we see that the additional effects of predation counteract the impact of competition among resources to form a less pronounced intraspecies segregation of resources. Finally, we consider the combined effect of the short-range competition of both consumers and resources and short-range predation in Figure 4.7(g)–(i). We find competition-induced intraspecies segregation in this case, and this is confirmed by $C_{cc}(|\xi|, t) < 1$ and $C_{rr}(|\xi|, t) < 1$, respectively. We also observe interspecies segregation between consumers and resources confirmed by $C_{cr}(|\xi|, t) < 1$ due to the short-range predation.

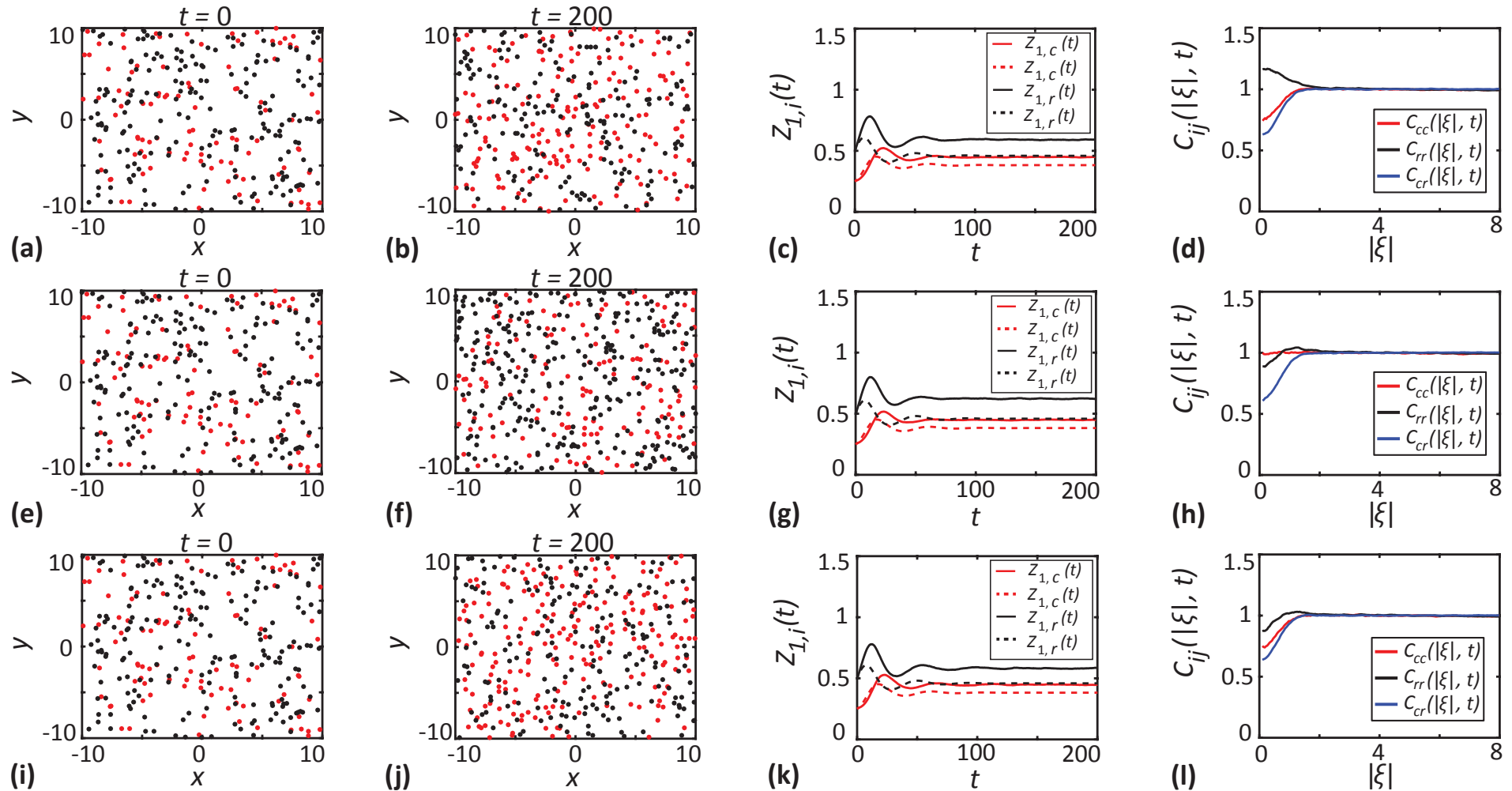


Figure 4.7: Short-range competition and short-range predation. Results in **a-d** correspond to short range competition of consumers ($\sigma_{cc}^c = 0.5$ and $\gamma_{cc}^c = 0.064$) and short-range predation ($\sigma_{cr}^p = \sigma_{rc}^p = 0.5$). Results in **e-h** correspond to short-range competition of resources ($\sigma_{rr}^c = 0.5$ and $\gamma_{rr}^c = 0.064$) and short-range predation. Results in **i-l** correspond to short-range competition of both species ($\sigma_{cc}^c = \sigma_{rr}^c = 0.5$ and $\gamma_{cc}^c = \gamma_{rr}^c = 0.064$) and short-range predation. **a, e, i** show the locations of consumers (red dots) and resources (black dots) at $t = 0$. **b, f, j** show the locations of consumers and resources at $t = 200$. **c, g, k** show the densities of consumers (red lines) and resources (black lines) as a function of time. Solid lines correspond to the averaged results from 1000 realisations of the IBM and dashed lines correspond to the solution of the mean-field model, Equations (4.6)-(4.7). **d, h, l** show the PCFs computed at $t = 200$ as a function of separation distance. All other parameters are same as in Table 4.1.

4.5.6 Spatial structure drives qualitative departure from the mean-field model

In this final set of simulations, we present a dramatic case where three spatial structure forming mechanisms act in unison to produce results that are fundamentally at odds with the predictions of the mean-field model. These results highlight the danger in neglecting spatial structure since the mean-field model leads to dramatically misleading predictions in this case.

The density dynamics of consumers and resources from the IBM simulation in Figure 4.8(a) show the eventual extinction of consumers while the resource species continues to grow to a steady density. In stark contrast, the solution of the mean-field model predicts the long-time coexistence of consumers and resources. These results demonstrate that the mean-field model and IBM can predict two qualitatively different outcomes when there is a strong spatial structure. In Figure 4.8(b)–(g), we show the evolution of the spatial structure of the community by presenting snapshots from the IBM as well as the PCFs at various points in time. We see intraspecies clustering among both consumers and resources, confirmed by $C_{cc}(|\xi|, t) > 1$ and $C_{rr}(|\xi|, t) > 1$, and interspecies segregation, confirmed by $C_{cr}(|\xi|, t) < 1$ at earlier times before reaching the long-time limit. Strong clustering at these intermediate times is due to the short-range dispersal of both consumers and resources ($\sigma_c^d = \sigma_r^d = 0.1$). Competition tends to reduce the extent of clustering. But, dispersal dominates competition since we use very small dispersal range compared to the competition range ($\sigma_{cc}^c = \sigma_{rr}^c = 0.5$). Short-range predation separate consumers and resources from each other by the consumption of close-lying resources by consumers. This results in interspecies segregation. As time progresses, these effects result in consumers becoming isolated from resources and eventually go extinct.

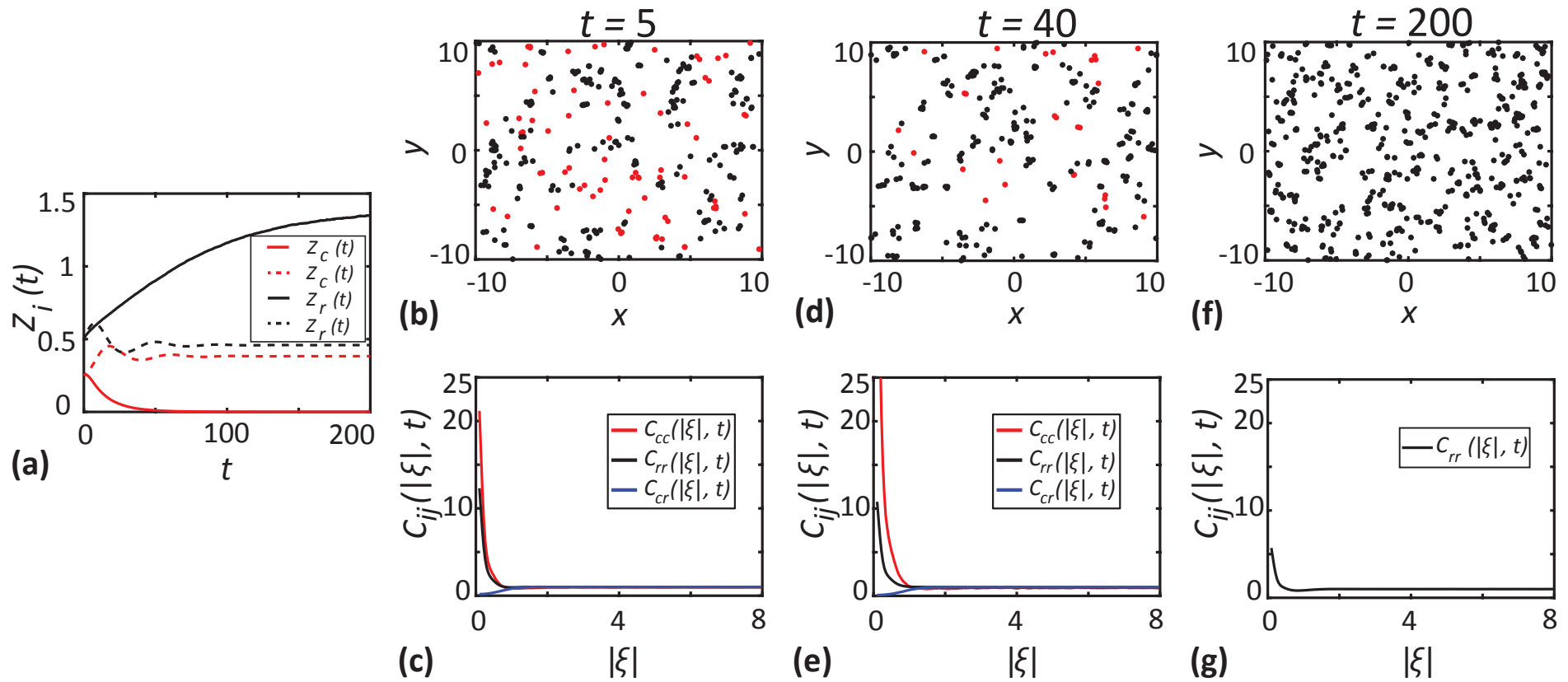


Figure 4.8: Short-range competition, short-range predation and short-range dispersal. **a** shows the densities of consumers (red lines) and resources (black lines) as a function of time. Solid lines correspond to the averaged results from 1000 realisations of the IBM and dashed lines correspond to the solution of the mean-field model, Equations (4.6)-(4.7). **b-c** show the locations of consumers (red dots) and resources (black dots) at $t = 5$ and PCFs computed at $t = 5$ as a function of separation distance. **d-e** show the locations of consumers and resources at $t = 40$ and PCFs computed at $t = 40$ as a function of separation distance. **f-g** show the locations of consumers and resources at $t = 200$ and PCFs computed at $t = 200$ as a function of separation distance. Parameter values are $\sigma_{cr}^p = \sigma_{rc}^p = \sigma_{cc}^c = \sigma_{rr}^c = 0.5$, $\gamma_{cr}^p = 0.192$, $\gamma_{rc}^p = 0.256$, $\gamma_{cc}^c = \gamma_{rr}^c = 0.064$, $\sigma_c^d = \sigma_r^d = 0.1$. All other parameters are same as in Table 4.1.

4.6 Conclusion

In this chapter, we present a relatively simple IBM describing the dynamics of a community of consumers and resources where we pay particular attention to the effects of short-range interactions and small-scale spatial structure. The IBM simulation results are compared with solutions of a mean-field model constructed by invoking the mean-field approximation. This analysis reveals various situations where the IBM suggests qualitatively different outcomes compared to the solution of the mean-field model. These observations highlight the importance of considering the role of spatial structure in community dynamics. Mean-field models are routinely used to explore various characteristics of population dynamics and predator-prey type interactions. These include predicting whether certain subpopulations go extinct or whether all subpopulation survive and co-exist (Kuperman et al., 2019). Our results suggest that the predictions of the mean-field models in these scenarios could be inaccurate if the communities in question exhibit significant spatial structure.

Many studies consider the comparison of IBMs and their mean-field approximations to explore scenarios where mean-field assumption breaks down and predicts conflicting outcomes due to short-range interactions and spatial structure in a consumer resource community (Wilson, 1998; Cantrell and Cosner, 2004). While our present work explores cases where the mean-field model fails to predict coexistence and extinction accurately, similar studies in the literature consider other interesting scenarios where IBMs can exhibit stable dynamics when mean-field models predict oscillatory dynamics (Hosseini, 2006; Brigatti et al., 2009). In these IBMs, limited motility and short-range interactions dampen the magnitude of population oscillations and stabilise the consumer-resource density dynamics (Cuddington and Yodzis, 2000; Hosseini, 2003). Another remarkable difference between our model and these previous modelling frameworks is here we use PCFs to identify the spatial configuration of the community. We base our inference about any observed changes in the density dynamics on findings revealed by PCFs about the spatial arrangement of the community. Additionally, we use a more realistic lattice-free IBM compared to the lattice-based models considered in these previous studies, which restrict the freedom of movement along fixed lattice directions.

Our modelling framework can be extended by incorporating various additional forms of neighbour-dependent interactions that are not considered here. An interesting extension would be to consider the effects of neighbour-dependent directional bias on the movement of consumers and resources. For example, in this work we make the simple assumption that the motility rate and direction of movement are independent of the local density. However, some recent IBMs introduce attractive or repulsive interactions where the motility rate and direction is affected by the local density, and these interactions can also drive significant differences in the macroscale spatial structure (Browning et al., 2018, 2020; Surendran et al., 2019; Binny et al., 2020). Incorporating these types of directional bias to the movement of consumers and resources may further influence the community dynamics beyond the effects explored in the

present study. Another important neighbour-dependent effect in the context of population dynamics in ecology and cell biology is the incorporation of an Allee effect where proliferation and death rates are incorporated into the IBM so that there can be a net negative growth rate at low density and a net positive growth rate at higher densities (Stephens et al., 1999; Johnston et al., 2017; Fadai et al., 2020). Understanding how these kinds of interactions that lead to Allee effects would influence the formation of spatial structure is an open question that could be analysed by extending the modelling framework that we have presented here.

Statement of Contribution of Co-Authors for Thesis by Published Paper

The authors listed below have certified that:

1. they meet the criteria for authorship and that they have participated in the conception, execution, or interpretation, of at least that part of the publication in their field of expertise;
2. they take public responsibility for their part of the publication, except for the responsible author who accepts overall responsibility for the publication;
3. there are no other authors of the publication according to these criteria;
4. potential conflicts of interest have been disclosed to (a) granting bodies, (b) the editor or publisher of journals or other publications, and (c) the head of the responsible academic unit, and
5. they agree to the use of the publication in the student's thesis and its publication on the [QUT's ePrints site](#) consistent with any limitations set by publisher requirements.

In the case of chapter 5:

Surendran Anudeep, Plank Michael J., Simpson Matthew J. 2020 Population dynamics with spatial structure and an Allee effect. Under review at Proceedings of the Royal Society A: Mathematical, Physical and Engineering Sciences.

Contributor	Statement of contribution*
Anudeep Surendran	Designed the study, derived the continuum moment dynamics equations, developed the codes for numerical simulation of the IBM and spatial moment model, performed numerical simulations, generated results, interpreted the results, and drafted the manuscript. <i>Anudeep Surendran</i>
19/08/2020	
Michael J. Plank	Designed the study, interpreted the results, and edited the manuscript during initial submission.
Matthew J. Simpson	Designed the study, supervised the research, interpreted the results, edited the manuscript during initial submission and acted as the corresponding author.

Principal Supervisor Confirmation

I have sighted email or other correspondence from all Co-authors confirming their certifying authorship.
(If the Co-authors are not able to sign the form please forward their email or other correspondence confirming the certifying authorship to the GRC).

MATTHEW SIMPSON

Name

M. Plank

Signature

26/8/2020

Date

Chapter 5

Population dynamics with spatial structure and an Allee effect

5.1 Preamble

This chapter is a paper published in the *Proceedings of the Royal Society A: Mathematical, Physical and Engineering Sciences*.

Surendran Anudeep, Plank Michael J., Simpson Matthew J. 2020 Population dynamics with spatial structure and an Allee effect. *Proceedings of the Royal Society A: Mathematical, Physical and Engineering Sciences* 476: 20200501. DOI:[10.1098/rspa.2020.0501](https://doi.org/10.1098/rspa.2020.0501). bioRxiv Preprint.

In this chapter, we address the research question 4 of the thesis: What impact do short-range interactions and spatial structure have on the Allee dynamics? We address this research question by extending the models developed in Chapter 2, to accommodate a strong Allee effect. The incorporation of Allee effects into the modelling framework requires substantial changes in the way we define birth and death rates of individuals compared to that in all of the previous Chapters 2-4. We notice that incorporating the Allee effect into the modelling framework requires a non-linear dependency of density on the event rates, which is different from all three previous cases. To reflect these differences, we derive a novel IBM and spatial moment dynamics framework in Chapter 5. We first show that our new models match the classical mean-field Allee dynamics in the long-range interaction limit (mean-field limit). We further demonstrate some dramatic consequences of short-range interactions and spatial structure on the Allee dynamics.

5.2 Abstract

Population dynamics including a strong Allee effect describe the situation where long-term population survival or extinction depends on the initial population density. A simple mathematical model of an Allee effect is one where initial densities below the threshold lead to

extinction, whereas initial densities above the threshold lead to survival. Mean field models of population dynamics neglect spatial structure that can arise through short-range interactions, such as competition and dispersal. The influence of non mean-field effects has not been studied in the presence of an Allee effect. To address this, we develop an individual-based model that incorporates short-range interactions and gives rise to an Allee effect. To explore the role of spatial structure we derive a mathematically tractable continuum approximation of the IBM in terms of the dynamics of spatial moments. In the limit of long-range interactions where the mean-field approximation holds, our modelling framework recovers the mean-field Allee threshold. We show that the Allee threshold is sensitive to spatial structure neglected by mean-field models. For example, there are cases where the mean-field model predicts extinction but the population actually survives. Through simulations we show that our new spatial moment dynamics model accurately captures the modified Allee threshold in the presence of spatial structure.

5.3 Introduction

Mathematical models of biological population dynamics are routinely built upon the classical logistic growth model where a population tends to a finite carrying capacity density for all positive initial densities (Murray, 1989; Edelstein-Keshet, 2005; Kot, 2003). While the logistic growth model is reasonable in some situations, there are other situations where the long-term survival of a population depends on the initial density, often called an Allee effect (Courchamp et al., 2008; Taylor and Hastings, 2005). A *strong Allee effect* is associated with a net negative growth rate at low densities leading to population extinction below the Allee threshold density. In contrast, a net positive growth rate at higher densities leads to the survival of the population when the initial density is greater than the Allee threshold (Courchamp et al., 1999a; Musgrave et al., 2015; Maciel and Lutscher, 2015). Another type of Allee effect, known as the *weak Allee effect*, describes population growth with a reduced but positive growth rate at low densities (Taylor and Hastings, 2005). Unlike the strong Allee effect, a weak Allee effect does not exhibit any threshold density due to the net positive growth rate. In this study, we focus on the strong Allee effect since we are interested in exploring threshold effects and factors that influence the Allee threshold. Initial evidence for the Allee effect came from ecological systems for various plant and animal populations (Allee and Bowen, 1932; Courchamp et al., 1999a; Groom, 1998; Lamont et al., 1993; Kuussaari et al., 1998; Lewis and Kareiva, 1993; Wittmer et al., 2005; Lutscher and Iljon, 2013), whereas more recent studies suggest a role for the Allee effect in populations of biological cells (Neufeld et al., 2017; Fadai and Simpson, 2020; Korolev et al., 2014; Johnston et al., 2017; Sarapata and dePillis, 2014; Johnston et al., 2020).

Most mathematical models of Allee population dynamics invoke a mean-field assumption (Courchamp et al., 1999a; Edelstein-Keshet, 2005; Morozov et al., 2004; Courchamp et al., 1999b) where, either implicitly or explicitly, interactions between individuals are assumed to

occur in proportional to the average density. Such models neglect spatial correlations between the locations of individuals (Law and Dieckmann, 2000). When short-range interactions are present, such as short-range competition, the mean-field approximation can become inaccurate (Bruna and Chapman, 2012a; Bruna and Chapman 2012b; Bruna et al., 2017; Martinez-Garcia et al., 2020). Short-range interactions can lead to the development of spatial structure that can affect the overall population dynamics (Law et al., 2003; Binny et al., 2016; Surendran et al., 2020a). Spatial structure in biological populations includes both clustering and segregation (Purves and Law, 2002; Gerum et al., 2018; Dini et al., 2018; Binder and Simpson, 2013; Simpson et al., 2013; Martinez-Garcia et al., 2015). Stochastic individual-based models (IBM) offer a straightforward means of exploring population dynamics without invoking a mean-field approximation (Chaplain et al., 2020; Macfarlane et al., 2019). However, IBM approaches are computationally prohibitive for large populations and provide limited mathematical insight into the population dynamics, for example how particular biological mechanisms affect the carrying capacity or the Allee threshold (Surendran et al., 2018).

A continuum approximation of the IBM in terms of the dynamics of spatial moments is a useful way to study how short-range interactions and spatial structure can influence population dynamics (Murrell and Law, 2000; Murrell 2009). Law et al. developed a spatial moment model, called the *spatial logistic model*, that quantifies the impact of spatial structure on classical logistic growth dynamics (Law et al., 2003). This work shows that spatial structure has a strong impact on the carrying capacity density. More recently, the spatial logistic model has been extended to consider other relevant mechanisms including interspecies and intraspecies interactions, neighbour-dependent motility bias, predator-prey dynamics and chase-escape interactions (Plank and Law, 2015; Binny et al., 2015; Barraquand and Murrell, 2012; Surendran et al., 2019).

In this chapter, we present an IBM and a novel spatial moment dynamics approximation that incorporates a strong Allee effect. This model is a generalisation of the spatial logistic model (Law et al., 2003). Localised density-dependent interactions, such as short-range competition, short-range cooperation and short-range offspring dispersal are incorporated. In the limit of large scale interactions where the mean-field approximation is valid, both the IBM and the spatial moment model are consistent with the classical mean-field Allee growth model. In contrast, when spatial structure is present, we find that the Allee threshold density can be very sensitive to the spatial structure. For example, under a combination of short-range competition and short-range dispersal, all initial densities lead to population extinction, whereas the classical mean-field model predicts that the population will survive. In contrast, the new spatial moment approximation gives an accurate prediction of the long-time outcome even when strong spatial structure is present.

In this chapter we broadly consider two different types of results. In the first set we focus on population-level outcomes with regard to whether a population eventually becomes extinct or whether it survives. We study these problems using a classical mean-field model, a new spatial

moment dynamics model as well as using repeated, identically-prepared stochastic simulations. For these results we are very careful to select initial conditions in the IBM simulations so that the vast majority of the repeated simulations lead to the same long-time outcome. For example, we consider parameter choices and initial conditions where more than > 99% of identically-prepared IBM simulations all lead to either long-term extinction or long-term survival. The extremely small proportion of outliers are then excluded from the calculation of ensemble data. In the second set of results we focus on repeated IBM simulations in situations where stochastic effects can lead to either long-term survival or long-term extinction. We characterise this transition in terms of a survival probability, defined as the fraction of IBM realisations in which the population does not become extinct. Both the classical mean-field model and the new spatial moment dynamics model are deterministic approximations of the IBM and do not describe any stochastic effects.

5.4 Individual-based model

The IBM describes the dynamics of $N(t)$ individuals, initially distributed randomly on a continuous two-dimensional domain of size $L \times L$. The location of the n^{th} individual is $\mathbf{x}_n \in \mathbb{R}^2$, and periodic boundary conditions are imposed. Individuals undergo birth, death and movement events, with event rates influenced by interactions between individuals. The IBM is developed for a spatially homogeneous, translationally-invariant environment, where the probability of finding an individual in a small region, averaged over multiple realisations of the IBM, is independent of the location of that region (Plank and Law., 2015; Surendran et al., 2019). Hence the model is relevant to populations that do not involve macroscopic gradients in the density of individuals (Jin et al., 2018).

Competition between individuals influences the death rate, modelling increased mortality as a result of competition for limited resources. We use an interaction kernel, $\omega_c(|\xi|)$, to describe the competition a particular reference individual experiences from another individual at a displacement, ξ . We specify the competition kernel to be a function of separation distance, $|\xi|$,

$$\omega_c(|\xi|) = \gamma_c \exp\left(-\frac{|\xi|^2}{2\sigma_c^2}\right), \quad (5.1)$$

where $\gamma_c > 0$ and $\sigma_c > 0$ are the competition strength and range, respectively. Specifying the competition kernel to be Gaussian means that the impact of competition is a decreasing function of separation distance, $|\xi|$. We define a random variable, X_n , that measures the neighbourhood density of the n^{th} individual weighted over by the competition kernel as,

$$X_n = \sum_{\substack{k=1 \\ k \neq n}}^{N(t)} \omega_c(|\mathbf{x}_k - \mathbf{x}_n|). \quad (5.2)$$

We consider the death rate of the n^{th} individual to be some function of X_n ,

$$\mathcal{D}_n = F(X_n). \quad (5.3)$$

For a specific choice of $F(X_n)$, the key parameters controlling how competition influences the death rate are σ_c and γ_c . Figure 5.1 illustrates two scenarios for the simplest choice of $F(X_n) = X_n$. The arrangement of agents in Figure 5.1(a) and (c) are identical but we consider a long-range competition kernel (large σ_c) in Figure 5.1(a)-(b) and a short-range competition kernel (small σ_c) in Figure 5.1(c)-(d). In Figure 5.1 we compute the death rate of a test individual located at any location \mathbf{x} . This allow us to treat \mathcal{D}_n as a continuous function of position. Level curves of \mathcal{D}_n are superimposed in Figure 5.1(a) and (c) and we see that the differences in the length-scale of interaction leads to very different local death rates. For example, when competition is long-range in Figure 5.1(a)-(b) the death rate for the relatively isolated green agent is $\mathcal{D}_n = 0.275$ whereas when the competition is short-range in Figure 5.1(c)-(d) the death rate of the same agent is very different, $\mathcal{D}_n = 0$. A similar set of results with a different choice of $F(X_n)$ in Section 5A.1 shows similar results.

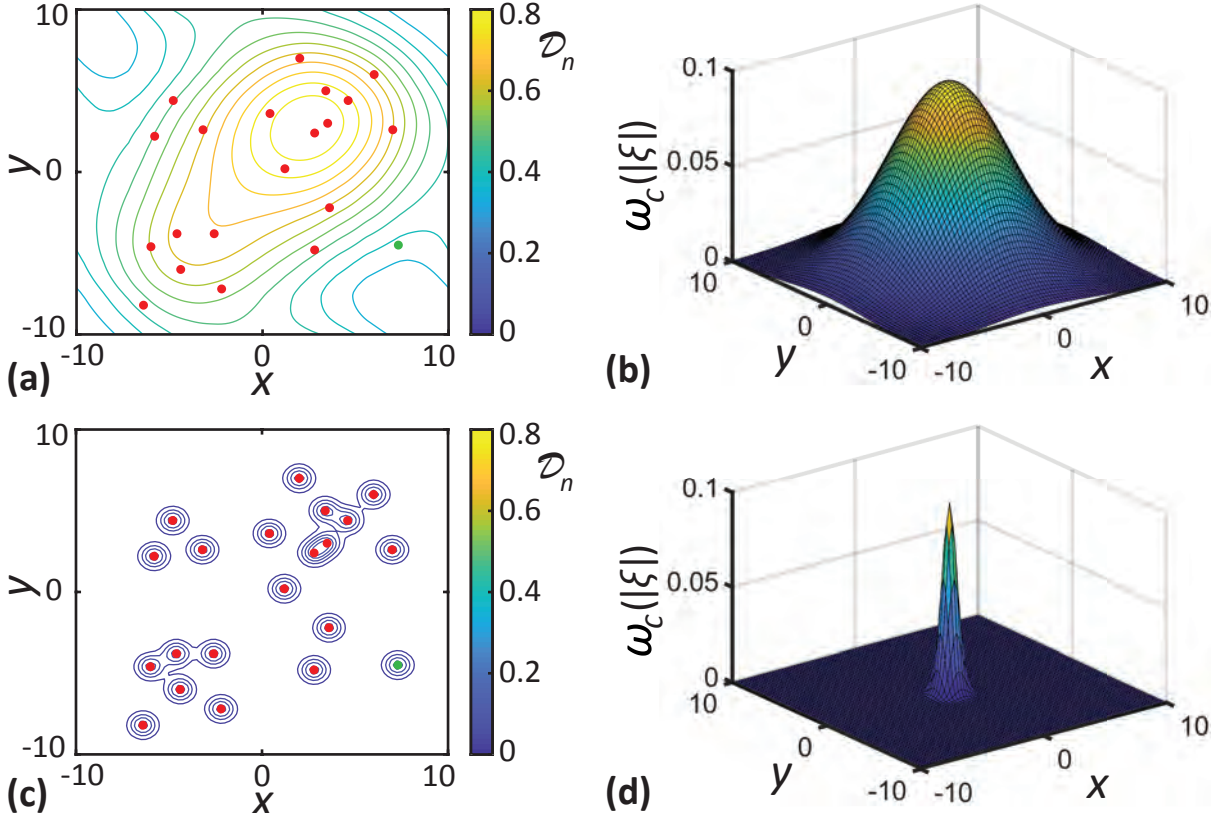


Figure 5.1: Visualising long- and short-range competition interactions. **a, c** locations of individuals (dots) superimposed with level curves of \mathcal{D}_n for long- and short-range competition, respectively. **b, d** shows the long- ($\sigma_c = 4.0$) and short-range ($\sigma_c = 0.5$) competition kernels, respectively, where these kernels are centred at the origin. Here, $F(X_n) = X_n$ and $\gamma_c = 0.1$.

We also consider a cooperative interaction between individuals that enhances the proliferation rate of individuals (Johnston et al., 2017). This is a model for sexual reproduction or

some other mutualistic interaction in which reproductive fitness increases in the presence of near neighbours. Similar to the competition kernel, we define a cooperation kernel,

$$\omega_p(|\xi|) = \gamma_p \exp\left(-\frac{|\xi|^2}{2\sigma_p^2}\right), \quad (5.4)$$

to account for the contribution of a neighbour at a displacement ξ to the reference individual's proliferation rate. Here, $\gamma_p > 0$ and $\sigma_p > 0$ represent the strength and range of the interaction, respectively. As with competition, we define a random variable, Y_n , that measures the neighbourhood density weighted by the cooperation kernel,

$$Y_n = \sum_{\substack{k=1 \\ k \neq n}}^{N(t)} \omega_p(|\mathbf{x}_k - \mathbf{x}_n|). \quad (5.5)$$

The proliferation rate of the n^{th} individual is taken to be some function of Y_n ,

$$\mathcal{P}_n = G(Y_n). \quad (5.6)$$

When an individual undergoes proliferation, a daughter agent is placed at a displacement sampled from a dispersal kernel, $\mu_p(\xi)$ that we choose to be a bivariate normal with mean zero and standard deviation σ_d .

For simplicity, we assume the movement rate is density-independent with a constant rate, m . An individual undergoing a motility event traverses a displacement, $(|\xi| \cos(\theta), |\xi| \sin(\theta))$ sampled from a movement kernel, $\mu_m(\xi)$. The direction of movement, $\theta \in [0, 2\pi]$ is uniformly distributed. The distance moved, $|\xi|$, is sampled from a relatively narrow, truncated Gaussian distribution with mean, μ_s , and standard deviation, σ_s , where $\sigma_s < \mu_s/4$. To ensure $|\xi|$ is positive, the Gaussian is truncated so that $\mu_s - 4\sigma_s < |\xi| < \mu_s + 4\sigma_s$.

This IBM is an extension of the spatial stochastic logistic model (Law et al., 2003), often simply called the spatial logistic model, which focuses on understanding the impact of short-range interactions and spatial structure on the classical logistic growth model (Murray, 1989). In the spatial logistic model, the death rate is taken to be the sum of the competition from the neighbours and the proliferation rate is constant, so there is no cooperation. Furthermore, the spatial logistic growth model does not involve any agent motility. We recover the spatial logistic model as a particular case of our model when we set $F(X_n) = X_n$, $G(Y_n) = p$ and $m = 0$. In Figure 5.2(a)-(c), we summarise the dynamics of the spatial logistic model when the interactions are long-range and the mean-field approximation is valid. Under these conditions the death rate is a linearly increasing function of density and the proliferation rate is constant, as shown in Figure 5.2(a). This choice leads to an unstable steady state $\bar{Z}_1^{(1)} = 0$ and a stable steady-state $\bar{Z}_1^{(2)} > 0$ as shown in Figure 5.2(b). Hence the mean-field implies that all initial population densities will eventually tend to $\bar{Z}_1^{(2)}$ as $t \rightarrow \infty$, as in Figure 5.2(c).

Our generalised IBM framework accommodates various non-linear functional forms for \mathcal{D}_n and \mathcal{P}_n . In Figure 5.2(d) we choose \mathcal{D}_n to be a concave up quadratic function and \mathcal{P}_n to be linearly increasing function of density. This leads to three equilibrium densities: $\bar{Z}_1^{(1)}$, $\bar{Z}_1^{(2)}$, and $\bar{Z}_1^{(3)}$, as in Figure 5.2(e). Here, $\bar{Z}_1^{(1)}$ and $\bar{Z}_1^{(3)}$ are stable equilibria, and $\bar{Z}_1^{(2)}$ is an unstable equilibrium. The population dynamics here with the long-range interactions where the mean-field approximation is valid is shown in Figure 5.2(f). Here we see that populations with an initial density less than the Allee threshold, $\bar{Z}_1^{(2)}$, eventually go extinct. In contrast, any initial density greater than the Allee threshold, $\bar{Z}_1^{(2)}$, eventually tends to $\bar{Z}_1^{(3)}$. This is the simplest mean-field model of an Allee effect in which the net population growth rate is a cubic function of population density (Kot, 2003). For the spatial logistic model, the stability of the mean-field equilibrium depends on the model parameters. For example, the unstable equilibrium point at $\bar{Z}_1^{(1)} = 0$, become a stable equilibrium point (population extinction) when competition and dispersal are short-range. Results in Section 5.7 reveal that similar observations hold for the IBM considered here.

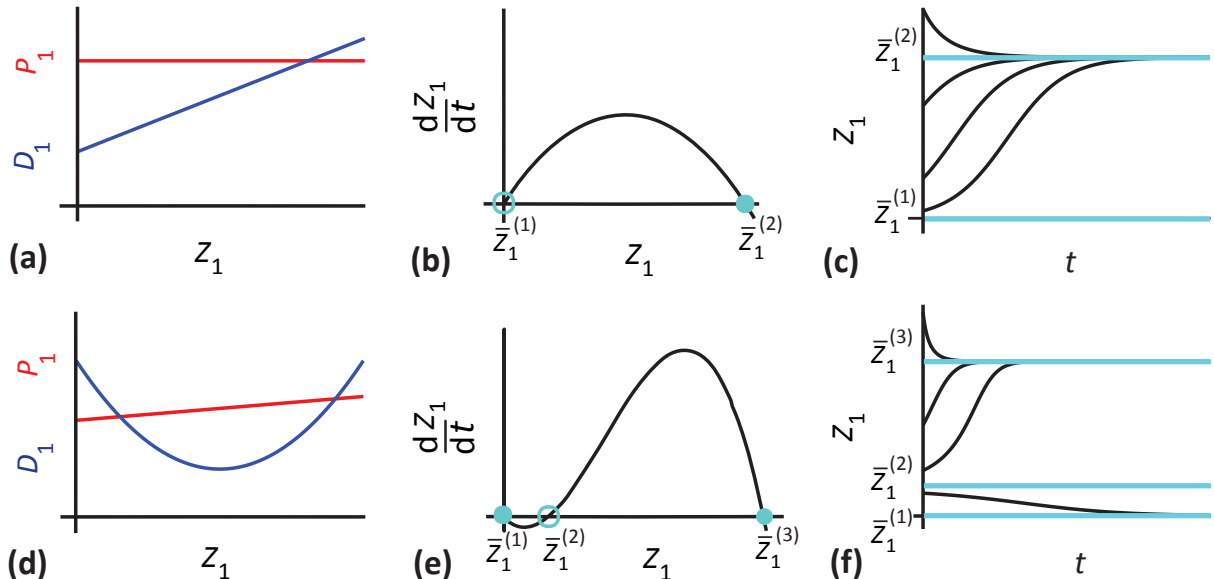


Figure 5.2: Comparison of the spatial logistic and Allee effect models under mean-field conditions. **a, d** proliferation (red) and death rates (blue) as functions of density. **b, e** density growth rate as a function of density. Stable and unstable equilibrium points are highlighted with filled and empty cyan dots, respectively. **c, f** dynamics for both models with the cyan lines indicating the equilibrium densities.

We simulate the IBM using the Gillespie algorithm (Gillespie, 1977) that is described in Section 5A.2. The population dynamics arising from the IBM is analysed by considering the average density of individuals, $Z_1(t) = N(t)/L^2$. Information about the spatial configuration of the population can be studied in terms of the average density of pairs of individuals expressed as a pair correlation function, $C(|\xi|, t)$ (Surendran et al., 2020a; Binder and Simpson 2013; Ovaskainen et al., 2014; Johnston et al., 2016). The pair-correlation function denotes the average density of pairs of individuals with separation distance $|\xi|$, at a time, t , normalised by the density of pairs in a population with the complete absence of spatial structure. Therefore, for a

population without any spatial structure, $C(|\xi|, t) = 1$. When $C(|\xi|, t) < 1$, there are fewer pairs of individuals with a separation distance, $|\xi|$, than in a population without any spatial structure. We refer to this spatial configuration as being *segregated*. When $C(|\xi|, t) > 1$, we have more pairs of individuals with a separation distance, $|\xi|$, than we would have in a population without any spatial structure and this spatial configuration is referred to as being *clustered*.

5.5 Spatial moment dynamics

In this section, we construct a continuum approximation of the IBM in terms of the dynamics of spatial moments. The first spatial moment, $Z_1(t)$, for a point process of the kind considered in the IBM is defined as the average density of individuals (Law et al., 2003; Plank and Law, 2015). The second spatial moment, $Z_2(\xi, t)$, is the average density of pairs of individuals separated by a displacement of ξ . The third spatial moment, $Z_3(\xi, \xi', t)$, is the average density of a triplet of individuals separated by displacements ξ and ξ' , respectively. A formal definition of spatial moments is provided in Section 5A.3. It is possible to define higher-order moments similarly, but for the present study, we restrict our attention to the first three spatial moments (Plank and Law, 2015; Omelyan, 2020).

To derive dynamical equations for the evolution of the spatial moments, we need to find expressions for the continuum analogue of the discrete event rates given in Equation (5.3) and Equation (5.6). This can be achieved by finding the expected death and proliferation rates, $\mathbb{E}[D_n] = \mathbb{E}[F(X_n)]$ and $\mathbb{E}[P_n] = \mathbb{E}[G(Y_n)]$, respectively. To calculate these expected rates expand $F(X_n)$ and $G(Y_n)$ in a Taylor series about $\bar{X} = \mathbb{E}[X_n]$ and $\bar{Y} = \mathbb{E}[Y_n]$. For the death rate we have

$$\begin{aligned}\mathbb{E}[F(X_n)] &= \mathbb{E}\left[F(\bar{X}) + F'(\bar{X})(X_n - \bar{X}) + \frac{F''(\bar{X})}{2!}(X_n - \bar{X})^2 + \frac{F'''(\bar{X})}{3!}(X_n - \bar{X})^3 + \dots\right], \\ &= F(\bar{X}) + \frac{F''(\bar{X})}{2!} \text{Var}[X_n] + \frac{F'''(\bar{X})}{3!} \mathbb{E}\left[(X_n - \bar{X})^3\right] + \dots\end{aligned}\quad (5.7)$$

While our IBM can incorporate any choice of $F(X_n)$, the higher-order terms in the truncated Taylor series in Equation (5.7) are, in general, non-zero. The most straightforward choice of $F(X_n)$ to generate the Allee effect is a quadratic, and this choice has the additional benefit that third and higher derivatives vanish, so we have

$$\mathbb{E}[F(X_n)] = F(\bar{X}) + \frac{F''(\bar{X})}{2!} \text{Var}[X_n].\quad (5.8)$$

The computation of expected death rates reduces to calculating $\mathbb{E}[X_n]$ and $\text{Var}[X_n]$, and substituting these into Equation (5.8). If we suppose the $L \times L$ domain is divided into $M = L^2/\delta A$ subregions, each of area δA , where these subregions are sufficiently small such that each sub-

region contains at most one individual, we have

$$\mathbb{E}[X_n] = \mathbb{E} \left[\sum_{k=1}^M \omega_c(|\mathbf{x}_k - \mathbf{x}_n|) \mathbb{I}_{\delta A}(\mathbf{x}_k - \mathbf{x}_n) \right], \quad (5.9)$$

where, $\mathbb{I}_{\delta A}(\mathbf{x}_k - \mathbf{x}_n) = 1$, if an individual is present in a region of area δA at a displacement $\mathbf{x}_k - \mathbf{x}_n$, and $\mathbb{I}_{\delta A}(\mathbf{x}_k - \mathbf{x}_n) = 0$, otherwise. Using the property of the indicator function that $\mathbb{E}[\mathbb{I}_{\delta A}(\mathbf{x}_k - \mathbf{x}_n)] = \mathbb{P}[\mathbb{I}_{\delta A}(\mathbf{x}_k - \mathbf{x}_n) = 1]$ (Ross, 2009), we have,

$$\mathbb{E}[X_n] = \sum_{k=1}^M \omega_c(|\mathbf{x}_k - \mathbf{x}_n|) \mathbb{P}[\mathbb{I}_{\delta A}(\mathbf{x}_k - \mathbf{x}_n) = 1]. \quad (5.10)$$

In the continuum limit, the right-hand side of Equation (5.10) is equivalent to multiplying the conditional probability of having an individual in a small window of size δA at a displacement ξ from the reference individual, with the corresponding interaction kernel and integrating over all possible displacements as $\delta A \rightarrow 0$ (Plank and Law, 2015). The conditional probability for the presence of a neighbour individual is $Z_2(\xi, t) \delta A / Z_1(t)$. A derivation of the conditional probability is provided in Section 5A.4. Hence we have,

$$\mathbb{E}[X_n] = \int \omega_c(|\xi|) \frac{Z_2(\xi, t)}{Z_1(t)} d\xi. \quad (5.11)$$

Note that the previous spatial moment models, including the spatial logistic model, assume that $F(X_n)$ is a linear function (Law et al., 2003; Plank and Law, 2015; Binny et al., 2016; Surendran et al., 2018). In that case, the death rate in Equation (5.8) depends only on $\mathbb{E}[X_n]$. But in the more general case where $F(X_n)$ is nonlinear, such as an Allee effect, we also require information about the variance. Therefore we compute $\text{Var}[X_n]$ in a similar fashion,

$$\begin{aligned} \text{Var}[X_n] &= \text{Var} \left[\sum_{k=1}^M \omega_c(|\mathbf{x}_k - \mathbf{x}_n|) \mathbb{I}_{\delta A}(\mathbf{x}_k - \mathbf{x}_n) \right], \\ &= \sum_{k=1}^M \omega_c^2(|\mathbf{x}_k - \mathbf{x}_n|) \text{Var}[\mathbb{I}_{\delta A}(\mathbf{x}_k - \mathbf{x}_n)] \\ &\quad + \sum_{\substack{i=1, j=1 \\ i \neq j}}^M \omega_c(|\mathbf{x}_i - \mathbf{x}_n|) \omega_c(|\mathbf{x}_j - \mathbf{x}_n|) \text{Cov} [\mathbb{I}_{\delta A}(\mathbf{x}_i - \mathbf{x}_n), \mathbb{I}_{\delta A}(\mathbf{x}_j - \mathbf{x}_n)]. \end{aligned} \quad (5.12)$$

Following a similar procedure used in the computation of continuum analogue of $\mathbb{E}[X_n]$ in Equation (5.11), we derive the expression for $\text{Var}[X_n]$ as,

$$\begin{aligned} \text{Var}[X_n] &= \int \omega_c^2(|\xi|) \left(\frac{Z_2(\xi, t)}{Z_1(t)} \right) d\xi \\ &\quad + \iint \omega_c(|\xi'|) \omega_c(|\xi''|) \left(\frac{Z_3(\xi', \xi'', t)}{Z_1(t)} - \frac{Z_2(\xi', t) Z_2(\xi'', t)}{Z_1^2(t)} \right) d\xi' d\xi''. \end{aligned} \quad (5.13)$$

For brevity, we omit the intermediate steps involved in the derivation of $\text{Var}[X_n]$ here. These details are provided in Section 5A.5.

We consider specific functional forms as $F(X_n) = d + X_n^2$ and $G(Y_n) = p + Y_n$. We make these choices because they are the simplest scenario that result in a strong Allee effect. To proceed, we compute the expected death rate of an individual, $D_1(t)$, by substituting the expressions for $\mathbb{E}[X_n]$ and $\text{Var}[X_n]$ in Equation (5.8) to give,

$$\begin{aligned} D_1(t) &= d + \left(\int \omega_c(|\xi|) \frac{Z_2(\xi, t)}{Z_1(t)} d\xi \right)^2 + \int \omega_c^2(|\xi|) \frac{Z_2(\xi, t)}{Z_1(t)} d\xi \\ &\quad + \iint \omega_c(|\xi|) \omega_c(|\xi'|) \left(\frac{Z_3(\xi, \xi', t)}{Z_1(t)} - \frac{Z_2(\xi, t) Z_2(\xi', t)}{Z_1^2(t)} \right) d\xi d\xi'. \end{aligned} \quad (5.14)$$

Similarly the expected proliferation rate for an individual is,

$$P_1(t) = p + \int \omega_p(|\xi|) \frac{Z_2(\xi, t)}{Z_1(t)} d\xi. \quad (5.15)$$

The dynamics of the first moment depend solely on the balance between proliferation and death. The movement of individuals does not result in a change in the population size. Hence the time evolution of the first spatial moment is given by,

$$\frac{d}{dt} Z_1(t) = \underbrace{P_1(t) Z_1(t)}_{\text{Increase in density due to proliferation}} - \underbrace{\widetilde{D_1(t) Z_1(t)}}_{\text{Decrease in density due to death}}. \quad (5.16)$$

Note that the dynamics of the first moment depends on the second and third moments through Equations (5.14)-(5.15), and to solve the dynamics of the first moment, we need to specify the values of these higher-order moments.

Now we derive the dynamical equation for the density of pairs of individuals. For the derivation, we need to calculate the event rates of individuals while they are in a pair with another individual at a displacement, ξ . The conditional probability of finding an individual at displacement ξ' , given that a pair of individuals exist with separation displacement ξ is $Z_3(\xi, \xi', t) \delta A / Z_2(\xi, t)$. The derivation of the expression for the conditional probability is given in Section 5A.4. Using this expression for the conditional probability, and following the same procedures used to arrive at Equation (5.11) and Equation (5.13), we compute $\mathbb{E}[X_n]$ and $\text{Var}[X_n]$ for an individual that forms a pair with another individual at a displacement ξ . Hence, the expected death rate of an individual, conditional on the presence of a neighbour at a displacement ξ , is given by,

$$D_2(\xi, t) = d + \left(\int \omega_c(|\xi'|) \frac{Z_3(\xi, \xi', t)}{Z_2(\xi, t)} d\xi' + \omega_c(|\xi|) \right)^2 + \int \omega_c^2(|\xi'|) \frac{Z_3(\xi, \xi', t)}{Z_2(\xi, t)} d\xi'. \quad (5.17)$$

Note that the subscript in $D_2(\xi, t)$ indicates the fact that we are computing the expected rate

for an individual that forms a pair with another individual at displacement ξ . The additional factor of $\omega_c(|\xi|)$ in the second term of Equation (5.17) accounts for the direct influence of the individual at displacement ξ . Similarly, the expected proliferation rate of an individual, conditional on the presence of a neighbour at a displacement ξ is,

$$P_2(\xi, t) = p + \int \omega_p(|\xi'|) \frac{Z_3(\xi, \xi', t)}{Z_2(\xi, t)} d\xi' + \omega_p(|\xi|). \quad (5.18)$$

The time evolution of $Z_2(\xi, t)$ depends on the creation of new pairs and the loss of existing pairs. The schematic in Figure 5.3 illustrates possible ways in which movement, proliferation or death event leads to the creation or destruction of pairs of individuals separated by a displacement of ξ . Figure 5.3(a) represents a pair of individuals at a separation displacement of ξ . A movement of either individual destroys this pair, as does the death of either individual. Figure 5.3(b)-(c) demonstrates two different ways to generate a new pair separated by a displacement ξ . When an individual among the pair separated by a displacement $\xi' + \xi$ in Figure 5.3(b) moves or places a daughter agent a displacement ξ' , a new pair is formed at a displacement ξ . In this case, the movement and proliferation occurs with rates $\mu_m(\xi') m$ and $\mu_p(\xi') P_2(\xi' + \xi, t)$, respectively. Another possibility for the creation of a pair with separation displacement ξ is when a single individual, as shown in Figure 5.3(c), places a daughter agent over a displacement $-\xi$. The rate for this event is $\mu_p(-\xi) P_1(t)$. The dynamics of the second moment is obtained by combining these possibilities as,

$$\begin{aligned} \frac{\partial}{\partial t} Z_2(\xi, t) = & \underbrace{-2D_2(\xi, t)Z_2(\xi, t)}_{\text{Loss of pairs at displacement } \xi \text{ due to the death of either individual}} \\ & \underbrace{-2m Z_2(\xi, t)}_{\text{Loss of pairs at displacement } \xi \text{ due to the movement of either individual}} \\ & \underbrace{+2 \int \mu_p(\xi') P_2(\xi + \xi', t) Z_2(\xi + \xi', t) d\xi'}_{\text{Formation of pairs at displacement } \xi \text{ due to the proliferation of individuals that form a pair at displacement } \xi + \xi'} \\ & \underbrace{+2m \int \mu_m(\xi') Z_2(\xi + \xi', t) d\xi'}_{\text{Formation of pairs at displacement } \xi \text{ due to the movement of individuals that form a pair at displacement } \xi + \xi'} \\ & \underbrace{+2\mu_p(-\xi) P_1(t) Z_1(t).}_{\text{Formation of pairs at displacement } \xi \text{ due to the placement of a daughter individual at a displacement } -\xi'} \end{aligned} \quad (5.19)$$

Since the event rates in Equations (5.17)-(5.18) depend on the third-order moment, $Z_3(\xi, \xi', t)$, we need some expression for the third moment to solve the system, and we anticipate that the dynamics of the third moment will depend upon higher moments. To deal with this hierarchy of equations we use the Power-2 asymmetric moment closure approximation (Law et al., 2003;

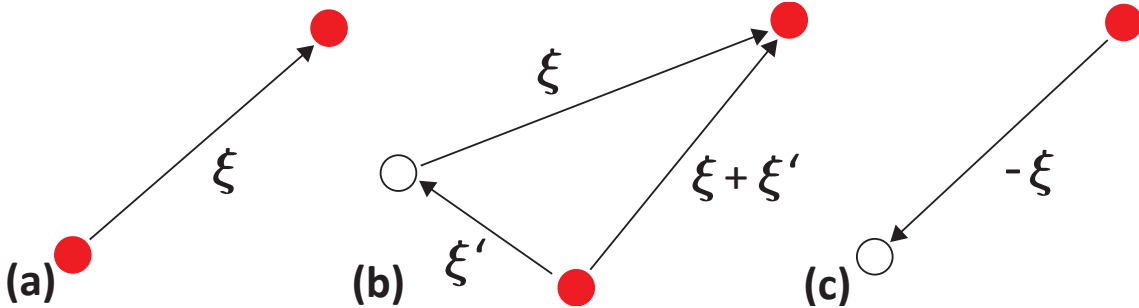


Figure 5.3: Possible events leading to a change in pair density. Red dots represent existing individuals and black open circles indicate potential locations of an individual after a movement or proliferation event. **a** A pair separated by a displacement ξ . Movement or death of either individual destroys the pair. **b** A pair separated by a displacement $\xi + \xi'$. A movement or placement of a daughter over a displacement of ξ' creates a new pair separated by displacement ξ . **c** A single individual where the placement of a daughter at displacement $-\xi$ creates a new pair with a displacement ξ .

Binny et al., 2016)

$$Z_3(\xi, \xi', t) = \frac{4Z_2(\xi, t)Z_2(\xi', t) + Z_2(\xi, t)Z_2(\xi' - \xi, t) - Z_2(\xi', t)Z_2(\xi' - \xi, t) - Z_1^4(t)}{5Z_1(t)}, \quad (5.20)$$

to approximately close the system in terms of the first and second moments only. Other closure approximations, such as the power-1 closure, the symmetric power-2 closure and the Kirkwood superposition approximation (Law et al., 2003; Murrell et al., 2004), are possible, and we compare the accuracy of these four different closure approximations in Section 5A.6. Details about the numerical methods involved in solving the dynamical equation for the second moment, Equation (5.19) is provided in Section 5A.7 and MATLAB code to implement the algorithm is available on [Github](#).

5.6 Mean-field dynamics

Under the classical mean-field approximation, interactions between individuals occur in proportion to the average density, and there is no spatial structure. These conditions correspond to having long-range interactions between individuals. Comparing the solutions of the classical mean-field model, IBM simulations and the solution of the new spatial moment dynamics model will provide insight into how spatial structure influences the population dynamics.

In terms of spatial moments, the mean-field implies that we have $Z_2(\xi, t) = Z_1^2(t)$ (Binny et al., 2016; Surendran et al., 2020a), which means that the expected death rate from Equation (5.14) simplifies to,

$$D_1(t) = d + Z_1^2(t) \left(\int \omega_c(|\xi|) d\xi \right)^2 + Z_1(t) \int \omega_c^2(|\xi|) d\xi. \quad (5.21)$$

Similarly, the expected proliferation rate in Equation (5.15) simplifies to

$$P_1(t) = p + Z_1(t) \int \omega_p(|\xi|) d\xi. \quad (5.22)$$

Since the interaction kernels have the property that $\int \omega_c(|\xi|) d\xi = 2\pi\gamma_c\sigma_c^2$ and $\int \omega_c^2(|\xi|) d\xi = \pi\gamma_c^2\sigma_c^2$, we substitute the mean-field death and proliferation rates in Equations (5.21)-(5.22) into Equation (5.16) to give

$$\frac{d}{dt}Z_1(t) = (p - d)Z_1(t) + (2\pi\gamma_p\sigma_p^2 - \pi\gamma_c^2\sigma_c^2)Z_1^2(t) - 4\pi^2\gamma_c^2\sigma_c^4Z_1^3(t), \quad (5.23)$$

which leads to three equilibrium densities:

$$\begin{aligned} \bar{Z}_1^{(1)} &= 0, \\ \bar{Z}_1^{(2)} &= \frac{2\gamma_p\sigma_p^2 - \gamma_c^2\sigma_c^2}{8\pi\gamma_c^2\sigma_c^4} - \frac{\sqrt{(2\gamma_p\sigma_p^2 - \gamma_c^2\sigma_c^2)^2 + 16\gamma_c^2\sigma_c^4(p - d)}}{8\pi\gamma_c^2\sigma_c^4}, \\ \bar{Z}_1^{(3)} &= \frac{2\gamma_p\sigma_p^2 - \gamma_c^2\sigma_c^2}{8\pi\gamma_c^2\sigma_c^4} + \frac{\sqrt{(2\gamma_p\sigma_p^2 - \gamma_c^2\sigma_c^2)^2 + 16\gamma_c^2\sigma_c^4(p - d)}}{8\pi\gamma_c^2\sigma_c^4}, \end{aligned} \quad (5.24)$$

where $\bar{Z}_1^{(3)} > \bar{Z}_1^{(2)} > \bar{Z}_1^{(1)}$ for the parameters we consider in this study. In this classical mean-field context, $\bar{Z}_1^{(2)}$ is the Allee threshold and $\bar{Z}_1^{(3)}$ is the carrying capacity density. The equilibrium densities and dynamics associated with Equation (5.23) are depicted in Figure 5.2(e)-(f).

5.7 Results and Discussion

We now present IBM simulation results together with numerical solutions of both the spatial moment and the mean-field models to explore the influence of spatial structure on the population dynamics. In each case that we consider (Figures 5.4–5.7) we plot the time evolution of the average density of individuals from repeated, identically-prepared IBM simulations. Information about the spatial structure of the population is given in terms of the pair correlation function computed at the end of the simulation. Since the IBM is stochastic, there is a non-zero probability that any individual simulation will lead to extinction, regardless of whether the average outcome is that the population would survive. In the first set of results we present we take care to choose parameters and initial conditions such that at least 99% of the 1000 identically prepared simulations leads to the same long-term population-level outcome (i.e. extinction or survival) and any outliers, if present, are excluded from the calculation of ensemble averages. For each parameter combination, we consider three different initial conditions: (i) $\bar{Z}_1^{(1)} < Z_1(0) < \bar{Z}_1^{(2)}$; (ii) $\bar{Z}_1^{(2)} < Z_1(0) < \bar{Z}_1^{(3)}$; and (iii) $Z_1(0) > \bar{Z}_1^{(3)}$. In the IBM simulations we control the initial density by choosing a different value of $N(0)$.

As a starting point we consider a simple case with relatively weak long-range interactions so that the mean-field approximation is valid in Figure 5.4. Choosing long-range dispersion and competition kernels ensures that there is minimal correlation between the locations of agents in the simulations. As expected, results with $\bar{Z}_1^{(1)} < Z_1(0) < \bar{Z}_1^{(2)}$ lead to extinction, and results with $\bar{Z}_1^{(2)} < Z_1(0) < \bar{Z}_1^{(3)}$ and $Z_1(0) > \bar{Z}_1^{(3)}$ leads to the population eventually settling to the carrying capacity density by $t = 30$. The comparison of the averaged IBM results, the mean-field and spatial moment models in 5.4(g)-(i) shows that all three approaches are consistent and the eventual long-time population contains no spatial structure since the pair correlation function is unity in Figure 5.4(k)-(l). Note that we do not show the pair correlation function in Figure 5.4(j) since, in this case, the long-time result is that the population goes extinct.

Having verified that both the IBM and spatial moment dynamics model replicate solutions of the mean-field model for relatively weak long-range interaction and dispersal kernels, we now focus on short-range interactions that can lead to spatial structure.

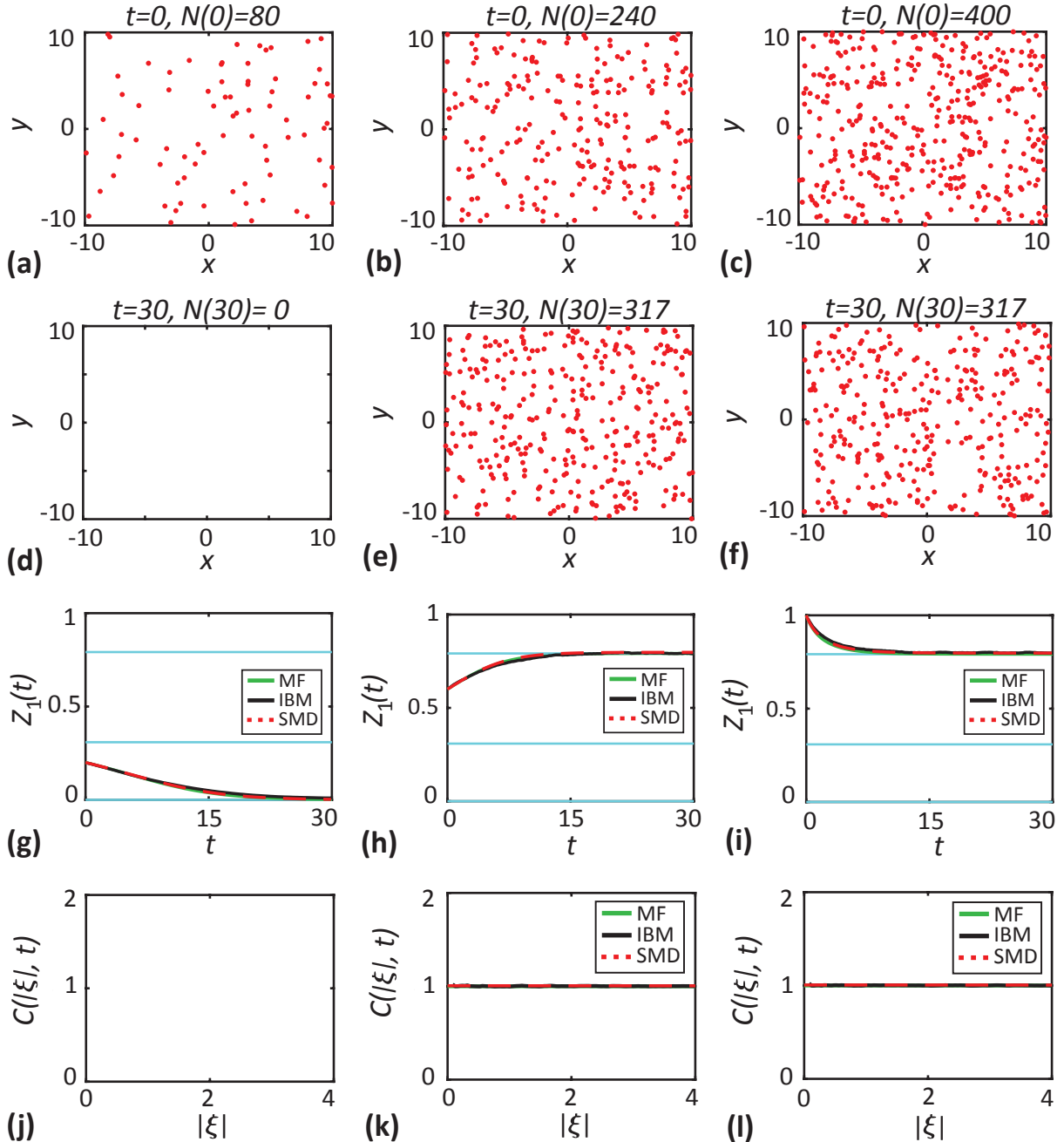


Figure 5.4: Long-range interactions and dispersal kernels ($\sigma_c = \sigma_p = \sigma_d = 4.0$) with weak interaction strengths ($\gamma_c = 0.009$ and $\gamma_p = 0.009$) lead to mean-field conditions. **a-c** initial locations of individuals (dots) for three different initial population sizes, $N(0) = 80, 240$ and 400 , respectively. **d-f** location of individuals at $t = 30$. **g-i** density of individuals as a function of time. Black solid lines correspond to averaged results from 1000 identically-prepared IBM realisations, red dashed lines correspond to the solutions of the spatial moment dynamics model and green solid lines are the solution of the mean-field model. The cyan lines show the equilibrium densities. **j-l** pair-correlation function, $C(|\xi|, 30)$. Here we see that the simulation results from IBM and solutions of both spatial moment model and mean-field models match well for all cases considered. Since the population extinction occurs by $t = 30$ for the case with $N(0) = 80$, we do not show any individuals in **d** and any pair correlation function in **j**. Parameter values are $d = 0.4, p = 0.2, m = 0.1, \mu_s = 0.4$ and $\sigma_s = 0.1$.

5.7.1 Short-range competition reduces the Allee threshold

Results in Figure 5.5 are presented in the same format as in Figure 5.4 except that we consider short-range competition by setting $\sigma_c = 0.5$ without changing the cooperation or dispersal kernels.

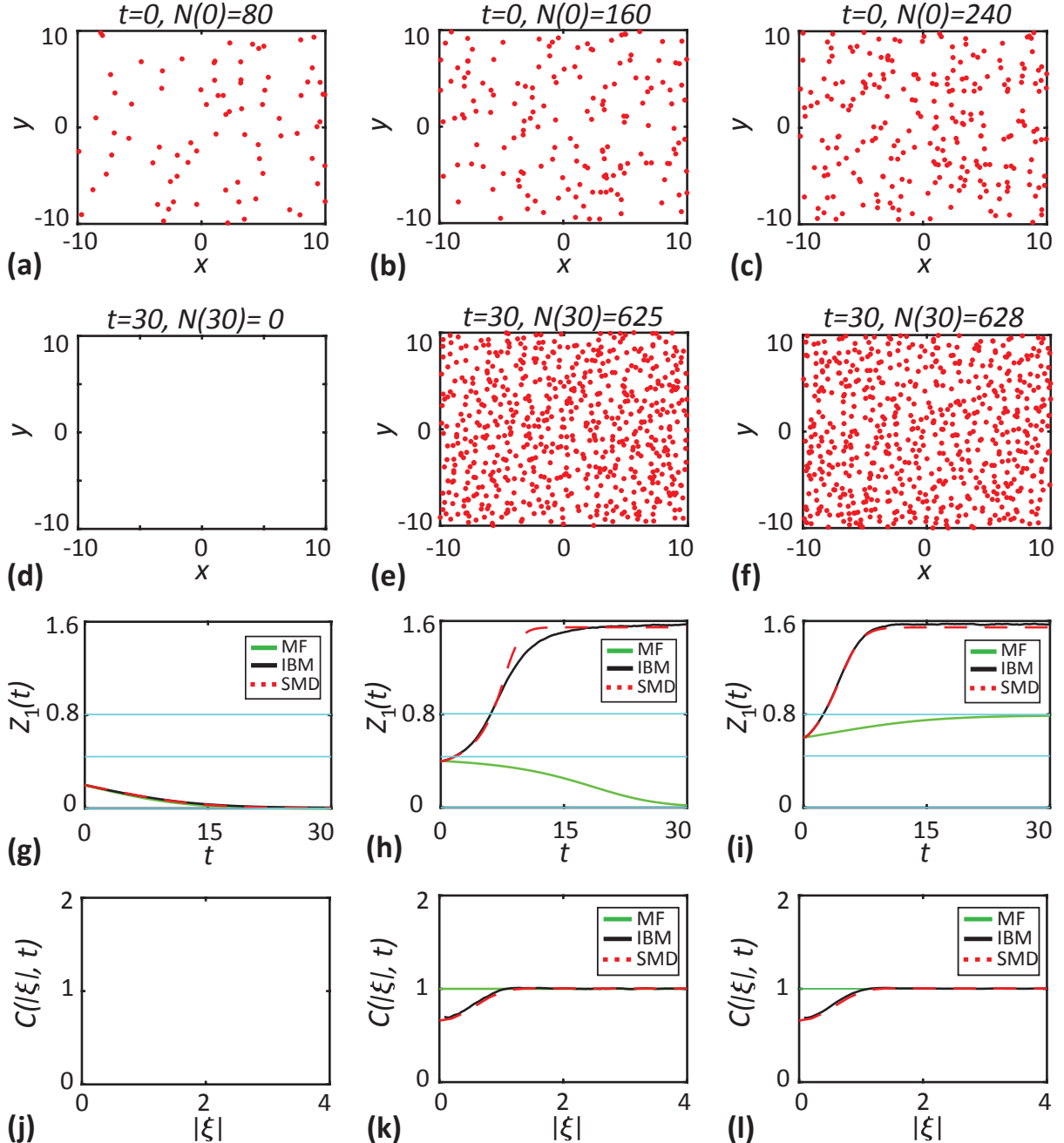


Figure 5.5: Short-range competition ($\sigma_c = 0.5$ and $\gamma_c = 0.448$) reduces the Allee threshold. **a-c** initial locations of individuals (red) for three different population sizes, $N(0) = 80, 160$ and 240 , respectively. **d-f** location of individuals at $t = 30$. **g-i** density of individuals as a function of time. Black solid lines correspond to the averaged results from 1000 identically-prepared IBM realisations, red dashed lines correspond to the solutions of the spatial moment dynamics model and green solid lines are the solution of the mean-field model. The cyan lines show the equilibrium densities. **j-l** pair-correlation function, $C(|\xi|, 30)$. Parameter values are $d = 0.4$, $p = 0.2$, $m = 0.1$, $\mu_s = 0.4$ and $\sigma_s = 0.1$.

Figure 5.5(a)-(c) shows the initial randomly-placed populations, $N(0) = 80, 160$ and 240 , respectively. Results in the left-most column with $Z_1(0) = 80/400 < \bar{Z}_1^{(2)}$ leads to extinction. Results in the central column with $Z_1(0) = 160/400 < \bar{Z}_1^{(2)}$ are very interesting because the initial density is below the classical mean-field Allee threshold and so standard models would predict extinction, yet we see that the population grows to reach a positive carrying capacity density. This difference is caused by the spatial structure, which we can see in Figure 5.5(k) is segregated at short distances. When competition is short range and the population is segregated, individuals in the IBM experience less competition than would be expected in a population without spatial structure under mean-field conditions. This decrease in competition means that the population increases despite the initial density being less than the mean-field Allee threshold. These observations highlight the interplay between the competition and dispersal ranges. In Figure 5.6, we present results when both competition and dispersal are short-range, and we demonstrate that those results are entirely different from those in Figure 5.5. We observe a discrepancy between the IBM and the spatial moment model results for the transient dynamics, approximately between $t = 10$ and $t = 20$, in Figure 5.5(h). We attribute this discrepancy to the accuracy of the moment closure approximation since similar results are observed in lattice-based models [8].

Results in the right-most column in Figure 5.5 show that when the initial density is above the mean-field Allee threshold, $Z_1(0) > \bar{Z}_1^{(2)}$, we see that the population increases to reach the same carrying capacity density as in Figure 5.5(h). Here we find that the carrying capacity density reached by the IBM is much higher than the mean-field carrying capacity density. This means that the classical mean-field model under-predicts the long-time density. In contrast, the spatial moment dynamics model leads to an accurate prediction of the averaged density from the IBM. This result, that the spatial structure can impact the carrying capacity density is consistent with previous observations for the spatial logistic model (Law et al., 2003), but our observation that spatial structure changes the Allee threshold has not been reported previously.

5.7.2 Short-range competition and dispersal encourage population extinction

Results in Figure 5.6 consider both short-range competition and short-range dispersal by setting $\sigma_c = \sigma_d = 0.5$. The format of the results in Figure 5.6 is the same as in Figures 5.4-5.5. An additional set of results in Section 5A.8 present some cases where we consider just short-range dispersal.

IBM simulations in Figure 5.6 show that short-range dispersal and competition leads to clustering and extinction. When the dispersal is short-range, daughter individuals are placed in close proximity to the parent individual, which leads to the formation of clusters. Short-range competition means that the competition within those clusters is strong, and significantly increases the local death rate of individuals. In the classical mean-field model we expect ex-

tinction to occur only when $Z_1(0) < \bar{Z}_1^{(2)}$ but our IBM results show that the population goes extinct when we set $Z_1(0) > \bar{Z}_1^{(2)}$ in Figure 5.6(h), and even more surprisingly we see that the IBM simulations lead to extinction even when $Z_1(0) > \bar{Z}_1^{(3)}$ in Figure 5.6(i). This means that the spatial structure in this case leads the population to extinction. While the mean-field model completely fails to predict the observed extinction in the IBM, we find that the spatial moment model accurately reproduces the population dynamics of the IBM.

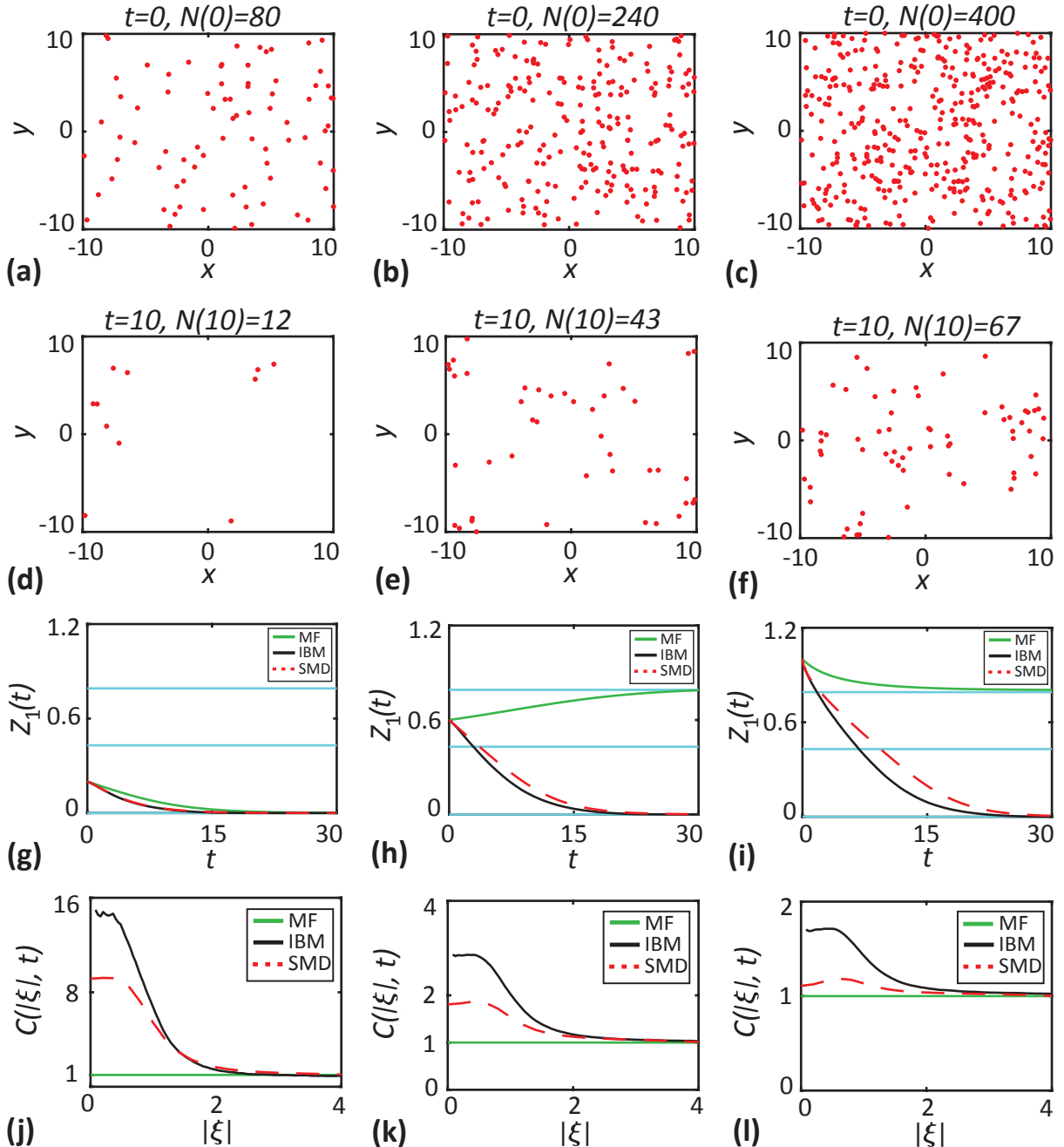


Figure 5.6: Short-range competition and short-range dispersal drive the population to extinction. In this case we consider short-range competition and dispersal ($\sigma_c = \sigma_d = 0.5$) with $\gamma_c = 0.488$. **a-c** initial locations of individuals (red) for three different population sizes, $N(0) = 80, 240$ and 400 , respectively. **d-f** location of individuals at $t = 30$. **g-i** density of individuals as a function of time. Black solid lines correspond to the averaged results from 1000 identically-prepared IBM realisations, red dashed lines correspond to the solutions of spatial moment dynamics model and green solid lines are the solution of the mean-field model. The cyan lines show the equilibrium densities. **j-l** pair-correlation function, $C(|\xi|, 30)$. Parameter values are $d = 0.4, p = 0.2, m = 0.1, \mu_s = 0.4$ and $\sigma_s = 0.1$.

5.7.3 Short-range cooperation and intermediate-range dispersal promotes population growth

We now consider a further case where IBM simulations are qualitatively different from the classical mean-field model. Results in Figure 5.7 correspond to short-range cooperation ($\sigma_p = 0.5$) and intermediate-range dispersal ($\sigma_d = 2.0$).

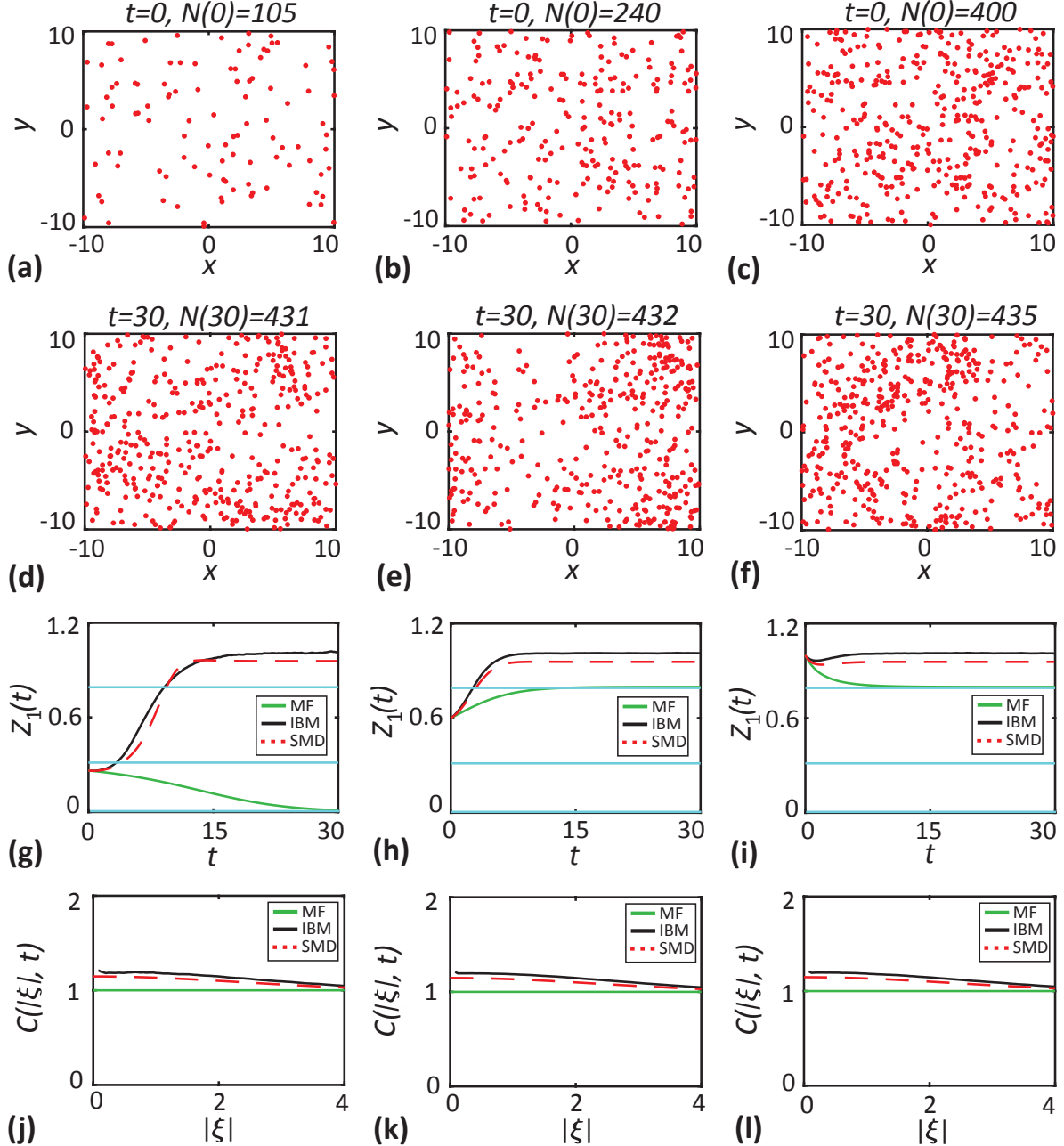


Figure 5.7: Short-range cooperation and dispersal promotes population growth. In this case we consider short-range cooperation $\sigma_p = 0.5$ and an intermediate-range dispersal $\sigma_d = 2.0$ with $\gamma_p = 0.576$. **a-c** the initial locations of individuals (red dots) for three different population sizes, $N(0) = 105, 240$ and 400 . **d-f** show the location of individuals at $t = 30$. **g-i** show the density of individuals as a function of time. Black solid lines correspond to the averaged results from 1000 realisations of the IBM, red dashed lines correspond to the solutions of spatial moment dynamics and green solid lines correspond to the solution of the mean-field model. The cyan lines show the critical densities. **j-l** show the $C(|\xi|, t)$ computed at $t = 30$ as a function of separation distance. Parameter values are $d = 0.4, p = 0.2, m = 0.1, \mu_s = 0.4$ and $\sigma_s = 0.1$.

Some clustering in Figure 5.7(d)-(f) is evident, and this clustering is induced by the intermediate-range dispersal and leads to enhanced proliferation because of strong short-range cooperation. This case is very interesting because we observe population growth even when the initial density is below the classical mean-field Allee threshold in Figure 5.7(g). For all three choices of initial density in Figure 5.7, the population survives and eventually reaches a carrying capacity density that is greater than the carrying capacity density predicted by the classical mean-field model.

5.7.4 Survival probability

We conclude our results by using the IBM to estimate the survival probability, $\mathbb{P}(\text{survival})$, as a function of initial density in Figure 5.8. To calculate $\mathbb{P}(\text{survival})$, we perform a large number of identically-prepared realisations over a sufficiently long period of time, $t = 100$. From these simulations we record the fraction of realisations in which the population does not become extinct in this time interval.

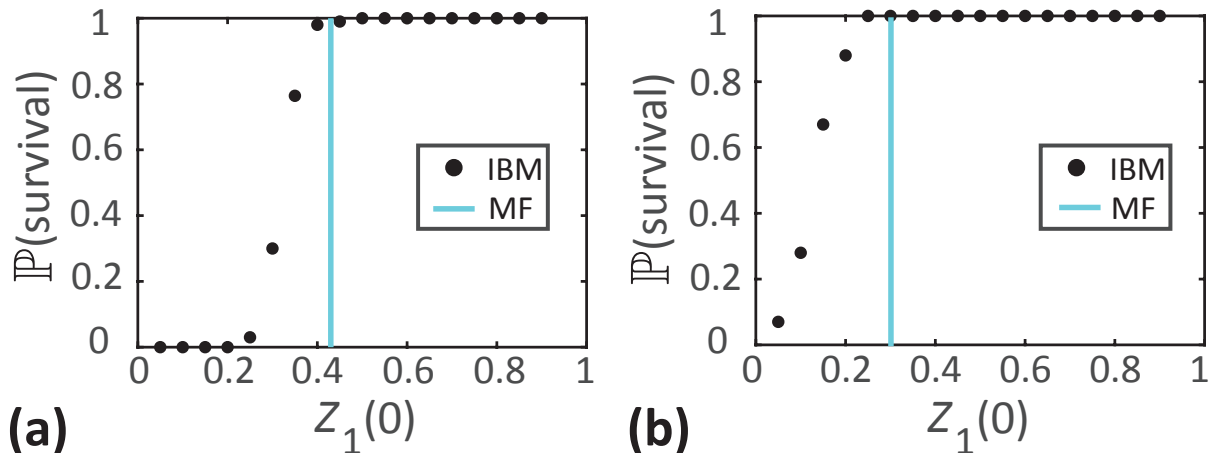


Figure 5.8: Survival probability as a function of $Z_1(0)$ for: **a** short-range competition ($\sigma_c = 0.5$, $\gamma_c = 0.488$), and **b** short-range cooperation and intermediate-range dispersal ($\sigma_p = 0.5$, $\sigma_d = 2.0$, $\gamma_p = 0.576$). Cyan lines show the classical mean-field Allee threshold and black dots show $\mathbb{P}(\text{survival})$ estimated from 100 identically-prepared IBM realisations. Other parameter values are $d = 0.4$, $p = 0.2$, $m = 0.1$, $\mu_s = 0.4$ and $\sigma_s = 0.1$.

Results in Figure 5.8(a) show $\mathbb{P}(\text{survival})$ for a population with short-range competition. The mean-field Allee threshold for this choice of parameters is $\bar{Z}_1^{(2)} = 0.43$. In contrast, we find that a certain proportion of populations with $Z_1(0) < \bar{Z}_1^{(2)}$ can survive. This difference between the classical mean-field result is due to the presence of spatial structure, and for this choice of parameters we have a segregated population, as illustrated in Figure 5.5. Another factor that influences the survival probability is the stochastic nature of the IBM. Even in the absence of spatial structure, the stochasticity can lead to a continuous transition of $\mathbb{P}(\text{survival})$ from 0 to 1 in the IBM, but possibly quite narrow and centred around the mean-field model Allee threshold. The spatial structure can shift the transition left or right (depending on whether it makes survival more or less likely) and potentially broaden the transition curve. Results in

Figure 5.8(b) show $\mathbb{P}(\text{survival})$ for a population with short-range cooperation and intermediate-range dispersal where the classical mean-field Allee threshold is $\bar{Z}_1^{(2)} = 0.3$. Again we see that populations with an initial density below the Allee threshold can survive. This difference between the classical mean-field result is due to the presence of spatial structure, which in this case leads to clustering, as shown in Figure 5.7, and the stochasticity of the IBM.

5.8 Conclusions

In this study we consider an IBM that describes population dynamics that incorporates short-range interactions and spatial structure. The model construction allows us to incorporate a strong Allee effect, and in particular to explore the impact of spatial structure on the Allee threshold. Classical mathematical models of population dynamics that incorporate an Allee effect are based on making a mean-field approximation. This approximation implies that individuals interact in proportion to their average density and leads to the neglect of spatial structure, such as clustering and segregation.

We explore how short-range competition, short-range cooperation and short-range dispersal leads to spatial structure in a dynamic population and we focus on examining how this spatial structure influences the Allee threshold density. Overall, we find that the Allee threshold can be very sensitive to the presence of spatial structure to the point that classical mean-field predictions are invalid. For example, when we consider short-range dispersal and short-range competition we find that the population becomes extinct, despite the fact that the classical mean-field model predicts that the population will always survive when $Z_1(0) > \bar{Z}_1^{(2)}$. While our IBM results disagree with the classical mean-field prediction when the spatial structure is present, we also derive and solve a novel spatial moment dynamics model that is able to accurately capture how the Allee threshold depends upon spatial structure and we find that the spatial moment model reliably predicts population dynamics when spatial structure is present. Our results on the estimation of $\mathbb{P}(\text{survival})$ show that a certain proportion of populations seemed to have non-zero survival probability despite the fact that the initial population density is below the Allee threshold due to the presence of spatial structure. Note that the spatial moment model developed in this study is deterministic and hence cannot be used to estimate $\mathbb{P}(\text{survival})$. Instead, the spatial moment model predicts a threshold initial density above which the population survives. Overall our results show that the spatial moment model predicts this threshold more accurately than the mean-field model.

There are many potential avenues to extend the features in this study. For example, in this work we make the simplest possible assumption that agent movement is random and density-independent. This feature could be refined. For example, if the model was applied to study a population of biological cells, it might be more appropriate to consider a density-dependent movement rate and some directional bias where individuals are either attracted to or repelled from other agents in their neighbourhood (Cai et al., 2006; Binny et al., 2020). In this study,

we restrict our exploration to a simple population where all individuals are of the same type. Another interesting extension of the model would be to consider a multi-species where the total population consists of individuals from various distinct species (Markham et al., 2013; Wittmer et al., 2005). We leave both these extensions for future consideration.

Chapter 5A

Additional results for Chapter 5

5A.1 Comparison of long-range and short-range competition

Here we present a second set of results comparing the impact of short-range and long-range competition on the death rate, \mathcal{D}_n , analogous to the results in Figure 5.1. These additional results, in Figure 5A.1, are generated with precisely the same parameters and spatial arrangement of individuals as those in Figure 5.1, with the exception that here we consider a quadratic functional form for the death rate ($F(X_n) = X_n^2$). Comparing the results in Figure 5.1 with the additional results in Figure 5A.1 indicates that the choice of $F(X_n) = X_n^2$, reduces the death rates of individuals.

Similar to the results in Figure 5.1, the long-range competition leads to \mathcal{D}_n being influenced by neighbours that are further apart, as shown in Figure 5A.1(a)-(b). But the difference here is that overall we see a decrease in the death rate. For example, even though the death rate of the relatively isolated individual shown with the green dot is non-zero due to the long-range competition, the value of $\mathcal{D}_n = 0.076$ here is lower than $\mathcal{D}_n = 0.275$ computed using $F(X_n) = X_n$ in Figure 5.1. Under short-range competition, as shown in Figure 5A.1(c)-(d), only the contribution from immediate neighbours is significant. As a result, the isolated individual (green dot), does not experience competition from its neighbours, leading to $\mathcal{D}_n = 0$.

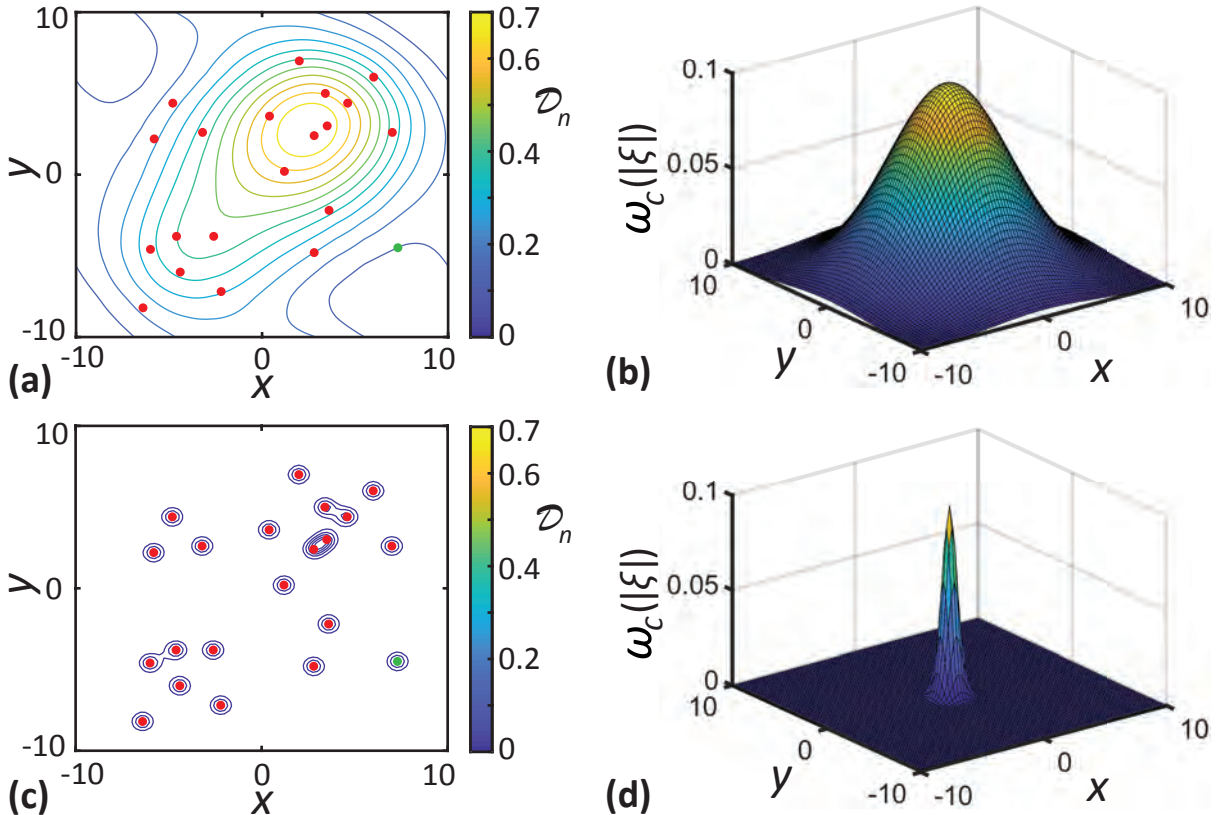


Figure 5A.1: Visualisation of the impact of long-range and short-range neighbour-dependent interactions. Results in **a**, **c** show the location of individuals (red dots) superimposed with the level curves of \mathcal{D}_n for long-range and short range-competition, respectively. Results in **b**, **d** show the long-range ($\sigma_c = 4.0$) and short-range ($\sigma_c = 0.5$) competition kernel, respectively, where these kernels are centred at the origin. For the computation of \mathcal{D}_n , we use $F(X_n) = X_n^2$ and $\gamma_c = 0.1$.

5A.2 Numerical implementation of the individual-based model

Here we outline the numerical implementation of our individual-based model (IBM) using the Gillespie algorithm (Gillespie, 1977). The codes used for the simulation of the IBM are available on [Github](#). In each simulation, we initially populate the computational domain, of size $L \times L$, with $N(0)$ individuals placed at random. We use periodic boundary conditions along all boundaries. For each potential event, we compute the death and proliferation rates of individuals using Equation (5.3) and Equation (5.6). The movement of individuals is density independent, and the constant intrinsic movement rate is m . The sum of event rates of all individuals is given by,

$$\lambda(t) = \sum_{n=1}^{N(t)} (\mathcal{D}_n + \mathcal{P}_n + m). \quad (5A.1)$$

Each time the IBM is updated, one of the three possible events occurs, and the time interval between successive events is exponentially distributed with mean $1/\lambda(t)$. The probability for any of the events to occur is proportional to the rate of the corresponding event. For a proliferation

event, an offspring is placed at a displacement sampled from the dispersal kernel, $\mu_p(\xi)$, and the population size increases by one. For a death event, the population size reduces by one. For a movement event, an individual traverses a displacement that is sampled from the movement displacement kernel, $\mu_m(\xi)$.

We compute the average density of individuals at a particular time by dividing the population size, $N(t)$, by the area of the computational domain, L^2 . To compute the pair-correlation function, $C(|\xi|, t)$, we consider a reference individual located at \mathbf{x}_n and calculate all distances $|\xi| = |\mathbf{x}_k - \mathbf{x}_n|$, associated with the other $N(t) - 1$ individuals (Law et al., 2003; Surendran et al., 2018). We repeat this process with each of the remaining individuals until every individual has acted as the reference individual. The pair-correlation function is calculated by enumerating the distances which fall into the interval, $[|\xi| - \delta|\xi|/2, |\xi| + \delta|\xi|/2]$. We normalise the bin count by a factor of $2\pi|\xi|\delta|\xi|N(t)(N(t) - 1)/L^2$ to ensure that $C(|\xi|, t) = 1$ in the absence of spatial structure. The choice of bin width, $\delta|\xi|$, is crucial in computing the pair-correlation function. When $\delta|\xi|$ is very small, we obtain a noise dominated $C(|\xi|, t)$. In contrast, very large $\delta|\xi|$ leads to an overly smooth $C(|\xi|, t)$ that fails to describe the effects of short-range interactions. In all our simulations, we use an intermediate value of $\delta|\xi| = 0.2$ which helps us to avoid the two extremities.

5A.3 Definition of spatial moments

Here, we provide a more formal mathematical definition for the spatial moments (Plank and Law, 2015; Law and Dieckmann, 2000; Binny et al., 2016). Let us suppose $D_{\delta A}(\mathbf{x}) \subset \mathbb{R}^2$ is a disc of area δA centred at position $\mathbf{x} \in \mathbb{R}^2$ and the number of individuals in the region $D_{\delta A}(\mathbf{x})$, at a time t , is denoted by the random variable $N(D_{\delta A}(\mathbf{x}), t)$. The first spatial moment, $Z_1(t)$, can be computed by dividing the population size of individuals by the area of the domain. Hence we have,

$$Z_1(t) = \lim_{\delta A \rightarrow 0} \frac{1}{\delta A} \mathbb{E}[N(D_{\delta A}(\mathbf{x}), t)]. \quad (5A.2)$$

The second spatial moment, $Z_2(\xi, t)$, is the average density of pairs of individuals separated by a displacement ξ at time t . For a pair of individuals separated by a displacement ξ , we have,

$$Z_2(\xi, t) = \lim_{\delta A \rightarrow 0} \frac{1}{\delta A^2} \mathbb{E}[N(D_{\delta A}(\mathbf{x}), t) N(D_{\delta A}(\mathbf{x} + \xi), t) - N(D_{\delta A}(\mathbf{x}) \cap D_{\delta A}(\mathbf{x} + \xi), t)]. \quad (5A.3)$$

The second term in the expectation in Equation (5A.3) is necessary to avoid counting self-pairs. For non-overlapping regions $D_{\delta A}(\mathbf{x})$ and $D_{\delta A}(\mathbf{x} + \xi)$, this term becomes zero as $\delta A \rightarrow 0$. The

third spatial moment is the density of triplets of individuals, and is similarly defined as,

$$\begin{aligned} Z_3(\xi, \xi', t) = \lim_{\delta A \rightarrow 0} \frac{1}{\delta A^3} \mathbb{E} & \left[N(D_{\delta A}(\mathbf{x}), t) N(D_{\delta A}(\mathbf{x} + \xi), t) N(D_{\delta A}(\mathbf{x} + \xi'), t) \right. \\ & - N(D_{\delta A}(\mathbf{x}) \cap D_{\delta A}(\mathbf{x} + \xi), t) N(D_{\delta A}(\mathbf{x} + \xi'), t) \\ & - N(D_{\delta A}(\mathbf{x}) \cap D_{\delta A}(\mathbf{x} + \xi'), t) N(D_{\delta A}(\mathbf{x} + \xi), t) \\ & - N(D_{\delta A}(\mathbf{x} + \xi) \cap D_{\delta A}(\mathbf{x} + \xi'), t) N(D_{\delta A}(\mathbf{x}), t) \\ & \left. + 2N(D_{\delta A}(\mathbf{x}) \cap D_{\delta A}(\mathbf{x} + \xi') \cap D_{\delta A}(\mathbf{x} + \xi), t) \right]. \end{aligned} \quad (5A.4)$$

Again, the extra terms in Equation (5A.4) are needed to avoid counting non-distinct triplets.

5A.4 Conditional probabilities for the presence of individuals

In this section we derive expressions for the probabilities of finding individuals at specific displacements conditional on the presence of other individuals. In the limit, $\delta A \rightarrow 0$, the probability of having one individual in the region $D_{\delta A}(\mathbf{x})$ is given by,

$$\mathbb{P}[N(D_{\delta A}(\mathbf{x}), t) = 1] = \mathbb{E}[N(D_{\delta A}(\mathbf{x}), t)]. \quad (5A.5)$$

Now, the probability of having two individuals located in non overlapping regions $D_{\delta A}(\mathbf{x})$ and $D_{\delta A}(\mathbf{x} + \xi)$, respectively, is given by,

$$\mathbb{P}[N(D_{\delta A}(\mathbf{x}), t) = 1 \cap N(D_{\delta A}(\mathbf{x} + \xi), t) = 1] = \mathbb{E}[N(D_{\delta A}(\mathbf{x}), t) N(D_{\delta A}(\mathbf{x} + \xi), t)]. \quad (5A.6)$$

Similarly, the probability for having three individuals at non overlapping regions $D_{\delta A}(\mathbf{x})$, $D_{\delta A}(\mathbf{x} + \xi)$ and $D_{\delta A}(\mathbf{x} + \xi')$, respectively, is given by,

$$\begin{aligned} \mathbb{P}[N(D_{\delta A}(\mathbf{x}), t) = 1 \cap N(D_{\delta A}(\mathbf{x} + \xi), t) = 1 \cap N(D_{\delta A}(\mathbf{x} + \xi'), t) = 1] \\ = \mathbb{E}[N(D_{\delta A}(\mathbf{x}), t) N(D_{\delta A}(\mathbf{x} + \xi), t) N(D_{\delta A}(\mathbf{x} + \xi'), t)]. \end{aligned} \quad (5A.7)$$

To compute the event rates, we need to find the probabilities of individuals being present at a given displacement, conditional on the presence of other individuals. To compute the conditional probabilities, we use the property that,

$$\mathbb{P}[A | B] = \frac{\mathbb{P}[A \cap B]}{\mathbb{P}[B]}. \quad (5A.8)$$

The conditional probability of finding an individual at a displacement $\mathbf{x} + \boldsymbol{\xi}$, given that the reference individual is located at \mathbf{x} , is,

$$\mathbb{P}[N(D_{\delta A}(\mathbf{x} + \boldsymbol{\xi}), t) = 1 | N(D_{\delta A}(\mathbf{x}), t) = 1] = \frac{\mathbb{P}[N(D_{\delta A}(\mathbf{x} + \boldsymbol{\xi}), t) = 1 \cap N(D_{\delta A}(\mathbf{x}), t) = 1]}{\mathbb{P}[N(D_{\delta A}(\mathbf{x}), t) = 1]}. \quad (5A.9)$$

Using the definitions of probabilities in Equations (5A.5)-(5A.6) and the definitions of spatial moments in Equations (5A.2)-(5A.3), we rewrite the numerator and denominator of Equation (5A.9) as,

$$\mathbb{P}[N(D_{\delta A}(\mathbf{x}), t) = 1] = Z_1(t) \delta A, \quad (5A.10)$$

$$\mathbb{P}[N(D_{\delta A}(\mathbf{x} + \boldsymbol{\xi}), t) = 1 \cap N(D_{\delta A}(\mathbf{x}), t) = 1] = Z_2(\boldsymbol{\xi}, t) (\delta A)^2. \quad (5A.11)$$

Hence the conditional probability of finding an individual at a displacement $\mathbf{x} + \boldsymbol{\xi}$ from a reference individual at \mathbf{x} is given by,

$$\mathbb{P}[N(D_{\delta A}(\mathbf{x} + \boldsymbol{\xi}), t) = 1 | N(D_{\delta A}(\mathbf{x}), t) = 1] = \frac{Z_2(\boldsymbol{\xi}, t) \delta A}{Z_1(t)}. \quad (5A.12)$$

Similarly, we compute the conditional probability of finding an individual at a displacement $\mathbf{x} + \boldsymbol{\xi}'$, given that a pair of individuals where constituent individuals are located at $\mathbf{x} + \boldsymbol{\xi}$ and \mathbf{x} , respectively, as

$$\begin{aligned} & \mathbb{P}[N(D_{\delta A}(\mathbf{x} + \boldsymbol{\xi}'), t) = 1 | N(D_{\delta A}(\mathbf{x} + \boldsymbol{\xi}), t) = 1 \cap N(D_{\delta A}(\mathbf{x}), t) = 1] \\ &= \frac{\mathbb{P}[N(D_{\delta A}(\mathbf{x} + \boldsymbol{\xi}'), t) = 1 \cap N(D_{\delta A}(\mathbf{x} + \boldsymbol{\xi}), t) = 1 \cap N(D_{\delta A}(\mathbf{x}), t) = 1]}{\mathbb{P}[N(D_{\delta A}(\mathbf{x} + \boldsymbol{\xi}), t) = 1 \cap N(D_{\delta A}(\mathbf{x}), t) = 1]}, \\ &= \frac{Z_3(\boldsymbol{\xi}, \boldsymbol{\xi}', t) \delta A}{Z_2(\boldsymbol{\xi}, t)}. \end{aligned} \quad (5A.13)$$

5A.5 Computation of variance

Here we outline the steps involved in the derivation of expression for variance of the neighbourhood density in Equation (5.13). The fundamental definition of the variance is,

$$\begin{aligned} \text{Var}[X] &= \text{Var} \left[\sum_{k=1}^M \omega_c(|\mathbf{x}_k - \mathbf{x}_n|) \mathbb{I}_{\delta A}(\mathbf{x}_k - \mathbf{x}_n) \right], \\ &= \sum_{k=1}^M \omega_c^2(|\mathbf{x}_k - \mathbf{x}_n|) \text{Var}[\mathbb{I}_{\delta A}(\mathbf{x}_k - \mathbf{x}_n)] \\ &\quad + \sum_{\substack{i=1, j=1 \\ i \neq j}}^M \omega_c(|\mathbf{x}_i - \mathbf{x}_n|) \omega_c(|\mathbf{x}_j - \mathbf{x}_n|) \text{Cov}[\mathbb{I}_{\delta A}(\mathbf{x}_i - \mathbf{x}_n), \mathbb{I}_{\delta A}(\mathbf{x}_j - \mathbf{x}_n)]. \end{aligned} \quad (5A.14)$$

Now, using the properties of indicator function, $\mathbb{E}[\mathbb{I}_{\delta A}(\mathbf{x}_k - \mathbf{x}_n)] = \mathbb{P}[\mathbb{I}_{\delta A}(\mathbf{x}_k - \mathbf{x}_n) = 1]$ and $\text{Var}[\mathbb{I}_{\delta A}(\mathbf{x}_k - \mathbf{x}_n)] = \mathbb{P}[\mathbb{I}_{\delta A}(\mathbf{x}_k - \mathbf{x}_n) = 1] - (\mathbb{P}[\mathbb{I}_{\delta A}(\mathbf{x}_k - \mathbf{x}_n) = 1])^2$ (Ross, 2009), we rewrite Equation (5A.14) as,

$$\begin{aligned} \text{Var}[X] &= \sum_{k=1}^M \omega_c^2(|\mathbf{x}_k - \mathbf{x}_n|) \left(\mathbb{P}[\mathbb{I}_{\delta A}(\mathbf{x}_k - \mathbf{x}_n)] - \mathbb{P}[\mathbb{I}_{\delta A}(\mathbf{x}_k - \mathbf{x}_n)]^2 \right) \\ &\quad + \sum_{\substack{i=1, j=1 \\ i \neq j}}^M \omega_c(|\mathbf{x}_i - \mathbf{x}_n|) \omega_c(|\mathbf{x}_j - \mathbf{x}_n|) \times \\ &\quad \left(\mathbb{P}[\mathbb{I}_{\delta A}(\mathbf{x}_i - \mathbf{x}_n) = 1 \cap \mathbb{I}_{\delta A}(\mathbf{x}_j - \mathbf{x}_n) = 1] - \mathbb{P}[\mathbb{I}_{\delta A}(\mathbf{x}_i - \mathbf{x}_n) = 1] \mathbb{P}[\mathbb{I}_{\delta A}(\mathbf{x}_j - \mathbf{x}_n) = 1] \right). \end{aligned} \quad (5A.15)$$

Using Equation (5A.8), we write,

$$\begin{aligned} \mathbb{P}[\mathbb{I}_{\delta A}(\mathbf{x}_i - \mathbf{x}_n) = 1 \cap \mathbb{I}_{\delta A}(\mathbf{x}_j - \mathbf{x}_n) = 1] &= \mathbb{P}[\mathbb{I}_{\delta A}(\mathbf{x}_i - \mathbf{x}_n) = 1 | \mathbb{I}_{\delta A}(\mathbf{x}_j - \mathbf{x}_n) = 1] \\ &\quad \times \mathbb{P}[\mathbb{I}_{\delta A}(\mathbf{x}_j - \mathbf{x}_n) = 1]. \end{aligned} \quad (5A.16)$$

These definitions allow us to rewrite Equation (5A.15) in terms of continuous variables by multiplying the corresponding conditional probabilities for the presence of individuals with the interaction kernels and summing over all possible displacements as,

$$\begin{aligned} \text{Var}[X] &= \int \omega_c^2(|\boldsymbol{\xi}|) \left(\frac{Z_2(\boldsymbol{\xi}, t)}{Z_1(t)} \right) d\boldsymbol{\xi} \\ &\quad + \iint \omega_c(|\boldsymbol{\xi}'|) \omega_c(|\boldsymbol{\xi}''|) \left(\frac{Z_3(\boldsymbol{\xi}', \boldsymbol{\xi}'', t)}{Z_1(t)} - \frac{Z_2(\boldsymbol{\xi}', t) Z_2(\boldsymbol{\xi}'', t)}{(Z_1(t))^2} \right) d\boldsymbol{\xi}' d\boldsymbol{\xi}''. \end{aligned} \quad (5A.17)$$

5A.6 Comparison of moment closure methods

The moment closure methods help to approximate the third-order spatial moments in terms of the first and second spatial moments. In this section, we compare the performance of popular moment closure methods. The closure methods considered are the power-1 closure (P1), the symmetric power-2 closure (P2S), the asymmetric power-2 closure (P2A) and the Kirkwood superposition approximation (KSA) (Law et al., 2003; Murrell et al., 2004).

The power-1 closure (P1) method use an approximation for the third moment, $Z_3(\boldsymbol{\xi}, \boldsymbol{\xi}', t)$, given by,

$$Z_3(\boldsymbol{\xi}, \boldsymbol{\xi}', t) = Z_1(t)Z_2(\boldsymbol{\xi}, t) + Z_1(t)Z_2(\boldsymbol{\xi}', t) + Z_1(t)Z_2(\boldsymbol{\xi}' - \boldsymbol{\xi}, t) - 2Z_1^3(t). \quad (5A.18)$$

The symmetric power-2 closure is given by,

$$Z_3(\boldsymbol{\xi}, \boldsymbol{\xi}', t) = \frac{Z_2(\boldsymbol{\xi}, t)Z_2(\boldsymbol{\xi}', t) + Z_2(\boldsymbol{\xi}, t)Z_2(\boldsymbol{\xi}' - \boldsymbol{\xi}, t) - Z_2(\boldsymbol{\xi}', t)Z_2(\boldsymbol{\xi}' - \boldsymbol{\xi}, t) - Z_1^4(t)}{2Z_1(t)}. \quad (5A.19)$$

The asymmetric power-2 closure is given by,

$$Z_3(\xi, \xi', t) = \frac{4Z_2(\xi, t)Z_2(\xi', t) + Z_2(\xi, t)Z_2(\xi' - \xi, t) - Z_2(\xi', t)Z_2(\xi' - \xi, t) - Z_1^4(t)}{5Z_1(t)}. \quad (5A.20)$$

The Kirkwood superposition approximation (KSA) is given by,

$$Z_3(\xi, \xi', t) = \frac{Z_2(\xi, t)Z_2(\xi', t)Z_2(\xi' - \xi, t)}{Z_1^3(t)}. \quad (5A.21)$$

To compare the accuracy of closure methods, we compute the solutions of the spatial moment model with each of the four closure methods and compare it with the averaged data from the IBM simulation. We calculate the density dynamics and pair-correlation function for a population with initial population size, $N(0) = 150$, and random initial arrangement of individuals. The density dynamics computed using all four closure methods, as well as from the IBM simulations for this population, are shown in Figure 5A.2(a). Our results indicate that the asymmetric power-2 closure provides the best match with the average results from the IBM. Similarly, the pair-correlation function computed using the asymmetric power-2 closure most accurately reproduces $C(|\xi|, t)$ from the IBM, as shown in Figure 5A.2(b). While our results suggest that the asymmetric power-2 closure provides the best approximation to IBM for the parameters considered, the motive of this study is not to advocate for one particular closure approximation over others. Instead, we provide a general moment dynamics model that can be implemented using different closure methods if one particular closure approximation is preferred over others.

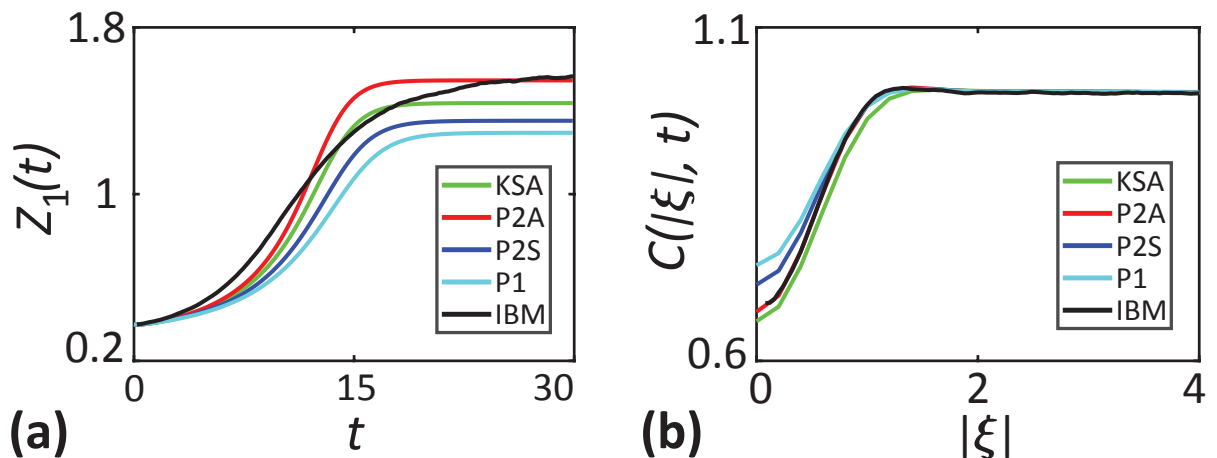


Figure 5A.2: Comparison of moment closure methods. **a** shows the density of individuals as a function of time. **b** shows the $C(|\xi|, t)$ computed at $t = 30$ as a function of separation distance. Parameter values are $\sigma_c = 0.5$, $\gamma_c = 0.448$, $\sigma_p = \sigma_d = 4.0$, $\gamma_p = 0.009$, $d = 0.4$, $p = 0.2$, $m = 0.1$, $\mu_s = 0.4$ and $\sigma_s = 0.1$.

5A.7 Numerical methods for solving the moment dynamics equation

Here we describe the numerical methods used for solving the dynamical equation for the second spatial moment, Equation (5.19). Temporal derivatives are approximated using an explicit Euler approximation implemented in MATLAB. The codes used are available on [Github](#). The numerical scheme involves spatial discretisation of the displacement, $\xi = (\xi_x, \xi_y)$, over the domain $\{-\xi_{\max} \leq \xi_x, \xi_y \leq \xi_{\max}\}$ using a constant grid spacing of $\Delta\xi$. We use a sufficiently large ξ_{\max} such that $Z_2(\xi, t) = Z_1^2(t)$ at the boundary since we anticipate that the usual mean-field condition will hold for sufficiently large displacements. We approximate the integral terms in Equations (5.17)-(5.19) using the trapezoid rule. The evaluation of these integral terms require the values of $Z_2(\xi + \xi', t)$ for all values of ξ and ξ' . A potential issue here is when both ξ and ξ' , are large, there is a possibility that $Z_2(\xi + \xi', t)$ lies outside of the computational domain. In such cases, we replace those terms with the value of $Z_2(\xi, t)$ at the boundary, $Z_2((\xi_{\max}, \xi_{\max}), t)$. The movement and dispersal kernels are normalised such that $\int \mu_m(\xi) d\xi = 1$ and $\int \mu_p(\xi) d\xi = 1$, using the trapezoid rule.

Solving for the dynamics of the second spatial moment, Equation (5.19), requires the evaluation of $Z_1(t)$. Since we consider a sufficiently large computational domain compared to the interaction ranges, the usual mean-field condition, $Z_2(\xi, t) = Z_1^2(t)$ will be valid at large displacements. Using this property, we evaluate the first moments without actually solving the Equation (5.16). At each time step, the first moment is computed using, $Z_1(t) = \sqrt{Z_2((\xi_{\max}, \xi_{\max}), t)}$. To compare the results from the spatial moment model with that of the IBM, we calculate the pair-correlation function as, $Z_2(\xi, t)/Z_1^2(t)$. We use an initial condition, $Z_2(\xi, 0) = Z_1^2(0)$. In all of our computation we use a constant time step, $dt = 0.1$, grid spacing, $\Delta\xi = 0.2$ and $\xi_{\max} = 16$. We find that these values of dt , and $\Delta\xi$ are sufficiently small to produce grid-independent results. Further, we find that choosing larger values of ξ_{\max} does not affect our results.

5A.8 Effect of short-range dispersal

Here, we investigate the effect of short-range dispersal of offspring in Figure 5A.3. For these suites of simulations, we consider long-range competition and cooperation among individuals ($\sigma_c = \sigma_p = 4.0$) so that we can describe solely the dynamics resulting from the close dispersal of offspring ($\sigma_d = 0.5$). Again we consider three cases with initial population size, $N(0) = 80, 240$ and 400 , where individuals are randomly distributed over the domain, as shown in Figure 5A.3(a)-(c). The three initial conditions considered here are the same as those considered in Figure 5.4.

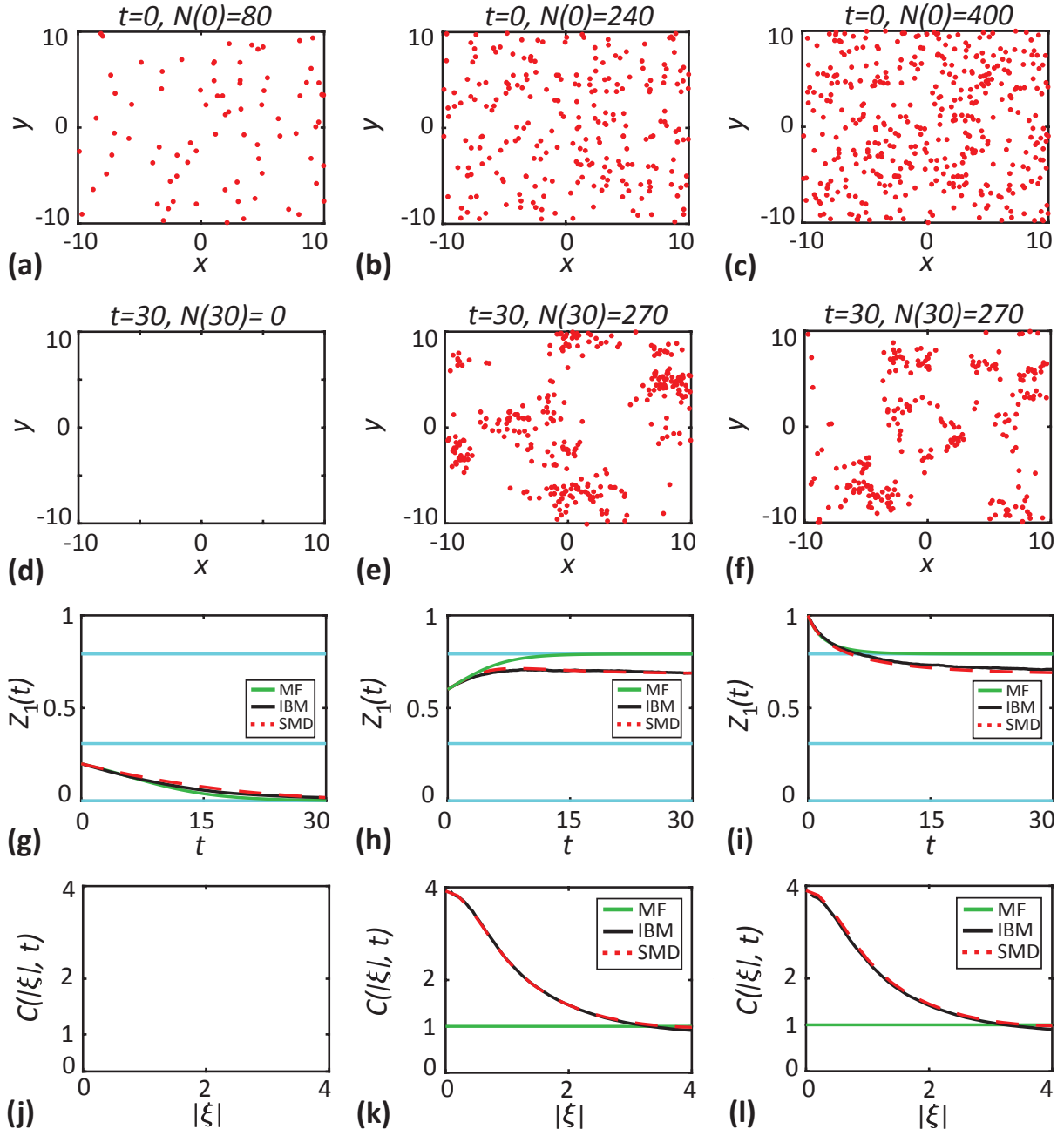


Figure 5A.3: Effect of short-range dispersal. In these set of simulations, dispersal range is lowered to $\sigma_d = 0.5$. **a-c** show the initial locations of individuals (red dots) for three different population sizes, $N(0) = 80, 240$ and 400 . **d-f** show the location of individuals at $t = 30$. **g-i** show the density of individuals as a function of time. Black solid lines correspond to the averaged results from 1000 realisations of the IBM, red dashed lines correspond to the solutions of spatial moment dynamics and green solid lines correspond to the solution of the mean-field model. The cyan lines show the critical densities. **j-l** show the $C(|\xi|, t)$ computed at $t = 30$ as a function of separation distance. Parameter values are $d = 0.4$, $p = 0.2$, $m = 0.1$, $\mu_s = 0.4$ and $\sigma_s = 0.1$.

When $Z_1(0) < \bar{Z}_1^{(2)}$, the population goes extinct since the total death rate is higher compared to the proliferation rate. For the two cases where $Z_1(0) > \bar{Z}_1^{(2)}$, the population survives, and the locations of individuals at the final time are shown in Figure 5A.3(e)-(f). As time progresses, individuals tend to be found in close groups corresponding to a clustered spatial structure. The clustering arises in the population through short-range dispersal, where offspring are placed in the close vicinity of parents. As time evolves, more and more individuals are placed in close

neighbourhoods creating a strong clustering. Since we consider long-range competition, there is no mechanism to counteract or reduce the magnitude of the cluster formation. The presence of spatial clustering in the population is further confirmed by $C(|\xi|, t) > 1$ in Figure 5A.3(k)-(l). Now the competition within these clusters enhances the net death rate. As a result, the population grows to a carrying capacity that is lower than $\bar{Z}_1^{(3)}$. The spatial moment model accurately captures cluster formation due to short-scale dispersal and the resulting reduction in the carrying capacity.

Chapter 6

Conclusions

In this chapter, we summarise our research findings and propose potential avenues for extensions of this work.

6.1 Summary of the research

In this thesis, we develop new mathematical models that incorporate short-range interactions and spatial structure of the population into the modelling framework. These models allow us to explore how short-range interactions generate macro-scale spatial structures and enable us to investigate the effect of spatial structure on the population dynamics. To consider the interactions and events occurring at the individual level, we construct an IBM. In this framework, the incorporation of localised interaction mechanisms helps us make various event rates of an individual, such as motility and proliferation rates and the direction of motion, all to depend on the extent of crowding around that individual. Another outcome of this thesis is that we derive a mathematically tractable continuum description of the IBM using spatial moments. Spatial moment models help us to capture population-level macroscopic behaviours of the population. Unlike the traditional continuum models based on the mean-field assumption, the moment dynamics models account for the presence of spatial structure by describing the dynamics of the average density of pairs of individuals.

The main objectives of this thesis were to:

1. Develop an IBM and spatial moment model of birth-death-movement processes for cells in an obstacle field by incorporating the realistic effects of short-range interactions, crowding effects and spatial structure.
2. Extend the modelling frameworks developed in objective 1 to consider chase-escape interactions observed in ecology and cell biology processes.
3. Develop an IBM that incorporates predator-prey dynamics and compare the simulation results to the classical mean-field model's solutions to gain insight into scenarios where

mean-field approximation fails.

4. Develop an IBM and spatial moment model that incorporate the Allee effect and compare the results to the classical mean-field model's solutions to gain insight into how spatial structure impacts the Allee kinetics.

We successfully address these objectives in the four journal publications presented in Chapters 2-5 of this thesis. Now we provide a summary of the research outcomes here.

In Chapter 2, we construct an IBM describing birth-death-movement processes of cells among a population of stationary and non-proliferative biological obstacles. The localised interactions in between individual cells and between cells and obstacles are accommodated in the modelling framework by defining interaction kernels. The incorporation of interactions between individuals through the interaction kernels also helps in modelling crowding effects such as contact inhibition of proliferation, where the proliferation rate of an individual decreases when it is in a crowded region. A continuum approximation of the stochastic dynamics arising out of IBM is derived using the spatial moment framework. Our modelling framework allows us to explore how different properties of obstacles such as density, size and interaction strength influence the dynamics and emergence of spatial structure in the population. We see the development of interesting spatial patterns through our exploration as we vary the properties of obstacles. For example, our results show that the long time steady arrangement of cells is segregated if the obstacle density is sufficiently low. In contrast, when the obstacle density is large enough, we observe a clustered spatial structure of cells. Overall we see that the details of the dynamics and the spatial structure of the population predicted using many identically prepared realisations of the IBM is reasonably well approximated by the solution of the spatial moment model.

In Chapter 3 we explore how the directional movement of individuals arising out of chase-escape interactions leads to the development of the spatial structure. The most striking feature of this analysis is that we find spatial structure formation driven purely by motility. Our study is particularly interesting because most spatial moment models that have their origin in plant ecology assume the birth and death mechanisms play the critical role in generating the spatial structure rather than motility (Bolker and Pacala, 1997; Bolker and Pacala, 1999; Law and Dieckmann, 2000; Law et al., 2003). Some of the recent moment dynamics models that mimic cell biology experiments consider simultaneous movement and proliferation. These models attribute spatial structure formation to the combined effects of motility and proliferation (Binny et al., 2016b; Browning et al., 2018). In Chapter 3, we present the first study that applies spatial moment analysis to a conservative community, composed of multiple distinct populations, without birth or death events.

The IBM and spatial moment dynamics models developed in Chapter 3 is particularly relevant for considering asymmetric interactions between distinct populations within a community. For example, these models allow the interaction of chasers to the escapees to be attractive,

while escapees to the chasers to be repulsive. We explore a range of complex spatial structures arising from the combined impacts of various intraspecies and interspecies interactions, which involve different types of attractive or repulsive bias between individuals in a two-species community. We study the important features of the interactions by systematically varying the interaction strength, the spatial extent of interaction and relative densities of individuals. Our investigation reveals several interesting and possibly counter-intuitive results. For example, under self-repulsion of escapees and chase-escape behaviour, the increase in density of chasers relative to escapees results in weakening of segregation between chasers and enhancement of segregation among escapees.

In Chapter 4, we explore the impact of short-range interactions and spatial structure on predator-prey dynamics. In this chapter, we construct an IBM describing the dynamics of a community of consumers and resources by incorporating short-range interaction mechanisms such as short-range predation, competition and dispersal of offsprings. The IBM simulation results are compared with solutions of a mean-field model constructed by invoking the mean-field approximation. Our analysis reveals various situations in which the IBM suggests qualitatively different outcomes compared to the solution of the mean-field model and emphasise the importance of considering the role of spatial structure in community dynamics. By comparing the IBM and mean-field model solutions, we find that the mechanisms leading to intraspecific clustering and interspecific segregation, such as short-range predation and short-range dispersal, tend to increase the size of the resource relative to the mean-field prediction. Our results also indicate that under specific parameter regimes, these mechanisms lead to the extinction of consumers, whereas the classical mean-field model predicts the coexistence. In the mathematical biology literature, the mean-field models are regularly invoked for exploring different characteristics of predator-prey interactions. For instance, the mean-field models are used in the prediction of coexistence versus extinct or in the prediction of stable versus oscillatory dynamics in predator-prey systems (Kuperman et al., 2019). Our results suggest that the predictions of the mean-field models in these scenarios could be inaccurate if the communities in question exhibit significant spatial structure.

In Chapter 5, we explore the impact of short-range interactions and spatial structure on Allee dynamics. We construct an IBM and spatial moment model that considers short-range competition, short-range cooperation, and short-range dispersal and incorporates a strong Allee effect. Similar to what we have done in Chapter 4, we compare the results of these new models with the corresponding mean-field model solutions with a focus on examining how the spatial structure influences the Allee threshold density. Our investigation reveals some interesting scenarios where spatial structure impacts the Allee dynamics. For instance, under the influence of short-range dispersal and short-range competition, the population found to go extinct, even though the classical mean-field model predicts the survival of the population for any initial density above the critical Allee threshold. Overall, we find that the Allee threshold can be very sensitive to the presence of spatial structure to the point that classical mean-field predic-

tions are invalid. Again, the results in this chapter confirm that the spatial moment dynamics framework can be a suitable method to replicate the population-level outcomes of the IBM. While the mean-field prediction disagrees with the IBM simulation results, the spatial moment model accurately captures how the Allee threshold depends upon the spatial structure of the population.

6.2 Future work

While the modelling framework presented in this thesis is relatively general and considers various scenarios where spatial structure plays a crucial role in determining the dynamics, there are many ways that it could be extended. We now discuss these potential extensions.

6.2.1 Non-homogeneous models

In all of the cases considered in this thesis, we presented our models in a spatially homogeneous environment with randomly distributed initial arrangement of individuals. While these considerations allow us to study the formation of spatial structure and its impact on population dynamics, a generalisation to non-homogeneous environments would broaden potential applications. Non-homogeneous models would be of particular interest in the case of certain cell biology experiments, such as *scratch assays* (Liang et al., 2007), as shown in Figure 6.1, that are initiated by considering an initial density of cells that varies spatially.

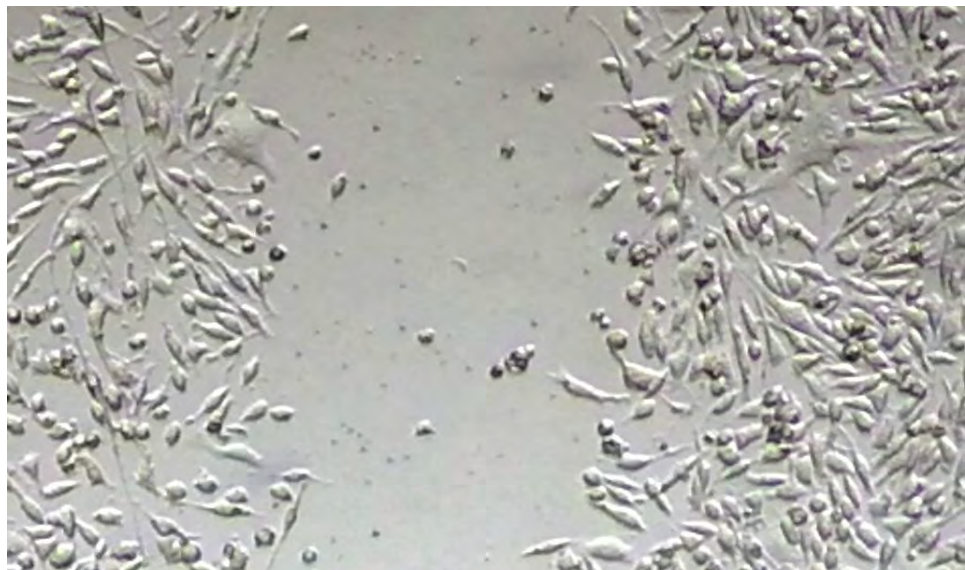


Figure 6.1: An image showing the scratch assay of Rhabdomyosarcoma cancer cells (image by Dhifaf Zeki reprinted from Wikipedia under CC BY-SA).

Also, such extensions are required to consider spatial processes such as moving fronts that are relevant to many biological processes, including malignant invasion and developmental

morphogenesis (Smith and Yates, 2018). The extension of IBM to a non-homogeneous setting would be relatively straightforward. On the other hand, numerical computation of spatial moments as a function of locations in space rather than as a function of separation displacement can be computationally challenging. There have been some recent attempts at deriving and numerically solving the spatial moment dynamics in a non-homogeneous setting (Omelyan and Kozitsky, 2019). But these models consider relatively simple birth-death models in one-dimensional space.

6.2.2 Three-dimensional models

In this thesis, we consider the movement of individuals in a two-dimensional (2D) spatial domain. The 2D models are suitable for modelling ecological systems where typical locations of individuals are confined to 2D spaces and for many of the 2D cell biology experimental assays. However, realistic modelling of *in vivo* cell migration and *in vitro* experiments that involve movement of cells through 3D scaffolds (Wolf et al., 2009; Herrmann et al., 2014), such as shown in Figure 6.2, requires consideration of three-dimensional (3D) space. While the extension of the IBM framework and moment dynamics analysis to 3D is relatively straightforward, the numerical evaluation of moment dynamics in 3D can become increasingly complicated.

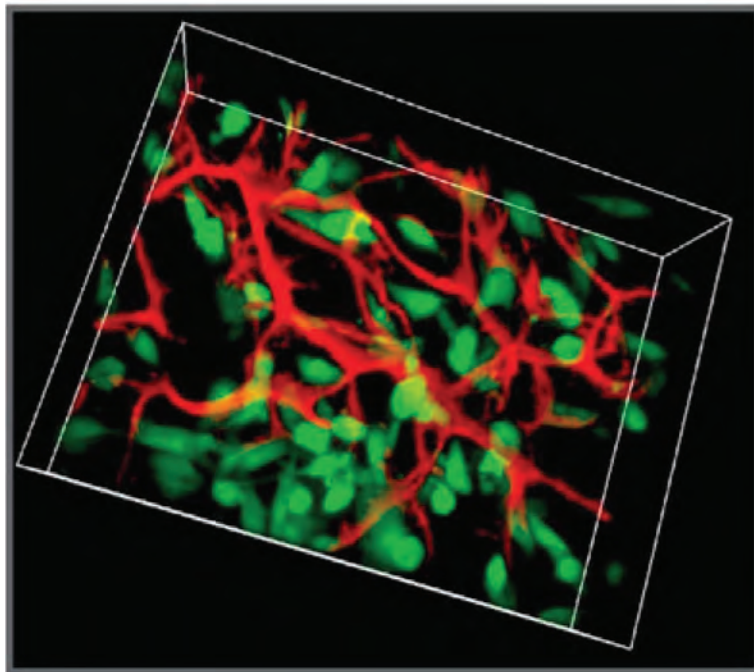


Figure 6.2: An image showing the movement of fibroblasts cells (green) through a three-dimensional highly porous collagen-glycosaminoglycan scaffold. (reprinted from Harley et al., 2008, with permission from Elsevier).

6.2.3 Incorporation of experimental data and parameter estimation

The main focus of this thesis is on the development of stochastic and continuum models with application in ecologically and biologically relevant scenarios. In each of the applications con-

sidered, we varied various parameters such as different interaction ranges, over a range of values and studied how this led to the generation of spatial structure and how that, in turn, influences the population dynamics. While considering simulations over a range of parameter space and elucidating the emergence of spatial structure is an important first step, the incorporation of experimental data to validate the model predictions as well as for parameter estimation is an interesting avenue for future research. An interesting extension here would be to work out how to best design cell biology and ecology experiments that can get at the precise parameter values that are critical to this modelling approach.

6.2.4 Higher order moment closure methods

The moment closure method is an important factor that influences the accuracy of the moment dynamics model solutions. For all the cases considered in this thesis, we close the hierarchy of moment dynamics equations at second order by approximating the third-order moments in terms of first and second moments. While this second-order closure provides a reasonable approximation of the IBM, higher-order moments may retain some information about the spatial structure of the population. The consideration of the dynamics of higher-order moments may provide a better approximation to the simulation results of IBM.

6.2.5 Multi-species model of Allee effects

When we explore the impact of spatial structure on the Allee dynamics in Chapter 5, we restrict our exploration to populations where all individuals are of the same type. An interesting extension of the model would be to consider a multi-species case where the total population consists of individuals from various distinct species. The consideration of the Allee effect for multiple species might be particularly useful for analysing the role of the Allee effect in predator-prey systems.

6.2.6 Impact of directional bias on predator-prey dynamics and Allee kinetics

While developing the models for studying the effect of spatial structure on predator-prey dynamics in Chapter 4 and on Allee kinetics in Chapter 5, we make a simplifying assumption that motility rate and direction of movement are independent of the local density. This feature could be refined by considering the effects of neighbour-dependent directional bias on the movement of individuals, which we incorporated in models presented in Chapters 2-3. Incorporating these types of directional bias on movement may further influence the community dynamics beyond the effects explored in those respective chapters.

6.2.7 Eco-evolutionary dynamics

It has been recently shown that an emergent population spatial structure, together with evolution acting on the range of a prey-predator interaction, may influence coexistence times in prey-predator communities (Colombo et al., 2019). An interesting extension of the spatial predator-prey model developed in Chapter 4 would be to consider the effect of evolution and examine how the population dynamics predicted by our model differ in the presence of evolution.

6.3 Final remarks

In this thesis, we have explored the importance of considering the effect of short-range interactions and spatial structure while developing mathematical models of population dynamics. Through different examples from ecology and cell biology, we demonstrate that the classical mean-field model solutions could be erroneous under various scenarios where short-range interaction between individuals play a significant role in the population dynamics. Typically, mathematical models of ecological and cell biology processes are employed to make useful predictions on the system's possible state over a period of time. For instance, in conservation ecology, an important question can be how many individuals of an endangered species survive over a specific time span considering various predatory and other interactions they face in the ecosystem. For these types of applications, the accurate modelling of the population dynamics is of paramount importance. The IBM and the spatial moment dynamics framework developed in this thesis can be of great help to accurately model many of these realistic scenarios in ecology and cell biology.

Bibliography

- [1] Abercrombie M. 1979 Contact inhibition and malignancy. *Nature* 281: 259–262.
- [2] Abrams PA. 2000 The evolution of predator-prey interactions: theory and evidence. *Annual Review of Ecology and Systematics* 31: 79–105.
- [3] Abrams PA, Ginzburg LR. 2000 The nature of predation: prey dependent, ratio dependent or neither? *Trends in Ecology and Evolution* 15: 337–341.
- [4] Agnew DJG, Green JEF, Brown TM, Simpson MJ, Binder BJ. 2014 Distinguishing between mechanisms of cell aggregation using pair-correlation functions. *Journal of Theoretical Biology* 352: 16–23.
- [5] Akira S, Uematsu S, Takeuchi O. 2006 Pathogen recognition and innate immunity. *Cell* 124: 783–801.
- [6] Allee WC, Bowen ES. 1932 Studies in animal aggregations: mass protection against colloidal silver among goldfishes. *Journal of Experimental Zoology* 61: 185–207.
- [7] Bajenoff M, Egen JG, Koo LY, Laugier JP, Brau F, Glaichenhaus N, Germain RN. 2006 Stromal cell networks regulate lymphocyte entry, migration, and territoriality in lymph nodes. *Immunity* 25: 989–1001.
- [8] Baker RE, Simpson MJ. 2010 Correcting mean-field approximations for birth-death-movement processes. *Physical Review E* 82: 041905.
- [9] Baker RE, Parker A, Simpson MJ. 2019 A free boundary model of epithelial dynamics. *Journal of Theoretical Biology* 481: 61–74.
- [10] Barbaric I, Biga V, Gokhale PJ, Jones M, Stavish D, Glen A, Coca D, Andrews PW. 2014 Time-lapse analysis of human embryonic stem cells reveals multiple bottlenecks restricting colony formation and their relief upon culture adaptation. *Stem Cell Reports* 3: 142–155.
- [11] Barbosa P, Castellanos I. 2005 Ecology of predator-prey interactions. Oxford University Press.

- [12] Barraquand F, Murrell DJ. 2012 Intense or spatially heterogeneous predation can select against prey dispersal. *PLoS One* 7: e28924
- [13] Barraquand F, Murrell DJ. 2013 Scaling up predator-prey dynamics using spatial moment equations. *Methods in Ecology and Evolution* 4: 276–289.
- [14] Bazazi S, Buhl J, Hale JJ, Anstey ML, Sword GA, Simpson SJ, Couzin ID. 2008 Collective motion and cannibalism in locust migratory bands. *Current Biology* 18: 735-739.
- [15] Binder BJ, Simpson MJ. 2013 Quantifying spatial structure in experimental observations and agent-based simulations using pair-correlation functions. *Physical Review E* 88: 022705.
- [16] Binder BJ, Simpson MJ (2015) Spectral analysis of pair-correlation bandwidth: application to cell biooogy images. *Royal Society Open Science* 2: 140494.
- [17] Binny RN, Haridas P, James A, Law R, Simpson MJ, Plank MJ. 2016a Spatial structure arising from neighbour-dependent bias in collective cell movement. *PeerJ* 4: e1689.
- [18] Binny RN, James A, Plank MJ. 2016b Collective cell behaviour with neighbour-dependent proliferation, death and directional bias. *Bulletin of Mathematical Biology* 78: 2277–2301.
- [19] Binny RN, Law R, Plank MJ. 2020 Living in groups: Spatial-moment dynamics with neighbour-biased movements. *Ecological Modelling* 415: 108825.
- [20] Binny RN, Plank MJ, James A. 2015 Spatial moment dynamics for collective cell movement incorporating a neighbour-dependent directional bias. *Journal of the Royal Society Interface* 12: 20150228.
- [21] Bolker B, Pacala SW. 1997 Using moment equations to understand stochastically driven spatial pattern formation in ecological systems. *Theoretical Population Biology* 52: 179–197.
- [22] Bolker BM, Pacala SW. 1999 Spatial moment equations for plant competition: understanding spatial strategies and the advantages of short dispersal. *The American Naturalist* 153: 575–602.
- [23] Brigatti E, Oliva M, Nunez-Lopez M, Oliveros-Ramos R, Benavides J. 2009 Pattern formation in a predator-prey system characterized by a spatial scale of interaction. *Europhysics Letters* 88: 68002.
- [24] Britton N. 2003 *Essential mathematical biology*. Springer, London.

- [25] Browning AP, McCue SW, Binny RN, Plank MJ, Shah ET, Simpson MJ. 2018 Inferring parameters for a lattice-free model of cell migration and proliferation using experimental data. *Journal of Theoretical Biology* 437: 251–260.
- [26] Browning AP, Jin W, Plank MJ, Simpson MJ. 2020 Identifying density-dependent interactions in collective cell behaviour. *Journal of the Royal Society Interface* 17: 20200143.
- [27] Bruna M, Chapman SJ. 2012a Excluded-volume effects in the diffusion of hard spheres. *Physical Review E* 85: 011103.
- [28] Bruna M, Chapman SJ. 2012b Diffusion of multiple species with excluded-volume effects. *Journal of Chemical Physics* 137: 204116.
- [29] Bruna M, Chapman SJ, Robinson M. 2017 Diffusion of particles with short-range interactions. *SIAM Journal on Applied Mathematics* 77: 2294–2316.
- [30] Cai AQ, Landman KA, Hughes BD. 2006 Modelling directional guidance and motility regulation in cell migration. *Bulletin of Mathematical Biology* 68: 25–52.
- [31] Cai AQ, Landman KA, Hughes BD. 2007 Multi-scale modeling of a wound-healing cell migration assay. *Journal of Theoretical Biology* 245: 576–594.
- [32] Cantrell RS, Cosner C. 2004 Deriving reaction–diffusion models in ecology from interacting particle systems. *Journal of Mathematical Biology* 48: 187–217.
- [33] Chaplain MAJ, Lorenzi T, Macfarlane FR. 2020 Bridging the gap between individual-based and continuum models of growing cell populations. *Journal of Mathematical Biology* 80: 343–371.
- [34] Colombo EH, Martínez-García R, López C, Hernández-García E. 2019 Spatial eco-evolutionary feedbacks mediate coexistence in prey-predator systems. *Scientific Reports* 9: 18161.
- [35] Condeelis J, Segail JE. 2003 Intravital imaging of cell movement in tumours. *Nature Reviews Cancer* 3: 921–930.
- [36] Courchamp F, Berec L, Gascoigne J. 2008 *Allee effects in ecology and conservation*. Oxford University Press.
- [37] Courchamp F, Clutton-Brock TH, Grenfell BT. 1999 Inverse density dependence and the Allee effect. *Trends in Ecology and Evolution* 14: 405–410.
- [38] Courchamp F, Grenfell BT, Clutton-Brock TH. 1999 Population dynamics of obligate cooperators. *Proceedings of the Royal Society of London Series B Biological Sciences* 266: 557–563.

- [39] Cuddington KM, Yodzis P. 2000 Diffusion-limited predator-prey dynamics in euclidean environments: An allometric individual-based model. *Theoretical Population Biology* 58: 259–278.
- [40] Delcourt J, Bode NWF, Denoel M. 2016 Collective vortex behaviors: Diversity, proximate, and ultimate causes of circular animal group movements. *The Quarterly Review of Biology* 91: 1–24.
- [41] Delfau J, Ollivier H, and López C, Blasius B, Hernández-García E. 2016 Pattern formation with repulsive soft-core interactions: Discrete particle dynamics and Dean-Kawasaki equation. *Physical Review E* 94: 042120.
- [42] Dini S, Binder BJ, Green JEF. 2018 Understanding interactions between populations: Individual based modelling and quantification using pair correlation functions. *Journal of Theoretical Biology* 439: 50–64.
- [43] Dittmann L, Schausberger P. 2017 Adaptive aggregation by spider mites under predation risk. *Scientific Reports* 7: 10609.
- [44] Dobramysl U, Tauber UC. 2013 Environmental versus demographic variability in two-species predator-prey models. *Physical Review Letters* 110: 048105.
- [45] Dyson L, Baker RE. 2015 The importance of volume exclusion in modelling cellular migration. *Journal of Mathematical Biology* 71: 691–711.
- [46] Edelstein-Keshet L. 2005 *Mathematical models in biology*. Society for Industrial and Applied Mathematics, New York.
- [47] Ellery AJ, Simpson MJ, McCue SW, Baker RE. 2014 Characterising transport through a crowded environment with different obstacle sizes. *The Journal of Chemical Physics* 140: 054108.
- [48] Ellery AJ, Baker RE, McCue SW, Simpson MJ. 2016 Modelling transport through an environment crowded by a mixture of obstacles of different shapes and sizes. *Physica A: Statistical Mechanics and its Applications* 449: 74–84.
- [49] Fadai NT, Johnston ST, Simpson MJ. 2020 Unpacking the Allee effect: determining individual-level mechanisms that drive population dynamics. *Proceedings of the Royal Society A: Mathematical, Physical and Engineering Sciences* 476: 20200350.
- [50] Fadai NT, Simpson MJ. 2020 Population dynamics with threshold effects give rise to a diverse family of Allee effects. *Bulletin of Mathematical Biology* 82: 74.
- [51] Finkelshtein D, Kondratiev Y, Kutoviy O. 2009 Individual based model with competition in spatial ecology. *SIAM Journal on Mathematical Analysis* 41: 297–317

- [52] Frasca M, Sharkey KJ. 2016 Discrete-time moment closure models for epidemic spreading in populations of interacting individuals. *Journal of Theoretical Biology* 399: 13–21.
- [53] Friedl P, Wolf K. 2003 Tumour-cell invasion and migration: diversity and escape mechanisms. *Nature Reviews Cancer* 3: 362–374.
- [54] Galetti M, Moleon M, Jordano P, Pires MM, Guimaraes PR Jr, Pape T, Nichols E, Hansen D, Olesen JM, Munk M, de Mattos JS, Schweiger AH, Owen-Smith N, Johnson CN, Marquis RJ, Svenning JC. 2018 Ecological and evolutionary legacy of megafauna extinctions. *Biological Reviews* 93: 845–862.
- [55] Gavagnin E, Yates CA. 2018 *Handbook of statistics: integrated population biology and modelling* Elsevier.
- [56] Gerum R, Richter S, Fabry B, Bohec CL, Bonadonna F, Nesterova A, Zitterbart DP 2018 Structural organisation and dynamics in king penguin colonies. *Journal of Physics D: Applied Physics* 51: 164004.
- [57] Ghosh SK, Cherstvy AG, Grebenkov DS, Metzler R. 2016 Anomalous, non-Gaussian tracer diffusion in crowded two-dimensional environments. *New Journal of Physics* 18: 013027.
- [58] Gillespie DT. 1977 Exact stochastic simulation of coupled chemical reactions. *The Journal of Physical Chemistry* 81: 2340–2361.
- [59] Green JEF, Waters SL, Whiteley JP, Edelstein-Keshet L, Shakesheff KM, Byrne HM. 2010 Non-local models for the formation of hepatocyte–stellate cell aggregates. *Journal of Theoretical Biology* 267: 106–120.
- [60] Grimm V, Berger U, Bastiansen F, Eliassen S, Ginot V, Giske J, Goss-Custard J, Grand T, Heinz SK, Huse G, Huth A, Jepsen JU, Jorgensen C, Mooij WM, Muller B, Peer G, Piou C, Railsback SF, Robbins AM, Robbins MM, Rossmanith E, Ruger N, Strand E, Souissi S, Stillman RA, Vabo R, Visser U, DeAngelis DL. 2006 A standard protocol for describing individual-based and agent-based models. *Ecological Modelling* 198: 115–126.
- [61] Groom MJ. 1998 Allee effects limit population viability of an annual plant. *The American Naturalist* 151: 487–496.
- [62] Grunbaum D (2012) The logic of ecological patchiness. *Interface Focus* 2: 150–155.
- [63] Guttal V, Romanczuk P, Simpson SJ, Sword GA, Couzin ID. 2015 Cannibalism can drive the evolution of behavioural phase polyphenism in locusts. *Ecology Letters* 15: 1158–1166.

- [64] Hansen MM, Meijer LH, Spruijt E, Maas RJ, Rosquelles MV, Groen J, Heus HA, Huck WT. 2016 Macromolecular crowding creates heterogeneous environments of gene expression in picolitre droplets. *Nature Nanotechnology* 11: 191–197.
- [65] Harley BA, Kim HD, Zaman MH, Yannas IV, Lauffenburger DA, Gibson LJ. 2008 Microarchitecture of three-dimensional scaffolds influences cell migration behaviour via junction interactions. *Biophysical Journal* 95: 4013–4024.
- [66] Herrmann D, Conway JRW, Vennin C, Magenau A, Hughes WE, Morton JP, Timpson P. 2014 Three-dimensional cancer models mimic cell–matrix interactions in the tumour microenvironment. *Carcinogenesis* 35: 1671–1679.
- [67] Hillen T, Painter KJ. 2009 A user’s guide to PDE models for chemotaxis. *Journal of Mathematical Biology* 58: 183–217.
- [68] Hosseini PR. 2003 How localized consumption stabilizes predator-prey systems with finite frequency of mixing. *The American Naturalist* 161: 567–585.
- [69] Hosseini PR. 2006 Pattern formation and individual-based models: The importance of understanding individual-based movement. *Ecological Modelling* 194: 357–371.
- [70] Hu K, Ji L, Applegate KT, Danuser G, Waterman-Storer CM. 2007 Differential transmission of actin motion within focal adhesions. *Science* 315: 111–115.
- [71] Hunt VM, Brown JS. 2018 Coexistence and displacement in consumer-resource systems with local and shared resources. *Theoretical Ecology* 11: 83–93.
- [72] Ilina O, Friedl P. 2009 Mechanisms of collective cell migration at a glance. *Journal of Cell Science* 122: 3203–3208.
- [73] Inaba M, Yamanaka H, Kondo S. 2012 Pigment pattern formation by contact-dependent depolarization. *Science* 335: 677.
- [74] Janosov M, Virág C, Vásárhelyi G, Vicsek T. 2017 Group chasing tactics: how to catch a faster prey. *New Journal of Physics* 19: 053003.
- [75] Jin W, McCue SW, Simpson MJ. 2018 Extended logistic growth models for heterogeneous populations. *Journal of Theoretical Biology* 445: 51–61.
- [76] Johnston ST, Shah ET, Chopin LK, McElwain DLS, Simpson MJ. 2015 Estimating cell diffusivity and cell proliferation rate by interpreting IncuCyte ZOOMTM assay data using the Fisher-Kolmogorov model. *BMC Systems Biology* 9: 38.
- [77] Johnston ST, Baker RE, McElwain DLS, Simpson MJ. 2017 Co-operation, competition and crowding: A discrete framework linking Allee kinetics, nonlinear diffusion, shocks and sharp-fronted travelling waves. *Scientific Reports* 7: 42134.

- [78] Johnston ST, Ross JV, Binder BJ, McElwain DLS, Haridas P, Simpson MJ. 2016 Quantifying the effect of experimental design choices for in vitro scratch assays. *Journal of Theoretical Biology* 400: 19–31.
- [79] Johnston ST, Simpson MJ, Crampin EJ. 2020 Predicting population extinction in lattice-based birth-death-movement models. *Proceedings of the Royal Society A: Mathematical, Physical and Engineering Sciences* 476: 20200089.
- [80] Kay J, Chu M, Sanes J. 2012 MEGF10 and MEGF11 mediate homotypic interactions required for mosaic spacing of retinal neurons. *Nature* 483: 465–469.
- [81] Keeley PW, Zhou C, Lu L, Williams RW, Melmed S, Reese BE. 2014 Pituitary tumor-transforming gene 1 regulates the patterning of retinal mosaics. *Proceedings of the National Academy of Sciences of the United States of America* 111: 9295–9300.
- [82] Keller EF, Segel LA. 1971 Model for chemotaxis. *Journal of Theoretical Biology* 30: 225–234.
- [83] Khalil N, Lopez C, Hernandez-Garcia E. 2017 Nonlocal birth-death competitive dynamics with volume exclusion. *Journal of Statistical Mechanics: Theory and Experiment* 2017: 063505.
- [84] Kim N, Koh E, Chen X, Gumbiner BM. 2011 E-cadherin mediates contact inhibition of proliferation through Hippo signaling-pathway components. *Proceedings of the National Academy of Sciences of the United States of America* 108: 11930–11935.
- [85] King AJ, Wilson AM, Wilshin SD, Lowe J, Haddadi H, Hailes S, Morton AJ. 2012 Selfish-herd behaviour of sheep under threat. *Current Biology* 22: R561-R562.
- [86] Korolev KS, Xavier JB, Gore J. 2014 Turning ecology and evolution against cancer. *Nature Reviews Cancer* 14: 371–380.
- [87] Kot M. 2003 *Elements of Mathematical ecology*. Cambridge University Press, Cambridge.
- [88] Kuperman MN, Laguna MF, Abramson G, Monjeau JA. 2019 Meta-population oscillations from satiation of predators. *Physica A: Statistical Mechanics and its Applications* 527: 121288.
- [89] Kurosaka S, Kashina A. 2008 Cell biology of embryonic migration. *Birth Defects Research Part C - Embryo Today* 84: 102–122.
- [90] Kuussaari M, Saccheri I, Camara M, Hanski I. 1998 Allee effect and population dynamics in the Glanville fritillary butterfly. *Oikos* 82: 384–392.

- [91] Lamont BB, Klinkhamer PGL, Witkowski ETF. 1993 Population fragmentation may reduce fertility to zero in *Banksia goodii* - a demonstration of the Allee effect. *Oecologia* 94: 446–450.
- [92] Law R, Dieckmann U. 2000 A dynamical system for neighbourhoods in plant communities. *Ecology* 81: 2137–2148.
- [93] Law R, Illian J, Burslem DFRP, Gratzer G, Gunatilleke CVS, Gunatilleke IAUN. 2009 Ecological information from spatial patterns of plants: insights from point process theory. *Journal of Ecology* 97: 616–628.
- [94] Law R, Murrell DJ, Dieckmann U. 2003 Population growth in space and time: spatial logistic equations. *Ecology* 84: 252–262.
- [95] Le Clainche C, Carlier M. 2008 Regulation of actin assembly associated with protrusion and adhesion in cell migration. *Physiological Reviews* 88: 489–513.
- [96] Lewis MA. 2000 Spread rate for a nonlinear stochastic invasion. *Journal of Mathematical Biology* 41: 430–454.
- [97] Lewis MA, Kareiva P. 1993 Allee dynamics and the spread of invading organisms. *Theoretical Population Biology* 43: 141–158.
- [98] Liang C, Park A, Guan J. 2007 In vitro scratch assay: a convenient and inexpensive method for analysis of cell migration in vitro. *Nature Protocols* 2: 329–333.
- [99] Lin Z, Wu C, Ho C. 2018 Warming neutralizes host-specific competitive advantages between a native and invasive herbivore. *Scientific Reports* 8: 11130.
- [100] Liu Q, Doelman A, Rottschäfer V, Jager M, Herman P, Rietkerk M, van de Koppel J. 2013 Phase separation explains a new class of self-organized spatial patterns in ecological systems. *Proceedings of the National Academy of Sciences of the United States of America* 110: 11905–11910.
- [101] Liu Q, Rietkerk M, Herman PM, Piersma T, Fryxell JM, van de Koppel J. 2016 Phase separation driven by density-dependent movement: A novel mechanism for ecological patterns. *Physics of Life Reviews* 19:107–121.
- [102] Lutscher F, Iljon T. 2013 Competition, facilitation and the Allee effect. *Oikos* 122: 621–631.
- [103] Macfarlane FR, Chaplain MAJ, Lorenzi T. 2019 A stochastic individual-based model to explore the role of spatial interactions and antigen recognition in the immune response against solid tumours. *Journal of Theoretical Biology* 480: 43–55.

- [104] Maciel GA, Lutscher F. 2015 Allee effects and population spread in patchy landscapes. *Journal of Biological Dynamics* 9: 109–123.
- [105] Markham DC, Simpson MJ, Maini PK, Gaffney EA, Baker RE. 2013 Incorporating spatial correlations into multispecies mean-field models. *Physical Review E* 88: 052713.
- [106] Martin P. 1997 Wound healing—aiming for perfect skin regeneration. *Science* 276: 75–81.
- [107] Martinez-Garcia R, Fleming CH, Seppelt R, Fagan WF, Calabrese JM. 2020 How range residency and long-range perception change encounter rates. *Journal of Theoretical Biology* 498: 110267.
- [108] Martinez-Garcia R, Murgui C, Hernandez-Garcia E, Lopez C. 2015 Pattern formation in populations with density-dependent movement and two interaction scales. *PLoS One* 10: e0132261.
- [109] Mathworks. 2019 [Solve nonstiff differential equations — medium order method](#). Accessed December 2019
- [110] Middleton AM, Fleck C, Grima R. 2014 A continuum approximation to an off-lattice individual-cell based model of cell migration and adhesion. *Journal of Theoretical Biology* 359: 220–232.
- [111] Mobilia M, Georgiev IT, Tauber UC. 2006 Fluctuations and correlations in lattice models for predator-prey interaction. *Physical Review E* 73: 040903(R).
- [112] Mobilia M, Georgiev IT, Tauber UC. 2007 Phase transitions and spatio-temporal fluctuations in stochastic lattice Lotka–Volterra models. *Journal of Statistical Physics* 128: 447–483.
- [113] Morozov A, Petrovskii S, Li BL. 2004 Bifurcations and chaos in a predator–prey system with the Allee effect. *Proceedings of the Royal Society of London Series B Biological Sciences* 271: 1407–1414.
- [114] Murray JD. 1989 *Mathematical biology*. Springer, New York.
- [115] Murrell DJ, Law R. 2000 Beetles in fragmented woodlands: a formal framework for dynamics of movement in ecological landscapes. *Journal of Animal Ecology* 69: 471–483.
- [116] Murrell DJ, Law R. 2003 Heteromyopia and the spatial coexistence of similar competitors. *Ecology Letters* 6: 48–59.
- [117] Murrell DJ, Dieckmann U, Law R. 2004 On moment closures for population dynamics in continuous space. *Journal of Theoretical Biology* 229: 421–432.

- [118] Murrell DJ. 2005 Local spatial structure and predator-prey dynamics: counterintuitive effects of prey enrichment. *The American Naturalist* 166: 354–367.
- [119] Murrell DJ. 2009 On the emergent spatial structure of size-structured populations: when does self-thinning lead to a reduction in clustering? *Journal of Ecology* 97: 256–266.
- [120] Musgrave J, Girard A, Lutscher F. 2015 Population spread in patchy landscapes under a strong Allee effect *Theoretical Ecology* 8: 313–326.
- [121] Neufeld Z, von Witt W, Lakatos D, Wang J, Hegedus B, Czirok A. 2017 The role of Allee effect in modelling post resection recurrence of glioblastoma. *PLoS Computational Biology* 13: e1005818.
- [122] North A, Ovaskainen O. 2007 Interactions between dispersal, competition, and landscape heterogeneity. *Oikos* 116: 1106–1119.
- [123] North A, Cornell SJ, Ovaskainen O. 2011 Evolutionary responses of dispersal distance to landscape structure and habitat loss. *Evolution* 65: 1739–1751.
- [124] Oliveira S, Rosowski EE, Huttenlocher A. 2016 Neutrophil migration in infection and wound repair: going forward in reverse. *Nature Reviews Immunology* 16: 378–391.
- [125] Omelyan I. 2020 Spatial population dynamics: Beyond the Kirkwood superposition approximation by advancing to the Fisher–Kopeliovich ansatz. *Physica A: Statistical Mechanics and its Applications* 544: 123546.
- [126] Omelyan I, Kozitsky Y. 2020 Spatially inhomogeneous population dynamics: beyond the mean field approximation. *Journal of Physics A: Mathematical and Theoretical* 52: 305601.
- [127] Oshanin G, Vasilyev O, Krapivsky PL, Klafter J. 2009 Survival of an evasive prey. *Proceedings of the National Academy of Sciences of the United States of America* 106: 13696–13701.
- [128] Ovaskainen O, Cornell SJ. 2006 Asymptotically exact analysis of stochastic metapopulation dynamics with explicit spatial structure. *Theoretical Population Biology* 69: 13–33.
- [129] Ovaskainen O, Finkelshtein D, Kutoviy O, Cornell SJ, Bolker B, Kondratiev Y. 2014 A general mathematical framework for the analysis of spatiotemporal point processes. *Theoretical Ecology* 7: 101–113.
- [130] Pavel M, Renna M, Park SJ, Menzies FM, Ricketts T, Füllgrabe J, Ashkenazi A, Frake RA, Lombarte AC, Bento CF, Franze K, Rubinsztein DC. 2018 Contact inhibition controls cell survival and proliferation via YAP/TAZ-autophagy axis. *Nature Communications* 9: 2961.

- [131] Penczykowski RM, Laine A, Koskella B. 2016 Understanding the ecology and evolution of host–parasite interactions across scales. *Evolutionary Applications* 9: 37–52.
- [132] Plank MJ, Law R. 2015 Spatial point processes and moment dynamics in the life sciences: A parsimonious derivation and some extensions. *Bulletin of Mathematical Biology* 77: 586–613.
- [133] Plank MJ, Simpson MJ. 2012 Models of collective cell behaviour with crowding effects: comparing lattice based and lattice-free approaches. *Journal of the Royal Society Interface* 9: 2983–2996.
- [134] Plank MJ, Simpson MJ. 2013 Lattice-free models of cell invasion: discrete simulations and travelling waves. *Bulletin of Mathematical Biology* 75: 2150–2166.
- [135] Plank MJ, Simpson MJ, Binny RN. 2019 Small-scale spatial structure influences large-scale invasion rates. *Theoretical Ecology* <https://doi.org/10.1007/s12080-020-00450-1>.
- [136] Purves DW, Law R. 2002 Fine-scale spatial structure in a grassland community: quantifying the plant’s-eye view. *Journal of Ecology* 90: 121–129.
- [137] Raghib M, Hill NA, Dieckmann U. 2011 A multiscale maximum entropy moment closure for locally regulated space-time point process models of population dynamics. *Journal of Mathematical Biology* 62: 605–653.
- [138] Raz E, Mahabaleshwar H. 2009 Chemokine signaling in embryonic cell migration: a fisheye view. *Development* 136: 1223–1229.
- [139] Rincon DF, Canas LA, Hoy CW. 2017 Modeling changes in predator functional response to prey across spatial scales. *Theoretical Ecology* 10: 403–415.
- [140] Romanczuk P, Couzin ID, Schimansky-Geier L. 2009 Collective motion due to individual escape and pursuit response. *Physical Review Letters* 102: 010602.
- [141] Ross SM. 2009 *Introduction to probability and statistics for engineers and scientists*. Elsevier Academic Press, Massachusetts.
- [142] Roycroft A, Mayor R. 2015 Forcing contact inhibition of locomotion. *Trends in cell biology* 25: 373–375.
- [143] Santora JA, Reiss CS, Loeb VJ, Veit RR. 2010 Spatial association between hotspots of baleen whales and demographic patterns of Antarctic krill *Euphausia superba* suggests size-dependent predation. *Marine Ecology Progress Series* 405: 255–269.
- [144] Sarapata EA, de Pillis LG. 2014 A Comparison and catalog of intrinsic tumor growth models. *Bulletin of Mathematical Biology* 76: 2010–2024.

- [145] Sharkey KJ, Fernandez C, Morgan KL, Peeler E, Thrush M, Turnbull JF, Bowers RG. 2006 Pair-level approximations to the spatio-temporal dynamics of epidemics on asymmetric contact networks. *Journal of Mathematical Biology* 53: 61–85.
- [146] Shaw TJ, Martin P. 2009 Wound repair at a glance. *Journal of Cell Science* 122: 3209–3213.
- [147] Simpson MJ, Landman KA, Hughes BD. 2009 Multi-species simple exclusion processes. *Physica A: Statistical Mechanics and its Applications* 388: 399–406.
- [148] Simpson MJ, Landman KA, Hughes BD. 2010 Cell invasion with proliferation mechanisms motivated by time-lapse data. *Physica A: Statistical Mechanics and its Applications* 389: 3779–3790.
- [149] Simpson MJ, Towne C, McElwain DLS, Upton Z. 2010 Migration of breast cancer cells: Understanding the roles of volume exclusion and cell-to-cell adhesion. *Physical Review E* 82: 041901.
- [150] Simpson MJ, Binder BJ, Haridas P, Wood BK, Treloar KK, McElwain DLS, Baker RE. 2013a Experimental and modelling investigation of monolayer development with clustering. *Bulletin of Mathematical Biology* 75: 871–889.
- [151] Simpson MJ, Jazaei F, Clement TP. 2013b How long does it take for aquifer recharge or aquifer discharge processes to reach steady state? *Journal of Hydrology* 501: 241–248.
- [152] Simpson MJ, Plank MJ. 2017 Simplified calculation of diffusivity for a lattice-based random walk with a single obstacle. *Results in Physics* 7: 3346-3348.
- [153] Smith S, Cianci C, Grima R. 2017 Macromolecular crowding directs the motion of small molecules inside cells. *Journal of the Royal Society Interface* 14: 20170047.
- [154] Smith CA, Yates CA. 2018 Spatially extended hybrid methods: a review. *Journal of the Royal Society Interface* 15: 20170931.
- [155] Soehnlein O, Steffens S, Hidalgo A, Weber C. 2017 Neutrophils as protagonists and targets in chronic inflammation. *Nature Reviews Immunology* 17: 248–261.
- [156] Stephens PA, Sutherland WJ, Freckleton RP. 1999 What is the Allee effect? *Oikos* 87: 185–190.
- [157] Strömbom D, Mann RP, Wilson AM, Hailes S, Morton AJ, Sumpter DJ, King AJ. 2014 Solving the shepherding problem: heuristics for herding autonomous, interacting agents. *Journal of the Royal Society Interface* 11: 20140719.

- [158] Sun M, Zaman MH. 2017 Modelling, signaling and cytoskeleton dynamics: integrated modelling-experimental frameworks in cell migration. *Wiley Interdisciplinary Reviews: Systems Biology and Medicine* 9: e1365.
- [159] Surendran A, Plank MJ, Simpson MJ. 2018 Spatial moment description of birth-death-movement processes incorporating the effects of crowding and obstacles. *Bulletin of Mathematical Biology* 80: 2828–2855.
- [160] Surendran A, Plank MJ, Simpson MJ. 2019 Spatial structure arising from chase-escape interactions with crowding. *Scientific Reports* 9: 14988.
- [161] Surendran A, Plank MJ, Simpson MJ. 2020 Small-scale spatial structure affects predator-prey dynamics and coexistence. *Theoretical Ecology* 13: 537–550.
- [162] Surendran A, Plank MJ, Simpson MJ. 2020 Population dynamics with spatial structure and an Allee effect. *Proceedings of the Royal Society A: Mathematical, Physical and Engineering Sciences* 476: 20200501.
- [163] Tambe DT, Hardin CC, Angelini TE, Rajendran K, Park CY, Serra-Picamal X, Zhou EH, Zaman MH, Butler JP, Weitz DA, Fredberg JJ, Trepat X. Collective cell guidance by cooperative intercellular forces. *Nature Materials* 10: 469–475.
- [164] Tan C, Saurabh S, Bruchez MP, Schwartz R, LeDuc P. 2013 Molecular crowding shapes gene expression in synthetic cellular nanosystems. *Nature Nanotechnology* 8: 602–608.
- [165] Taylor CM, Hastings A. 2005 Allee effects in biological invasions. *Ecology Letters* 8: 895–908.
- [166] Thomas RJ, Bennett A, Thomson B, Shakesheff KM. 2006 Hepatic stellate cells on poly(dl-lactic acid) surfaces control the formation of 3d hepatocyte co-culture aggregates in vitro. *European Cells and Materials* 11: 16–26.
- [167] Tobin P, Bjornstad ON. 2003 Spatial dynamics and cross-correlation in a transient predator-prey system. *Journal of Animal Ecology* 72: 460–467.
- [168] Treloar KK, Simpson MJ, Binder BJ, McElwain DLS, Baker RE. 2015 Assessing the role of spatial correlations during collective cell spreading. *Scientific Reports* 4: 5713.
- [169] Vicsek T. 2010 Closing in on evaders. *Nature* 466: 43–44.
- [170] Vijay K. 2018 Toll-like receptors in immunity and inflammatory diseases: Past, present, and future. *International Immunopharmacology* 59: 391–412.
- [171] Wang H, Nagy JD, Gilg O, Kuang Y. 2009 The roles of predator maturation delay and functional response in determining the periodicity of predator-prey cycles. *Mathematical Biosciences* 221: 1–10.

- [172] Warne DJ, Baker RE, Simpson MJ. 2017 Optimal quantification of contact inhibition in cell populations. *Biophysical Journal* 113: 1920–1924.
- [173] Wedemeier A, Merlitz H, Langowski J. 2009 Anomalous diffusion in the presence of mobile obstacles. *Europhysics Letters* 88: 38004.
- [174] Weijer CJ. 2009 Collective cell migration in development. *Journal of Cell Science* 122: 3215–3223.
- [175] Welch MD. 2015 Cell migration, freshly squeezed. *Cell* 160: 581–582.
- [176] Williams MLK, Solnica-Krezel L. 2017 Regulation of gastrulation movements by emergent cell and tissue interactions. *Current Opinion in Cell Biology* 48: 33–39.
- [177] Wilson WG. 1998 Resolving discrepancies between deterministic population models and individual-based simulations. *The American Naturalist* 151: 116–134.
- [178] Wittmer HU, Sinclair ARE, McLellan BN. 2005 The role of predation in the decline and extirpation of woodland caribou. *Oecologia* 144: 257–267.
- [179] Wolf K, Alexander S, Schacht V, Coussens LM, von Andrian UH, van Rheenen J, Deryugina E, Friedl P. 2009 Collagen-based cell migration models in vitro and in vivo. *Seminars in Cell and Developmental Biology*, 20: 931–941.
- [180] Wood AJ, Ackland GJ. 2007 Evolving the selfish herd: emergence of distinct aggregating strategies in an individual-based model. *Proceedings of the Royal Society B: Biological Sciences* 274: 1637–1642.
- [181] Young W, Roberts A, Stuhne G. 2001 Reproductive pair correlations and the clustering of organisms. *Nature* 412: 328–331.
- [182] Yue B. 2014 Biology of the extracellular matrix: an overview. *Journal of Glaucoma* 23: S20–S23.
- [183] Zaman MH, Trapani LM, Sieminski AL, Mackellar D, Gong H, Kamm RD, Wells A, Lauffenburger DA, Matsudaira P. 2006 Migration of tumor cells in 3D matrices is governed by matrix stiffness along with cell-matrix adhesion and proteolysis. *Proceedings of the National Academy of Sciences of the United States of America* 103: 10889–10894.